Rigorous Bounds for Bond Percolation Thresholds of Three-dimensional Lattices

by

Gaoran Yu

A dissertation submitted to Johns Hopkins University in conformity with the requirements for the degree of Doctor of Philosophy.

Baltimore, Maryland

October, 2018

Abstract

In this dissertation we introduce and apply a new growth process methodology that provides rigorous upper bounds for the percolation thresholds of several three-dimensional bond percolation models. By studying rigorous upper and lower bounds of bond percolation thresholds, one hopes to obtain guidelines or hints for determining exact percolation thresholds. Meanwhile, rigorous upper and lower bounds may provide verifications or disproofs of the simulation estimates or conjectured values of the corresponding thresholds. A trustworthy result for the percolation threshold, whether exactly solved or obtained from simulations, provides an accurate phase transition point above which percolation (or infinite connectivity) occurs on the associated porous media, which is of great interest in industrial and scientific fields. Examples of applications include characterization of permeability, conductivity, diffusivity of porous media, biological evolution, spread of information, and many others.

The dissertation focuses on three-dimensional bond percolation models. Currently, none of the percolation thresholds of three-dimensional bond percolation models have

been solved exactly. Moreover, there are few rigorous upper and lower bounds, and those that exist are not very precise. However, since most real-world media are three-dimensional, these models are of great importance in physics applications. This motivates us to study the percolation thresholds of such models.

To obtain upper bounds for the bond percolation thresholds of three-dimensional lattices, we develop a growth process approach. The growth process approach analyzes the static connected component in a random graph by considering it to be a dynamic process. The process describes the connected component as a growing set of vertices that may keep adding a subset of their current neighbors depending on the random states of the incident edges. Subsequently, we analyze whether or not this growth process stops growing to study whether percolation occurs on the associated lattice or not.

The methodology provides us with a powerful tool to study a variety of three-dimensional bond percolation models. The growth process approach works on a family of lattices called stacked lattices. It can also be slightly modified and applied to other well-studied three dimensional lattices such as the face-centered cubic lattice and the body-centered cubic lattice.

In this dissertation we provide detailed description, justification and applications

of the growth process method. The results we obtain are quite satisfactory, compared with the previous rigorous bounds for our problem models. For instance, we prove that the bond percolation threshold of the cubic lattice, for which high-precision simulation estimates yield 0.24881, is smaller than 0.34730, in contrast to the previous best upper bound, 0.44779. We thus successfully narrow the difference between the rigorous upper bound and simulation estimates for the percolation threshold of the cubic lattice bond percolation model by approximately 50%. However, there is still much room for further improvement. Future research may explore more approaches for bounding percolation thresholds, or even solving them; generalizing the growth process approach to a wider family of models (e.g., mixed percolation models and directed percolation models); and using our improved bounds as references and applying the substitution method to obtain bounds for other models.

Primary Reader: John C. Wierman

Secondary Reader: James A. Fill

Acknowledgments

There are many people that have offered me great help during my time in graduate school. I would like to thank four groups of people, without whom this thesis would not have been possible: my thesis advisor, my thesis committee members, and my family and friends.

My thesis advisor: Prof. John C. Wierman

I owe my deepest gratitude to my research advisor, Prof. John C. Wierman. On the academic level, Prof. Wierman taught me fundamentals of conducting scientific research in the percolation area. He not only guided me through mathematical thinking and learning, but also improved my research writing and communication skills. On a personal level, Prof. Wierman's integrity, reliability and hard-working nature greatly influenced me. I really benefited a lot, in every aspect, by working under his supervision.

My thesis committee members: Prof. Amitabh Basu, Prof. James A. Fill, and

ACKNOWLEDGMENTS

Prof. John C. Wierman

I would like to thank Prof. Basu for his participation in my PhD qualification exams and his guidance concerning the combinatorial field. He inspired me to implement my own symbolic calculation toolbox in Matlab. I would like to thank Prof. Fill for his critical and helpful comments in proofreading my dissertation, along with the wisdom he shared in his probability courses. Finally, I would also like to thank Prof. Wierman again for reading my dissertation repetitively and provide countless suggestions and advice.

My family: Dr. Xuejun Yu, Mrs. Haiyan Gao, and Dr. Hongfan Chen

My most sincere thanks to my parents, Xuejun and Haiyan, for their continuous and unconditional support. I also want to express my appreciation to my wife, Hongfan, for her inspiring encouragement and trust.

My friends: Dr. W. Allen Cheng, Dr. Runze Tang, and Dr. Shangsi Wang.

I thank my dearest friends for the meaningful and colorful days we shared together.

Contents

List of Tables

List of Figures

Chapter 1

Introduction

1.1 Percolation Models

1.1.1 Origin

Percolation theory was introduced in order to model fluid flow in random media. Consider the following problem: If we immerse a large porous stone into water, then what is the probability that the center of the stone is saturated? In 1957, Broadbent and Hammersley [4] introduced the "percolation model" as a simple stochastic model for this complicated problem. In the three-dimensional case, their model amounts to the following. Let $\mathbb{L}^3$ be the simple cubic lattice (Figure 1.1) and q be a number satisfying $0 \leqslant q \leqslant 1$. Each edge of $\mathbb{L}^3$ is designated to be open with probability q and closed otherwise, independently of all the other edges. The edges of $\mathbb{L}^3$ represent the

inner passageways of the stone and the parameter q is the proportion of the passages which are broad enough to allow water molecules to pass through. The edges correspond to the broad passageways are called open edges, and the other edges are called closed edges. Once the stone is immersed in the water, a vertex v inside the stone is wetted if and only if there is an open path (a path consisting of only open edges) in $\mathbb{L}^3$ from v to a vertex on the boundary of the stone. Percolation theory is concerned primarily with the existence of such open paths.

Notice that edges in the lattice $\mathbb{L}^3$ represent the microscopic structure of the porous stone. Thus, a path from the stone surface to a vertex v buried near the center must contain a large number of edges. Therefore, the probability that v is saturated by water can be approximated by the probability that the vertex v lies on an infinite open path in $\mathbb{L}^3$. In other words, the probability of large-scale penetration of the stone by water is closely related to the probability of the existence of an infinite open cluster, which is a collection of endpoints of the connected open passageways. The latter probability equals 0 if $q = 0$ and equals 1 if $q = 1$, and it is non-decreasing as q increases. By Kolmogorov's zero-one law, for each fixed $q \in [0, 1]$, the probability of the existence of an infinite open cluster is either 0 or 1. Combining Kolmogorov's zero-one law with the monotonicity property, there exists a critical value $p_c(\mathbb{L}^3)$, which is the proportion of open edges such that all open clusters are finite almost surely when $q < p_c(\mathbb{L}^3)$ and there exists an infinite open cluster

almost surely when $q > p_c(\mathbb{L}^3)$. This critical value $p_c(\mathbb{L}^3)$ is called the *bond percolation threshold of the cubic lattice*. A major goal of percolation theory is to solve for such a critical value p_c, while the underlying graph may no longer be the cubic lattice.

1.1.2 Model Generalization

Since the genesis of percolation theory, the model described by Broadbent and Hammersley has been generalized extensively. The structure of the lattice is not restricted to the cubic lattice, but more general families of infinite graphs are allowed. For instance, Archimedean lattices, which are planar lattices in which all polygons are regular and each vertex is surrounded by the same sequence of polygons, are one of the most well-studied families of graphs. Also, the model can be further generalized by introducing different sources of randomness. The Bernoulli bond percolation model, where each edge (bond) is open with probability p and water molecules can travel through the open bonds, is the most well-studied model. The Bernoulli site percolation model, where each vertex (site) is open with probability p, and the water molecules can travel through a bond if and only if both endpoints of the bond are open, is a more general model than the bond model, in the sense that a bond model on a graph G is equivalent to the site model on the line graph of G. Apart from use of different lattices and source of randomness, one may generalize from the homogeneous bond model, in which each bond is open with the same probability p, to the

inhomogeneous bond model, in which different bonds may have different probabilities to be designated as open.

1.1.3 Model Descriptions

In this dissertation, we focus on the percolation threshold of the homogeneous bond percolation model. We begin by describing these terms in more detail.

Definition 1.1.1 (The homogeneous Bernoulli bond percolation model)**.** For a connected graph $G = (V, E)$, the *homogeneous Bernoulli bond percolation model on* G is a random designation of states (open or closed) to each edge of G, with each edge independently designated as open with probability p and closed otherwise.

Throughout this dissertation, we assume that the underlying graph G is connected and contains infinitely many vertices. Following the model definition, we define the corresponding probability space as follows.

Definition 1.1.2 (The probability space of the homogeneous bond percolation model)**.** Let $\Omega = \{0,1\}^E$ be the configuration space. A set $C \in \Omega$ is a finite cylinder set if there exists $E_s \subset E$ such that $|E_s| < \infty$ and $C = \{0,1\}^{E\setminus E_s} \times \{1\}^{E_s}$. Let $\mathcal{F}$ be the σ-field generated by the finite cylinder sets of Ω. Define the probability measure P_p on $(\Omega, \mathcal{F})$ to be the product measure

$$P_p = \prod_{e\in E} \mu_e,$$

where $\omega(e) = \mathbb{1}_{\{\text{e is open}\}}$, and μ_e is Bernoulli distributed with parameter p for each $e \in E$. We call $(\Omega, \mathcal{F}, P_p)$ the *probability space of the homogeneous percolation model*.

We then introduce the definition of the percolation probability.

Definition 1.1.3 (Open cluster)**.** For a bond percolation model on $G = (V, E)$, a fixed vertex $v \in V$, and a configuration $\omega \in \Omega$, the *open cluster* containing v is defined by $C_v(\omega) = \{u \in V \mid u \text{ is connected to } v \text{ by } \omega\text{-open edges in } E\}$.

Definition 1.1.4 (Percolation probability)**.** For a homogeneous bond model on G, and a fixed vertex $v \in V$, the *percolation probability* $\theta_v^G(p)$ is defined as $\theta_v^G(p) = P_p^G(|C_v| = \infty)$.

With the definition of the percolation probability, we can define the percolation threshold of a homogeneous bond model.

Definition 1.1.5 (Bond percolation threshold)**.** For a homogeneous bond model on a graph G, its *bond percolation threshold* is $p_c(G) = \sup\{p : \theta_v^G(p) = 0\}$.

Here $p_c(G)$ is independent of the choice of the vertex in the definition of percolation probability if G is connected. To see this, consider any two vertices $v_1, v_2 \in V$. Let l be the length of the shortest path (not necessarily open) in G connecting v_1 to v_2. By definition of the percolation probability, we have $\theta_{v_1}^G(p) \geqslant p^l \cdot \theta_{v_2}^G(p)$ and $\theta_{v_2}^G(p) \geqslant p^l \cdot \theta_{v_1}^G(p)$. Thus, $\theta_{v_1}^G(p) = 0 \Leftrightarrow \theta_{v_2}^G(p) = 0$, making $p_c(G)$ independent of the choice of the vertex in the definition of percolation probability.

1.2 Lattices of Interest

In this section, we describe several three-dimensional lattices whose bond percolation thresholds are of particular interest to physicists and mathematicians. Among them, the cubic lattice, the face centered cubic (FCC) lattice, and the body centered cubic (BCC) lattice are the most studied. In addition to the three lattices listed above, stacked lattices, especially the stacked triangular lattice, are also considered in the physics literature [8, 27, 32]. Unfortunately, for all of these three-dimensional lattices, the exact values of their bond percolation thresholds remain unknown.

1.2.1 The Cubic Lattice

The cubic lattice bond model is the most studied three-dimensional percolation model. Figure 1.1 illustrates an induced subgraph of the cubic lattice containing $4 \times 4 \times 4$ cubic units. We denote the unsolved percolation threshold of the cubic lattice by $p_c(\mathbb{L}^3)$. There is an extensive literature providing approximations, numerical estimates, and rigorous bounds for it (See Table 1.1). From the 1960s through the 1980s, a collection of estimates ranging from 0.248 to 0.254 were obtained by Monte Carlo simulations [10,12,29,33,41]. During the same period, other approximations were produced by series expansion [1,9,30], which proposed values ranging from 0.247 to 0.248, and by the renormalization approach [7,22,25], which provided results

ranging from 0.209 to 0.265. With the development of advanced algorithms and increasing computational performance, simulation results are becoming more accurate and trustworthy. From the 1990s onward, simulation results [6,11,18,28,32,34] began to agree on the first four decimal places, at 0.2488. In particular, the most recent simulations [6, 18, 34] produced high-precision estimates that this bond percolation threshold is near 0.248812.

As for rigorous bounds for $p_c(\mathbb{L}^3)$, no reasonably tight upper bound has been proved to date. In 1985, Campanino and Russo [5] proved that the site percolation threshold of the cubic lattice is strictly smaller than 0.5. Since the bond percolation threshold is no greater than the site percolation threshold of the same underlying lattice, the bond percolation threshold of the cubic lattice is strictly less than 0.5 as well. Currently, the best rigorous upper bound is $p_c(\mathbb{L}^3) \leqslant 0.447792$ by Wierman [37]. Meanwhile, a lower bound for $p_c(\mathbb{L}^3)$ follows from self-avoiding walk (SAW) enumeration by Schram *et al.* [26], who enumerated SAWs on the cubic lattice up to length 36 using the length-doubling method. The method generates a length n self-avoiding walk by concatenating length $n/2$ SAWs, two at a time. The enumeration results provide an upper bound for the connective constant of the cubic lattice, whose reciprocal is a lower bound for the corresponding bond percolation threshold. Schram's results translate into the lower bound for $p_c(\mathbb{L}^3)$ that $p_c(\mathbb{L}^3) \geqslant 0.2090827$. The length-doubling method can be applied to SAW enumerations on vertex transitive graphs.

In separate work [42], we generalized this algorithm and applied it to graphs that are not vertex transitive.

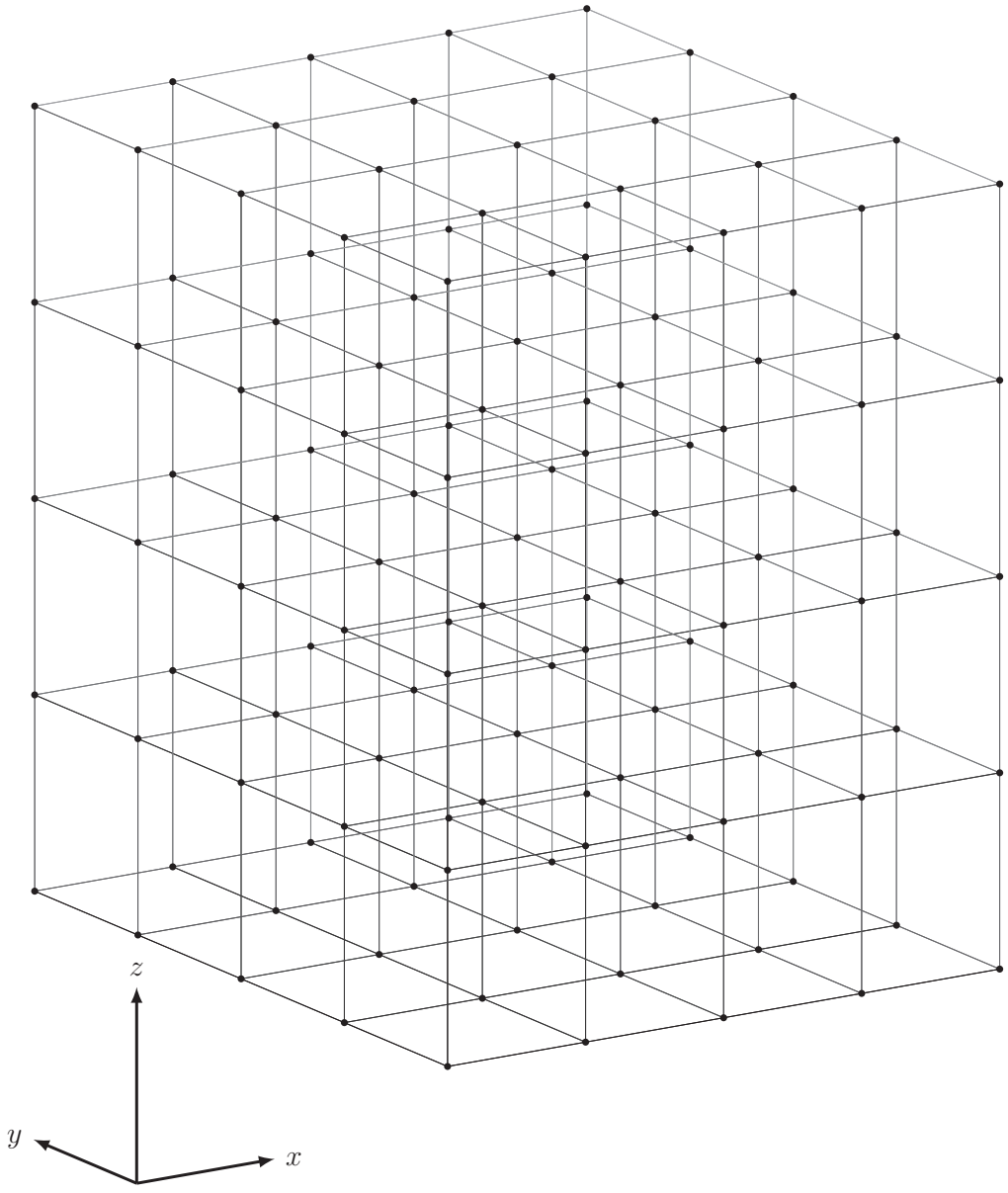

Figure 1.1: An illustration of the cubic lattice. The figure shows a subgraph of $\mathbb{L}^3$ containing $4 \times 4 \times 4$ cubic units.

Author	Year	Method	Result	Reference
Vyssotsky *et al*	1961	Monte Carlo	0.254	[33]
Heermann & Stauffer	1981	Monte Carlo	0.248	[12]
Wilke	1983	Monte Carlo	0.2492	[41]
Grassberger	1986	Monte Carlo	0.24875	[10]
Stauffer & Zabolitzky	1986	Monte Carlo	0.2494	[29]
Grassberger	1992	Monte Carlo	0.248814	[11]
Stauffer *et al*	1994	Monte Carlo	0.2488	[28]
van der Marck	1997	Monte Carlo	0.2487	[32]
Lorenz & Ziff	1998	Monte Carlo	0.248812	[18]
Dammer & Hinrichsen	2004	Monte Carlo	0.2488125	[6]
Wang *et al*	2013	Monte Carlo	0.24881182	[34]
Sykes & Essam	1964	Series expansion	0.247	[30]
Gaunt & Sykes	1983	Series expansion	0.2479	[9]
Adler	1984	Series expansion	0.2479	[1]
Adler *et al*	1990	Series expansion	0.2488	[2]
Galam & Mauger	1997	Universal Formula	0.2488	[8]
de Magalhães *et al*	1980	Renormalization	0.2526	[7]
Sahimi *et al*	1983	Renormalization	0.265	[25]
Odagaki & Chang	1984	Renormalization	0.209	[22]
Vyssotsky *et al*	1961	Conjecture	0.2500	[33]

Table 1.1: A summary of estimates for $p_c(\mathbb{L}^3)$.

1.2.2 The FCC Lattice and the BCC Lattice

The FCC lattice and the BCC lattice are two other important lattices in the cubic crystal system (a crystal system where the unit cell is in the shape of a cube). Both lattices have a unit cell in the shape of a cube. The unit cell of the FCC lattice and that of the BCC lattice are illustrated in Figure 1.2 and Figure 1.3, respectively. In both figures, we use solid lines to illustrate edges of the corresponding lattices, and use dashed lines to illustrate the two cubic units. It is worth noticing that the dashed lines are not edges of the corresponding lattices.

Estimates for the bond percolation thresholds of these two lattices are $p_c(\text{FCC}) = 0.119$ and $p_c(\text{BCC}) = 0.180$ by Stauffer *et al.* [28], $p_c(\text{FCC}) = 0.1200 \pm 0.0002$ and $p_c(\text{BCC}) = 0.1802 \pm 0.0002$ by van der Marck [32], and $p_c(\text{FCC}) = 0.1201635 \pm 0.0000010$ and $p_c(\text{BCC}) = 0.1802875 \pm 0.0000010$ by Lorenz and Ziff [18]. All these results were obtained using Monte Carlo simulation. Currently, there are no non-trivial rigorous bounds for either of the percolation thresholds.

Remarks 1.2.1.

(a) The face centered cubic lattice and body centered cubic lattice we study throughout this dissertation are the versions that appear in the physics literature. There are alternative versions of these two lattices. We name the alternative versions the FCC$(4, 18)$ lattice and the BCC$(8, 14)$ lattice. The values in each pair of parentheses indicate the degrees of the vertices in each vertex "class" of the

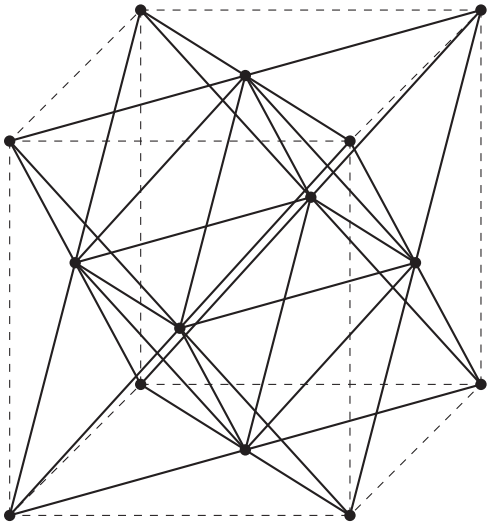

Figure 1.2: One cubic unit of the FCC lattice. Notice that the dashed line segments illustrate the cube, but are not edges of the FCC lattice.

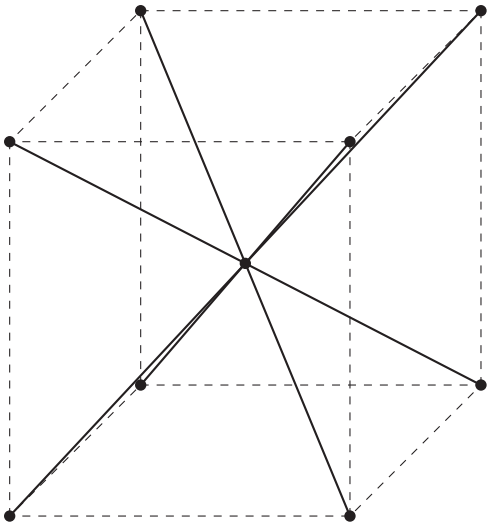

Figure 1.3: One cubic unit of the BCC lattice. Notice that the dashed line segments illustrate the cube, but are not edges of the BCC lattice.

corresponding lattice. Lower bounds for the bond percolation thresholds of the FCC$(4, 18)$ lattice and the BCC$(8, 14)$ lattice have been obtained by self-avoiding

walk enumerations [42].

(b) Our literature search found no other results regarding the percolation thresholds of the FCC$(4, 18)$ lattice and the BCC$(8, 14)$ lattice.

1.2.3 Stacked Lattices

Apart from lattices in the cubic crystal system, we are also interested in the bond percolation thresholds of stacked lattices. Informally speaking, a stacked lattice is obtained by piling up isomorphic planar graphs, forming a three-dimensional graph containing infinitely many layers. For instance, the cubic lattice can be regarded as the stacked square lattice. In the stacked lattice family other than the cubic lattice, the stacked triangular lattice (Figure 1.4) bond percolation model is the most commonly studied. Simulation results for its percolation threshold are 0.1859 by van der Marck [32] and 0.1860 by Schrenk *et al.* [27]. Meanwhile, van der Marck also provides simulation results for other stacked lattices. Further discussion regarding these lattices is in Chapter 8.

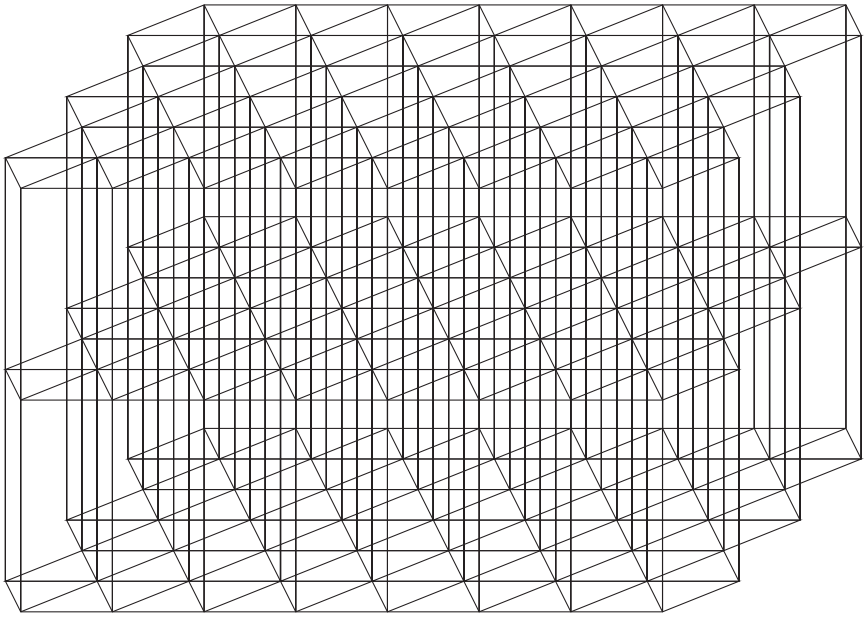

Figure 1.4: The stacked triangular lattice.

1.3 Bounding Percolation Thresholds

1.3.1 Exactly Solved Percolation Thresholds

At present, there are several two-dimensional lattice models in which the exact percolation thresholds are known. These models stand as benchmarks when bounding the percolation thresholds of the unsolved models. To be more specific, rigorous bounds obtained by the containment principle, the contraction principle, the substitution method, and the growth process approach, which is developed in this dissertation, are all based on relating unsolved percolation models to solved ones. Generally speaking, we have two families of models whose percolation thresholds are exactly solved. They are the bond models on self-dual graphs (hypergraphs included) and the site

models on self-matching graphs. For readers interested in further details regarding finding exact percolation thresholds, please refer to Kesten [17], Sykes & Essam [30], Wierman & Ziff [40], Ziff [43], Ziff & Scullard [44], and Ziff *et al.* [45]

Ideally, we would like to solve for percolation thresholds exactly. For the unsolved models, various methodologies are developed to bound their percolation thresholds rigorously. Rigorous bounds for percolation thresholds are useful in verifying the correctness of the simulation results of the corresponding thresholds. More importantly, they provide insight that might help solve the models exactly in the future. In this dissertation, we focus on the growth process approach.

1.3.2 The Growth Process Approach

The growth process approach analyzes whether or not a growth process describing the "projected open cluster" of a three-dimensional bond percolation model stops expanding. It is inspired by a method introduced by Men'shikov and Pelikh [20] to analyze site percolation models with multiple defect types. (The standard site percolation model has two defect types: open and closed.) The method was further modified by van den Berg and Ermakov [31] to provide a rigorous lower bound for the percolation threshold of the square lattice site model. The core idea of this method is that we no longer consider the open cluster of a random graph to be a static collection of vertices, but a dynamically growing process. In this dissertation, we refer to and

generalize this idea to analyze bond percolation models on three-dimensional lattices.

The intuitive idea of the growth process approach can be described as follows. We establish a growth process, denoted by $\mathbf{G}^{(3)}$, that describes the expansion of the open cluster in a three-dimensional bond percolation model. Performing the natural projection of $\mathbf{G}^{(3)}$ results in a projected process $\mathbf{G}^{(2)}$. Intuitively, $\mathbf{G}^{(2)}$ is a growth process on a two-dimensional lattice, but is also related to the open cluster of the three-dimensional lattice since it illustrates the expansion of the "projected open cluster". Meanwhile, we consider the open cluster in a bond percolation model on the two-dimensional lattice to be another growth process $\mathbf{G}^{(c)}$. Notice that both $\mathbf{G}^{(2)}$ and $\mathbf{G}^{(c)}$ are defined on the two-dimensional lattice. We relate them by comparing their growth, using stochastic ordering inequalities. We choose the parameter of the two-dimensional model above criticality such that the two-dimensional model percolates. Subsequently, we choose the parameter of the three-dimensional model large enough such that $\mathbf{G}^{(2)}$ grows faster than $\mathbf{G}^{(c)}$. Finally, we use the survival of $\mathbf{G}^{(c)}$ to prove the survival of $\mathbf{G}^{(2)}$. This implies that the parameter value chosen for the three-dimensional model is an upper bound for its percolation threshold.

We apply the growth process approach to our models of interest, and obtain upper bounds for their bond percolation thresholds.

Problem Lattice	Upper Bound for p_c	Simulation Results	References
Simple Cubic	0.34730	0.2488	[6, 18, 34]
Face-centered Cubic	0.19170	0.1201, 0.1200	[18], [32]
Body-centered Cubic	0.27455	0.1803, 0.1802	[18], [32]
Stacked Kagome	0.38516	0.2563	[32]
Stacked Honeycomb	0.41614	0.3093	[32]
Stacked Triangular	0.27455	0.1859, 0.1860	[32], [27]
Stacked Dice	0.37754	0.2378	[32]
Stacked Bow-tie	0.31884	0.2092	[32]
Stacked Octagonal	0.30712	0.1752	[32]

Table 1.2: A summary of the results obtained by the growth process approach. Previously published simulation results and their references are listed for comparison.

The rest of this dissertation is organized as follows. A sketch of the basic idea of the justification of the growth process approach is given in Chapter 2. A detailed proof is provided in Chapters 3–7. Formal definitions of $\mathbf{G}^{(2)}$ and $\mathbf{G}^{(3)}$ are given in Chapter 3. The Markov property of $\mathbf{G}^{(2)}$ and $\mathbf{G}^{(3)}$ is proved in Chapter 4. The transition probabilities of $\mathbf{G}^{(2)}$ are calculated in Chapter 5. The couplings between the two processes are constructed in Chapter 6. The survival of $\mathbf{G}^{(2)}$ is analyzed using the step-wise couplings in Chapter 7. Direct applications of the approach to the stacked lattices and BCC lattice are included in Chapter 8. Finally, modifications of the approach are provided in Chapter 9, in which we further improve the upper

bound for $p_c(\mathbb{L}^3)$ and derive an upper bound for $p_c(\text{FCC})$.

Chapter 2

Growth Model Approach: An Overview

In this chapter, we shall provide an overview of how the growth process approach bounds the bond percolation threshold from above, and a sketch of the justification that the approach is correct. We illustrate the idea using the cubic lattice as an example.

2.1 Description of the Problem

Denote the d-dimensional hyper-cubic lattice by $\mathbb{L}^d = (\mathbb{Z}^d, \mathbb{E}^d)$. In the canonical embedding of $\mathbb{L}^d$, vertices in $\mathbb{Z}^d$ are associated with the points with integer coordi-

nates in d-dimensional Euclidean space and edges in $\mathbb{E}^d$ are associated with pairs of vertices whose Euclidean distance is 1. In particular, the d-dimensional hyper-cubic lattice is called the square lattice if $d = 2$, and the cubic lattice if $d = 3$.

In the hyper-cubic lattice bond percolation model, all edges of $\mathbb{E}^d$ are designated to be open with the same probability, and closed otherwise. The designation of each edge in $\mathbb{E}^d$ is assumed to be independent of all the other edges. A configuration on $\mathbb{L}^d$ is a realization of this model. More specifically, a configuration $\omega^{(d)} = \{\omega^{(d)}(e)\}_{e\in\mathbb{E}^d} \in \{0,1\}^{\mathbb{E}^d}$ is an infinite dimensional vector indexed by $e \in \mathbb{E}^d$, where $\omega^{(d)}(e) = 1$ indicates the edge e is open and $\omega^{(d)}(e) = 0$ indicates edge e is closed.

In this dissertation, we will focus on the cubic lattice (See Figure 2.1) bond percolation model. Let q be the parameter of this model, representing the probability of each edge in $\mathbb{E}^3$ being open, and $P_q^{(3)}$ be the corresponding probability measure of the cubic lattice percolation bond model. Let $\mathbf{0}^{(3)} := (0,0,0)$ denote the origin of $\mathbb{L}^3$.

We introduce analogous notation for the square lattice bond percolation model: let p be the probability of each edge in $\mathbb{E}^2$ being open, and $P_p^{(2)}$ be the corresponding probability measure of the square lattice bond percolation model. Lastly, let $\mathbf{0}^{(2)} := (0,0)$ denote the origin of $\mathbb{L}^2$. We will show that $p_c(\mathbb{L}^3) \leqslant 0.365606302$ by

relating the cubic lattice bond model to the square lattice bond model.

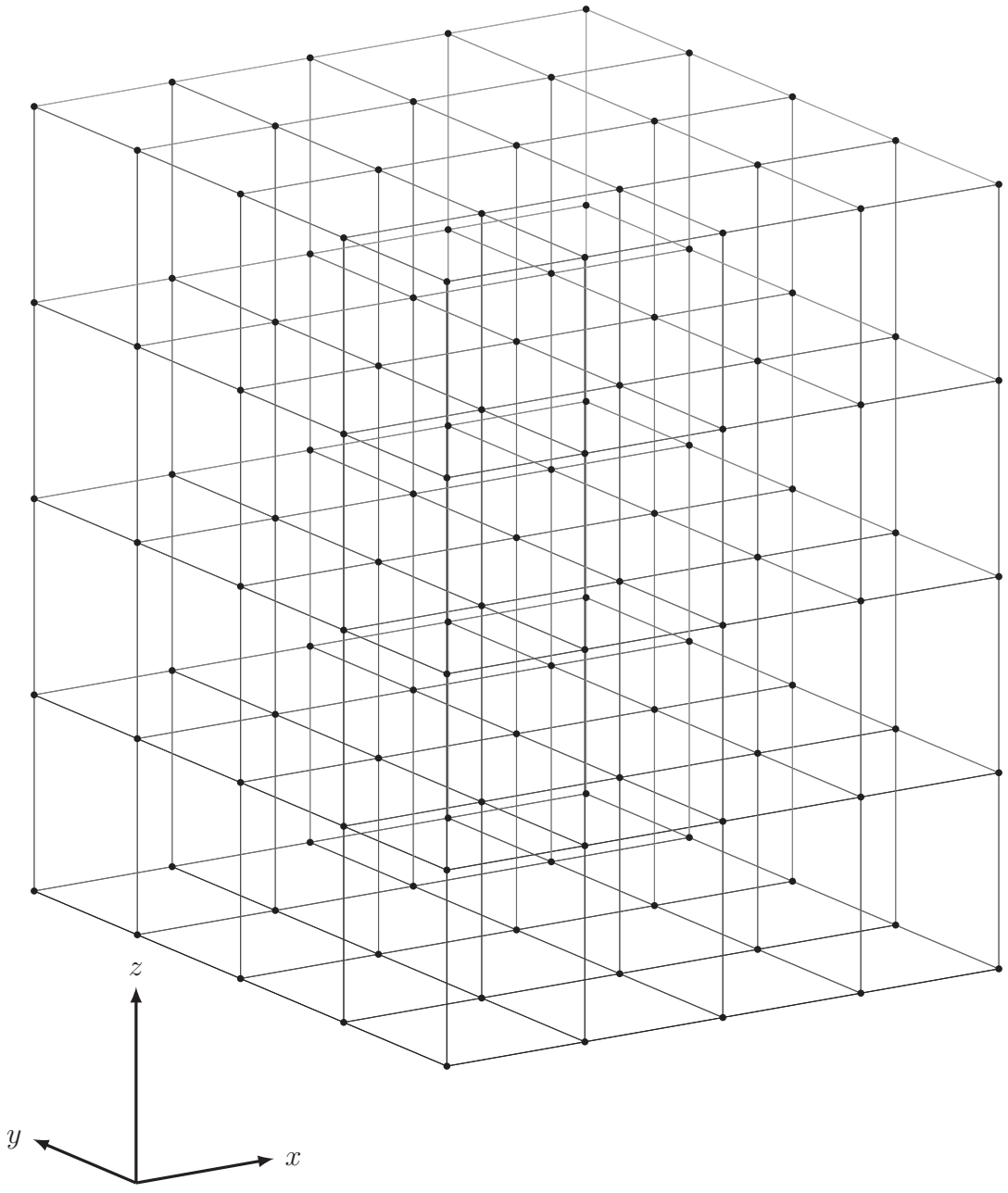

Figure 2.1: An illustration of the cubic lattice. The figure shows the subgraph of $\mathbb{L}^3$ in $[-2, 2]^3$.

2.2 General Idea

We briefly sketch the intuitive idea of our proof, while detailed descriptions of the proof are provided in Chapter 3–7. For a given configuration $\omega^{(3)}$ on $\mathbb{L}^3$ (See Figure 2.2), we think of its open cluster $D(\omega^{(3)})$ as a set of vertices that may spread from one vertex to its neighbors step-by-step, depending on the states of the incident edges. Thus we obtain a growth process $\mathbf{G}^{(3)}$ (See Figure 2.3): the edge cluster is initialized to be the empty set, while at each step of $\mathbf{G}^{(3)}$, a subset of edges connecting the vertices in $D(\omega^{(3)})$ to $\mathbf{0}^{(3)}$ may be added to the cluster based on their ω-values.

After that, we "project" $\mathbf{G}^{(3)}$ onto $\mathbb{L}^2$ and obtain a growth process on $\mathbb{L}^2$ (See Figure 2.4). Denote this projected growth process by $\mathbf{G}^{(2)}$. At each step of $\mathbf{G}^{(2)}$, edges in $\mathbb{E}^2$ that are incident to a certain vertex are considered and a subset of the edges are included (See Figure 2.5). These included edges connect $\mathbf{0}^{(2)}$ to vertices in the "projected open cluster".

We then analyze the probability measure of the set of edges that are added at each step of $\mathbf{G}^{(2)}$. Subsequently, we are able to find q large enough so that at each step, the joint probability of edges that are included by $\mathbf{G}^{(2)}$, denoted by $Q^{(2)}$, stochastically dominates the product measure of independent Bernoulli distribution with parameter p, which is denoted by Q.

Under this stochastic dominance relationship, we will establish a sequence of "step-wise" couplings. More specifically, in order to relate the projected growth process $\mathbf{G}^{(2)}$ to a standard bond percolation model on $\mathbb{L}^2$, we define two processes, $\mathbf{G}^{(r)}$ and $\mathbf{G}^{(c)}$, such that $\mathbf{G}^{(r)}$ is a "replication" of $\mathbf{G}^{(2)}$ and $\mathbf{G}^{(c)}$ is "coupled" with $\mathbf{G}^{(r)}$. More rigorously, the replicated process $\mathbf{G}^{(r)}$ is a growth process on $\mathbb{L}^2$ such that at each step, the joint distribution of edges included by $\mathbf{G}^{(r)}$ is $Q^{(2)}$ (See Figure 2.6). Meanwhile, the process $\mathbf{G}^{(c)}$ is coupled with $\mathbf{G}^{(r)}$ in the following manner. At each step of $\mathbf{G}^{(r)}$, we explore from some vertex in $\mathbb{Z}^2$ by considering its incident edges. A subset of the incident edges is added to the cluster following the $Q^{(2)}$ distribution. Meanwhile, these incident edges are added to $\mathbf{G}^{(c)}$ following the Q distribution, satisfying the coupling relation that the edges added to $\mathbf{G}^{(c)}$ are a subset of edges added to the edge cluster of $\mathbf{G}^{(r)}$. The existence of such coupling is ensured by the stochastic dominance that $Q^{(2)} \geqslant_{\text{st}} Q$.

To view this differently, we may consider edges in $\mathbf{G}^{(c)}$ to be open, and edges considered by $\mathbf{G}^{(r)}$ but not in $\mathbf{G}^{(c)}$ to be closed. The coupling procedure makes each edge considered by $\mathbf{G}^{(r)}$ open independently with probability p, and provides us with a global coupling that all edges considered to be open are a subset of edges in the edge cluster of $\mathbf{G}^{(r)}$ as we move on to future steps (See Figure 2.7). For edges in $\mathbb{E}^2$ that are not considered during the coupling procedure, they are considered to be open independently with probability p. By doing so, we obtain a random subgraph

of $\mathbb{L}^2$ consisting of open edges, and each edge in $\mathbb{L}^2$ is open with probability p (See Figure 2.8).

Thus, if p is chosen such that $p > p_c(\mathbb{L}^2) = \frac{1}{2}$, there exists an open cluster in the random subgraph of $\mathbb{L}^2$ with probability $\theta^{\mathbb{L}^2}(p) > 0$, which indicates that there are infinitely many edges included by $\mathbf{G}^{(r)}$ with strictly positive probability by the coupling relation (See Figure 2.9). Notice that $\mathbf{G}^{(r)}$ is a replication of $\mathbf{G}^{(2)}$ in the sense that they have the same distribution. Thus, there are infinitely many edges included by $\mathbf{G}^{(2)}$ with positive probability as well. This further results in infinitely many edges being included by $\mathbf{G}^{(3)}$ (See Figure 2.10). Consequently, $D(\omega^{(3)})$ contains infinitely many vertices with positive probability. Thus, the pair of p and q satisfies $p > p_c(\mathbb{L}^2)$ and the stochastic dominance shows that q is an upper bound for $p_c(\mathbb{L}^3)$ (See Figure 2.11). By letting $p \downarrow \frac{1}{2}$, the smallest q satisfying the stochastic dominance goes down to 0.365606302, which implies that $p_c(\mathbb{L}^3) \leqslant 0.365606302$.

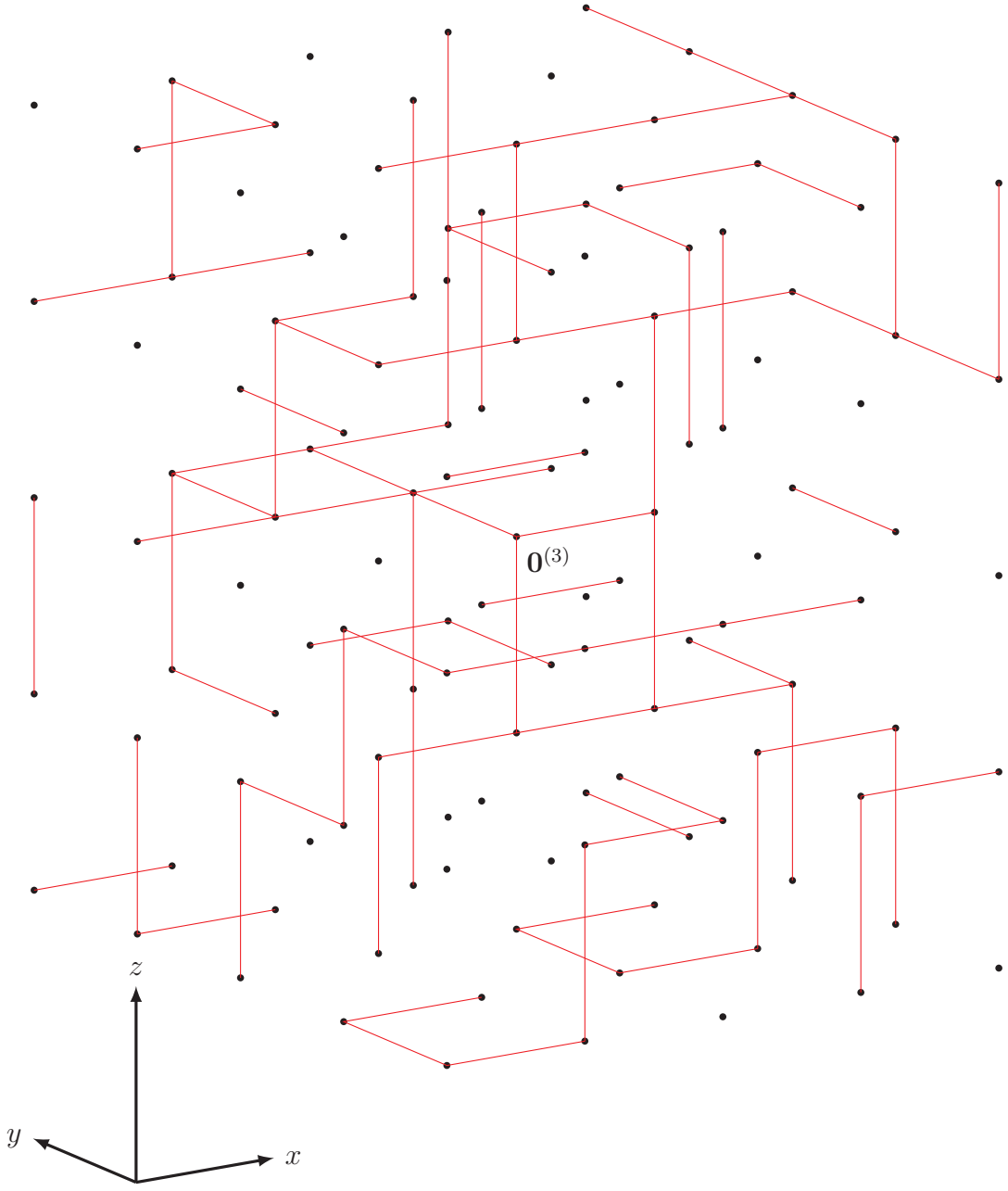

Figure 2.2: A configuration on $\mathbb{L}^3$, generated by setting $q = 0.3$. The red edges are open.

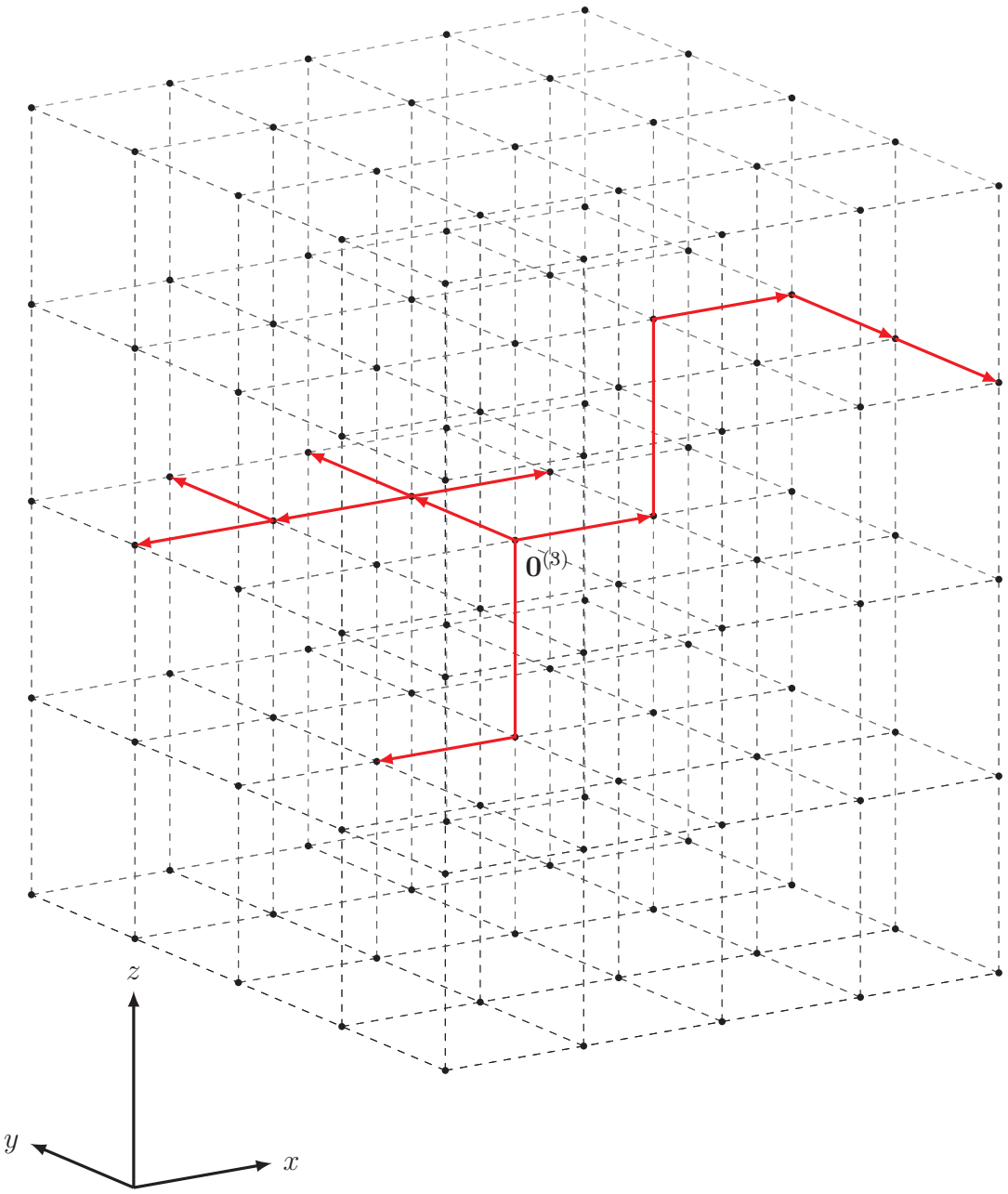

Figure 2.3: The growth process $\mathbf{G}^{(3)}$ associated with the configuration given in Figure 2.2. The arrows of paths show how the open cluster expands at different steps. Edges outside the $4 \times 4 \times 4$ cube are not considered.

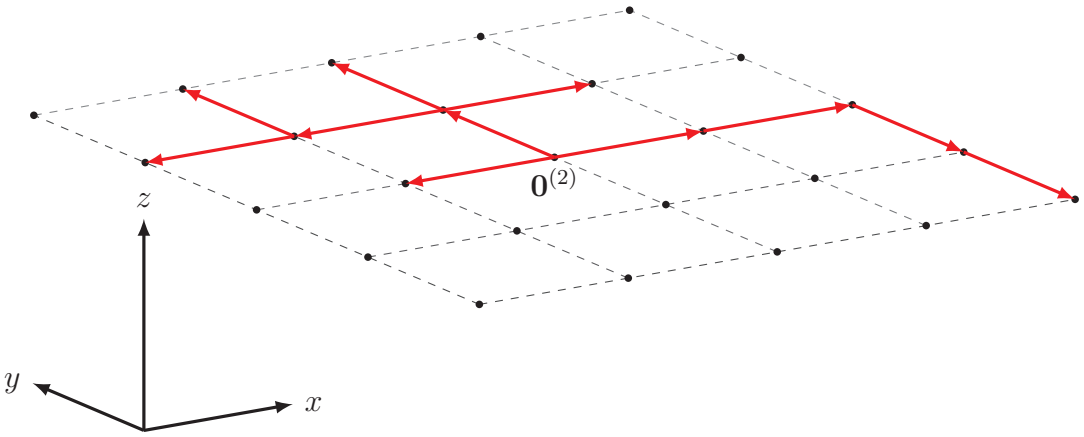

Figure 2.4: An illustration of the projection of the growth process $\mathbf{G}^{(3)}$ associated with the configuration given in Figure 2.2. The arrows of edges show how the "projected open cluster" expands, not that the edges are directed. We denote this process by $\mathbf{G}^{(2)}$.

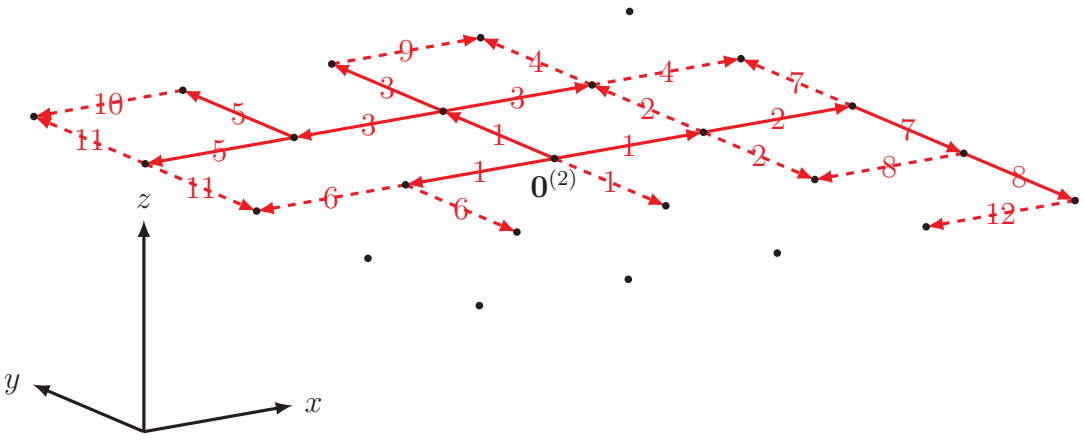

Figure 2.5: Another illustration of $\mathbf{G}^{(2)}$. The label on each edge shows the step at which the edge is considered by $\mathbf{G}^{(2)}$. Solid line segments represent edges that are included in $\mathbf{G}^{(2)}$, and dashed line segments represent edges that are considered but fail to be included.

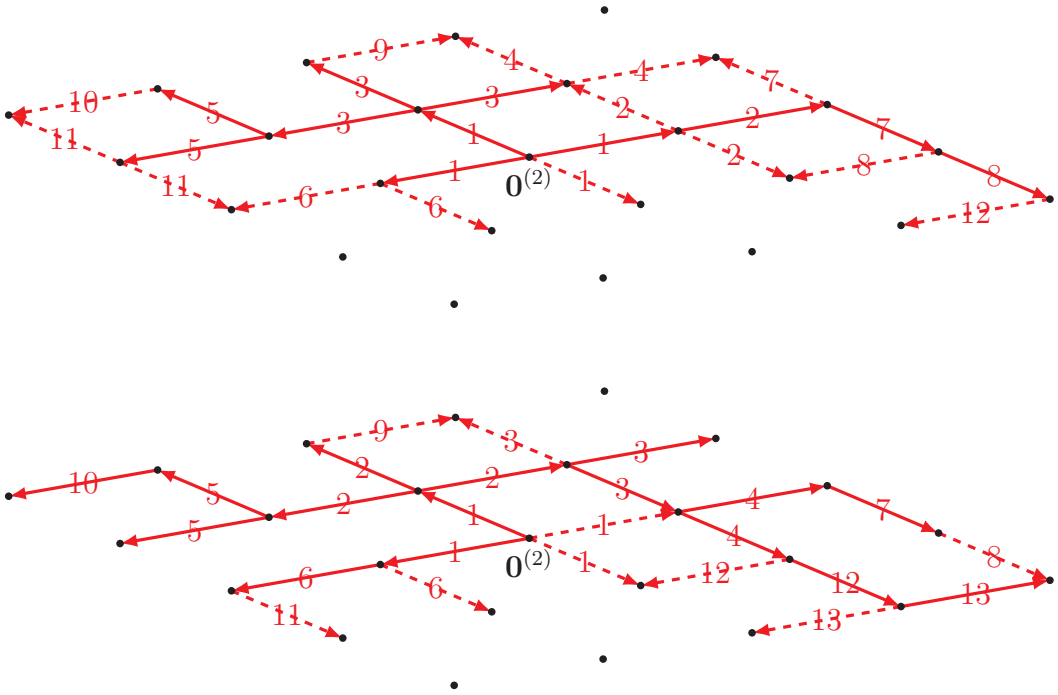

Figure 2.6: An illustration of $\mathbf{G}^{(2)}$ and its replication $\mathbf{G}^{(r)}$. The top figure illustrates $\mathbf{G}^{(2)}$, with solid line segments representing edges in the cluster and dashed line segments representing edges that are considered but are not in the cluster. The bottom figure illustrates $\mathbf{G}^{(r)}$. Notice that $\mathbf{G}^{(2)}$ is obtained from the underlying configuration on $\mathbb{L}^3$, while $\mathbf{G}^{(r)}$ is not. Both processes share the same distribution but their realizations are not necessarily equal. The label of each edge shows the step at which the edge is explored by the corresponding process.

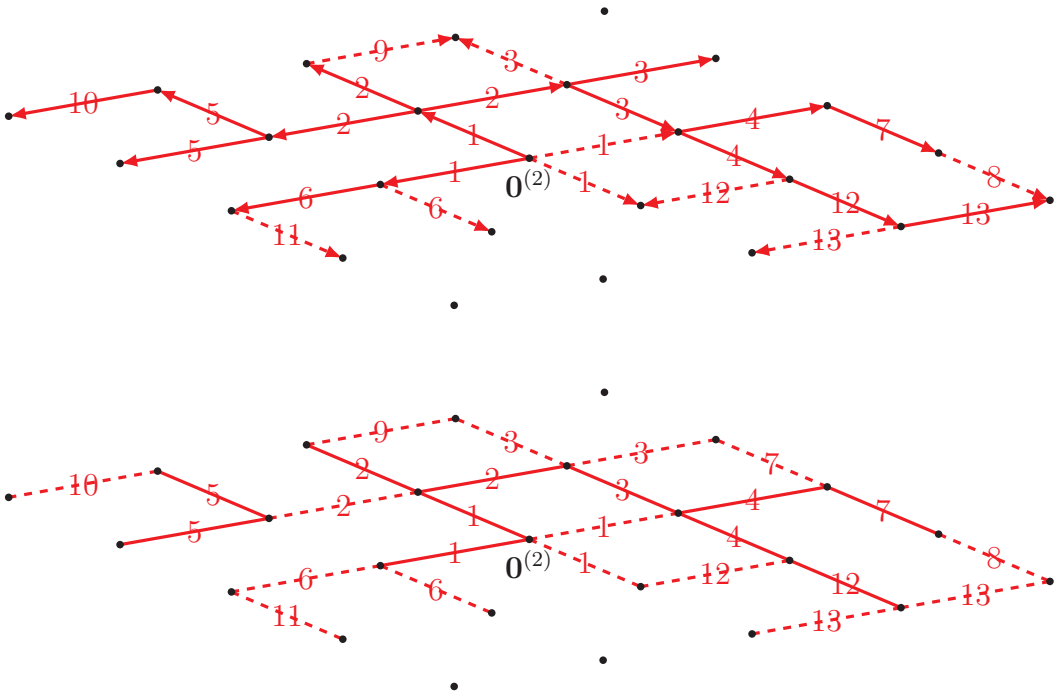

Figure 2.7: An illustration of the "step-wise" couplings forming a "global" coupling. The top figure illustrates $\mathbf{G}^{(r)}$, with solid lines representing edges in the cluster and dashed lines representing edges that are considered but are not in the cluster. The bottom figure illustrates edge designations during the coupling procedure, with solid lines representing edges designated to be open and dashed lines representing edges designated to be closed. The label on each edge shows the step at which the coupling is established: at step n of the coupling, each edge considered by $\mathbf{G}^{(r)}$ is designated to be open with probability p, while the open edges are a subset of the edges included in $\mathbf{G}^{(r)}$. To visualize, for each n, the set of solid edges with label n in the bottom figure is always a subset of the corresponding edges in the top figure, providing a "global" coupling that the set of open edges is a subset of edges included in $\mathbf{G}^{(r)}$.

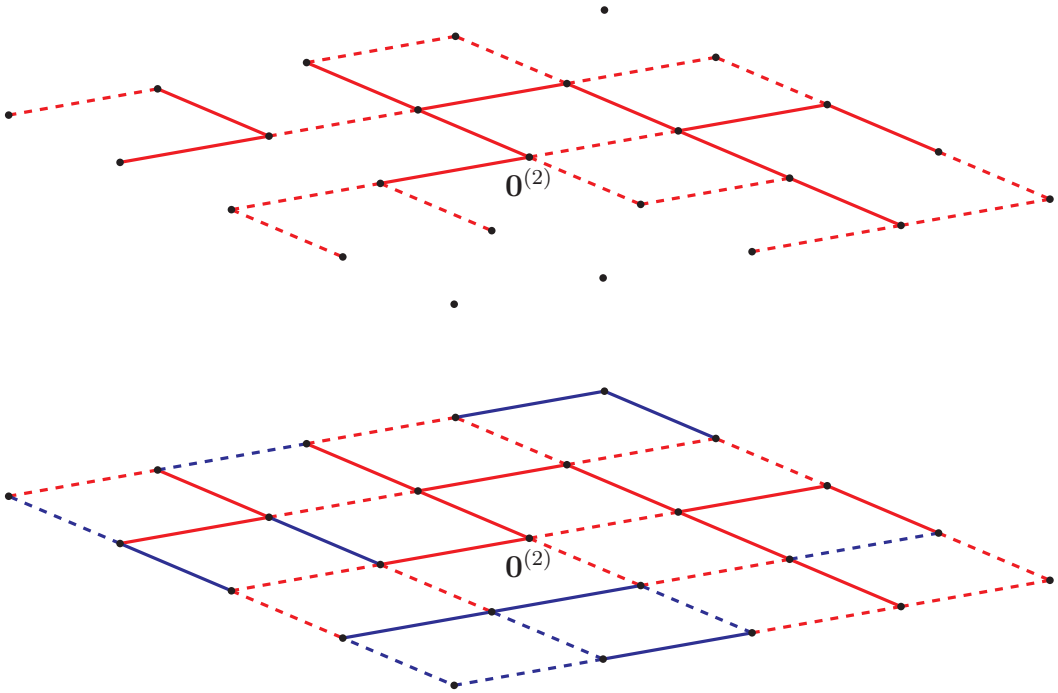

Figure 2.8: Using the coupling results to construct a configuration on $\mathbb{L}^2$. The top figure is an illustration of edge designation during the coupling procedure, which is consistent with Figure 2.7. In the bottom figure, red edges are edges that are designated to be open or closed during the coupling establishment. Blue edges are the rest of the edges in $\mathbb{E}^2$. Each blue edge is open independently with probability p (solid line), and closed otherwise (dashed line). Such coloring gives us a configuration on $\mathbb{L}^2$, which is denoted by $\omega^{(2)}$.

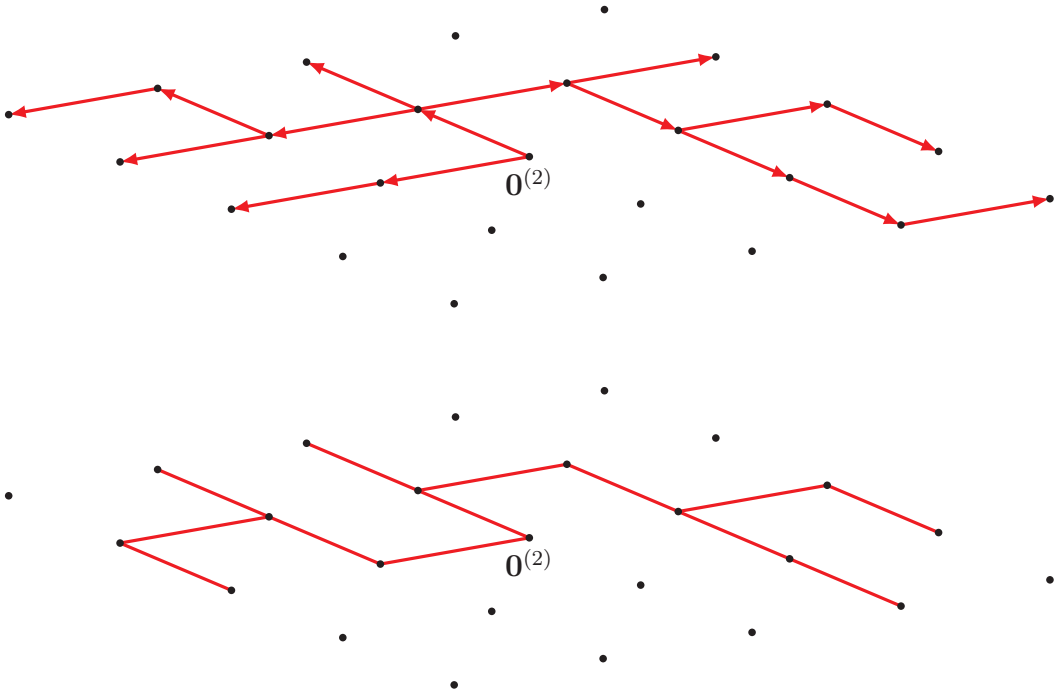

Figure 2.9: An illustration of the vertex cluster of $\mathbf{G}^{(r)}$ containing $D(\omega^{(2)})$. The top figure illustrates the replicated process $\mathbf{G}^{(r)}$, with the red arrows representing edges in the edge cluster of $\mathbf{G}^{(r)}$. The bottom figure illustrates the open cluster of $\omega^{(2)}$, which is the configuration on $\mathbb{L}^2$ in Figure 2.8. For each vertex in the open cluster (bottom figure), at least one edge included by $\mathbf{G}^{(r)}$ (top figure) has this vertex as a endpoint. Thus, if the open cluster contains infinitely many vertices, $\mathbf{G}^{(r)}$ contains infinitely many edges.

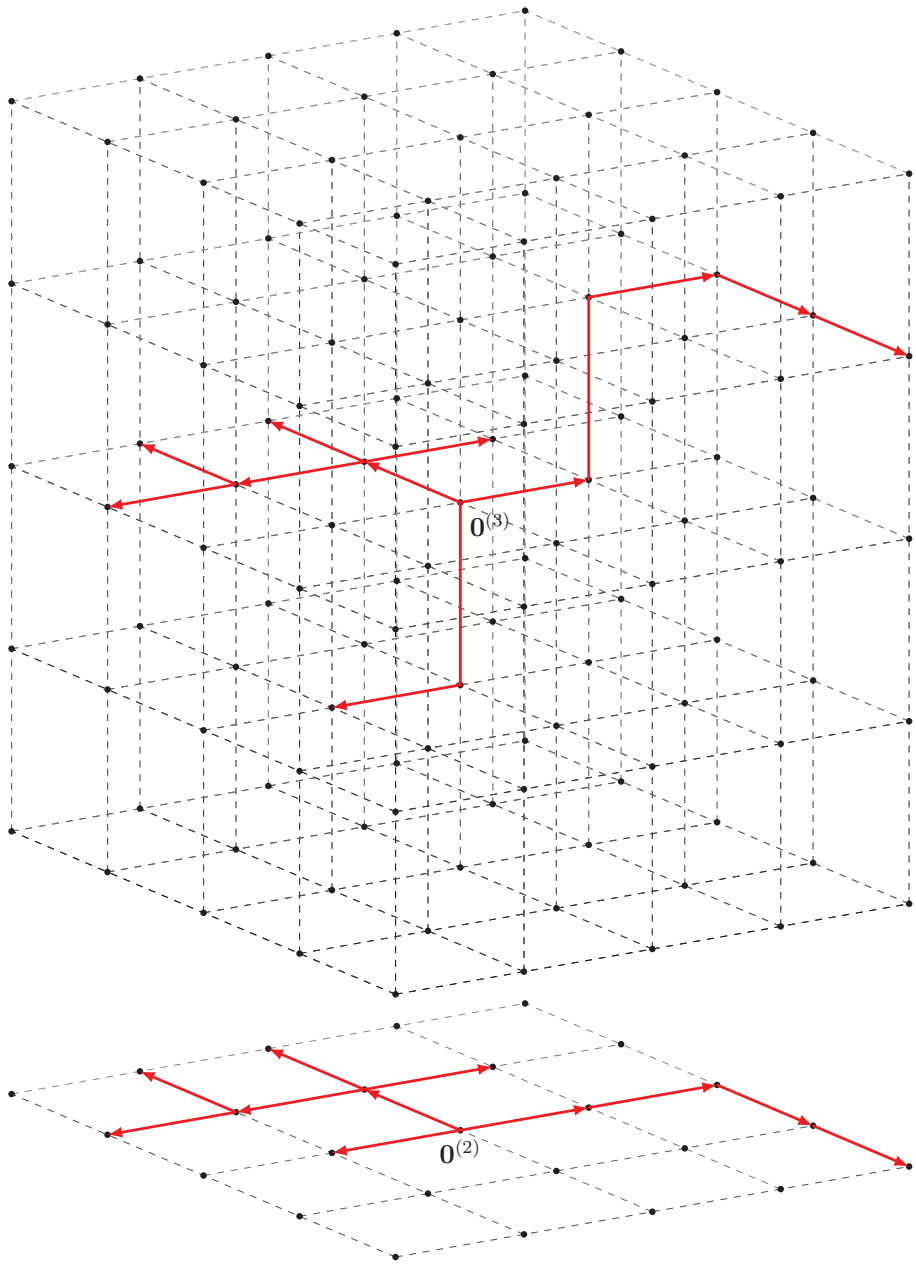

Figure 2.10: An illustration showing how edges included in $\mathbf{G}^{(2)}$ correspond to the edges included in $\mathbf{G}^{(3)}$. For each edge e in the edge cluster of $\mathbf{G}^{(2)}$ (bottom figure), it corresponds to one edge included in $\mathbf{G}^{(3)}$ (top figure) such that it is the projection of its corresponding edge onto $\mathbb{R}^2$. Consequently, if the number of edges included in $\mathbf{G}^{(2)}$ is infinite, so is the number of edges included in $\mathbf{G}^{(3)}$.

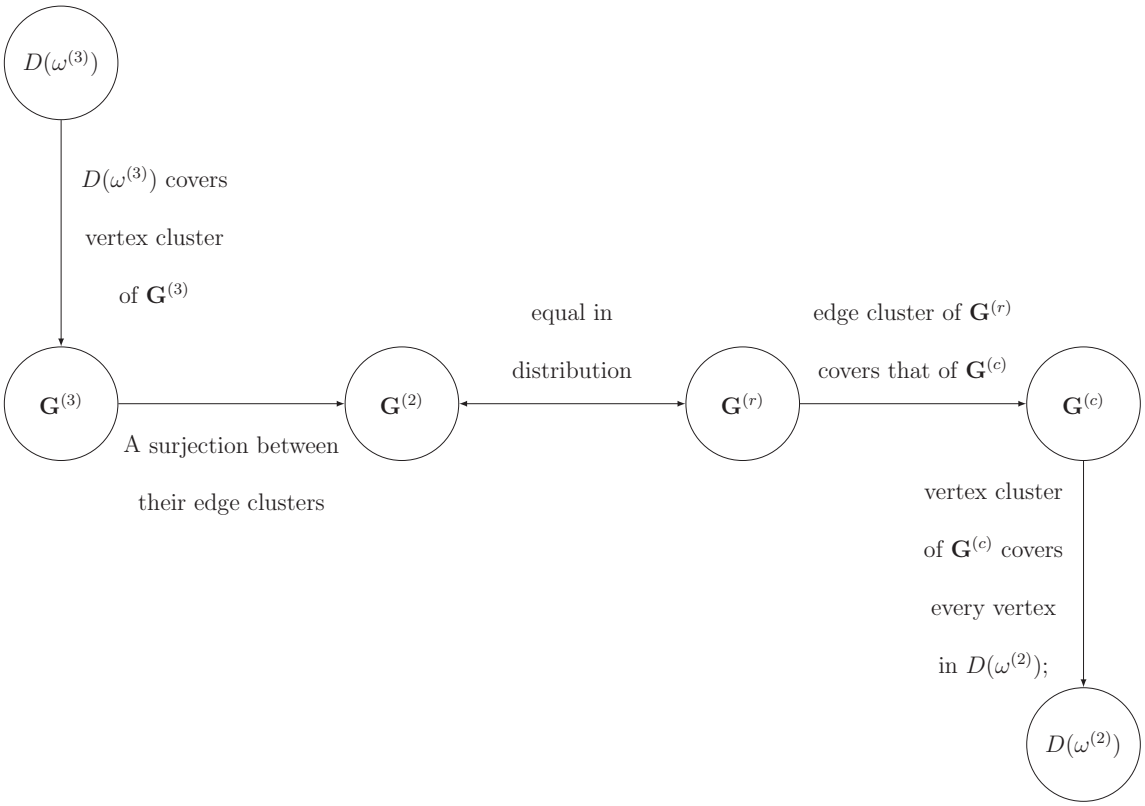

Figure 2.11: A summary of the proof logic of the growth process approach. Starting from the configuration $\omega^{(2)}$ on $\mathbb{L}^2$, if $|D(\omega^{(2)})| = \infty$, then $\mathbf{G}^{(c)}$ and $\mathbf{G}^{(r)}$ contains infinitely many edges by the coupling relation (See Figure 2.9). Thus, the probability of $\mathbf{G}^{(r)}$ containing infinitely many edges is no less than $\theta^{\mathbb{L}^2}(p)$. This further implies that $\mathbf{G}^{(2)}$, and furthermore $\mathbf{G}^{(3)}$, contain infinitely many edges with probability no less than $\theta^{\mathbb{L}^2}(p)$. Consequently, the pair (p, q) satisfying $\theta^{\mathbb{L}^2}(p) > 0$ and the stochastic dominance makes q an upper bound of $p_c(\mathbb{L}^3)$.

Chapter 3

Constructing the Growth Process $\mathbf{G}^{(3)}$

3.1 Preliminaries and Definitions

We introduce the following three definitions that correspond to a pre-specified graph $G = (V, E)$. Throughout Chapters 3–7, G refers to the square lattice or the cubic lattice. In Chapters 8 and 9, G refers to some other periodic graphs, including the stacked lattices, the body-centered cubic lattice, and the face-centered cubic lattice.

Definition 3.1.1 (Endpoint set)**.** For any collection of edges $F \subseteq E$, the *endpoint set* of F, denoted by $\bigcup_F := \{v \in V \mid \text{there exists } u \in V \text{ with } \{u, v\} \in F\}$, is the collection of all vertices in V that are endpoints of edges in F.

Definition 3.1.2 (Incident edge set)**.** For any collection of vertices $S \subset V$, the *incident edge set* of S, denoted by $I[S]$, is the set of edges in E incident to at least one vertex in S.

Definition 3.1.3 (Configuration)**.** A *configuration* on G is an outcome of the bond percolation model on G. Mathematically, a configuration is a point $\omega := \{\omega(e) \mid e \in E\}$ in $\{0,1\}^E$, where $\omega(e) = 1$ indicates that the underlying edge e is open and $\omega(e) = 0$ indicates that e is closed.

Definition 3.1.4 ((F,ω)-connected)**.** Let u and v be two vertices in V, let F be a subset of E, and let ω be a configuration on G. Define $u \overset{F,\omega}{\longleftrightarrow} v$ as the indicator that there exists a path that only consists of edges in F starting from u and ending with v, satisfying that the ω-value of each edge in the path is 1. Additionally, if the configuration ω has been pre-specified and is clear from context, we shall omit the ω by writing the indicator as $u \overset{F}{\longleftrightarrow} v$.

For simplicity, we no longer distinguish the hypercubic lattices $\mathbb{L}^d$ and their canonical embeddings, where $d \in \{2,3\}$. In other words, vectors in $\mathbb{R}^d$ with integer coordinates are defined polymorphically: for any $\boldsymbol{x} \in \mathbb{Z}^d$, it represents both the vertex of the d-dimensional hypercubic lattice that is associated with $\boldsymbol{x}$, and a d-dimensional vector in the Euclidean space. Similarly, $\mathbb{Z}^3$ represents both the set of vertices of $\mathbb{L}^3$ and the set of points in $\mathbb{R}^3$ having integer coordinates.

Definition 3.1.5 ($\boldsymbol{x}$-column)**.** For any $\boldsymbol{x} = (x_1, x_2) \in \mathbb{Z}^2$ and $z \in \mathbb{Z}$, let $\boldsymbol{x} \times z :=$

(x_1, x_2, z) be a point in $\mathbb{Z}^3$. The $\boldsymbol{x}$-*column* is $\boldsymbol{x} \times \mathbb{Z} := \{\boldsymbol{x} \times z \mid z \in \mathbb{Z}\}$.

Definition 3.1.6 (Projection)**.** For any $\boldsymbol{x} = (x_1, x_2, x_3) \in \mathbb{Z}^3$, the *projection* of $\boldsymbol{x}$ is $\mathrm{proj}(\boldsymbol{x}) := (x_1, x_2)$.

Definition 3.1.7 (Associated column)**.** For any $\boldsymbol{x} \in \mathbb{Z}^3$, we define its *associated column* as $\mathrm{col}(\boldsymbol{x}) := \mathrm{proj}(\boldsymbol{x}) \times \mathbb{Z}$. More generally, for any $A \subset \mathbb{Z}^3$, the *associated columns* are $\mathrm{col}(A) := \bigcup_{\boldsymbol{x} \in A} \mathrm{col}(\boldsymbol{x})$.

Definition 3.1.8 (Labeling function)**.** A *labeling function on* $\mathbb{Z}^2$ is a one-to-one function $l : \mathbb{Z}^2 \to \mathbb{N}$. For $v \in \mathbb{Z}^2$, the *label* of v is $l(v)$.

Definition 3.1.9 (Label of vertices)**.** Given a labeling function l on $\mathbb{Z}^2$, and any $v \in \mathbb{Z}^3$, the *label* of v is $l(v) := l(\mathrm{proj}(v))$.

Definition 3.1.10 (Column-neighbor)**.** The *column-neighbors* of a vertex $\boldsymbol{x} \in \mathbb{Z}^3$ is the set of vertices in $\mathbb{Z}^3$ defined by $\{\boldsymbol{y} = (y_1, y_2, y_3) \in \mathbb{Z}^3 \mid \|\mathrm{proj}(\boldsymbol{x}) - \mathrm{proj}(\boldsymbol{y})\|_2 = 1\}$.

Definition 3.1.11 (Probability space of cubic lattice bond model)**.** Let $\Omega^{(3)} := \{0,1\}^{\mathbb{E}^3}$ be the *configuration space* of $\mathbb{L}^3$ and $\mathcal{F}^{(3)}$ be the σ-field generated by the finite cylinder sets of $\Omega^{(3)}$. Let $P_q^{(3)}$ be the *probability measure* for the cubic lattice bond model defined by

$$P_q^{(3)} = \prod_{e \in \mathbb{E}^3} \mu_e^{(3)},$$

where for each $e \in \mathbb{E}^3, \omega^{(3)}(e) = \mathbb{1}_{\{\text{e is open}\}}$, and $\mu_e^{(3)}$ is Bernoulli distributed with parameter q.

Definition 3.1.12 (Probability space of square lattice bond model)**.** Let $\Omega^{(2)} := \{0,1\}^{\mathbb{E}^2}$ be the *configuration space* of $\mathbb{L}^2$ and $\mathcal{F}^{(2)}$ be the σ-field generated by the finite cylinder sets of $\Omega^{(2)}$. Let $P_p^{(2)}$ be the *probability measure* for the square lattice bond model defined by

$$P_p^{(2)} = \prod_{e \in \mathbb{E}^2} \mu_e^{(2)},$$

where for each $e \in \mathbb{E}^2, \omega^{(2)}(e) = \mathbb{1}_{\{\text{e is open}\}}$, and $\mu_e^{(2)}$ is Bernoulli distributed with parameter p.

Definition 3.1.13 (Nearest connected column-neighbor)**.** For an arbitrary vertex $\boldsymbol{x} \in \mathbb{Z}^3$, a collection of edges $B \subset \mathbb{E}^3$ and a configuration $\omega^{(3)} \in \Omega^{(3)}$, the *nearest connected column-neighbors* of $\boldsymbol{x}$, denoted by $N[\boldsymbol{x}, \omega^{(3)}, B]$, is a set of vertices each vertex $\boldsymbol{y}$ of which satisfies the following:

1. $\boldsymbol{y}$ is a column neighbor of $\boldsymbol{x}$,
2. $\boldsymbol{y} \xleftrightarrow{B,\omega^{(3)}} \boldsymbol{x}$,
3. for each $\boldsymbol{z} \in \mathbb{Z}^3$, satisfying
   (a) $\text{proj}(\boldsymbol{z}) = \text{proj}(\boldsymbol{y})$, and
   (b) $\boldsymbol{z} \xleftrightarrow{B,\omega^{(3)}} \boldsymbol{x}$,

   either $|y_3 - x_3| < |z_3 - x_3|$ or both $|y_3 - x_3| = |z_3 - x_3|$ and $(y_3 - x_3) > 0$. Additionally, if the configuration $\omega^{(3)}$ has been pre-specified and is clear from

context, we simply omit $\omega^{(3)}$ and refer the nearest connected column-neighbors of $\boldsymbol{x}$ as $N[\boldsymbol{x}, B]$.

Intuitively, the nearest connected column-neighbors of a vertex $\boldsymbol{x}$ are column-neighbors of $\boldsymbol{x}$ that are connected to $\boldsymbol{x}$ using open edges in B. They are the "nearest" in the sense that for each of these vertices, there are no vertices in the associated column that are connected to $\boldsymbol{x}$ but closer to $\boldsymbol{x}$ in terms of Euclidean distance. In case of ties (i.e., two connected column-neighbors sharing the same distance to $\boldsymbol{x}$) we choose the vertex that lies "above" $\boldsymbol{x}$. At each step of our growth process, we "explore" from a certain vertex already in the cluster by identifying its nearest connected column-neighbors and adding them to the cluster to form a larger one. Notice that a vertex in $\mathbb{Z}^{(3)}$ can have at most 4 nearest connected column-neighbors: one in each of the four adjacent columns. Consequently, at each step, we add at most four vertices to the cluster, which makes it computationally feasible to analyze the growth of the process.

Definition 3.1.14 (Open connection path)**.** Let $T \subset \mathbb{E}^3$ be a collection of connected edges that contains no cycles, and $u, v \in \mathbb{Z}^3$ be two vertices of $\mathbb{L}^3$. Then there exists a unique path from u to v using only edges in T. Denote the set of edges in such path by $\text{path}(u, v, T)$.

Later, we shall take T to be a subset of the incident edge set of the associated column of the vertex from which we explore. Thus, T contains no cycles. We are

particularly interested in paths connecting the vertex to its nearest connected column-neighbors, since these paths are contained in some open paths that connect $\mathbf{0}^{(3)}$ to the nearest connected column-neighbors.

3.2 The Growth Process Associated with $\omega^{(3)}$

For a fixed configuration $\omega^{(3)}$ on the cubic lattice, its open cluster containing the origin $\mathbf{0}^{(3)}$, denoted by $D(\omega^{(3)})$, is a "static" collection of vertices. On the other hand, we may consider $D(\omega^{(3)})$ to be obtained from a dynamic process. Initially, we have a *vertex cluster* containing only the origin $\mathbf{0}^{(3)}$ and an *edge cluster* being the empty set. At step n, we explore from a certain vertex $v_n^{(3)}$ that is in the vertex cluster obtained at step $n-1$. We let $A_n^{(3)} := \{v_1^{(3)}, ..., v_n^{(3)}\}$ be the *antecedent vertices* at step n, indicating that we have explored from all the vertices in $A_n^{(3)}$ by the end of step n. Naturally, the choice of $v_n^{(3)}$ should satisfy the condition that $v_n^{(3)} \notin A_{n-1}^{(3)}$ to avoid duplicate exploration from the same vertex. Afterwards, we identify the nearest connected column-neighbors of $v_n^{(3)}$ by looking at the underlying configuration $\omega^{(3)}$ restricted to a specific region called the *exploration region*. We denote the exploration region by $B_n^{(3)}$. We then add $v_n^{(3)}$'s nearest connected column-neighbors (if any) to the vertex cluster to form a larger cluster of vertices. Meanwhile, we add the edges in $B_n^{(3)}$ which connect $v_n^{(3)}$ to its nearest connected column-neighbors to the edge cluster to

form a larger cluster of edges. Consequently, during this dynamic process, we obtain a non-decreasing sequence of vertex clusters, and a non-decreasing sequence of edge clusters. We denote them by $D_n^{(3)}$ and $C_n^{(3)}$, respectively.

A more formal description and notation are given in the following definition, where we define such a growth process recursively.

Definition 3.2.1 (3D growth process)**.** Let $(\Omega^{(3)}, \mathcal{F}^{(3)}, P_q^{(3)})$ be the probability space of the homogeneous bond percolation model of $\mathbb{L}^3$ with parameter q, and let l be a labeling function on $\mathbb{Z}^2$. We initialize $(A_0^{(3)}, D_0^{(3)}, C_0^{(3)})$ as follows:

$$A_0^{(3)} := \emptyset,$$

$$D_0^{(3)} := \{\mathbf{0}^{(3)}\},$$

$$C_0^{(3)} := \emptyset.$$

Based on the initialization, define a stochastic process $(v_n^{(3)}, A_n^{(3)}, B_n^{(3)}, C_n^{(3)}, D_n^{(3)}) : \Omega^{(3)} \to \mathbb{Z}^3 \times 2^{\mathbb{Z}^3} \times 2^{\mathbb{E}^3} \times 2^{\mathbb{E}^3} \times 2^{\mathbb{Z}^3}$ on $(\Omega^{(3)}, \mathcal{F}^{(3)}, P_q^{(3)})$ for $n \geqslant 1$ recursively as follows. For each $\omega^{(3)} \in \Omega^{(3)}$, assume that this stochastic process has been defined up to step

n. At step $n+1$, if $D_n^{(3)} \setminus A_n^{(3)} \neq \emptyset$, we define

$$\begin{aligned}
v_{n+1}^{(3)} &:= \arg\min\{l(v) : v \in D_n^{(3)} \setminus A_n^{(3)}\},\\
A_{n+1}^{(3)} &:= A_n^{(3)} \cup \{v_{n+1}^{(3)}\},\\
B_{n+1}^{(3)} &:= I[\mathrm{col}(v_{n+1}^{(3)})] \setminus I[\mathrm{col}(D_n^{(3)} \setminus \{v_{n+1}^{(3)}\})],\\
D_{n+1}^{(3)} &:= D_n^{(3)} \cup N[v_{n+1}^{(3)}, B_{n+1}^{(3)}, \omega^{(3)}],\\
C_{n+1}^{(3)} &:= C_n^{(3)} \cup \left(\bigcup_{v \in N[v_{n+1}^{(3)}, B_{n+1}^{(3)}]} \mathrm{path}(v_{n+1}^{(3)}, v, B_{n+1}^{(3)}) \right).
\end{aligned}$$

Otherwise, we define

$$\begin{aligned}
v_{n+1}^{(3)} &:= v_n^{(3)},\\
A_{n+1}^{(3)} &:= A_n^{(3)},\\
B_{n+1}^{(3)} &:= \emptyset,\\
D_{n+1}^{(3)} &:= D_n^{(3)},\\
C_{n+1}^{(3)} &:= C_n^{(3)},
\end{aligned}$$

The *growth process associated with* $\omega^{(3)}$ is the stochastic process $\mathbf{G}_n^{(3)} := (A_n^{(3)}, C_n^{(3)})$ defined on the probability space $(\Omega^{(3)}, \mathcal{F}^{(3)}, P_q^{(3)})$.

In the remaining part of this section, we describe how the growth process associated with $\omega^{(3)}$ defined above corresponds to the intuition that it illustrates how $D(\omega^{(3)})$ expands from $\mathbf{0}^{(3)}$ dynamically. We also explain what each notation in Definition 3.2.1 represents and the reasons why it is defined in such a way.

Process Notations

By convention, we let n indicate the index of the growth process. For each $n \in \mathbb{N}$, the process $\mathbf{G}_n^{(3)}$ maps the configuration $\omega^{(3)}$ to a subset of $\mathbb{Z}^3 \times \mathbb{E}^3$. More specifically, in $\mathbf{G}_n^{(3)} = (A_n^{(3)}, C_n^{(3)})$, the antecedent vertices $A_n^{(3)} \subseteq \mathbb{Z}^3$ record all the vertices from which $\mathbf{G}^{(3)}$ has explored through step n (inclusive); and $C_n^{(3)} \subset \mathbb{E}^3$ keeps track of the edges included in the edge cluster until step n. The growth process $\mathbf{G}^{(3)}$ does not contain $v_n^{(3)}$, $B_n^{(3)}$ and $D_n^{(3)}$. These three notations are introduced only for convenience of description. In fact, the growth process is well defined in the sense that we can still obtain $(A^{(3)}, C^{(3)})$ recursively without using $v^{(3)}, B^{(3)}$ and $D^{(3)}$. To see this, we notice that $v_n^{(3)}$, the vertex from which $\mathbf{G}^{(3)}$ explores at step n, satisfies $\{v_n^{(3)}\} = A_n^{(3)} \setminus A_{n-1}^{(3)}$. Meanwhile, $D_n^{(3)}$, the vertex cluster at step n, satisfies $D_n^{(3)} = \bigcup_{C_n^{(3)}} \setminus \mathrm{col}(A_n^{(3)}) \cup A_n^{(3)}$. Finally, the exploration region, $B_n^{(3)} = I[\mathrm{col}(v_{n+1}^{(3)})] \setminus I[\mathrm{col}(D_n^{(3)} \setminus \{v_{n+1}^{(3)}\})]$, is defined in terms of $v^{(3)}$ and $D^{(3)}$, both of which are determined by $A^{(3)}$ and $C^{(3)}$.

In the definition of $\mathbf{G}^{(3)}$, both $C^{(3)}$ and $D^{(3)}$ describe the growth of $D(\omega^{(3)})$, in terms of edges and vertices, respectively. Since we focus on whether $D(\omega^{(3)})$ is an infinite cluster or not, readers may consider it redundant to define $C^{(3)}$, in the sense that the cluster containing infinitely many edges indicates that the cluster contains infinitely many vertices, and vice versa. There are two reasons why we introduce $C^{(3)}$, and describe the growth of the cluster in terms of $C^{(3)}$, instead of $D^{(3)}$. First, it

simplifies our description of projecting $\mathbf{G}^{(3)}$ onto $\mathbb{L}^2$ to form $\mathbf{G}^{(2)}$. Second, it simplifies the argument that establishes the "step-wise" coupling relation later.

Nearest Connected Column-Neighbors

The process $\mathbf{G}^{(3)}$ grows in a carefully designed manner. More specifically, assuming that we are at step n of $\mathbf{G}^{(3)}$, we make the following three choices.

1. Instead of the neighbors of $v_n^{(3)}$, it is the column-neighbors that are considered.

2. Among all the column-neighbors of $v_n^{(3)}$ that are connected to $v_n^{(3)}$, only those connected to $v_n^{(3)}$ by paths in the exploration region $B_n^{(3)}$ can possibly be added to $D_n^{(3)}$.

3. Among all the column-neighbors that are connected to $v_n^{(3)}$ by paths in $B_n^{(3)}$, only the nearest connected column-neighbors are added to $D_n^{(3)}$.

We now provide detailed explanation of the above choices.

1. Firstly, we discuss the choice of column-neighbors. Intuitively, when describing the growth of $\{C_n^{(3)}(\omega^{(3)})\}$, it is natural that we explore from a vertex $v_n^{(3)}$ and add a subset of its neighbors, i.e., vertices in $\mathbb{Z}^3$ that are adjacent to $v_n^{(3)}$. However, our growth process differs from this straightforward idea in the sense that we are considering the column-neighbors of $v_n^{(3)}$, instead of its neighbors. The purpose of the definition is to help define $\mathbf{G}^{(2)}$ in terms of the projection of $\mathbf{G}^{(3)}$. The projected process $\mathbf{G}^{(2)}$ is intuitive: it explores from a vertex in $\mathbb{L}^2$

and adds a subset of the vertex's neighbors into the cluster at each step (Figure 3.13). Recall that it is the survival of $\mathbf{G}^{(2)}$, rather than $\mathbf{G}^{(3)}$, that we want to analyze. Thus, our $\mathbf{G}^{(3)}$ is defined in a non-straightforward way to ensure its projection $\mathbf{G}^{(2)}$ is defined in a straightforward way.

2. We now discuss the choice of exploration regions. Let v be a column neighbor of vertex $v_n^{(3)}$. An intuitive idea is that v is contained in $D_n^{(3)}$ if and only if v is connected to $v_n^{(3)}$ by an open path, i.e., $v \overset{\mathbb{E}^3}{\longleftrightarrow} v_n^{(3)}$. However, this makes it difficult to analyze the probability of such an event unless the connected path is restricted to a "local" region. That is, we consider the exploration region $B_n^{(3)}$ (Figure 3.4, 3.6, 3.8 and 3.10), and v is included in $D_n^{(3)}$ only if v is connected to $v_n^{(3)}$ by an open path in $B_n^{(3)}$, i.e., $v \overset{B_n^{(3)}}{\longleftrightarrow} v_n^{(3)}$.

Recall that $B_n^{(3)}$ is defined to be a subset of the incident edge set of $\mathrm{col}(v_n^{(3)})$, where the geometry of the incident edge set is illustrated in Figure 3.4. The geometries of the exploration regions $\{B_n^{(3)}\}_{n=1}^{\infty}$, if non-empty, are similar: Each of them contains a vertical path in the associated column of $v_n^{(3)}$, and horizontal edges pointing to at most four directions in each layer (Figure 3.4, 3.6, 3.8, 3.10). Such geometry makes it possible for us to analyze the joint distribution of adding edges of $\mathbb{E}^2$ at each step of $\mathbf{G}^{(2)}$. This joint distribution describes how fast $\mathbf{G}^{(2)}$ grows, from which we can study the survival of $\mathbf{G}^{(2)}$. Meanwhile, for $n \geqslant 2$, there is at least one vertex that is a column-neighbor of $v_n^{(3)}$, but

has already been included in $D^{(3)}_{n-1}$. For such vertices, their associated columns are not considered at step $n+1$. This is because we want $\mathbf{G}^{(3)}$ to consider the configuration restricted to distinct sets of edges at different steps. In other words, we want the sequence $\{B^{(3)}_n\}$ to be pairwise disjoint. One big advantage of doing so is to make the process $\mathbf{G}^{(3)}$ and its projection $\mathbf{G}^{(2)}$ Markovian. A detailed proof is provided in the following chapter. With the Markov property, we analyze the transition probabilities and reduce them to a finite number of cases. Thus, in Definition 3.2.1, $B^{(3)}_n$ is defined as a subset of $I[\mathrm{col}(v^{(3)}_n)]$ that contains no edges incident to vertices in $\mathrm{col}(D^{(3)}_n \setminus \{v^{(3)}_{n+1}\})$.

3. Finally, we discuss the choice of nearest connected column-neighbors. When exploring from $v^{(3)}_n$, there can possibly be infinitely many column-neighbors of $v^{(3)}_n$ that are connected to $v^{(3)}_n$ by paths in $B^{(3)}_n$. For simplicity, we select a subset of them such that for the selected column-neighbors, their projections differ from each other. For instance, when $n = 1$, there are at most four vertices in $D^{(3)}_1$. Meanwhile, in terms of projection, having multiple vertices in the same column added to $D^{(3)}_n$ would result in the same projected process as having just one vertex in that column. Additionally, the definition of the nearest connected column-neighbors makes the vertices in $D^{(3)}$ have distinct projections so that vertices in $D^{(3)}_n \setminus A^{(3)}_n$ have distinct labels, which justifies the choice of $v^{(3)}_{n+1}$ (if it exists) as unique (Lemma 3.2.2).

Labeling Function

Recall that the process $\mathbf{G}^{(3)}$ is defined for each configuration $\omega^{(3)}$ on $\mathbb{L}^3$ and a fixed labeling function l. The process value depends on the configuration $\omega^{(3)}$. Meanwhile, for a fixed configuration, there might be a different process for each labeling function l. Thus, in the remaining part of the dissertation, we assume that l is fixed, and is specified as illustrated in Figure 3.1. From Definition 3.1.9, the label of each vertex in $\mathbb{L}^3$ is consistent with the label of its projection, as illustrated in Figure 3.2.

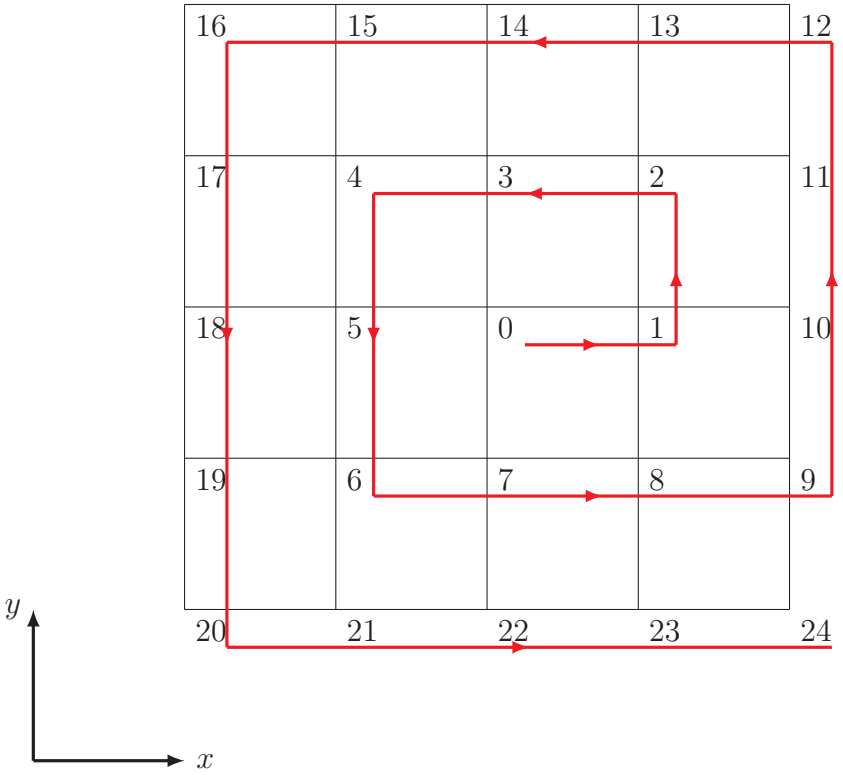

Figure 3.1: An illustration of a labeling function l on a subset of vertices in $\mathbb{L}^2$. The labels of the vertices are the integers, increasing in the direction shown by the red arrows.

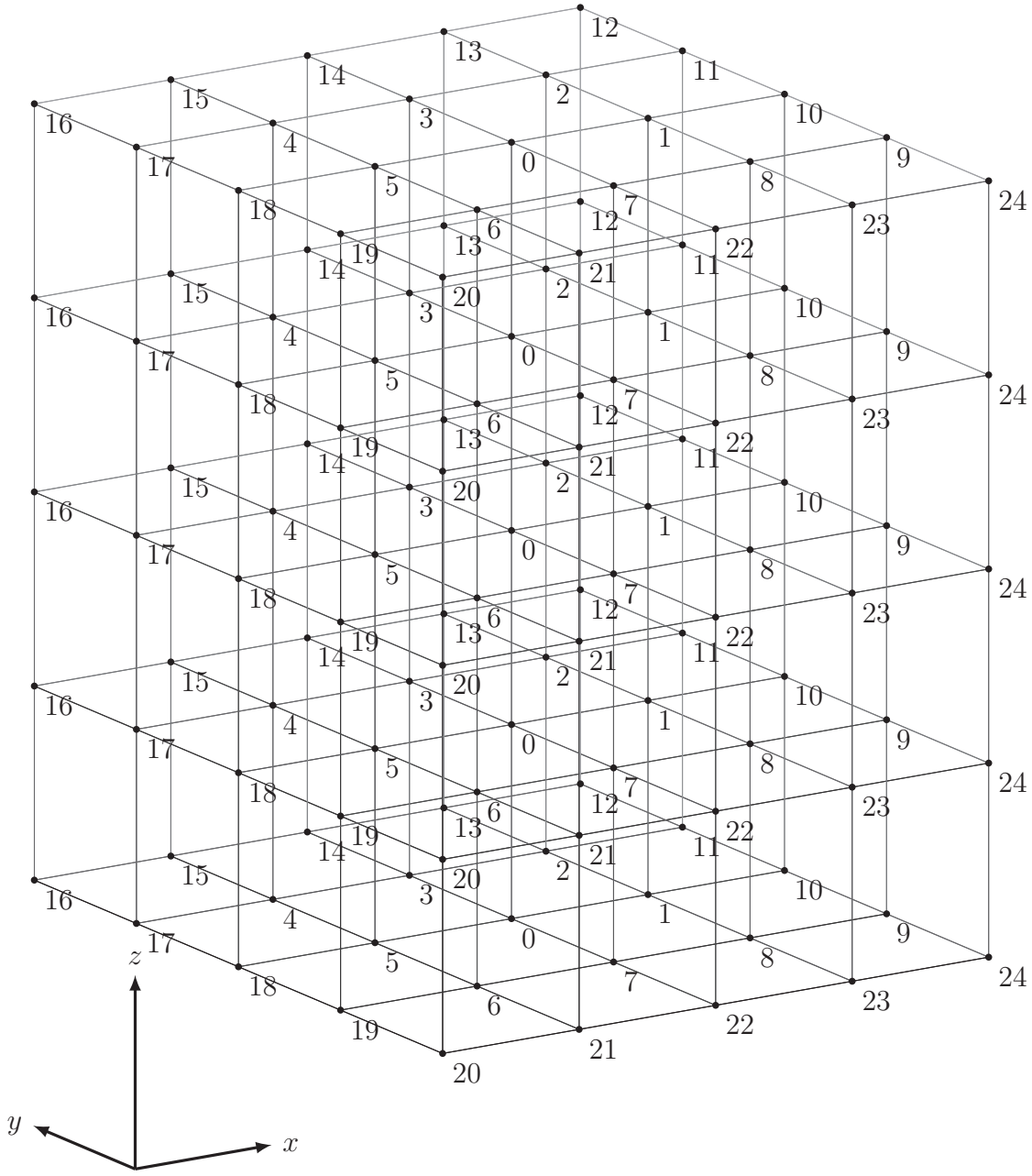

Figure 3.2: A labeling of vertices in $\mathbb{L}^3$. Recall that the $\mathbb{L}^2$ labeling is one-to-one, but now it is extended to 3 dimensions and is not one-to-one. All vertices in the same column are assigned the same label.

Unique Choice of Exploration Vertex

Before we finish the construction of $\mathbf{G}^{(3)}$, we justify $v_{n+1}^{(3)}$ as unique. Recall that $v_{n+1}^{(3)}$ is chosen as the vertex in $D_n^{(3)} \setminus A_n^{(3)}$ that has the smallest label. Thus, it is sufficient to show that every vertex in $D_n^{(3)} \setminus A_n^{(3)}$ has a different label, which is rephrased in the following lemma.

Lemma 3.2.2. *For any $n \in \mathbb{N}$, if there exists $\boldsymbol{x}, \boldsymbol{y} \in D_n^{(3)} \setminus A_n^{(3)}$ such that $\boldsymbol{x} \neq \boldsymbol{y}$, then $l(\boldsymbol{x}) \neq l(\boldsymbol{y})$.*

Proof. We prove this by induction on n with the induction hypothesis that for each $\boldsymbol{x}, \boldsymbol{y} \in D_n^{(3)} \setminus A_n^{(3)}$ with $\boldsymbol{x} \neq \boldsymbol{y}$, then $\text{proj}(\boldsymbol{x}) \neq \text{proj}(\boldsymbol{y})$.

For $n = 0$, we have $D_0^{(3)} \setminus A_0^{(3)} = \{\mathbf{0}^{(3)}\}$. The induction hypothesis holds trivially.

Suppose that the induction hypothesis is correct up to n. At $n+1$, for all $\boldsymbol{x}, \boldsymbol{y} \in D_{n+1}^{(3)} \setminus A_{n+1}^{(3)}$ such that $\boldsymbol{x} \neq \boldsymbol{y}$, we consider the following three cases:

1. $\boldsymbol{x}, \boldsymbol{y} \in D_{n+1}^{(3)} \setminus D_n^{(3)}$,
2. $\boldsymbol{x} \in D_{n+1}^{(3)} \setminus D_n^{(3)}$, and $\boldsymbol{y} \in D_n^{(3)}$,
3. $\boldsymbol{x}, \boldsymbol{y} \in D_n^{(3)}$.

In case 1, $\boldsymbol{x}, \boldsymbol{y} \in D_{n+1}^{(3)} \setminus D_n^{(3)}$: they both are nearest connected column-neighbors

of $v_{n+1}^{(3)}$. Consequently, $\text{proj}(\boldsymbol{x}) \neq \text{proj}(\boldsymbol{y})$ by Definition 3.1.13.

In case 2, we notice that $\boldsymbol{x} \in D_{n+1}^{(3)} \setminus D_n^{(3)} \subset \bigcup_{B_{n+1}^{(3)}}$ and $\boldsymbol{y} \in D_n^{(3)} \subset \text{col}(D_n^{(3)})$. Since $B_{n+1}^{(3)} = I[\text{col}(v_{n+1}^{(3)})] \setminus I[\text{col}(D_n^{(3)} \setminus \{v_{n+1}^{(3)}\})]$, its endpoint set contains no vertices in $\text{col}(D_n^{(3)} \setminus \{v_{n+1}^{(3)}\})$. Notice that $\boldsymbol{x}$ is a nearest connected column-neighbor of $v_{n+1}^{(3)}$, which implies $\boldsymbol{x} \notin \text{col}(v_{n+1}^{(3)})$. Consequently, $\boldsymbol{x} \notin \text{col}(D_n^{(3)})$ while $\boldsymbol{y} \in \text{col}(D_n^{(3)})$. These together imply that $\text{proj}(\boldsymbol{x}) \neq \text{proj}(\boldsymbol{y})$.

In case 3, we have $\boldsymbol{x}, \boldsymbol{y} \in D_n^{(3)}$ and $\boldsymbol{x}, \boldsymbol{y} \notin A_{n+1}^{(3)}$. Thus, $\boldsymbol{x}, \boldsymbol{y} \in D_n^{(3)} \setminus A_n^{(3)}$, which implies that $\text{proj}(\boldsymbol{x}) \neq \text{proj}(\boldsymbol{y})$ by induction hypothesis. □

3.3 An example of $\mathbf{G}^{(3)}$

In Chapter 2, we generated a configuration on $\mathbb{L}^3$ to illustrate the intuitive idea of our proof. In this section, we use the same configuration (Figure 3.3) to help readers understand how $\mathbf{G}^{(3)}$ is defined step by step. To avoid confusion in generating the corresponding growth process $\mathbf{G}^{(3)}$, we assume that edges outside these $4 \times 4 \times 4$ cubic units are all closed.

Given this configuration on $\mathbb{L}^3$ and the labeling function l (Figure 3.1), the corresponding $\mathbf{G}^{(3)}$ is constructed as follows.

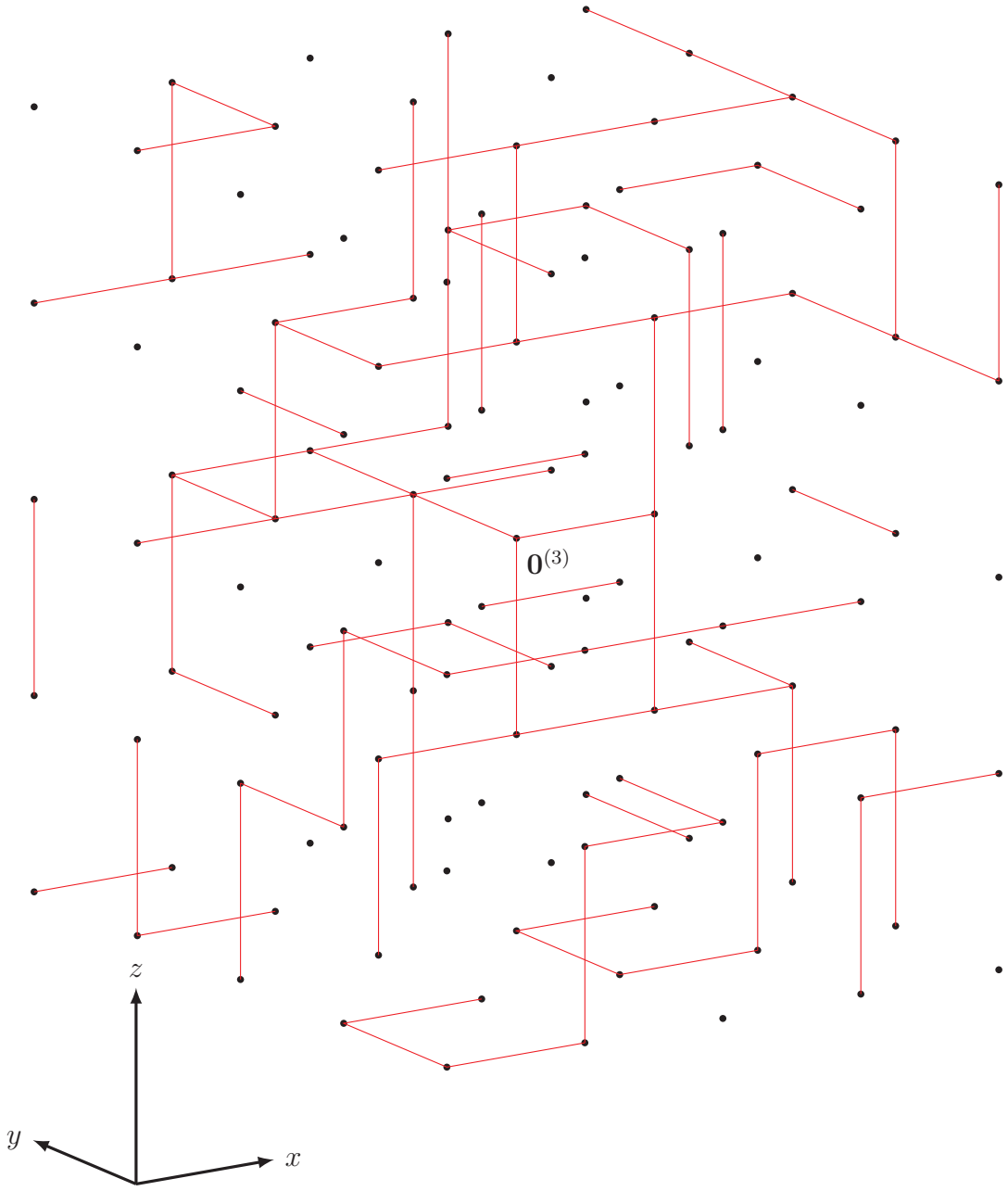

Figure 3.3: A configuration on $\mathbb{L}^3$ restricted to $[-2, 2]^3$, generated by setting $q = 0.3$. The red line segments illustrate the open edges.

At step 1, we explore from vertex $v_1^{(3)} = \mathbf{0}^{(3)}$. Let $B_1^{(3)}$ be the incident edge set of $\text{col}(v_1^{(3)})$. We notice that among the column-neighbors of $v_1^{(3)}$, vertices d_1, d_2, and d_3 are all connected to $\mathbf{0}^{(3)}$ by an open path in $B_1^{(3)}$ (Figure 3.4). Meanwhile, d_2' is also connected to $\mathbf{0}^{(3)}$ by open paths in $B_1^{(3)}$, but its third coordinate has an absolute value larger than d_2's, which means that d_2' is not the nearest connected column neighbor of $v_1^{(3)}$. Thus, we have $D_1^{(3)} = \{\mathbf{0}^{(3)}, d_1, d_2, d_3\}$ and $C_1^{(3)}$ contains open edges in $B_1^{(3)}$ that connect $\mathbf{0}^{(3)}$ to d_1, d_2 and d_3 (Figure 3.5). Finally, we set $A_1^{(3)} = \{v_1^{(3)}\} = \{\mathbf{0}^{(3)}\}$.

At step 2, we have $D_1^{(3)} \setminus A_1^{(3)} = \{d_1, d_2, d_3\}$. Pick $v_2^{(3)} = d_2$ since its label is the smallest (Figure 3.2). Meanwhile, set $B_2^{(3)}$ as edges in the incident edge set of $\text{col}(v_2^{(3)})$, except for those incident with vertices in $\text{col}(v_1^{(3)})$. By excluding edges incident with vertices in $\text{col}(v_1^{(3)})$, we have $B_1^{(3)} \cap B_2^{(3)} = \emptyset$ (Figure 3.6). We notice that for the column-neighbors of d_2, only d_4 and d_4' are connected to d_2 by open paths in $B_2^{(3)}$. We also notice that the distance between d_2 and d_4 equals the distance between d_2 and d_4', and d_4 lies "above" d_2. Thus, d_4 is added to $D_2^{(3)}$ to obtain $D_2^{(3)} = \{\mathbf{0}^{(3)}, d_1, d_2, d_3, d_4\}$ while d_4' is not. We then update $C_2^{(3)}$ by adding edges in $B_2^{(3)}$ that connect d_2 to d_4, as shown in Figure 3.7. Finally, we take the union of $A_1^{(3)}$ and $\{v_2^{(3)}\} = \{d_2\}$ to form $A_2^{(3)} = \{\mathbf{0}^{(3)}, d_2\}$.

At step 3, we explore from one of the vertices in $D_2^{(3)} \setminus A_2^{(3)} = \{d_1, d_3, d_4\}$ (Figure

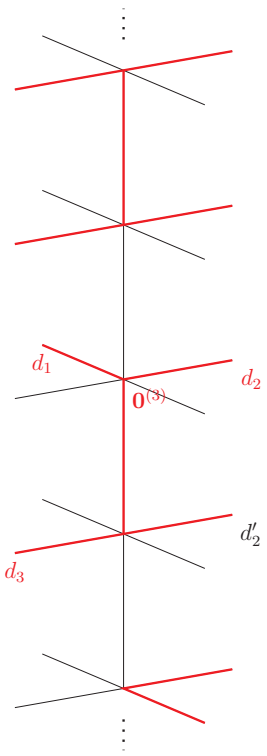

Figure 3.4: An illustration of the configuration restricted to the exploration region $B_1^{(3)}$, where the red line segments illustrate open edges in the given configuration.

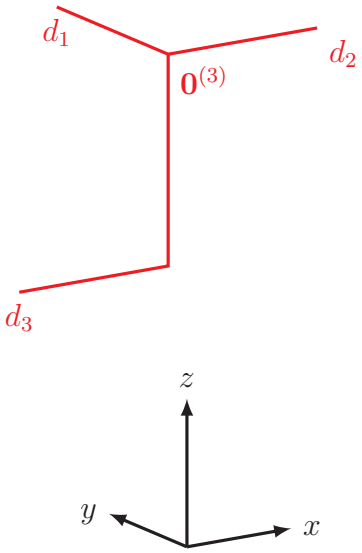

Figure 3.5: An illustration of edges included in $C_1^{(3)}$ (colored in red), and column neighbors that are added to $D_1^{(3)}$, which are d_1, d_2 and d_3.

3.8). Among them, d_1 has the smallest label. Thus, we explore from $v_3^{(3)} = d_1$ at this step. We let $B_3^{(3)}$ contain edges in the incident edge set of $\mathrm{col}(v_3^{(3)})$ that are not in the incident edge set of $\mathrm{col}(D_2^{(3)} \setminus \{v_3^{(3)}\}) = \mathrm{col}(\{\mathbf{0}^{(3)}, d_2, d_3, d_4\})$. Edges in $B_3^{(3)}$ are illustrated in Figure 3.8 using darker colors while edges in $B_1^{(3)}$ and $B_2^{(3)}$ are colored in lighter colors. Notice that d_5, d_6 and d_7 are the nearest connected

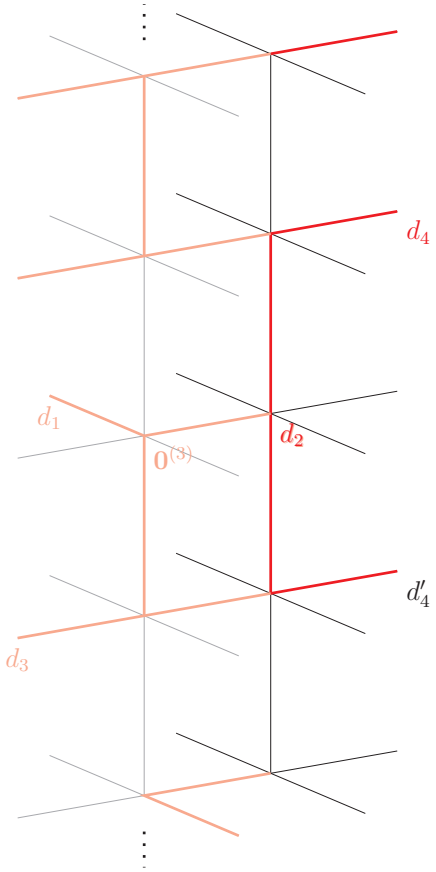

Figure 3.6: An illustration of the configuration restricted to $B_2^{(3)}$. Edges in $B_2^{(3)}$ are highlighted in darker colors, and open edges are colored in red.

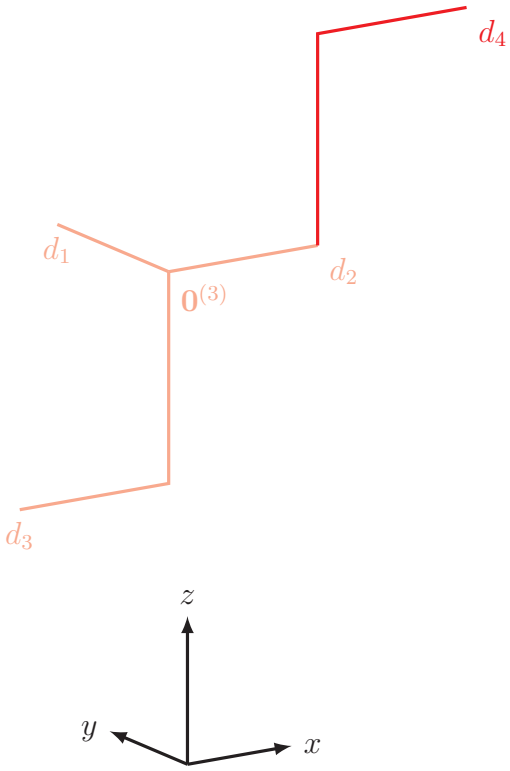

Figure 3.7: An illustration of edges included in $C_2^{(3)}$, where edges in $C_2^{(3)} \setminus C_1^{(3)}$ are highlighted in darker colors.

column-neighbors of $v_3^{(3)}$. Thus, we obtain $D_3^{(3)}$ by adding d_5, d_6 and d_7 to $D_2^{(3)}$ to get $D_3^{(3)} = \{\mathbf{0}^{(3)}, d_1, d_2, d_3, d_4, d_5, d_6, d_7\}$ and obtain $C_3^{(3)}$ by adding $(v_3^{(3)}, d_5), (v_3^{(3)}, d_6)$ and $(v_3^{(3)}, d_7)$ to $C_2^{(3)}$ (Figure 3.9). Finally, we let $A_3^{(3)} = A_2^{(3)} \cup \{v_3^{(3)}\} = \{\mathbf{0}^{(3)}, d_1, d_2\}$.

At step 4, $\mathbf{G}^{(3)}$ explores from vertex $v_4^{(3)} = d_7$. The corresponding exploration region $B_4^{(3)}$ is shown in Figure 3.10. Since no open edges in $B_4^{(3)}$ connect $v_4^{(3)}$ to any of its column-neighbors, we have $D_4^{(3)} = D_3^{(3)}$ and $C_4^{(3)} = C_3^{(3)}$ (Figure 3.11). Lastly, we set $A_4^{(3)} = A_3^{(3)} \cup \{v_4^{(3)}\} = \{\mathbf{0}^{(3)}, d_1, d_2, d_7\}$.

The process continues until $D_n^{(3)} = A_n^{(3)}$ for some $n \in \mathbb{N}$.

3.4 The Projected Growth Process $\mathbf{G}^{(2)}$

3.4.1 Projecting $\mathbf{G}^{(3)}$ to $\mathbf{G}^{(2)}$

The process $\mathbf{G}^{(3)}$ is closely related to $D(\omega^{(3)})$). However, it is hard to study the probability that $\mathbf{G}^{(3)}$ survives, i.e., $v_{n+1}^{(3)} \neq v_n^{(3)}$ for all $n \in \mathbb{N}$. If we can relate this growth process to a two-dimensional growth process, it will greatly simplify our problem. We achieve this goal by projecting the growth process $\mathbf{G}^{(3)}$ onto $\mathbb{L}^2$ to obtain a new process $\mathbf{G}^{(2)}$. Moreover, the new process $\mathbf{G}^{(2)}$ can be related to a canonical bond percolation process on $\mathbb{L}^2$. Notice that the bond percolation threshold of the square lattice $\mathbb{L}^2$ is exactly $\frac{1}{2}$ (See [16]). This is helpful in studying the probability

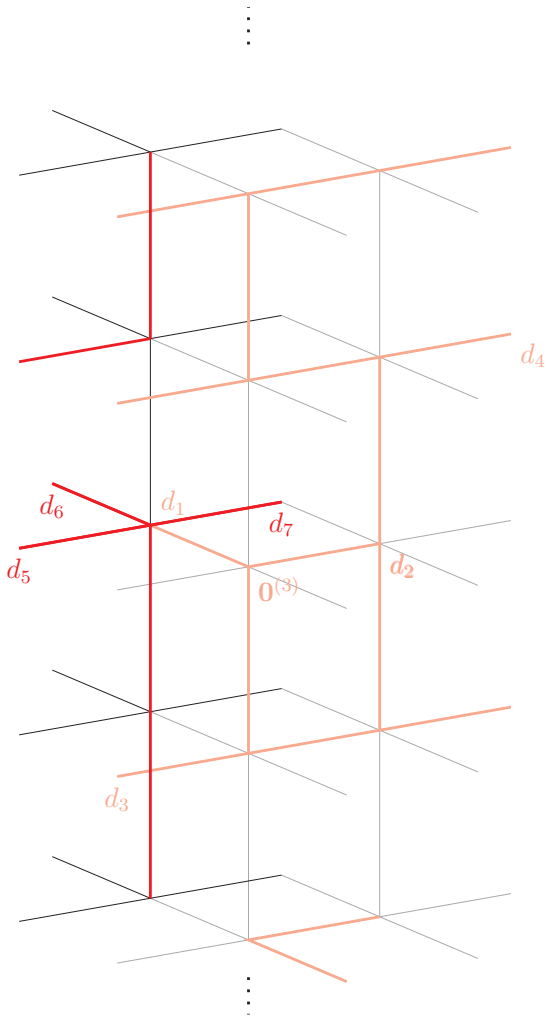

Figure 3.8: An illustration of $B_3^{(3)}$, where edges in $B_3^{(3)}$ are highlighted in darker color, and open edges are highlighted in red color.

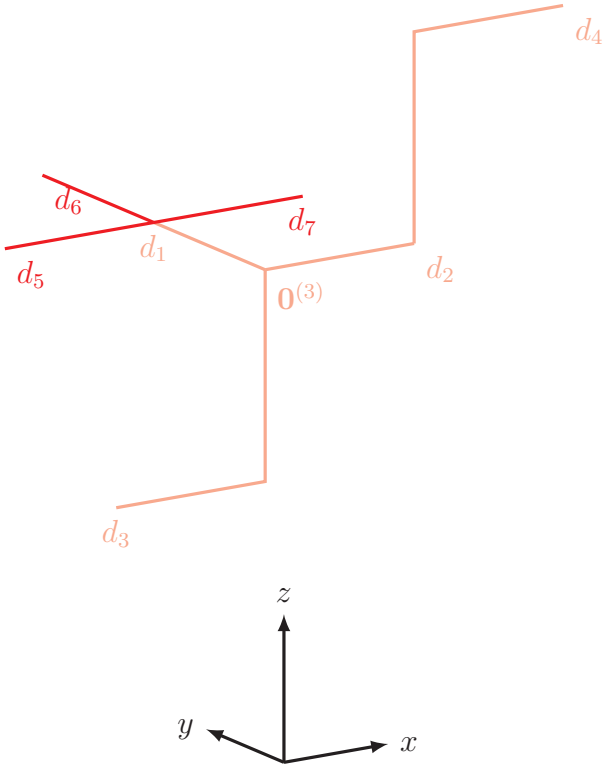

Figure 3.9: An illustration of edges included in $C_3^{(3)}$, where edges in $C_3^{(3)} \setminus C_2^{(3)}$ are highlighted in darker color.

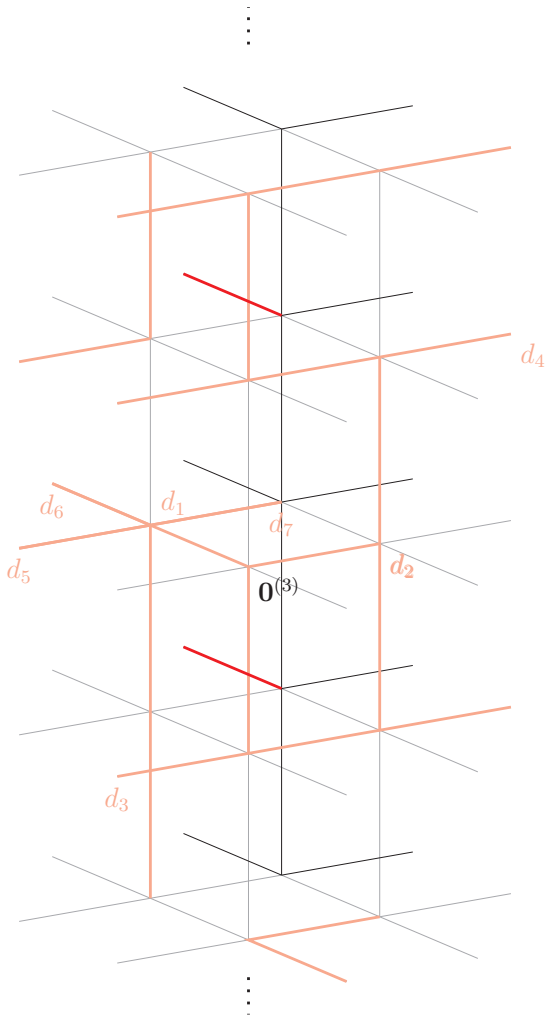

Figure 3.10: An illustration of $B_4^{(3)}$, where edges in $B_4^{(3)}$ are highlighted in darker color, and open edges are highlighted in red color.

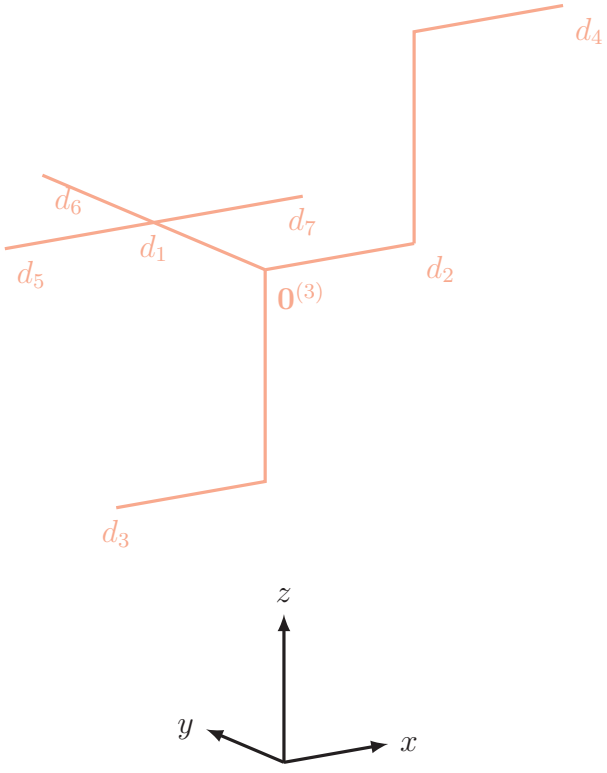

Figure 3.11: An illustration of edges included in $C_4^{(3)}$, where edges in $C_4^{(3)} \setminus C_3^{(3)}$ are highlighted with darker color.

that $\mathbf{G}^{(2)}$ survives. The survival of $\mathbf{G}^{(2)}$ can be used to prove the survival of $\mathbf{G}^{(3)}$, which implies the existence of an infinite open cluster on $\mathbb{L}^3$.

We now provide a rigorous description of this "projection" idea. Recall that for any vertex $\boldsymbol{x} = (x_1, x_2, x_3)$ in $\mathbb{Z}^3$, we define its projection as:

$$\text{proj}(\boldsymbol{x}) = (x_1, x_2) \in \mathbb{Z}^2.$$

Analogously, we have

Definition 3.4.1 (Edge projection)**.** For any edge $e = (\boldsymbol{x}, \boldsymbol{y}) \in \mathbb{E}^3$, we define its *projection* as:

$$\text{proj}(e) := \begin{cases} \emptyset & \text{if } \text{proj}(\boldsymbol{x}) = \text{proj}(\boldsymbol{y}), \\ (\text{proj}(\boldsymbol{x}), \text{proj}(\boldsymbol{y})) & \text{otherwise.} \end{cases}$$

Naturally, we can generalize this definition to a set of vertices or edges:

Definition 3.4.2 (Set projection)**.** For a set of vertices $V \subseteq \mathbb{Z}^3$, its *projection* is $\text{proj}(V) := \{\text{proj}(v) \mid v \in V\}$; for a set of edges $E \subseteq \mathbb{E}^3$, its *projection* is $\text{proj}(E) := \{\text{proj}(e) \mid e \in E\}$.

With the definitions above, the construction of "projected growth process" is straightforward:

Definition 3.4.3 (Projected growth process)**.** Let $\mathbf{G}^{(3)} = (A_n^{(3)}, C_n^{(3)})$ be the growth process associated with $\omega^{(3)}$. We define

$$\mathbf{G}_n^{(2)} := (A_n^{(2)}, C_n^{(2)}) := (\text{proj}(A_n^{(3)}), \text{proj}(C_n^{(3)}))$$

to be the *projected growth process associated with* $\omega^{(3)}$.

3.4.2 Interpretation of $\mathbf{G}^{(2)}$

The definition of $\mathbf{G}^{(3)}$ is complicated. Thus, if we consider $\mathbf{G}^{(2)}$ to be a projection of $\mathbf{G}^{(3)}$, it would be even more complicated. Instead, we regard $\mathbf{G}^{(2)}$ as a growth process on $\mathbb{L}^2$ so that it is more straightforward when compared with the square lattice bond percolation model. Thus, in this subsection, we rephrase the definition of $\mathbf{G}^{(2)}$.

We begin by revisiting the example in Section 3.3, and get a general idea of how $\mathbf{G}^{(2)}$ grows on $\mathbb{L}^2$. We consider the same configuration and the labeling function l that are used in the example (Figure 3.3 and Figure 3.1). In Figure 3.11, we illustrate the edges included in $C_4^{(3)}$. We modify it slightly in Figure 3.12 by adding directions to the edges to indicate how the edge cluster grows. Meanwhile, we mark the vertices from which $\mathbf{G}^{(3)}$ explores at each step. After that, we apply the projection operator to $\mathbf{G}^{(3)}$ to obtain $\mathbf{G}^{(2)}$, which is shown in Figure 3.13.

From Figure 3.13, intuitively, $\mathbf{G}^{(2)}$ can be considered as a growth process on $\mathbb{L}^2$. In fact, for any $n \in \mathbb{N}$, at step n of $\mathbf{G}^{(3)}$, we explore from the vertex $v_n^{(3)}$ and identify its nearest connected column-neighbors through edges in $B_n^{(3)}$. Meanwhile, edges contained in paths in $B_n^{(3)}$ that connect $v_n^{(3)}$ to its nearest column-neighbors are added to $C_n^{(3)}$. Correspondingly, in $\mathbb{L}^2$, the projection of $v_n^{(3)}$ is adjacent to the projection of its

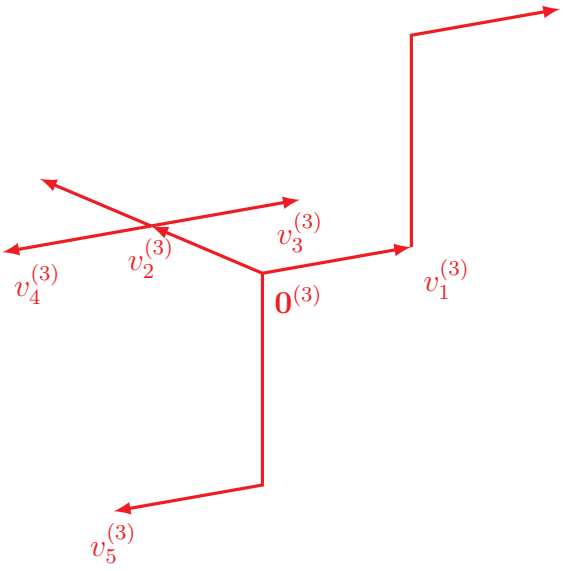

Figure 3.12: An illustration of edges in $C_4^{(3)}$. The edges are not directed edges. The arrows indicates how the edge cluster grows: at each step, $\mathbf{G}^{(3)}$ explores from one of the starting-points of the arrows.

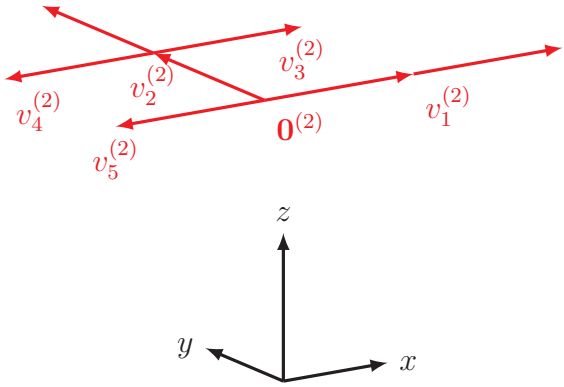

Figure 3.13: An illustration of projecting $\mathbf{G}^{(3)}$ onto $\mathbb{L}^2$ to obtain $\mathbf{G}^{(2)}$, where $v_i^{(2)} = \text{proj}(v_i^{(3)})$.

column-neighbors; the projection of $B_n^{(3)}$ are edges incident to the projection of $v_n^{(3)}$; and the projection of edges newly added to $C_n^{(3)}$ is a subset of $\text{proj}(B_n^{(3)})$. Thus, at step n of $\mathbf{G}^{(2)}$, it is justifiable that we consider $\mathbf{G}^{(2)}$ to be a growth process that explores from $v_n^{(2)} = \text{proj}(v_n^{(3)})$ by considering edges in $\text{proj}(B_n^{(3)})$ and adding a subset of them (which is $\text{proj}(C_n^{(3)})$) to $C_n^{(2)}$. By definition, for any $e = \{v, v_n^{(2)}\} \in \mathbb{E}^2$, the process $\mathbf{G}^{(2)}$ adds e into $C_n^{(2)}$ if and only if e is a projection of some edge in $C_n^{(3)}$. In other words, $e \in C_n^{(2)}$ if and only if there exists a vertex $u \in \mathbb{Z}^3$, satisfying $\text{proj}(u) = v$ and

$u \xleftrightarrow{B_n^{(3)}} v_n^{(3)}$. Meanwhile, we observe that $\{B_n^{(3)}\}$ are pairwise disjoint, which is quite straightforward from the figures, while a formal proof is postponed to the following chapter. Combined with the special geometry of the exploration regions, $\{\text{proj}(B_n^{(3)})\}$ are pairwise disjoint as well. This shows that $\mathbf{G}^{(2)}$ does not consider the same edge of $\mathbb{E}^2$ twice. Thus, it is justifiable that we consider $\mathbf{G}^{(2)}$ to be a growth process on $\mathbb{L}^2$ that explores from vertex $v_n^{(2)}$ at step n, while duplicate consideration of the same edge in $\mathbb{E}^2$ is avoided. A detailed definition is given in the following subsection.

3.4.3 Formal Definition of $\mathbf{G}^{(2)}$

Definition 3.4.4 (Projected process)**.** Let $(\Omega^{(3)}, \mathcal{F}^{(3)}, P_q^{(3)})$ be the probability space for the cubic lattice bond percolation model with parameter q, and l be a labeling function on $\mathbb{Z}^2$. We initialize $(A_0^{(2)}, C_0^{(2)})$ as follows:

$$A_0^{(2)} := \emptyset,$$

$$C_0^{(2)} := \emptyset.$$

For $n \geqslant 1$, we define a stochastic process $(v_n^{(2)}, z_{v_n^{(2)}}, A_n^{(2)}, B_n^{(2)}, C_n^{(2)}) : \Omega^{(3)} \to \mathbb{Z}^2 \times \mathbb{Z} \times 2^{\mathbb{Z}^2} \times 2^{\mathbb{E}^2} \times 2^{\mathbb{E}^2}$ on $(\Omega^{(3)}, \mathcal{F}^{(3)}, P_q^{(3)})$ recursively as follows.

For $n = 1$, we have

$$v_1^{(2)} := \mathbf{0}^{(2)},$$

$$z_{v_1^{(2)}} := 0,$$

$$A_1^{(2)} := A_0^{(2)} \cup \{v_1^{(2)}\},$$

$$B_1^{(2)} := I[v_1^{(2)}].$$

For any $e = \{v, v_1^{(2)}\} \in B_1^{(2)}$, define

$$\omega_\perp^{(2)}(e) := \begin{cases} 1 & \text{if there exists } z \in \mathbb{Z} \text{ such that } v \times z \xleftrightarrow{I[v_1^{(2)} \times \mathbb{Z}]} v_1^{(2)} \times z_{v_1^{(2)}}, \\ 0 & \text{otherwise.} \end{cases}$$

$$C_1^{(2)} := C_0^{(2)} \cup \{e \in B_1^{(2)} \mid \omega_\perp^{(2)}(e) = 1\}.$$

For each $v \in \bigcup_{C_1^{(2)}} \setminus A_1^{(2)}$, define z_v as the integer such that $v \times z_v \in N[v_1^{(2)} \times z_{v_1^{(2)}}, I[v_1^{(2)} \times \mathbb{Z}]]$.

Assume that this stochastic process has been defined up to step n. At step $n+1$, if $\bigcup_{C_n^{(2)}} \setminus A_n^{(2)} \neq \emptyset$, we define

$$v_{n+1}^{(2)} := \arg\min\{l(v) : v \in \bigcup_{C_n^{(2)}} \setminus A_n^{(2)}\},$$

$$A_{n+1}^{(2)} := A_n^{(2)} \cup \{v_{n+1}^{(2)}\},$$

$$B_{n+1}^{(2)} := I[\{v_{n+1}^{(2)}\}] \setminus I[\bigcup_{C_n^{(2)}} \setminus \{v_{n+1}^{(2)}\}]$$

For each $e = \{v, v_{n+1}^{(2)}\} \in B_{n+1}^{(2)}$, define

$$\omega_{\perp}^{(2)}(e) := \begin{cases} 1 & \text{if there exists } z \in \mathbb{Z} \text{ such that } v \times z \xleftrightarrow{I[v_{n+1}^{(2)} \times \mathbb{Z}]} v_{n+1}^{(2)} \times z_{v_{n+1}^{(2)}}, \\ 0 & \text{otherwise.} \end{cases}$$

$$C_{n+1}^{(2)} := C_n^{(2)} \cup \{e \in B_{n+1}^{(2)} \mid \omega_{\perp}^{(2)}(e) = 1\}.$$

For any $v \in C_{n+1}^{(2)} \setminus C_n^{(2)}$, define z_v as the integer such that $v \times z_v \in N[v_{n+1}^{(2)} \times z_{v_{n+1}^{(2)}}, I[v_{n+1}^{(2)} \times \mathbb{Z}]]$.

Otherwise, if $\bigcup_{C_n^{(2)}} \setminus A_n^{(2)} = \emptyset$ we define

$$v_{n+1}^{(2)} := v_n^{(2)},$$

$$A_{n+1}^{(2)} := A_n^{(2)},$$

$$B_{n+1}^{(2)} := \emptyset,$$

$$C_{n+1}^{(2)} := C_n^{(2)}.$$

The *projected growth process associated with* $\omega^{(3)}$ is the stochastic process $\mathbf{G}_n^{(2)} := (A_n^{(2)}, C_n^{(2)})$ defined on the probability space $(\Omega^{(3)}, \mathcal{F}^{(3)}, P_q^{(3)})$ with state space $\mathcal{S}$, where $\mathcal{S} = 2^{\mathbb{Z}^2} \times 2^{\mathbb{E}^2}$.

The above recursive definition is equivalent to the definition of $\mathbf{G}^{(2)}$ in terms of projection. More specifically, we have:

Lemma 3.4.5. *Assume that the processes defined in Definitions 3.2.1 and 3.4.4 have*

the same underlying configuration $\omega^{(3)} \in \Omega^{(3)}$. *Then the following relations hold:*

$$
\begin{aligned}
A_n^{(2)} &= \mathrm{proj}(A_n^{(3)}),\\
B_n^{(2)} &= \mathrm{proj}(B_n^{(3)}),\\
C_n^{(2)} &= \mathrm{proj}(C_n^{(3)}),\\
v_n^{(2)} &= \mathrm{proj}(v_n^{(3)}),\ \textit{furthermore}\ , v_n^{(2)} \times z_{v_n^{(2)}} = v_n^{(3)},\\
A_n^{(3)} &= \{v_i^{(2)} \times z_{v_i^{(2)}} \mid i \in \{1, 2, ..., n\}\},\\
B_n^{(3)} &= I[v_{n+1}^{(2)} \times \mathbb{Z}] \setminus I[(\textstyle\bigcup_{C_n^{(2)}} \setminus \{v_{n+1}^{(2)}\}) \times \mathbb{Z}],\\
D_n^{(3)} &= \{v \times z_v \mid v \in \textstyle\bigcup_{C_n^{(2)}}\},\\
C_n^{(3)} &= \bigcup_{i=1}^{n} \left(\bigcup_{v \in D_i^{(3)} \setminus D_{i-1}^{(3)}} \mathrm{path}(v_i^{(2)} \times z_{v_i^{(2)}}, v \times z_v, B_i^{(3)}) \right).
\end{aligned}
$$

In the remainder of the dissertation, we focus on analyzing $\mathbf{G}^{(2)}$. For brevity, we shall sometime refer to the notation used in defining the three-dimensional growth process to help us illustrate the properties of the two-dimensional projected growth process.

Chapter 4

Properties of $\mathbf{G}^{(3)}$ and $\mathbf{G}^{(2)}$

In the previous chapter, we introduced the cubic lattice growth process $\mathbf{G}^{(3)}$ and its planar projection $\mathbf{G}^{(2)}$. In this chapter, we study their properties, among which the most important are the Markov property of $\mathbf{G}^{(2)}$ and its corresponding transition probabilities. The Markov property provides us with theoretical justification that at each step of $\mathbf{G}^{(2)}$, to calculate the conditional probability measure of edges being added to $\mathbf{G}^{(2)}$ given the natural filtration, it is sufficient that we only condition on the state after the previous step. This allows us to study the growth of $\mathbf{G}^{(2)}$ in terms of its transition probabilities, which reduces the number of states we need to consider. Using the transition probabilities, we derive stochastic ordering inequalities that provide us with the "step-wise" coupling.

Given a sequence of probability measures $\{\mu_i\}_{i\in I}$, we let $\prod_{i\in I}\mu_i$ denote the prod-

uct measure. Meanwhile, for a given configuration $\omega^{(3)}$ on $\mathbb{L}^3$ and a given set of edges $B \subseteq \mathbb{E}^3$, we call $\{\omega^{(3)}(e)\}_{e\in B}$ the configuration restricted to B. Moreover, if B is pre-specified, and when the meaning is clear from the context, we simply call $\{\omega^{(3)}(e)\}_{e\in B}$ the restricted configuration.

4.1 Properties of $\mathbf{G}^{(3)}$

In this section, we introduce two properties of $\mathbf{G}^{(3)}$. The first helps in proving the Markov property of $\mathbf{G}^{(2)}$, and the latter relates the survival of $\mathbf{G}^{(3)}$ to the infinite cardinality of $D(\omega^{(3)})$, where $\omega^{(3)}$ is the underlying configuration on $\mathbf{G}^{(3)}$.

Lemma 4.1.1. *Let $\{B_n^{(3)}\}$ be defined as in Definition 3.2.1. Then the sets $\{B_n^{(3)}\}_{n=1}^{\infty}$ are pairwise disjoint.*

Proof. Recall that $B_n^{(3)}$ is the exploration region at step n of $\mathbf{G}^{(3)}$. We prove that $B_m^{(3)} \cap B_n^{(3)} = \emptyset$, for any $1 \leqslant m < n$.

Assume not. Then there exists an edge $e = (\boldsymbol{x}, \boldsymbol{y}) \in \mathbb{E}^3$ such that $e \in B_m^{(3)} \cap B_n^{(3)}$ for some $m < n$. Recall that $B_m^{(3)} = I[\mathrm{col}(v_m^{(3)})] \setminus I[\mathrm{col}(D_{m-1}^{(3)} \setminus \{v_m^{(3)}\})] \subseteq I[\mathrm{col}(v_m^{(3)})]$. Meanwhile, $v_m^{(3)} \in D_m^{(3)} \subset D_{n-1}^{(3)}$ and $v_m^{(3)} \neq v_n^{(3)}$. Thus, $v_m^{(3)} \in D_{n-1}^{(3)} \setminus \{v_n^{(3)}\}$. Consequently, $e \in B_m^{(3)} \subset I[\mathrm{col}(D_{n-1}^{(3)} \setminus \{v_n^{(3)}\})]$. By our assumption that $e \in B_n^{(3)}$, we have $e \in I[\mathrm{col}(v_n^{(3)})] \setminus I[\mathrm{col}(D_{n-1}^{(3)} \setminus \{v_n^{(3)}\})]$, which is a contradiction. □

Lemma 4.1.2. *For a configuration $\omega^{(3)}$ on $\mathbb{L}^3$, if $\mathbf{G}^{(3)}(\omega^{(3)})$ survives (i.e., if $A_{n+1}^{(3)}(\omega^{(3)}) \neq A_n^{(3)}(\omega^{(3)})$ for each $n \in \mathbb{N}$), then $|D(\omega^{(3)})| = \infty$.*

Proof. We prove that $D_n^{(3)} \subseteq D(\omega^{(3)})$ for every n by applying induction on n.

For $n = 1$, we have $D_1^{(3)} = \{\mathbf{0}^{(3)}\} \subseteq D(\omega^{(3)})$ by the definition of open cluster.

Given the induction hypothesis that $D_n^{(3)} \subseteq D(\omega^{(3)})$, we show that $D_{n+1}^{(3)} \subseteq D(\omega^{(3)})$. Notice that for any $v \in D_{n+1}^{(3)} \setminus D_n^{(3)}$, we have $v \xleftrightarrow{B_{n+1}^{(3)},\omega^{(3)}} v_{n+1}^{(3)}$. Notice also that $v_{n+1}^{(3)} \xleftrightarrow{\mathbb{E}^3,\omega^{(3)}} \mathbf{0}^{(3)}$ by the induction hypothesis. Thus, $v \xleftrightarrow{\mathbb{E}^3,\omega^{(3)}} \mathbf{0}^{(3)}$. Consequently, $D_{n+1}^{(3)} \subseteq D(\omega^{(3)})$.

Using induction, we have $D_n^{(3)} \subseteq D(\omega^{(3)})$ for each $n \in \mathbb{N}$, which implies that $A_n^{(3)} = \{v_1^{(3)}, ..., v_n^{(3)}\} \subseteq D_n^{(3)} \subseteq D(\omega^{(3)})$. Notice that if $\mathbf{G}^{(3)}$ survives, $A_n^{(3)}$ contains exactly n distinct vertices, implying that $|D(\omega^{(3)})| = \infty$.

□

4.2 Properties of $\mathbf{G}^{(2)}$

In the previous section, we proved that if the growth process $\mathbf{G}^{(3)}$ survives, then $|D(\omega^{(3)})| = \infty$. Thus, if the projected growth process $\mathbf{G}^{(2)}$ survives, then the original process $\mathbf{G}^{(3)}$ survives as well. This also results in $|D(\omega^{(3)})| = \infty$.

Lemma 4.2.1. *For a configuration $\omega^{(3)}$ on $\mathbb{L}^3$, if $\mathbf{G}^{(2)}(\omega^{(3)})$ survives (i.e., if $A^{(2)}_{n+1}(\omega^{(3)}) \neq A^{(2)}_n(\omega^{(3)})$ for each $n \in \mathbb{N}$), then $|D(\omega^{(3)})| = \infty$.*

We provide a proof using notation introduced in Definition 3.4.4. The idea of this proof is the same as the proof of Lemma 4.1.2.

Proof. We first prove that $v^{(2)}_n \times z_{v^{(2)}_n} \in D(\omega^{(3)})$ for every n by induction on n.

For $n = 1$, $v^{(2)}_1 \times z_{v^{(2)}_1} = \mathbf{0}^{(3)} \in D(\omega^{(3)})$ by definition.

Assume the induction hypothesis that $v^{(2)}_k \times z_{v^{(2)}_k} \in D(\omega^{(3)})$ is true for each $k \leqslant n$. We now show that $v^{(2)}_{n+1} \in D(\omega^{(3)})$. If $v^{(2)}_{n+1} = v^{(2)}_n$, the process is not exploring any new vertex, and the induction hypothesis holds true. Otherwise, notice that $v^{(2)}_{n+1} \in \bigcup_{C^{(2)}_n} \setminus A^{(2)}_n$, and by the definition of $C^{(2)}_n$, there exists $m \leqslant n$ such that $\{v^{(2)}_m, v^{(2)}_{n+1}\} \in \mathbb{E}^2$ and $\omega^{(2)}_\perp(\{v^{(2)}_m, v^{(2)}_{n+1}\}) = 1$. Recall that $\omega^{(2)}_\perp(\{v^{(2)}_m, v^{(2)}_{n+1}\})$ is the indicator that $v^{(2)}_m \times z_{v^{(2)}_m} \xleftrightarrow{I[v^{(2)}_m \times \mathbb{Z}], \omega^{(3)}} v^{(2)}_{n+1} \times z_{v^{(2)}_{n+1}}$ for some $z_{v^{(2)}_{n+1}} \in \mathbb{Z}$. By the induction hypothesis, $v^{(2)}_m \times z_{v^{(2)}_m} \xleftrightarrow{\mathbb{E}^3,\ \omega^{(3)}} \mathbf{0}^{(3)}$. Consequently, $v^{(2)}_{n+1} \times z_{v^{(2)}_{n+1}}$ is connected to $\mathbf{0}^{(3)}$ as well, i.e., $v^{(2)}_{n+1} \times z_{v^{(2)}_{n+1}} \in D(\omega^{(3)})$.

By induction, the sequence $\{v^{(2)}_n \times z_{v^{(2)}_n}\}_n \subseteq D(\omega^{(3)})$. If $\{v^{(2)}_n\}$ are distinct vertices of $\mathbb{Z}^2$, then $\{v^{(2)}_n \times z_{v^{(2)}_n}\}$ are distinct vertices of $\mathbb{Z}^3$. Consequently, if $\mathbf{G}^{(2)}$ survives, $|D(\omega^{(3)})| = \infty$. □

4.2.1 Markov Property of $\mathbf{G}^{(2)}$

In the following, we prove that $\mathbf{G}^{(2)}$ is a Markov process. We observe that the probability measure $P_q^{(3)}$ satisfies the translation invariance property, resulting from the vertex transitive property of the cubic lattice. In other words, we have the following lemma.

Lemma 4.2.2. *For any $\boldsymbol{z} \in \mathbb{Z}^3$ and $\omega^{(3)} \in \Omega^{(3)}$, let $T_{\boldsymbol{z}}(\omega^{(3)})$ be the configuration obtained by translating $\omega^{(3)}$ by vector $\boldsymbol{z}$. That is, $T_{\boldsymbol{z}}(\omega^{(3)})(\{\boldsymbol{x}, \boldsymbol{y}\}) = \omega^{(3)}(\{\boldsymbol{x}-\boldsymbol{z}, \boldsymbol{y}-\boldsymbol{z}\})$ for each $\{\boldsymbol{x}, \boldsymbol{y}\} \in \mathbb{E}^3$. Meanwhile, for each $F \in \mathcal{F}^{(3)}$, define $T_{\boldsymbol{z}}(F) = \{T_{\boldsymbol{z}}(\omega^{(3)}) \mid \omega^{(3)} \in F\}$. We have $P_q^{(3)}(F) = P_q^{(3)}(T_{\boldsymbol{z}}(F))$ for each $\boldsymbol{z} \in \mathbb{Z}^3$ and each $F \in \mathcal{F}^{(3)}$.*

Proof. We define the finite positive cylinder set of $\Omega^{(3)}$ as follows. For each $E \subseteq \mathbb{E}^3, |E| < \infty$, let $C_+(E) := \{\omega^{(3)} \in \Omega^{(3)} \mid \omega^{(3)}(e) = 1 \text{ for each } e \in E\}$ be its corresponding positive cylinder set. For notational convenience, we define $T_{\boldsymbol{z}}(E) :=$

$\{\{\boldsymbol{x}+\boldsymbol{z}, \boldsymbol{y}+\boldsymbol{z}\} \mid \{\boldsymbol{x}, \boldsymbol{y}\} \in E\}$. By the definition of $P_q^{(3)}$, we have

$$\begin{aligned}
P_q^{(3)}(C_+(E)) &= \left(\prod_{e\in\mathbb{E}^3} \mu_e^{(3)}\right)(C_+(E)) \\
&= \prod_{e\in E} \mu_e^{(3)}(1) \cdot \prod_{e\in\mathbb{E}^3\setminus E} [\mu_e^{(3)}(0) + \mu_e^{(3)}(1)] \\
&= q^{|E|} \cdot 1 \\
&= q^{|T_{\boldsymbol{z}}(E)|} \cdot 1 \\
&= \prod_{e\in T_{\boldsymbol{z}}(E)} \mu_e^{(3)}(1) \cdot \prod_{e\in\mathbb{E}^3\setminus T_{\boldsymbol{z}}(E)} [\mu_e^{(3)}(0) + \mu_e^{(3)}(1)] \\
&= \left(\prod_{e\in\mathbb{E}^3} \mu_e^{(3)}\right)(C_+(T_{\boldsymbol{z}}(E))) \\
&= P_q^{(3)}(T_{\boldsymbol{z}}(C_+(E))).
\end{aligned}$$

Notice that this holds true for any finite positive cylinder set $C_+(F)$. Notice also that

1. the σ-field generated by the finite positive cylinder sets of $\Omega^{(3)}$ is $\mathcal{F}^{(3)}$ (Remark 4.2.3.(a).),

2. and the finite positive cylinder sets of $\Omega^{(3)}$ form a π-system (Remark 4.2.3.(b).).

By the π-λ Theorem, we have $P_q^{(3)}(F) = P_q^{(3)}(T_{\boldsymbol{z}}(F))$ for all $F \in \mathcal{F}^{(3)}$. □

Remarks 4.2.3.

(a) In Campanino and Russo's paper [5], they use the positive cylinder sets to be the generating class for the σ-field of the site percolation model, this can be carried over to bond percolation model as well. In fact, for each finite cylinder

set $C_{\pm}(E_1, E_2) := \{\omega^{(3)} \in \Omega^{(3)} \mid \omega^{(3)}(e) = 1 \text{ for each } e \in E_1 \text{ and } \omega^{(3)}(e) = 0 \text{ for each } e \in E_2\}$, we may write it as $C_{\pm}(E_1, E_2) := C_+(E_1) \cap (\bigcap_{e \in E_2} C_+(\{e\})^c)$; For each positive cylinder $C_+(E)$, we may write it as $C_+(E) = C_{\pm}(E, \emptyset)$. Thus, the σ-field generated by both classes are the same.

(b) To see this, simplify use the fact that $C_+(E_1) \cap C_+(E_2) = C_+(E_1 \cup E_2)$. Thus, the positive cylinder sets are non-empty and closed under intersection, which makes it a π-system.

The translation invariance property provides us with the vertex transitivity property of $\mathbf{G}^{(2)}$, which is formalized in the following two theorems.

Theorem 4.2.4 (Vertex transitive property)**.** *For any fixed $n \in \mathbb{N}$, the conditional probability $P_q^{(3)}(\mathbf{G}_{n+1}^{(2)} \mid \mathbf{G}_n^{(2)}, z_{v_{n+1}^{(2)}} = z)$ is invariant with respect to z.*

Theorem 4.2.5 (Vertex transitive property)**.** *For any fixed n, the conditional probability $P_q^{(3)}(\mathbf{G}_{n+1}^{(2)} \mid \mathcal{F}_n^{(2)}, z_{v_{n+1}^{(2)}} = z)$ is invariant with respect to z, where $\mathcal{F}_n^{(2)} := \sigma(\mathbf{G}_1^{(2)}, ..., \mathbf{G}_n^{(2)})$ is the natural filtration of the projected growth process $\mathbf{G}_n^{(2)}$ through step n.*

Before the proof of the theorems above, we claim that both $v_{n+1}^{(2)}$ and $B_{n+1}^{(2)}$ are obtained from $\boldsymbol{G}_n^{(2)}$. Rigorously, we have

Lemma 4.2.6. *For any $n \in \mathbb{N}$, both $v_{n+1}^{(2)}$ and $B_{n+1}^{(2)}$ are $\sigma(\mathbf{G}_n^{(2)})$-measurable.*

This lemma is quite straightforward by looking at the definition of the corresponding notations. One may see that $v_{n+1}^{(2)}$ and $B_{n+1}^{(2)}$ are "determined" by $A_n^{(2)}$, $C_n^{(2)}$ and a

pre-specified labeling function l. Thus, the three terms are all $\sigma(\mathbf{G}_n^{(2)})$-measurable. A formal proof is given below.

Proof. We first show that $v_{n+1}^{(2)}$ is $\sigma(\mathbf{G}_n^{(2)})$-measurable. Equivalently, we show that $\min\{l(v) : v \in \bigcup_{C_n^{(2)}} \setminus A_n^{(2)}\}$ is $\sigma(\mathbf{G}_n^{(2)})$-measurable since l is a bijection between $\mathbb{Z}^2$ and $\mathbb{Z}_+$. For an arbitrary $x \in \mathbb{R}$, we have

$$\begin{aligned}
&\{\omega^{(3)} \in \Omega^{(3)} \mid \min\{l(v) : v \in \textstyle\bigcup_{C_n^{(2)}(\omega^{(3)})} \setminus A_n^{(2)}(\omega^{(3)})\} > x\} \\
&= \{\omega^{(3)} \in \Omega^{(3)} \mid l(v) > x \text{ for each } v \in \textstyle\bigcup_{C_n^{(2)}(\omega^{(3)})} \setminus A_n^{(2)}(\omega^{(3)})\}
\end{aligned}$$

Let $\mathcal{S}(x) := \{(A, C) \in \mathbb{Z}^2 \times \mathbb{E}^2 \mid \{l^{-1}(0), l^{-1}(1), ..., l^{-1}(\lfloor x \rfloor)\} \cap (\bigcup_C \setminus A) = \emptyset\}$ be a subset of the state space of $\mathbf{G}^{(2)}$, where $l^{-1}(i)$ is the vertex in $\mathbb{Z}^2$ whose labelling is i. For any $\omega^{(3)} \in \{\omega^{(3)} \in \Omega^{(3)} \mid l(v) > x \text{ for each } v \in \bigcup_{C_n^{(2)}(\omega^{(3)})} \setminus A_n^{(2)}(\omega^{(3)})\}$, we have $\mathbf{G}_n^{(2)}(\omega^{(3)}) \in \mathcal{S}(x)$. On the other hand, for any $\omega^{(3)}$ such that $\mathbf{G}_n^{(2)}(\omega^{(3)}) \in \mathcal{S}(x)$ for some $n \in \mathbb{N}$, $\mathbf{G}^{(2)}$ explores from a vertex whose labelling is strictly larger than x at step $n+1$. Consequently,

$$\begin{aligned}
&\{\omega^{(3)} \in \Omega^{(3)} \mid l(v) > x \text{ for each } v \in \textstyle\bigcup_{C_n^{(2)}(\omega^{(3)})} \setminus A_n^{(2)}(\omega^{(3)})\} \\
&= \mathbf{G}_n^{(2)^{-1}}(\mathcal{S}(x)) \\
&= \mathbf{G}_n^{(2)^{-1}}(\bigcup_{(A,C)\in\mathcal{S}(x)} (A, C)) \\
&= \bigcup_{(A,C)\in\mathcal{S}(x)} \mathbf{G}_n^{(2)^{-1}}((A, C)),
\end{aligned}$$

where by convention, $\mathbf{G}_n^{(2)^{-1}}(A, C) := \{\omega^{(3)} \in \Omega^{(3)} \mid \mathbf{G}_n^{(2)}(\omega^{(3)}) = (A, C)\}$.

The argument is complete once we have demonstrated that the index set $\mathcal{S}(x)$ is countable. Then $\{\omega^{(3)} \in \Omega^{(3)} \mid \min\{l(v) : v \in \bigcup_{C_n^{(2)}(\omega^{(3)})} \setminus A_n^{(2)}(\omega^{(3)})\} > x\}$ is a countable union of sets in $\sigma(\mathbf{G}_n^{(2)})$, thus is also in $\sigma(\mathbf{G}_n^{(2)})$. However, it is not necessary to prove (or disprove) that $\mathcal{S}(x)$ is countable.

Fortunately, $\bigcup_{(A,C)\in\mathcal{S}(x)} \mathbf{G}_n^{(2)^{-1}}((A,C))$ can be reduced to a union of finitely many sets. For any $n \in \mathbb{N}$, by the definition of $\mathbf{G}^{(2)}$ and induction, $C_n^{(2)}$ only contains edges in $[-n,n]^2$, where $[-n,n]^2$ represents edges of the $2n$ by $2n$ square units of the square lattice centered at $\mathbf{0}^{(2)}$. Let $\mathcal{S}_n(x) := \{(A,C) \in \mathcal{S}(x) \mid C \subseteq [-n,n]^2, A \subseteq \bigcup_C\}$. Since $A \subseteq \bigcup_C$ for any $(A,C) \in \mathcal{S}_n(x)$, $\mathcal{S}_n(x)$ contains finitely many elements. Additionally, for each $(A,C) \in \mathbb{Z}^2 \times \mathbb{E}^2 \setminus \mathcal{S}_n(x)$, we have $\mathbf{G}_n^{(2)^{-1}}((A,C)) = \emptyset$. In sum, we have

$$\begin{aligned}
&\{\omega^{(3)} \in \Omega^{(3)} \mid \min\{l(v) : v \in \textstyle\bigcup_{C_n^{(2)}(\omega^{(3)})} \setminus A_n^{(2)}(\omega^{(3)})\} > x\} \\
&= \bigcup_{(A,C)\in\mathcal{S}(x)} \mathbf{G}_n^{(2)^{-1}}((A,C)) \\
&= \bigcup_{(A,C)\in\mathcal{S}_n(x)} \mathbf{G}_n^{(2)^{-1}}((A,C)) \\
&\in \sigma(\mathbf{G}_n^{(2)})
\end{aligned}$$

Notice that this is true for arbitrary x, completing the proof that $v_{n+1}^{(2)}$ is $\sigma(\mathbf{G}_n^{(2)})$-measurable.

We now prove that $B_{n+1}^{(2)}$ is $\sigma(\mathbf{G}_n^{(2)})$-measurable using the fact that $v_{n+1}^{(2)}$ is $\sigma(\mathbf{G}_n^{(2)})$-

measurable. Consider $B^{(2)}_{n+1}$ to be a sequence of indicators $\{\mathbb{1}_{\{e\in B^{(2)}_{n+1}\}}\}$, indexed by $I := \{e \in \mathbb{E}^2, e \in [-(n+1), n+1]^2\}$. Notice that $\mathbb{1}_{\{e\in B^{(2)}_{n+1}\}} = 1$ if and only if one endpoint of e is $v^{(2)}_{n+1}$ and the other endpoint of e is not contained in $\bigcup_{C^{(2)}_n}$. Since $v^{(2)}_{n+1}$ is $\sigma(\mathbf{G}^{(2)}_n)$-measurable, $\mathbb{1}_{\{e\in B^{(2)}_{n+1}\}}$ is $\sigma(\mathbf{G}^{(2)}_n)$-measurable as well for any $e \in \mathbb{E}^2$. Notice that $B^{(2)}_{n+1}$ only contains edges in $[-(n+1), n+1]^2$. Consequently, the finite Cartesian product $\{\mathbb{1}_{\{e\in B^{(2)}_{n+1}\}}\}_{e\in I}$ is $\sigma(\mathbf{G}^{(2)}_n)$-measurable, which implies that $B^{(2)}_{n+1}$ is $\sigma(\mathbf{G}^{(2)}_n)$-measurable. □

We now return to the proof of Theorem 4.2.4. Informally speaking, given $v^{(2)}_{n+1}$, $B^{(2)}_{n+1}$ and $z_{v^{(2)}_{n+1}}$, the future state $\mathbf{G}^{(2)}_{n+1}$ is decided by the underlying configuration on $\Omega^{(3)}$ restricted to $I[v^{(2)}_{n+1} \times \mathbb{Z}]$. This is quite straightforward if one looks back to the example provided in Chapter 3, Section 3. This inspires us to define a collection of restricted configurations, denoted by $\Omega_{\mathbf{G}^{(2)}_n,\mathbf{G}^{(2)}_{n+1}}$ that can "transit" from state $\mathbf{G}^{(2)}_n$ to state $\mathbf{G}^{(2)}_{n+1}$.

Proof of Theorem 4.2.4. For $\mathbf{G}^{(2)}_n = (A^{(2)}_n, C^{(2)}_n)$, $\mathbf{G}^{(2)}_{n+1} = (A^{(2)}_{n+1}, C^{(2)}_{n+1})$ and a constant $z \in \mathbb{Z}$, let $\Omega_{\mathbf{G}^{(2)}_n,\mathbf{G}^{(2)}_{n+1}}(z) := \{\omega \in \Omega^{(3)} \mid$ there exists z' such that $v^{(2)}_{n+1} \times z \xleftarrow{I[v^{(2)}_{n+1}\times\mathbb{Z}],\ \omega} v' \times z'$ for each $v' \in \bigcup_{C^{(2)}_{n+1}} \setminus \bigcup_{C^{(2)}_n}$, and there does not exist $z'' \in \mathbb{Z}$ such that $v^{(2)}_{n+1} \times z \xleftarrow{I[v^{(2)}_{n+1}\times\mathbb{Z}],\omega} v'\times z''$ for each $v' \in \bigcup_{B^{(2)}_{n+1}} \setminus(\bigcup_{C^{(2)}_{n+1}})\}$. To interpret, the event $\Omega_{\mathbf{G}^{(2)}_n,\mathbf{G}^{(2)}_{n+1}}(z)$ is defined in such a way that on $\Omega_{\mathbf{G}^{(2)}_n,\mathbf{G}^{(2)}_{n+1}}(z)$, the projected growth process $\mathbf{G}^{(2)}$ makes a transition from state $\mathbf{G}^{(2)}_n$ to state $\mathbf{G}^{(2)}_{n+1}$, given that the vertex from which $\mathbf{G}^{(2)}$ explores has its third coordinate equal to z. More specifically, for any projected growth process at state $\mathbf{G}^{(2)}_n$ satisfying that it is exploring from a vertex with its

third coordinate equaling z at the next step, it is at state $\mathbf{G}^{(2)}_{n+1}$ at the next step if and only if the underlying configuration is in $\Omega_{\mathbf{G}^{(2)}_n,\mathbf{G}^{(2)}_{n+1}}(z)$. Notice that the above set of configurations is well-defined in the sense that $v^{(2)}_{n+1}$ and $I[v^{(2)}_{n+1}\times\mathbb{Z}]$ are both obtained from $\mathbf{G}^{(2)}_n$. We assume that $\Omega_{\mathbf{G}^{(2)}_n,\mathbf{G}^{(2)}_{n+1}}(z)\neq\emptyset$. The proof is trivial otherwise.

Meanwhile, for any fixed $z\in\mathbb{Z}$ and each $\omega\in\Omega_{\mathbf{G}^{(2)}_n,\mathbf{G}^{(2)}_{n+1}}(z)$, we translate this configuration by the vector $\boldsymbol{z}=(0,0,-z)$, forming a new configuration $T_{\boldsymbol{z}}(\omega)$, i.e., $T_{\boldsymbol{z}}(\omega)(\{\boldsymbol{x},\boldsymbol{y}\}):=\omega(\{(x_1,x_2,x_3+z),(y_1,y_2,y_3+z)\})$ for each $\{\boldsymbol{x},\boldsymbol{y}\}\in\mathbb{E}^3$. Using the vertex transitive property of $\mathbb{L}^3$, $v^{(2)}_{n+1}\times z \xleftrightarrow{I[v^{(2)}_{n+1}\times\mathbb{Z}],\ \omega} v'\times z'$ if and only if $v^{(2)}_{n+1}\times 0 \xleftrightarrow{I[v^{(2)}_{n+1}\times\mathbb{Z}],\ T_{\boldsymbol{z}}(\omega)} v'\times(z'-z)$, as illustrated in Figure 4.2. Thus, $T_{\boldsymbol{z}}(\omega)\in\Omega_{\mathbf{G}^{(2)}_n,\mathbf{G}^{(2)}_{n+1}}(0)$, i.e., $\Omega_{\mathbf{G}^{(2)}_n,\mathbf{G}^{(2)}_{n+1}}(0)=T_{\boldsymbol{z}}(\Omega_{\mathbf{G}^{(2)}_n,\mathbf{G}^{(2)}_{n+1}}(z))$. Consequently, we have

$$
\begin{aligned}
&P^{(3)}_q(\mathbf{G}^{(2)}_{n+1}\mid\mathbf{G}^{(2)}_n, z_{v^{(2)}_{n+1}}=z)\\
=&P^{(3)}_q(\Omega_{\mathbf{G}^{(2)}_n,\mathbf{G}^{(2)}_{n+1}}(z))\\
=&P^{(3)}_q(T_{\boldsymbol{z}}(\Omega_{\mathbf{G}^{(2)}_n,\mathbf{G}^{(2)}_{n+1}}(z)))\\
=&P^{(3)}_q(\Omega_{\mathbf{G}^{(2)}_n,\mathbf{G}^{(2)}_{n+1}}(0))\\
=&P^{(3)}_q(\mathbf{G}^{(2)}_{n+1}\mid\mathbf{G}^{(2)}_n, z_{v^{(2)}_{n+1}}=0),
\end{aligned}
$$

where the third equality is obtained from the translation invariance property of $P^{(3)}_q$ measure. □

The proof of Theorem 4.2.5 is based on the same reasoning, thus is omitted in this dissertation.

Remark 4.2.7.

In Figure 4.1, we illustrate the specific case that $|B^{(2)}_{n+1}| = 3$, $\mathbf{G}^{(2)}_n = (A^{(2)}_n, C^{(2)}_n)$, $\mathbf{G}^{(2)}_{n+1} = (A^{(2)}_n \cup \{v^{(2)}_{n+1}\}, C^{(2)}_n \cup \{e_2, e_3\})$, and $z_{v^{(2)}_{n+1}} = z$. Consider a configuration $\omega \in \Omega^{(3)}$ restricted to $I[v^{(2)}_{n+1} \times \mathbb{Z}] \setminus I[(\bigcup_{C^{(2)}_n} \setminus \{v^{(2)}_{n+1}\}) \times \mathbb{Z}]$, which is illustrated in Figure 4.1 by letting red edges represent open edges and black edges represent closed ones. Observe that a projected growth process, given its $z_{v^{(2)}_{n+1}} = z$, makes a transition from state $\mathbf{G}^{(2)}_n$ to $\mathbf{G}^{(2)}_{n+1}$ if the underlying configuration restricted to $I[v^{(2)}_{n+1} \times \mathbb{Z}] \setminus I[(\bigcup_{C^{(2)}_n} \setminus \{v^{(2)}_{n+1}\}) \times \mathbb{Z}]$ is consistent with the one shown in Figure 4.1. More rigorously, for any configuration $\omega' \in \Omega^{(3)}$ satisfying $\mathbf{G}^{(2)}_n(\omega') = \mathbf{G}^{(2)}_n$ and $z_{v^{(2)}_{n+1}}(\omega') = z$, we have $\mathbf{G}^{(2)}_{n+1}(\omega') = \mathbf{G}^{(2)}_{n+1}$ if $\omega'(e) = \omega(e)$ for all $e \in I[v^{(2)}_{n+1} \times \mathbb{Z}] \setminus I[(\bigcup_{C^{(2)}_n} \setminus \{v^{(2)}_{n+1}\}) \times \mathbb{Z}]$.

After translating the restricted configuration by vector $(0, 0, -z)$, we get a new configuration $T_{\boldsymbol{z}}(\omega)$, whose restriction to $I[v^{(2)}_{n+1} \times \mathbb{Z}] \setminus I[(\bigcup_{C^{(2)}_n} \setminus \{v^{(2)}_{n+1}\}) \times \mathbb{Z}]$ is illustrated in Figure 4.2. The translated restricted configuration transits from state $\mathbf{G}^{(2)}_n$ to $\mathbf{G}^{(2)}_{n+1}$, given $z_{v^{(2)}_{n+1}} = 0$. Thus, there is a bijection $T_{\mathbf{z}}$ from the configurations restricted to $B^{(3)}_{n+1}$ that the corresponding projected growth process transits from $\mathbf{G}^{(2)}_n$ to $\mathbf{G}^{(2)}_{n+1}$ given $z_{v^{(2)}_{n+1}} = z$, to other configurations restricted to $B^{(3)}_{n+1}$ that the corresponding projected growth process transits from $\mathbf{G}^{(2)}_n$ to $\mathbf{G}^{(2)}_{n+1}$ given $z_{v^{(2)}_{n+1}} = 0$, i.e., $\Omega_{\mathbf{G}^{(2)}_n, \mathbf{G}^{(2)}_{n+1}}(0) = T_z(\Omega_{\mathbf{G}^{(2)}_n, \mathbf{G}^{(2)}_{n+1}}(z))$.

Recall that in Definition 3.4.4, for each $e = \{v, v_{n+1}^{(2)}\} \in B_{n+1}^{(2)}$, we define $\omega_{\perp}^{(2)}(e)$ as follows:

$$\omega_{\perp}^{(2)}(e) := \begin{cases} 1 & \text{if there exists } z \in \mathbb{Z} \text{ such that } v \times z \xleftrightarrow{I[v_{n+1}^{(2)} \times \mathbb{Z}]} v_{n+1}^{(2)} \times z_{v_{n+1}^{(2)}}, \\ 0 & \text{otherwise.} \end{cases}$$

Notice that only edges in $B_{n+1}^{(2)}$ are considered at step $n+1$ of $\mathbf{G}^{(2)}$. Thus, $v \times z$ connecting to $v_{n+1}^{(2)} \times z_{v_{n+1}^{(2)}}$ by an open path in $I[v_{n+1}^{(2)} \times \mathbb{Z}]$ is equivalent to these two vertices being connected by an open path in $I[v_{n+1}^{(2)} \times \mathbb{Z}] \setminus I[(\bigcup_{C_n^{(2)}} \setminus \{v_{n+1}^{(2)}\}) \times \mathbb{Z}] = B_{n+1}^{(3)}$. This provides us with an alternative definition of $\omega_{\perp}^{(2)}$:

$$\omega_{\perp}^{(2)}(e) := \begin{cases} 1 & \text{if there exists } z \in \mathbb{Z} \text{ such that } v \times z \xleftrightarrow{B_{n+1}^{(3)}} v_{n+1}^{(2)} \times z_{v_{n+1}^{(2)}}, \\ 0 & \text{otherwise.} \end{cases}$$

Using the vertex transitive property, Lemma 4.1.1, and the alternative definition of $\omega_{\perp}^{(2)}$, we can prove the following theorem.

Theorem 4.2.8. *The growth process $\mathbf{G}^{(2)}$ is a Markov process.*

Recall that $\mathbf{G}^{(2)}$ is a stochastic process defined on the probability space $(\Omega^{(3)}, \mathcal{F}^{(3)}, P_q^{(3)})$. Informally, for each $n \in \mathbb{N}$, at step $n+1$ of $\mathbf{G}^{(2)}$, the vertex $v_{n+1}^{(2)}$ is determined by $\mathbf{G}_n^{(2)}$. Meanwhile, $B_{n+1}^{(2)}$, the set of edges that could possibly be added to the cluster is determined by $\mathbf{G}_n^{(2)}$ as well. Moreover, whether a certain subset of $B_{n+1}^{(2)}$ should be added to $C_{n+1}^{(2)}$ is determined by the configuration restricted to $B_{n+1}^{(3)}$, which is disjoint from $\bigcup_{i=1}^{n} B_i^{(3)}$. Thus, given $B_{n+1}^{(3)}$, whether edges in $B_{n+1}^{(2)}$ should be added to $C_{n+1}^{(2)}$ is conditionally independent of all the previous states of $\mathbf{G}^{(2)}$. The proof of

Theorem 4.2.8 would be intuitively simple if $B^{(2)}_{n+1}, v^{(2)}_{n+1}$, and $z_{v^{(2)}_{n+1}}$ were all determined by $\mathbf{G}^{(2)}_n$. However, the actual proof is more complicated because even though $v^{(2)}_{n+1}$ and $B^{(2)}_{n+1}$ can be obtained from $\mathbf{G}^{(2)}_n$, and that $z_{v^{(2)}_{n+1}}$ can not. In the following proof, we illustrate the intuition above while focusing on dealing with $z_{v^{(2)}_n}$ using the vertex transitive property.

Proof. Let $\mathcal{F}^{(2)}_n = \sigma(\mathbf{G}^{(2)}_1, ..., \mathbf{G}^{(2)}_n)$ be the natural filtration of $\mathbf{G}^{(2)}$ until step n. We prove that $P^{(3)}_q(\mathbf{G}^{(2)}_{n+1} \mid \mathcal{F}^{(2)}_n) = P^{(3)}_q(\mathbf{G}^{(2)}_{n+1} \mid \mathbf{G}^{(2)}_n)$ for each $n \in \mathbb{N}$. Assume that $A^{(2)}_n \neq A^{(2)}_{n+1}$, since the proof is trivial otherwise. Notice that $v^{(2)}_{n+1}$ and $B^{(2)}_{n+1}$ are both $\sigma(\mathbf{G}^{(2)}_n)$-measurable, and that $B^{(3)}_{n+1}$ is $\sigma(\mathbf{G}^{(2)}_n)$-measurable as well. By the definition of $\mathbf{G}^{(2)}$, we have

$$P^{(3)}_q(\mathbf{G}^{(2)}_{n+1} \mid \mathcal{F}^{(2)}_n) = P^{(3)}_q(\mathbf{G}^{(2)}_{n+1} \mid \mathbf{G}^{(2)}_n) = 0$$

if and only if

$$A^{(2)}_{n+1} \setminus A^{(2)}_n \neq \{v^{(2)}_{n+1}\} \text{ or } C^{(2)}_{n+1} \setminus C^{(2)}_n \not\subseteq B^{(2)}_{n+1}.$$

Otherwise, consider the situation that $A^{(2)}_{n+1} \setminus A^{(2)}_n = \{v^{(2)}_{n+1}\}$ and $C^{(2)}_{n+1} \setminus C^{(2)}_n \subseteq B^{(2)}_{n+1}$. Notice that $\{B^{(3)}_i\}^{n+1}_{i=1}$ are disjoint. Notice also that given $B^{(2)}_{n+1}, v^{(2)}_{n+1}$ and $z_{v^{(2)}_{n+1}}$, the indicators $\{\omega^{(2)}_\perp(e) : e \in B^{(2)}_{n+1}\}$ only depend on the configuration restricted to $B^{(3)}_{n+1}$, which is $\{\omega^{(3)}(e)\}_{e \in B^{(3)}_{n+1}}$. This makes $\{\omega^{(2)}_\perp(e)\}_{e \in B^{(2)}_{n+1}}$ conditionally independent of $\mathcal{F}^{(2)}_n$ given $B^{(2)}_{n+1}, v^{(2)}_{n+1}$ and $z_{v^{(2)}_{n+1}}$. Subsequently, since both $B^{(2)}_{n+1}$ and $v^{(2)}_{n+1}$ are $\sigma(\mathbf{G}^{(2)}_n)$-

measurable, and thus $\mathcal{F}_n^{(2)}$-measurable, we have

$$\begin{aligned}
&P_q^{(3)}(\mathbf{G}_{n+1}^{(2)} \mid \mathcal{F}_n^{(2)}) \\
=&P_q^{(3)}(\omega_\perp^{(2)}(e) = \mathbb{1}_{\{e \in C_{n+1}^{(2)} \setminus C_n^{(2)}\}} \text{ for each } e \in B_{n+1}^{(2)} \mid \mathcal{F}_n^{(2)}) \\
=&P_q^{(3)}(\omega_\perp^{(2)}(e) = \mathbb{1}_{\{e \in C_{n+1}^{(2)} \setminus C_n^{(2)}\}} \text{ for each } e \in B_{n+1}^{(2)} \mid \mathcal{F}_n^{(2)}, B_{n+1}^{(2)}, v_{n+1}^{(2)}).
\end{aligned}$$

Using the law of total probability by conditioning on $z_{v_{n+1}^{(2)}}$, and applying the vertex transitive property, we have

$$\begin{aligned}
&P_q^{(3)}(\mathbf{G}_{n+1}^{(2)} \mid \mathcal{F}_n^{(2)}) \\
=&\sum_{z \in \mathbb{Z}} P_q^{(3)}(\omega_\perp^{(2)}(e) = \mathbb{1}_{\{e \in C_{n+1}^{(2)} \setminus C_n^{(2)}\}} \text{ for each } e \in B_{n+1}^{(2)} \mid \mathcal{F}_n^{(2)}, B_{n+1}^{(2)}, v_{n+1}^{(2)}, z_{v_{n+1}^{(2)}} = z) \\
&\quad \times P_q^{(3)}(z_{v_{n+1}^{(2)}} = z \mid \mathcal{F}_n^{(2)}, B_{n+1}^{(2)}, v_{n+1}^{(2)}) \\
=&\sum_{z \in \mathbb{Z}} P_q^{(3)}(\omega_\perp^{(2)}(e) = \mathbb{1}_{\{e \in C_{n+1}^{(2)} \setminus C_n^{(2)}\}} \text{ for each } e \in B_{n+1}^{(2)} \mid \mathcal{F}_n^{(2)}, B_{n+1}^{(2)}, v_{n+1}^{(2)}, z_{v_{n+1}^{(2)}} = 0) \\
&\quad \times P_q^{(3)}(z_{v_{n+1}^{(2)}} = z \mid \mathcal{F}_n^{(2)}, B_{n+1}^{(2)}, v_{n+1}^{(2)}) \\
=&P_q^{(3)}(\omega_\perp^{(2)}(e) = \mathbb{1}_{\{e \in C_{n+1}^{(2)} \setminus C_n^{(2)}\}} \text{ for each } e \in B_{n+1}^{(2)} \mid \mathcal{F}_n^{(2)}, B_{n+1}^{(2)}, v_{n+1}^{(2)}, z_{v_{n+1}^{(2)}} = 0).
\end{aligned}$$

Given $B_{n+1}^{(2)}, v_{n+1}^{(2)}$, and $z_{v_{n+1}}$, by the conditional independence of $\{\omega_\perp^{(2)}(e)\}_{e \in B_{n+1}^{(2)}}$ and $\mathcal{F}_n^{(2)}$, we can remove $\mathcal{F}_n^{(2)}$ in the formula above, which gives us

$$\begin{aligned}
&P_q(\mathbf{G}_{n+1}^{(2)} | \mathcal{F}_n^{(2)}) \\
=&P_q^{(3)}(\omega_\perp^{(2)}(e) = \mathbb{1}_{\{e \in C_{n+1}^{(2)} \setminus C_n^{(2)}\}} \text{ for each } e \in B_{n+1}^{(2)} \mid B_{n+1}^{(2)}, v_{n+1}^{(2)}, z_{v_{n+1}^{(2)}} = 0).
\end{aligned}$$

Applying conditional independence of $\{\omega_\perp^{(2)}(e)\}_{e \in B_{n+1}^{(2)}}$ and $\mathbf{G}_n^{(2)}$, and then simplifying the equation using the statement that $B_{n+1}^{(2)}$ and $z_{v_{n+1}^{(2)}}$ are $\sigma(\mathbf{G}_n^{(2)})$-measurable, we

obtain

$$\begin{aligned}
&P_q^{(3)}(\mathbf{G}_{n+1}^{(2)} \mid \mathcal{F}_n^{(2)}) \\
=&P_q^{(3)}(\omega_\perp^{(2)}(e) = \mathbb{1}_{\{e \in C_{n+1}^{(2)} \setminus C_n^{(2)}\}} \text{ for each } e \in B_{n+1} \mid \mathbf{G}_n^{(2)}, B_{n+1}^{(2)}, v_{n+1}^{(2)}, z_{v_{n+1}^{(2)}} = 0) \\
=&P_q^{(3)}(\omega_\perp^{(2)}(e) = \mathbb{1}_{\{e \in C_{n+1}^{(2)} \setminus C_n^{(2)}\}} \text{ for each } e \in B_{n+1} \mid \mathbf{G}_n^{(2)}, z_{v_{n+1}^{(2)}} = 0) \\
=&P_q^{(3)}(\mathbf{G}_{n+1}^{(2)} \mid \mathbf{G}_n^{(2)}, z_{v_{n+1}^{(2)}} = 0)
\end{aligned}$$

Meanwhile, using a similar argument, for any $n \in \mathbb{N}$, we have

$$\begin{aligned}
&P_q^{(3)}(\mathbf{G}_{n+1}^{(2)} \mid \mathbf{G}_n^{(2)}) \\
=&\sum_{z \in \mathbb{Z}} P_q(\mathbf{G}_{n+1}^{(2)} \mid \mathbf{G}_n^{(2)}, z_{v_{n+1}^{(2)}} = z) P_q^{(3)}(z_{v_{n+1}^{(2)}} = z \mid \mathbf{G}_n^{(2)}) \\
=&\sum_{z \in \mathbb{Z}} P_q(\mathbf{G}_{n+1}^{(2)} \mid \mathbf{G}_n^{(2)}, z_{v_{n+1}^{(2)}} = 0) P_q^{(3)}(z_{v_{n+1}^{(2)}} = z \mid \mathbf{G}_n^{(2)}) \\
=&P_q^{(3)}(\mathbf{G}_{n+1}^{(2)} \mid \mathbf{G}_n^{(2)}, z_{v_{n+1}^{(2)}} = 0)
\end{aligned}$$

Thus, $P_q^{(3)}(\mathbf{G}_{n+1}^{(2)} \mid \mathcal{F}_n^{(2)}) = P_q(\mathbf{G}_{n+1}^{(2)} \mid \mathbf{G}_n^{(2)})$, which implies that $\mathbf{G}^{(2)}$ is a Markov process. □

4.2.2 Transition Probabilities of $\mathbf{G}^{(2)}$

For the Markov process $\mathbf{G}^{(2)}$, it is natural to ask for its transition probabilities, namely, the conditional joint distributions of $\{\omega_\perp^{(2)}(e) : e \in B_{n+1}^{(2)}\}$ given $\mathbf{G}_n^{(2)}$ for each $n \in \mathbb{N}$. Notice that $\mathbb{L}^3$ is vertex transitive. As a result, the joint distribution of $\{\omega_\perp^{(2)}(e) : e \in B_{n+1}^{(2)}\}$ is independent of the exact coordinates of $v_{n+1}^{(2)}$ and the value

of $z_{v_{n+1}^{(2)}}$. Additionally, the conditional joint distribution depends only on the number of edges in $B_{n+1}^{(2)}$. For instance, assume that there exists some $m, n \in \mathbb{N}$ such that both $B_{m+1}^{(2)} = \{e_1, e_2\}$ and $B_{n+1}^{(2)} = \{e_3, e_4\}$ contain two edges, satisfying that e_1 and e_2 are parallel, and e_3 and e_4 are perpendicular. The conditional joint distribution of $(\omega_\perp^{(2)}(e_1), \omega_\perp^{(2)}(e_2))$ given $\mathbf{G}_m^{(2)}$ is equal to the conditional joint distribution of $(\omega_\perp^{(2)}(e_3), \omega_\perp^{(2)}(e_4))$ given $\mathbf{G}_n^{(2)}$.

We provide an informal explanation of the argument above using a specific example illustrated by Figure 4.3 and 4.4. In Figure 4.3, where e_1 and e_2 are parallel, we pick a configuration on $\mathbb{L}^3$ restricted to $B_{m+1}^{(3)}$ satisfying $(\omega_\perp^{(2)}(e_1), \omega_\perp^{(2)}(e_2)) = (1, 1)$. Meanwhile, we can "bend" and "translate" this restricted configuration and obtain a new configuration restricted to $B_{n+1}^{(3)}$ (Figure 4.4). The new restricted configuration satisfies that for perpendicular e_3 and e_4, $(\omega_\perp^{(2)}(e_3), \omega_\perp^{(2)}(e_4)) = (1, 1)$. In other words, there is a bijection between the two sets of restricted configurations. The restricted configurations in the former set add parallel edges e_1 and e_2 to $C_{m+1}^{(2)}$, whereas the restricted configuration in the latter set add perpendicular edges e_3 and e_4 to $C_{n+1}^{(2)}$. Consequently, the conditional joint distribution of $(\omega_\perp^{(2)}(e_1), \omega_\perp^{(2)}(e_2)) = (1, 1)$ is the same as the conditional probability of $(\omega_\perp^{(2)}(e_3), \omega_\perp^{(2)}(e_4)) = (1, 1)$, given $\mathbf{G}_m^{(2)}$ and $\mathbf{G}_n^{(2)}$, respectively (Remark 4.2.9). The idea can be generalized to other values in $\{0, 1\}^2$ and other possibilities of $B_{n+1}^{(2)}$.

By the reasoning above, it is justifiable for us to use the notation $Q^{(2)}_{|B^{(2)}_{n+1}|,q}$ as the conditional distribution of $\{\omega^{(2)}_{\perp}(e) : e \in B^{(2)}_{n+1}\}$ given $\mathbf{G}^{(2)}_n$, with the corresponding sample space being $\{0,1\}^{|B^{(2)}_{n+1}|}$ (Figure 4.5–4.7). For simplicity, we shall refer to $\{Q^{(2)}_{m,q}\}_{(m,q)\in\{1,2,3\}\times[0,1]}$ as $Q^{(2)}$, indicating that the corresponding statement holds for all $(m,q) \in \{1,2,3\} \times [0,1]$.

Remarks 4.2.9.

(a) Readers may have noticed that the argument above is not rigorous. Our illustration that a bijection exists between the two sets of restricted configurations does not guarantee that these two sets share the same probabilities under $P^{(3)}_q$ measure.

(b) A rigorous proof of this argument is similar to the proof of Theorem 4.2.4. The basic idea is to prove that for any positive cylinder set, its probability under $P^{(3)}_q$ measure is invariant under the "bend" and "translate" operations. A detailed proof is omitted.

The transition probability of $\mathbf{G}^{(2)}$ can be explicitly expressed as:

$$P_q^{(3)}(\mathbf{G}_{n+1}^{(2)}|\mathbf{G}_n^{(2)}) = \begin{cases} 0 & \text{if } A_{n+1}^{(2)} \setminus A_n^{(2)} \neq \{v_{n+1}^{(2)}\}, \\ 0 & \text{if } C_{n+1}^{(2)} \setminus C_n^{(2)} \not\subseteq B_{n+1}^{(2)}, \\ Q^{(2)}_{|B_{n+1}|,q}(\mathbf{e}_{|C_{n+1}^{(2)} \setminus C_n^{(2)}|,|B_{n+1}^{(2)}|}) & \text{otherwise,} \end{cases} \tag{4.1}$$

where $\mathbf{e}_{|C_{n+1}^{(2)} \setminus C_n^{(2)}|,|B_{n+1}^{(2)}|}$ is a length $|B_{n+1}^{(2)}|$ vector with its first $|C_{n+1}^{(2)} \setminus C_n^{(2)}|$ entries equal to 1 and the rest of its entries equal to 0.

The distributions $Q_{m,q}^{(2)}, m \in \{1,2,3\}$ satisfy the following property.

Lemma 4.2.10. *$Q_{m,q}^{(2)}$ is a marginal distribution of $Q_{3,q}^{(2)}$ for each $m \leqslant 2$ and $q \in [0,1]$.*

Proof. We prove that the lemma holds true when $m = 2$. For $m = 1$, it can be proved by similar reasoning.

Consider a (deterministic) exploration region B such that $\text{proj}(B) = \{e_1, e_2\}$. We add some extra vertices and edges to B to form B' so that B' is also an exploration region and $\text{proj}(B') = \{e_1, e_2, e_3\}$. We let each extra edge be open independently with probability q. We assume $e_i = \{u, u_i\}$ for all $i \in \{1,2,3\}$. For each $\boldsymbol{e} \in \{0,1\}^{(2)}$, by definition of $Q^{(2)}$ measure and the vertex transitive property, we have

$$Q_{2,q}^{(2)}(\boldsymbol{e}) = P_q^{(3)}((u \times 0 \overset{B}{\leftrightarrow} u_i \times \mathbb{Z}) = e_i, i \in \{1,2\})$$

By the geometry of B and B', if there is an open path in B' connecting $u \times 0$ to some vertex in $u_i \times \mathbb{Z}$, then such path uses only edges in B. Meanwhile, if there is no open path in B connecting $u \times 0$ to any vertex in $u_i \times \mathbb{Z}$, then such path does not exist in B' as well. Thus,

$$\begin{aligned}
&P_q^{(3)}((u \times 0 \overset{B}{\longleftrightarrow} u_i \times \mathbb{Z}) = e_i, i \in \{1,2\}) \\
&= P_q^{(3)}((u \times 0 \overset{B'}{\longleftrightarrow} u_i \times \mathbb{Z}) = e_i, i \in \{1,2\}) \\
&= P_q^{(3)}((u \times 0 \overset{B'}{\longleftrightarrow} u_i \times \mathbb{Z}) = e_i, i \in \{1,2\}, (u \times 0 \overset{B'}{\longleftrightarrow} u_3 \times \mathbb{Z}) = 0) \\
&\quad + P_q^{(3)}((u \times 0 \overset{B'}{\longleftrightarrow} u_i \times \mathbb{Z}) = e_i, i \in \{1,2\}, (u \times 0 \overset{B'}{\longleftrightarrow} u_3 \times \mathbb{Z}) = 1) \\
&= Q_{3,q}^{(2)}((e_1, e_2, 0)) + Q_{3,q}^{(2)}((e_1, e_2, 1)),
\end{aligned}$$

where $u \times 0 \overset{B}{\longleftrightarrow} u_i \times \mathbb{Z}$ is the indicator that there exists $z \in \mathbb{Z}$ such that $u \times 0 \overset{B}{\longleftrightarrow} u_i \times z$. Consequently, $Q_{2,q}^{(2)}$ is a marginal distribution of $Q_{3,q}^{(2)}$. □

Lemma 4.2.10 allows us to focus only on the calculation of $Q_{3,q}^{(2)}$. The detailed calculations are rather complicated. We provide them in Chapter 5. Here, we present our final results:

$$
\begin{aligned}
&Q^{(2)}_{3,q}(1,1,1)\\
=&\frac{(1-\bar{q})^3(1-\bar{q}^3+2\bar{q}^4-\bar{q}^5)\times}{(1+\bar{q}+\bar{q}^2+\bar{q}^3-2\bar{q}^4-3\bar{q}^5+2\bar{q}^6+\bar{q}^7+2\bar{q}^8-4\bar{q}^9+\bar{q}^{10})}\\
&\frac{}{[(1-\bar{q}+\bar{q}^2)(1-\bar{q}^2+\bar{q}^3)(1-\bar{q}^3+\bar{q}^4)]^2}
\end{aligned}
$$

$$
\begin{aligned}
&Q^{(2)}_{3,q}(1,1,0)=Q^{(2)}_{3,q}(1,0,1)=Q^{(2)}_{3,q}(0,1,1)\\
=&\frac{(1-\bar{q})^2\bar{q}^3\times}{(1+2\bar{q}^2-4\bar{q}^3+2\bar{q}^4+4\bar{q}^6-8\bar{q}^7+7\bar{q}^8-6\bar{q}^9+6\bar{q}^{10}-4\bar{q}^{11}+\bar{q}^{12})}\\
&\frac{}{[(1-\bar{q}+\bar{q}^2)(1-\bar{q}^2+\bar{q}^3)(1-\bar{q}^3+\bar{q}^4)]^2}
\end{aligned}
$$

$$
\begin{aligned}
&Q^{(2)}_{3,q}(1,0,0)=Q^{(2)}_{3,q}(0,1,0)=Q^{(2)}_{3,q}(0,0,1)\\
=&\frac{(1-\bar{q})\bar{q}^4(1-\bar{q}^5+2\bar{q}^6-\bar{q}^7)}{[(1-\bar{q}^2+\bar{q}^3)(1-\bar{q}^3+\bar{q}^4)]^2}
\end{aligned}
$$

$$
\begin{aligned}
&Q^{(2)}_{3,q}(0,0,0)\\
=&\frac{\bar{q}^5}{(1-\bar{q}^3+\bar{q}^4)^2},
\end{aligned}
$$

where from simplicity of the integer coefficients, we denote $(1-q)$ by $\bar{q}$.

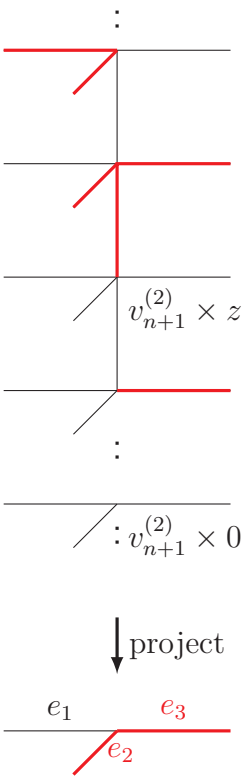

Figure 4.1: An illustration of ω restricted to $I[v_{n+1}^{(2)} \times \mathbb{Z}] \setminus I[(\bigcup_{C_n^{(2)}} \setminus \{v_{n+1}^{(2)}\}) \times \mathbb{Z}]$. In the specific case that $A_{n+1}^{(2)} \setminus A_n^{(2)} = \{v_{n+1}^{(2)}\}$, $B_{n+1}^{(2)}$ has three "branches", $z_{v_{n+1}^{(2)}} = z$ and $C_{n+1}^{(2)} \setminus C_n^{(2)} = \{e_2, e_3\}$, the restricted configuration transits from state $\mathbf{G}_n^{(2)}$ to state $\mathbf{G}_{n+1}^{(2)}$.

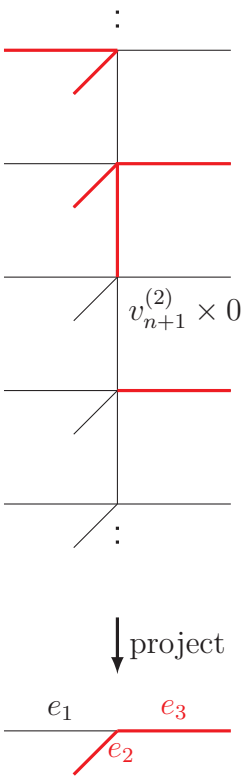

Figure 4.2: An illustration of $T_{\boldsymbol{z}}(\omega)$ restricted to $I[v_{n+1}^{(2)} \times \mathbb{Z}] \setminus I[(\bigcup_{C_n^{(2)}} \setminus \{v_{n+1}^{(2)}\}) \times \mathbb{Z}]$, obtained from translating the restricted configuration in Figure 4.1 by the vector $(0, 0, -z)$. Given $z_{v_{n+1}^{(2)}} = 0$, this restricted configuration transits from state $\mathbf{G}_n^{(2)}$ to state $\mathbf{G}_{n+1}^{(2)}$.

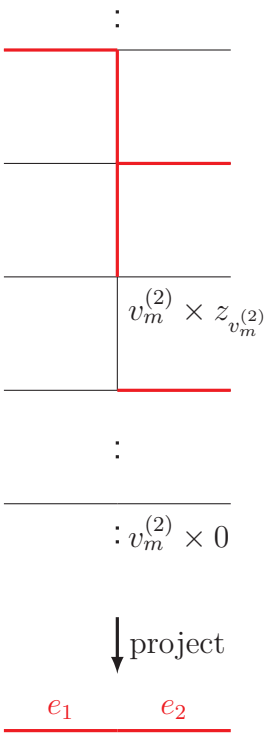

Figure 4.3: An illustration of a configuration restricted to $B_{m+1}^{(3)} = \{e_1, e_2\}$, satisfying $(\omega_\perp^{(2)}(e_1), \omega_\perp^{(2)}(e_2)) = (1, 1)$. Open edges in the configuration are marked in red and closed edges are marked in black.

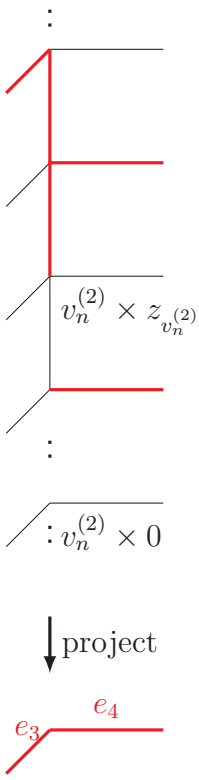

Figure 4.4: We "bend" and "translate" the restricted configuration in Figure 4.3 and obtain a new configuration restricted to $B_{n+1}^{(3)}$. The new "restricted" configuration satisfies $(\omega_\perp^{(2)}(e_3), \omega_\perp^{(2)}(e_4)) = (1, 1)$.

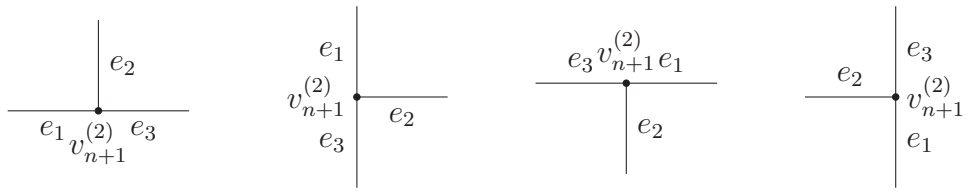

Figure 4.5: Four possible cases of $B_{n+1}^{(2)}$ satisfying $|B_{n+1}^{(2)}| = 3$. The joint distributions of $(\omega_{\perp}^{(2)}(e_1), \omega_{\perp}^{(2)}(e_2), \omega_{\perp}^{(2)}(e_3))$ in all these four cases are the same, namely, $Q_{3,q}^{(2)}$.

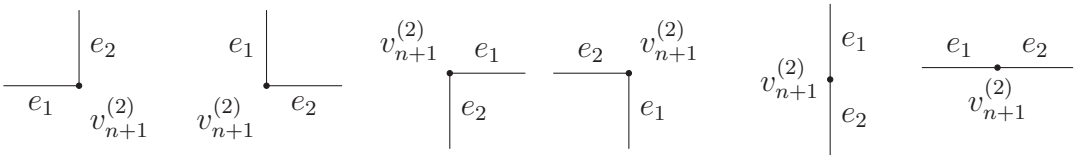

Figure 4.6: Six possible cases of $B_{n+1}^{(2)}$ satisfying $|B_{n+1}^{(2)}| = 2$. The joint distributions of $(\omega_{\perp}^{(2)}(e_1), \omega_{\perp}^{(2)}(e_2))$ in all these six cases are the same, namely, $Q_{2,q}^{(2)}$.

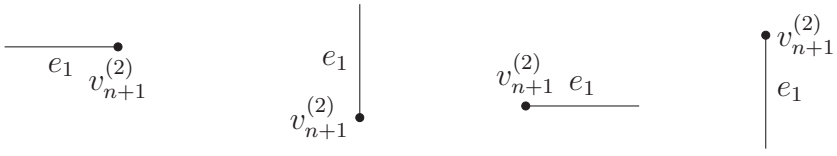

Figure 4.7: Four possible cases of $B_{n+1}^{(2)}$ satisfying $|B_{n+1}^{(2)}| = 1$. The distributions of $\omega_{\perp}^{(2)}(e_1)$ in all these four cases are the same, namely, $Q_{1,q}^{(2)}$.

Chapter 5

Calculation of Transition Probabilities

In Chapter 3, we introduced the the projected growth process $\mathbf{G}^{(2)}$ associated with $D(\omega^{(3)})$. Later in Chapter 4, we proved that $\mathbf{G}^{(2)}$ is Markovian. In this chapter, we provide detailed calculations of its transition probabilities.

5.1 Calculation of Transition Probabilities

Recall that in Chapter 4, the transition probabilities of $\mathbf{G}^{(2)}$ can be explicitly expressed as:

$$P_q^{(3)}(\mathbf{G}_{n+1}^{(2)}|\mathbf{G}_n^{(2)}) = \begin{cases} 0 & \text{if } A_{n+1}^{(2)} \setminus A_n^{(2)} \neq \{v_{n+1}^{(2)}\}, \\ 0 & \text{if } C_{n+1}^{(2)} \setminus C_n^{(2)} \not\subseteq B_{n+1}^{(2)}, \\ Q^{(2)}_{|B_{n+1}|,q}(\mathbf{e}_{|C_{n+1}^{(2)} \setminus C_n^{(2)}|,|B_{n+1}^{(2)}|}) & \text{otherwise,} \end{cases} \tag{5.1}$$

where $\mathbf{e}_{|C_{n+1}^{(2)} \setminus C_n^{(2)}|,|B_{n+1}^{(2)}|}$ is a length $|B_{n+1}^{(2)}|$ vector with the first $|C_{n+1}^{(2)} \setminus C_n^{(2)}|$ entries equal to 1 and the rest of the entries equal to 0, and $Q_{m,q}^{(2)}$ are probability distributions on $\{0,1\}^m$ with $m \in \{1,2,3\}$.

We briefly go through the definition of $Q_{m,q}^{(2)}$. For $m = 3$, consider a configuration $\omega^{(3)} \in \Omega^{(3)}$. A path in $\mathbb{L}^3$ is an open path if all its edges have $\omega^{(3)}$-value 1. Consider some $n \in \mathbb{N}$ such that at step n of $\mathbf{G}^{(2)}$, $B_n^{(2)}$ contains three edges in $\mathbb{E}^2$. The corresponding $B_n^{(3)}$ consists of infinitely many layers and the column of edges at $v_n^{(3)}$. For each layer, there is a set containing three edges which form a T-shape (Figure 5.1). Denote the three edges in $B_n^{(2)}$ by $e_i = \{v_n^{(2)}, u_i\}, i = 1,2,3$. Recall that if there exists an L-shaped open path in $B_n^{(3)}$ by which $v_n^{(2)} \times z_{v_n^{(2)}}$ is connected to $u_i \times z_{u_i}$ for some $z_{u_i} \in \mathbb{Z}$, then $\omega_\perp^{(2)}(e_i) = 1$ (Figure 5.2). At step n, $\mathbf{G}^{(2)}$ explores from vertex $v_n^{(2)}$ by considering if the three edges $B_n^{(2)} = \{e_1, e_2, e_3\}$ incident to $v_n^{(2)}$ have the corresponding $\omega_\perp^{(2)}$-values equal to 1. The joint distribution of $(\omega_\perp^{(2)}(e_1), \omega_\perp^{(2)}(e_2), \omega_\perp^{(2)}(e_3))$ is $Q_{3,q}^{(2)}$. The distributions $Q_{1,q}^{(2)}$ and $Q_{2,q}^{(2)}$ are defined analogously.

In this chapter, we focus on the calculations of $Q_{3,q}^{(2)}$ since $Q_{1,q}^{(2)}$ and $Q_{2,q}^{(2)}$ are cor-

responding marginal distributions of $Q^{(2)}_{3,q}$. Moreover, we shall justify in Chapter 6 that stochastic dominance of $Q^{(2)}_{3,q}$ and $Q_{3,p}$ is sufficient for establishing a step-wise coupling in the construction of a "coupled" growth process $\mathbf{G}^{(c)}$ on $\mathbb{Z}^2$.

In order to calculate this joint distribution, one straightforward idea is to identify whether each open path connecting $v^{(2)}_n \times z_{v^{(2)}_n}$ to $u_i \times z_{u_i}$ goes "up" or "down" along the vertical path in $B^{(3)}_n$, i.e., whether $z_{u_i} > z_{v^{(2)}_n}$ or $z_{u_i} < z_{v^{(2)}_n}$ for each $i \in \{1,2,3\}$ (Figure 5.2). This leads us to define the following random variables. Let $\omega^+_\perp(e_i)$ be the indicator that there exists an open path in $B^{(3)}_n$ by which $v^{(2)}_n \times z_{v^{(2)}_n}$ is connected to $u_i \times z$ for some $z > z_{v^{(2)}_n}$. Similarly, let $\omega^-_\perp(e_i)$ be the indicator that there exists an open path in $B^{(3)}_n$ by which $v^{(2)}_n \times z_{v^{(2)}_n}$ is connected to $u_i \times z$ for some $z < z_{v^{(2)}_n}$.

For simplicity, we introduce vector representations of the vectors of interest. Let $\boldsymbol{\omega}^{(2)}_\perp := (\omega^{(2)}_\perp(e_1), \omega^{(2)}_\perp(e_2), \omega^{(2)}_\perp(e_3))$ be a random vector on $\Omega^{(3)}$ taking $\{0,1\}^3$ values. Our goal is to calculate the joint distribution of $\boldsymbol{\omega}^{(2)}_\perp$. From the previous paragraph, we need to study the joint distributions of the following two vectors: $\boldsymbol{\omega}^-_\perp := (\omega^-_\perp(e_1), \omega^-_\perp(e_2), \omega^-_\perp(e_3))$ and $\boldsymbol{\omega}^+_\perp := (\omega^+_\perp(e_1), \omega^+_\perp(e_2), \omega^+_\perp(e_3))$. Both random vectors are defined on $\Omega^{(3)}$. To further simplify our notation, for any $\boldsymbol{x} \in \{0,1\}^3$, let $P_{\boldsymbol{\omega}^{(2)}_\perp}(\boldsymbol{x}) := P^{(3)}_q(\boldsymbol{\omega}^{(2)}_\perp = \boldsymbol{x}) = Q^{(2)}_{3,q}(\boldsymbol{x})$ be the joint distribution of $\boldsymbol{\omega}^{(2)}_\perp$. Analogously, let $P_{\boldsymbol{\omega}^+_\perp}$ and $P_{\boldsymbol{\omega}^-_\perp}$ be the joint distributions of $\boldsymbol{\omega}^+_\perp$ and $\boldsymbol{\omega}^-_\perp$, respectively. By symmetry and vertex transitivity, it is trivial that $P_{\boldsymbol{\omega}^-_\perp}(\boldsymbol{x}) = P_{\boldsymbol{\omega}^+_\perp}(\boldsymbol{x})$ for each $\boldsymbol{x} \in \{0,1\}^3$. In

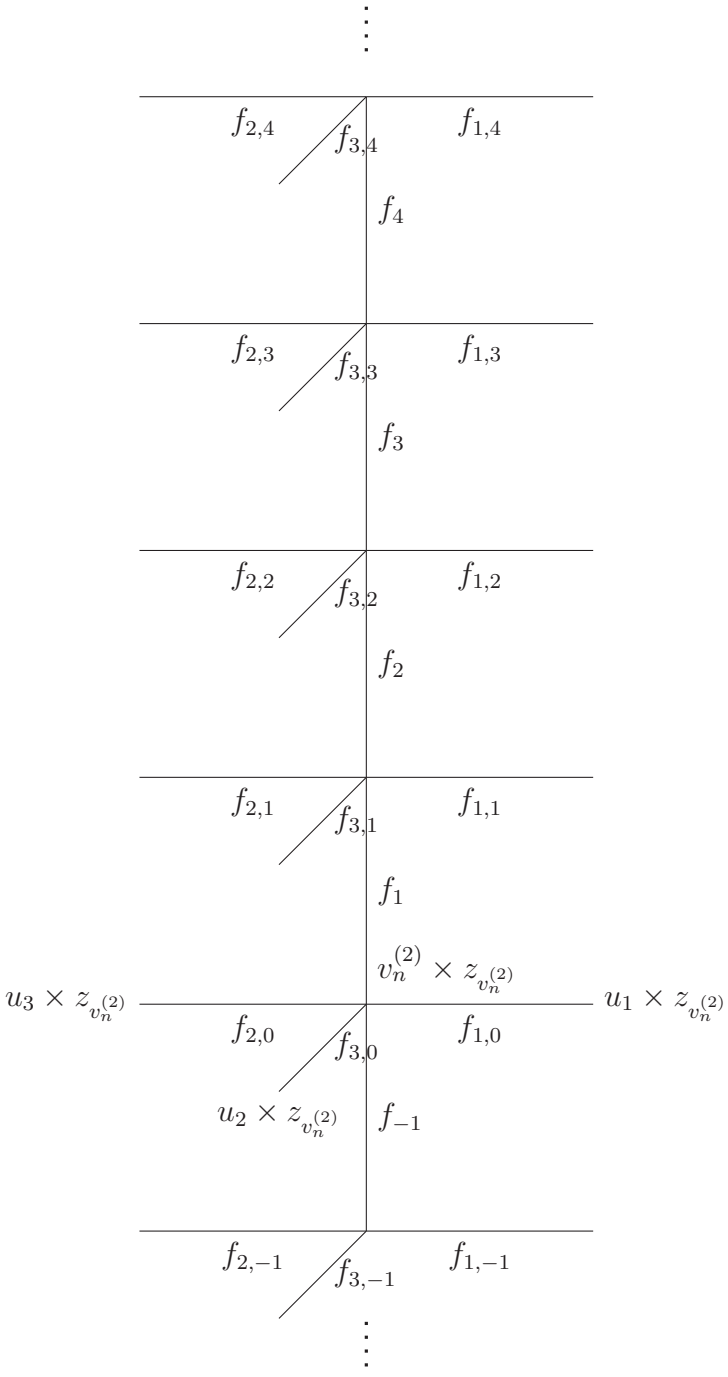

Figure 5.1: An illustration of $B_n^{(3)}$ where the corresponding $B_n^{(2)}$ contains three edges. Edges in $B_n^{(3)}$ are labeled to help illustrate the calculation procedure.

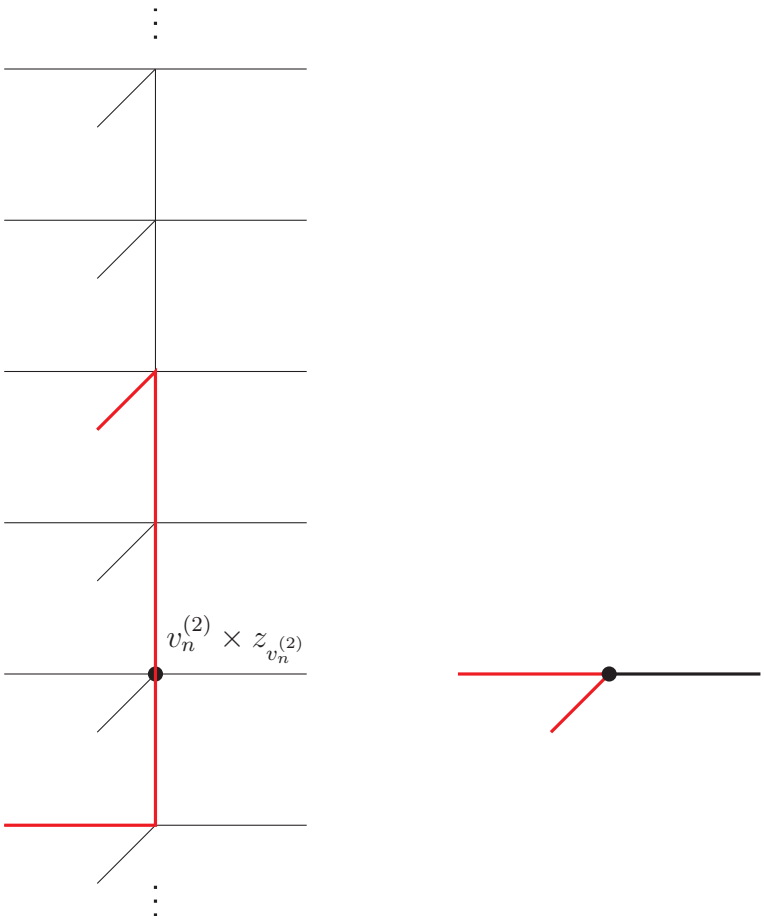

Figure 5.2: An illustration of the definition of $\omega_\perp^{(2)}(e_i)$. The red edges in the left side of the figure represent open edges in $B_n^{(3)}$. They form two L-shaped open paths, both of which start from $v_n^{(2)} \times z_{v_n^{(2)}}$. One of the open paths goes "up" along the vertical edges, while the other goes "down" along the vertical edges. Correspondingly, we have the $\omega_\perp^{(2)}$-values of edges in $B_n^{(2)}$ illustrated in the right side of the figure with the red edges representing edges with $\omega_\perp^{(2)}$-values equal to 1.

terms of the notations above, to calculate $P_{\boldsymbol{\omega}_\perp^{(2)}}$, we calculate $P_{\boldsymbol{\omega}_\perp^+}$ first. This is done in Section 5.1.1. We then use the result to obtain $P_{\boldsymbol{\omega}_\perp^{(2)}}$, which is described in Section 5.1.2.

5.1.1 Calculation of $P_{\boldsymbol{\omega}_\perp^+}$

We define an equivalence relation on $\{0,1\}^3$ in which two vectors are equivalent if and only if they have the same number of 1's. More formally, we define the equivalence relation as follows.

Definition 5.1.1 (Equivalence relation on $\{0,1\}^m$)**.** Two vectors $\boldsymbol{x}, \boldsymbol{y}$ in $\{0,1\}^m$ are equivalent, denoted by $\boldsymbol{x} \sim \boldsymbol{y}$, if and only if the numbers of 1's in them are equal.

By symmetry, to obtain the distribution of $\boldsymbol{\omega}_\perp^+$, it is sufficient that we calculate the probabilities of $\boldsymbol{\omega}_\perp^{(2)}$ taking values of the class representatives, i.e., $P_{\boldsymbol{\omega}_\perp^+}(\boldsymbol{e}_{0,3}), P_{\boldsymbol{\omega}_\perp^+}(\boldsymbol{e}_{1,3})$, $P_{\boldsymbol{\omega}_\perp^+}(\boldsymbol{e}_{2,3})$ and $P_{\boldsymbol{\omega}_\perp^+}(\boldsymbol{e}_{3,3})$, where $\mathbf{e}_{i,j}$ is a length j vector with the first i entries equal to 1 and the rest of the entries equal to 0. We label the edges of $B_n^{(3)}$ as illustrated in Figure 5.1, and let H be the largest positive integer such that the edges $f_1, ..., f_H$ are all open. By convention, we let $H = 0$ if f_1 is closed. We calculate $P_{\boldsymbol{\omega}_\perp^+}(\boldsymbol{e}_{0,3}), P_{\boldsymbol{\omega}_\perp^+}(\boldsymbol{e}_{1,3}), P_{\boldsymbol{\omega}_\perp^+}(\boldsymbol{e}_{2,3})$ and $P_{\boldsymbol{\omega}_\perp^+}(\boldsymbol{e}_{3,3})$ by conditioning on H. For instance, we notice that $P_q^{(3)}(\boldsymbol{\omega}_\perp^+ = \boldsymbol{e}_{0,3}|H) = P_q^{(3)}(f_{i,j}$ is closed for each $i \in \{1,2,3\}, 1 \leqslant j \leqslant H) = (1-q)^{3H}$. We further notice that $H+1$ follows a geometric distribution with

success probability $1-q$. These lead us to the following results:

$$\begin{aligned} P_{\boldsymbol{\omega}_\perp^+}(\boldsymbol{e}_{0,3}) &= \sum_{i=0}^{\infty} P_q^{(3)}(\boldsymbol{\omega}_\perp^+ = \boldsymbol{e}_{0,3} | H=i) P_q^{(3)}(H=i) \\ &= \sum_{i=0}^{\infty} (1-q)^{3i} \cdot q^i (1-q) \\ &= (1-q) \sum_{i=0}^{\infty} \left[q(1-q)^3 \right]^i \\ &= \frac{1-q}{1-q(1-q)^3}. \end{aligned}$$

In general, for $k \in \{1,2,3\}$, we have

$$\begin{aligned} & P_q^{(3)}(\omega_\perp^+(e_k) = 0 \mid H=i) \\ &= P_q^{(3)}(f_{k,j} \text{ is closed for each } 1 \leqslant j \leqslant i) \\ &= (1-q)^i. \end{aligned}$$

Since given H, $\omega_\perp^+(e_i)$ depends on the $\omega^{(3)}$-values of $\{f_{i,j}\}_{j=1}^{H}$ only, we also have

$\omega_\perp^+(e_1), \omega_\perp^+(e_2), \omega_\perp^+(e_3)$ are conditionally independent given H. Thus, we obtain:

$$
\begin{aligned}
& P_{\boldsymbol{\omega}_\perp^+}(\boldsymbol{e}_{1,3}) \\
&= \sum_{i=0}^{\infty} P_q^{(3)}(\boldsymbol{\omega}_\perp^+ = \boldsymbol{e}_{1,3} | H = i) P_q^{(3)}(H = i) \\
&= \sum_{i=0}^{\infty} (1-q)^{2i} [1 - (1-q)^i] \cdot q^i (1-q) \\
&= (1-q) \sum_{i=0}^{\infty} \left[q(1-q)^2 \right]^i - (1-q) \sum_{i=0}^{\infty} \left[q(1-q)^3 \right]^i \\
&= \frac{1-q}{1-q(1-q)^2} - \frac{1-q}{1-q(1-q)^3},
\end{aligned}
$$

$$
\begin{aligned}
& P_{\boldsymbol{\omega}_\perp^+}(\boldsymbol{e}_{2,3}) \\
&= \sum_{i=0}^{\infty} P_q^{(3)}(\boldsymbol{\omega}_\perp^+ = \boldsymbol{e}_{2,3} | H = i) P_q^{(3)}(H = i) \\
&= \sum_{i=0}^{\infty} (1-q)^i [1 - (1-q)^i]^2 \cdot q^i (1-q) \\
&= \sum_{i=0}^{\infty} (1-q)^i \left[1 - 2(1-q)^i + (1-q)^{2i} \right] \cdot q^i (1-q) \\
&= (1-q) \sum_{i=0}^{\infty} \left[q(1-q) \right]^i - 2(1-q) \sum_{i=0}^{\infty} \left[q(1-q)^2 \right]^i + (1-q) \sum_{i=0}^{\infty} \left[q(1-q)^3 \right]^i \\
&= \frac{1-q}{1-q(1-q)} - \frac{2(1-q)}{1-q(1-q)^2} + \frac{1-q}{1-q(1-q)^3},
\end{aligned}
$$

$$
\begin{aligned}
& P_{\boldsymbol{\omega}_\perp^+}(\boldsymbol{e}_{3,3}) \\
&= \sum_{i=0}^{\infty} P_q^{(3)}(\boldsymbol{\omega}_\perp^+ = \boldsymbol{e}_{3,3} | H = i) P_q^{(3)}(H = i) \\
&= \sum_{i=0}^{\infty} [1 - (1-q)^i]^3 \cdot q^i (1-q) \\
&= \sum_{i=0}^{\infty} \left[1 - 3(1-q)^i + 3(1-q)^{2i} - (1-q)^{3i}\right] \cdot q^i (1-q) \\
&= (1-q) \sum_{i=0}^{\infty} q^i - 3(1-q) \sum_{i=0}^{\infty} \left[q(1-q)\right]^i + 3(1-q) \sum_{i=0}^{\infty} \left[q(1-q)^2\right]^i \\
&\quad - (1-q) \sum_{i=0}^{\infty} \left[q(1-q)^3\right]^i \\
&= 1 - \frac{3(1-q)}{1-q(1-q)} + \frac{3(1-q)}{1-q(1-q)^2} - \frac{1-q}{1-q(1-q)^3}.
\end{aligned}
$$

5.1.2 Calculation of $P_{\boldsymbol{\omega}_\perp^{(2)}}$

Using $P_{\boldsymbol{\omega}_\perp^+}$, we are able to calculate $P_{\boldsymbol{\omega}_\perp^{(2)}}$, which is the probability distribution of $\boldsymbol{\omega}_\perp^{(2)}$. We focus on the calculation of $P_{\boldsymbol{\omega}_\perp^{(2)}}(\boldsymbol{e}_{0,3}), P_{\boldsymbol{\omega}_\perp^{(2)}}(\boldsymbol{e}_{1,3}), P_{\boldsymbol{\omega}_\perp^{(2)}}(\boldsymbol{e}_{2,3})$ and $P_{\boldsymbol{\omega}_\perp^{(2)}}(\boldsymbol{e}_{3,3})$. To do so, we condition on $\boldsymbol{\omega} := (\omega^{(3)}(f_{1,0}), \omega^{(3)}(f_{2,0}), \omega^{(3)}(f_{3,0}))$, where $f_{i,0}$ is the edge in $\mathbb{E}^3$ incident to $v_n^{(2)} \times z_{v_n^{(2)}}$ satisfying $\mathrm{proj}(f_{i,0}) = e_i$. For instance, we have

$$
\begin{aligned}
P_{\boldsymbol{\omega}_\perp^{(2)}}(\boldsymbol{e}_{0,3} | \boldsymbol{\omega} = \boldsymbol{e}_{0,3}) &= P_q^{(3)}(\boldsymbol{\omega}_\perp^{(2)} = \boldsymbol{e}_{0,3} | \boldsymbol{\omega} = \boldsymbol{e}_{0,3}) \\
&= P_q^{(3)}(\boldsymbol{\omega}_\perp^+ = \boldsymbol{e}_{0,3}, \boldsymbol{\omega}_\perp^- = \boldsymbol{e}_{0,3}) \\
&= P_{\boldsymbol{\omega}_\perp^+}(\boldsymbol{e}_{0,3})^2,
\end{aligned}
$$

where the last equation is by the independence of $\boldsymbol{\omega}_\perp^+$ and $\boldsymbol{\omega}_\perp^-$. Meanwhile, we have

$$P_{\boldsymbol{\omega}_\perp^{(2)}}(\boldsymbol{e}_{0,3}|\boldsymbol{\omega} = \boldsymbol{x}) = 0 \text{for each } \boldsymbol{x} \in \{0,1\}^3 \setminus \{\boldsymbol{e}_{0,3}\}.$$

Using $P_q^{(3)}(\boldsymbol{\omega} = \boldsymbol{e}_{0,3}) = (1-q)^3$, we get

$$P_{\boldsymbol{\omega}_\perp^{(2)}}(\boldsymbol{e}_{0,3}) = (1-q)^3 \cdot P_{\boldsymbol{\omega}_\perp^+}(\boldsymbol{e}_{0,3})^2.$$

Generally, from the definition of $\boldsymbol{\omega}_\perp, \boldsymbol{\omega}_\perp^+$, and $\boldsymbol{\omega}_\perp^-$, we have $\omega_\perp^{(2)}(e_i) = 1$ if and only if at least one of the three following conditions hold: $\omega^{(3)}(f_{i,0}) = 1$, $\omega_\perp^-(e_i) = 1$, or $\omega_\perp^+(e_i) = 1$. Thus we have, $\omega_\perp^{(2)}(e_i) = \max\{\omega_\perp^+(e_i), \omega_\perp^-(e_i), \omega^{(3)}(f_{i,0})\}$, for $i \in \{1,2,3\}$. Using the above argument, we represent the distribution of $\boldsymbol{\omega}_\perp$ in terms of $P_{\boldsymbol{\omega}_\perp^+}(\boldsymbol{e}_{i,3})$, where $i \in \{0,1,2,3\}$.

We then substitute in the values of $P_{\boldsymbol{\omega}_\perp^+}$ given in the previous subsection, and obtain the distribution of $\boldsymbol{\omega}_\perp$ in terms of q. Unfortunately, the calculation is too complicated to be carried out by hand. We input our partial results into MATLAB, and let the computer finish the calculations. Here, we provide pseudocode illustrating the ideas above. A complete version of the program is shown in the Appendix.

We briefly explain the pseudocode listed in Algorithm 1. From line 1 to 4, we implement the idea of calculating the distribution of $\boldsymbol{\omega}_\perp^+$. From line 5 to 7, we run through all the possible values of $\boldsymbol{\omega}_\perp^+, \boldsymbol{\omega}_\perp^-$, and $\boldsymbol{\omega}$. Given $\boldsymbol{\omega}_\perp^+ = \boldsymbol{x}_1, \boldsymbol{\omega}_\perp^- = \boldsymbol{x}_2$, and $\boldsymbol{\omega} = \boldsymbol{x}_3$, the corresponding $\boldsymbol{\omega}_\perp^{(2)} = \boldsymbol{x} := (\boldsymbol{x}_1 \vee \boldsymbol{x}_2) \vee \boldsymbol{x}_3$, where $\vee$ is the logical

Algorithm 1 Calculation of $P_{\boldsymbol{\omega}_\perp^{(2)}}$

1: **for all** $\boldsymbol{x} \in \{0,1\}^3$ **do**

2: $\quad n \leftarrow$ number of 1's in $\boldsymbol{x}$

3: $\quad P_{\boldsymbol{\omega}}(\boldsymbol{x}) \leftarrow q^n(1-q)^{3-n}$

4: $\quad P_{\boldsymbol{\omega}_\perp^+}(\boldsymbol{x}) \leftarrow \sum_{i=0}^{\infty} q^i(1-q)\left[1-(1-q)^i\right]^n\left[(1-q)^i\right]^{3-n}$

5: **for all** $\boldsymbol{x}_1 \in \{0,1\}^3$ **do**

6: $\quad$ **for all** $\boldsymbol{x}_2 \in \{0,1\}^3$ **do**

7: $\quad\quad$ **for all** $\boldsymbol{x}_3 \in \{0,1\}^3$ **do**

8: $\quad\quad\quad \boldsymbol{x} \leftarrow (\boldsymbol{x}_1 \vee \boldsymbol{x}_2) \vee \boldsymbol{x}_3$

9: $\quad\quad\quad P_{\boldsymbol{\omega}_\perp^{(2)}}(\boldsymbol{x}) \leftarrow P_{\boldsymbol{\omega}_\perp^{(2)}}(\boldsymbol{x}) + P_{\boldsymbol{\omega}_\perp^+}(\boldsymbol{x}_1) \cdot P_{\boldsymbol{\omega}_\perp^+}(\boldsymbol{x}_2) \cdot P_{\boldsymbol{\omega}}(\boldsymbol{x}_3)$

return $P_{\boldsymbol{\omega}_\perp^{(2)}}$

operation "or". This makes each entry in $\boldsymbol{x}$ the maximum of the corresponding entries in vector $\boldsymbol{x}_1$, $\boldsymbol{x}_2$ and $\boldsymbol{x}_3$. This is consistent with our previous argument that $\omega_\perp^{(2)}(e_i) = \max\{\omega_\perp^+(e_i), \omega_\perp^-(e_i), \omega^{(3)}(f_{i,0})\}$, for $i \in \{1,2,3\}$. Consequently, in line 9, we increment the probability $P_{\boldsymbol{\omega}_\perp^{(2)}}(\boldsymbol{x})$ by $P_{\boldsymbol{\omega}_\perp^+}(\boldsymbol{x}_1) \cdot P_{\boldsymbol{\omega}_\perp^+}(\boldsymbol{x}_2) \cdot P_{\boldsymbol{\omega}}(\boldsymbol{x}_3)$, where the latter is the probability that $\boldsymbol{\omega}_\perp^+ = \boldsymbol{x}_1, \boldsymbol{\omega}_\perp^- = \boldsymbol{x}_2$, and $\boldsymbol{\omega} = \boldsymbol{x}_3$. The output of the program is summarized in the lemma below, which describes the transition probabilities of the projected growth process $\mathbf{G}^{(2)}$.

Lemma 5.1.2.

$$P_{\boldsymbol{\omega}_\perp^{(2)}}(\boldsymbol{e}_{0,3}) = \frac{\bar{q}^5}{(1-\bar{q}^3+\bar{q}^4)^2}$$

$$P_{\boldsymbol{\omega}_\perp^{(2)}}(\boldsymbol{e}_{1,3}) = \frac{(1-\bar{q})\bar{q}^4(1-\bar{q}^5+2\bar{q}^6-\bar{q}^7)}{[(1-\bar{q}^2+\bar{q}^3)(1-\bar{q}^3+\bar{q}^4)]^2}$$

$$P_{\boldsymbol{\omega}_\perp^{(2)}}(\boldsymbol{e}_{2,3}) = \frac{\begin{array}{c}(1-\bar{q})^2\bar{q}^3\times \\ (1+2\bar{q}^2-4\bar{q}^3+2\bar{q}^4+4\bar{q}^6-8\bar{q}^7+7\bar{q}^8-6\bar{q}^9+6\bar{q}^{10}-4\bar{q}^{11}+\bar{q}^{12})\end{array}}{[(1-\bar{q}+\bar{q}^2)(1-\bar{q}^2+\bar{q}^3)(1-\bar{q}^3+\bar{q}^4)]^2}$$

$$P_{\boldsymbol{\omega}_\perp^{(2)}}(\boldsymbol{e}_{3,3}) = \frac{\begin{array}{c}(1-\bar{q})^3(1-\bar{q}^3+2\bar{q}^4-\bar{q}^5)\times \\ (1+\bar{q}+\bar{q}^2+\bar{q}^3-2\bar{q}^4-3\bar{q}^5+2\bar{q}^6+\bar{q}^7+2\bar{q}^8-4\bar{q}^9+\bar{q}^{10})\end{array}}{[(1-\bar{q}+\bar{q}^2)(1-\bar{q}^2+\bar{q}^3)(1-\bar{q}^3+\bar{q}^4)]^2},$$

where $\bar{q} = 1-q$.

Chapter 6

Establishing Step-wise Coupling and Global Coupling

In this chapter, we describe how $\mathbf{G}^{(2)}$ is related to the standard bond percolation model on $\mathbb{L}^2$.

Recall that $\mathbf{G}^{(2)}$ is a projected growth process associated with the open cluster of the cubic lattice bond percolation model. We want to compare it with a growth process associated with the open cluster in the square lattice bond percolation model having parameter p. Intuitively, if $\mathbf{G}^{(2)}$ grows "faster" than square lattice bond percolation process, we would expect that survival of square lattice bond percolation process results in the survival of $\mathbf{G}^{(2)}$.

Consider a growth process associated with the open cluster in the square lattice bond percolation model. Imagine what would happen if at a certain step n, the process explores from the same vertex as $\mathbf{G}^{(2)}$ does, which is the vertex $v_n^{(2)}$. Meanwhile, we further assume that the edges that can possibly be added to the cluster of the square lattice are the same as for $\mathbf{G}^{(2)}$ as well, namely, the edges in $B_n^{(2)}$. Then the joint distribution of edges in $B_n^{(2)}$ being added to the cluster of the square lattice bond model is the product measure of $|B_n^{(2)}|$ independent Bernoulli distributions with parameter p, since each edge in the model is open independently with probability p.

We define $Q_{m,p}$ as the joint law of m independent random variables, each with a Bernoulli distribution with parameter p. Assume that at some step n, both processes explore from the vertex $v_n^{(2)}$ and consider whether edges in $B_n^{(2)}$ should be included. For the process associated with the open cluster of the square lattice bond model, the joint distribution of adding edges in $B_n^{(2)}$ to the open cluster is $Q_{|B_n^{(2)}|,p}$. On the other hand, for process $\mathbf{G}^{(2)}$, the joint distribution of adding edges in $B_n^{(2)}$ to the projection of the open cluster in the cubic lattice is $Q^{(2)}_{|B_n^{(2)}|,q}$. Thus, a straightforward idea of comparing the growth of the two processes is to compare $Q^{(2)}_{|B_n^{(2)}|,q}$ with $Q_{|B_n^{(2)}|,p}$.

Recall that both $Q^{(2)}_{|B_n^{(2)}|,q}$ and $Q_{|B_n^{(2)}|,p}$ are defined on the same sample space $\{0,1\}^m$ (for $m = |B_n^{(2)}|$), which can naturally be regarded as a partially ordered set (See Definition 6.1.2). If $Q^{(2)}_{m,q} \geqslant_{\mathrm{st}} Q_{m,p}$ (See Definition 6.1.4)for each $m = 1, 2, 3$, then we

would be able to establish a coupling in which at each step, the set of edges added to the open cluster of the square lattice bond model is a subset of edges added to the projection of the open cluster of the cubic lattice bond model. Furthermore, if such a coupling can be established for any $n \in \mathbb{N}$, we would expect this collection of step-wise couplings to form a global coupling such that any edges that are added to the open cluster of the square lattice bond model are contained in the projection of the open cluster in the cubic lattice. Consequently, if the former open cluster is infinite, then the projection of the open cluster in the cubic lattice is infinite as well. By setting $p > \frac{1}{2}$, there is positive probability that the open cluster of the square lattice bond model is infinite. Consequently, the corresponding q satisfying the stochastic ordering inequalities would result in the existence an of an infinite open cluster in the cubic lattice with positive probability. Thus, q would be an upper bound for $p_c(\mathbb{L}^3)$.

The argument above is not rigorous since both processes may not explore from the same vertex at each step. Even if they do, the edges they consider may not be exactly the same. However, this idea does inspire us to consider the stochastic ordering inequalities between $Q^{(2)}$ and Q. We will resolve the problem that two processes may not explore from the same vertex and consider the same set of edges in Section 6.3.

6.1 Solving Stochastic Ordering Inequalities

For any fixed p, we solve for the smallest q such that $Q^{(2)}_{m,q} \geqslant_{\text{st}} Q_{m,p}$, $m = 1, 2, 3$. We notice that by Lemma 4.2.10, for $m \leqslant 2$, $Q^{(2)}_{m,q}$ and $Q_{m,p}$ are marginal distributions of $Q^{(2)}_{3,q}$ and $Q_{3,p}$, respectively. Thus, we only focus on solving $Q^{(2)}_{3,q} \geqslant_{\text{st}} Q_{3,p}$. Additionally, since the percolation threshold of the square lattice bond model is $p_c(\mathbb{L}^2) = \frac{1}{2}$ (See [16]), we are particularly interested in the special case that $p = \frac{1}{2}$, in which $Q_{3,p}(\mathbf{e}) = \frac{1}{8}$ for each $\mathbf{e} \in \{0,1\}^3$.

Recall that in Definition 5.1.1, we defined equivalence relations $\sim$ on $\{0,1\}^m$ for $m = 1, 2, 3$ that two vectors in $\{0,1\}^m$ are equivalent if and only if the number of 1's in them are equal. By symmetry of $Q^{(2)}_{m,q}$, for any two vectors in $\{0,1\}^m$ that are in the same equivalence class, their corresponding $Q^{(2)}_{m,q}$ measures are equal. The same property holds with respect to $Q_{m,p}$. More formally, we introduce the following lemma:

Lemma 6.1.1. *For any $\boldsymbol{x}, \boldsymbol{y} \in \{0,1\}^m$ with $\boldsymbol{x} \sim \boldsymbol{y}$, we have $Q^{(2)}_{m,q}(\boldsymbol{x}) = Q^{(2)}_{m,q}(\boldsymbol{y})$ and $Q_{m,p}(\boldsymbol{x}) = Q_{m,p}(\boldsymbol{y})$.*

This lemma is a partial result of Lemma 5.1.2.

We then define a partial order $\leqslant$ on $\{0,1\}^m$ as the canonical partial order on the Boolean algebra. More specifically, we define:

Definition 6.1.2 (Component-wise order $\leqslant$ on $\{0,1\}^m$)**.** For any $\boldsymbol{x}, \boldsymbol{y} \in \{0,1\}^m$, we say $\boldsymbol{x} \leqslant \boldsymbol{y}$ if and only if $x_i \leqslant y_i$ for all $i \in \{1,2,...,m\}$.

Definition 6.1.3 (Upset)**.** A subset U of $\{0,1\}^m$ is an *upset* if and only if for each $u_1 \in U$, $u_2 \in U$ for all $u_2 \geqslant u_1$.

Definition 6.1.4 (Stochastic ordering)**.** Let $Q^{(2)}$ and Q be two probability measures on $\{0,1\}^m$ and its corresponding σ-field. We say $Q^{(2)}$ *stochastically dominates* Q, denoted by $Q^{(2)} \geqslant_{\text{st}} Q$, if $Q^{(2)}(U) \geqslant Q(U)$ holds for all upset U.

One advantage of introducing the equivalence relation on the sample space $\{0,1\}^3$ is that it simplifies our calculation in proving stochastic dominance. Using similar reasoning to that of Theorem 8 of May's dissertation [19, Chapter 6, p. 119] (Remark 6.1.5.(a).), we obtain the following statement. If $Q^{(2)}_{3,q}(U) \geqslant Q_{3,p}(U)$ for each upset U that is a union of equivalence classes, then $Q^{(2)}_{3,q} \geqslant_{\text{st}} Q_{3,p}$.

In other words, let U_1, U_2, U_3 be three upsets in $\{0,1\}^3$ that are unions of equivalence classes:

$$\begin{aligned} U_1 &= \{(1,1,1)\}, \\ U_2 &= U_1 \cup \{(1,1,0),(1,0,1),(0,1,1)\}, \\ U_3 &= U_2 \cup \{(1,0,0),(0,1,0),(0,0,1)\}. \end{aligned}$$

We have $Q^{(2)}_{3,q} \geqslant_{\text{st}} Q_{3,\frac{1}{2}}$ if and only if the following three inequalities hold:

$$Q^{(2)}_{3,q}(U_1) = Q^{(2)}_{3,q}(1,1,1) \geqslant Q_{3,p}(U_1) = \left(\tfrac{1}{2}\right)^3,$$

$$Q^{(2)}_{3,q}(U_2) = Q^{(2)}_{3,q}(1,1,1) + 3Q^{(2)}_{3,q}(1,1,0) \geqslant Q_{3,p}(U_2) = 4\left(\tfrac{1}{2}\right)^3,$$

$$Q^{(2)}_{3,q}(U_3) = Q^{(2)}_{3,q}(1,1,1) + 3Q^{(2)}_{3,q}(1,1,0) + 3Q^{(2)}_{3,q}(1,0,0) \geqslant Q_{3,p}(U_3) = 7\left(\tfrac{1}{2}\right)^3.$$

The $Q^{(2)}$ measure is expressed in terms of q in Section 5.1.2. We substitute the results into the three inequalities above, and simplify the results to obtain the following:

$$\begin{aligned}
&(1-\bar{q})^3(1-\bar{q}^3+2\bar{q}^4-\bar{q}^5)\times \\
&\frac{(1+\bar{q}+\bar{q}^2+\bar{q}^3-2\bar{q}^4-3\bar{q}^5+2\bar{q}^6+\bar{q}^7+2\bar{q}^8-4\bar{q}^9+\bar{q}^{10})}{[(1-\bar{q}+\bar{q}^2)(1-\bar{q}^2+\bar{q}^3)(1-\bar{q}^3+\bar{q}^4)]^2} \geqslant \frac{1}{8}, \\
&(1-\bar{q})^2\times \\
&\frac{(1+2\bar{q}+\bar{q}^2-\bar{q}^4+2\bar{q}^5-\bar{q}^6-2\bar{q}^7+4\bar{q}^9-2\bar{q}^{10}-2\bar{q}^{11}+\bar{q}^{12})}{[(1-\bar{q}^2+\bar{q}^3)(1-\bar{q}^3+\bar{q}^4)]^2} \geqslant \frac{1}{2}, \\
&\frac{(1-\bar{q})(1+\bar{q}+\bar{q}^2)(1-\bar{q}^3+2\bar{q}^4-\bar{q}^5)}{(1-\bar{q}^3+\bar{q}^4)^2} \geqslant \frac{7}{8},
\end{aligned}$$

where $\bar{q} := 1-q$. Solving the inequalities above, we have $q \geqslant 0.29481591031887$, $q \geqslant 0.33010897776338$, and $q \geqslant 0.36560630186460$, respectively. Throughout the remainder of Chapter 6 and the whole Chapter 7, we choose $q = 0.365606302$ and $p > 0.5$ such that $Q^{(2)}_{3,q} \geqslant_{\text{st}} Q_{3,p}$. Notice that $Q^{(2)}_{1,q}, Q^{(2)}_{2,q}$ are marginal distributions of $Q^{(2)}_{3,q}$, while $Q_{1,p}, Q_{2,p}$ are respective marginal distributions of $Q_{3,p}$. Thus, $Q^{(2)}_{1,q} \geqslant_{\text{st}} Q_{1,p}$ and $Q^{(2)}_{2,q} \geqslant_{\text{st}} Q_{2,p}$ (Remark 6.1.5.(b).).

Remarks 6.1.5.

(a) For readers who do not have access to William D.May's dissertation [19], please refer to the proof in the Appendix (Section 6.7) at the end of this chapter.

(b) A brief justification that it is sufficient for us to only consider the stochastic ordering of $Q^{(2)}_{3,q}$ and $Q_{3,p}$ is provided in the Appendix (Section 6.7) at the end of this chapter.

6.2 Replicated Process $\mathbf{G}^{(r)}$ and Coupled Process $\mathbf{G}^{(c)}$

At the beginning of this chapter, we considered the open cluster in the square lattice bond model to be a growth process. We explained the difficulties of comparing this growth process to $\mathbf{G}^{(2)}$. One difficulty is that at each step, there is no guarantee that this process explores from the same vertex as $\mathbf{G}^{(2)}$ does. The other difficulty is that even if the two processes are exploring from the same vertex $v^{(2)}_n$, the sets of edges they consider may still be different.

In this section, we solve these two problems by "forcing" the two processes to explore from the same vertex at each step by considering the same set of edges. To be more specific, at step n of $\mathbf{G}^{(2)}$, edges in $B^{(2)}_n$ are added to $C^{(2)}_n$ with joint distribution $Q^{(2)}_{|B^{(2)}_n|,q}$. Meanwhile, edges in $B^{(2)}_n$ are considered to be open in the square lattice bond

percolation model with joint distribution $Q_{|B_n^{(2)}|,p}$. We can make these open edges a subset of edges that are added to $C_n^{(2)}$ by the stochastic ordering and coupling relation. We introduce the notation $C_n^{(c)}$, which is a subset of $\mathbb{E}^2$ that includes all the open edges that are considered to be open at the end of step n. By doing so step-by-step, we obtain a "global coupling" that $C_n^{(c)}$ is always a subset of $C_n^{(2)}$, for any $n \in \mathbb{N}$.

The argument above is not mathematically rigorous in terms of applying the stochastic ordering and coupling relation. This is because the existence of the coupling is guaranteed on a probability space that is not prespecified, while the probability space of $\mathbf{G}^{(2)}$ is pre-defined. For simplicity of introducing the intuitive idea, we will leave it non-rigorous here. We will make corresponding corrections in the following parts.

We notice that Strassen's theorem does not guarantee the existence of couplings on a pre-specified probability space, while the probability space of $\mathbf{G}^{(2)}$ is specified as $(\Omega^{(3)}, \mathcal{F}^{(3)}, P_q^{(3)})$. Thus, our first task is to "replicate" the process $\mathbf{G}^{(2)}$ so that the replicated process $\mathbf{G}^{(r)}$ has the same transition probabilities as $\mathbf{G}^{(2)}$, while it will be constructed using couplings. The notation for the components of $\mathbf{G}^{(r)}$ is defined analogously. The notation substitutes the superscript (r) for (2) to denote the replicated process. For instance, the process $\mathbf{G}^{(r)}$ explores edges in $B_n^{(r)}$ from the vertex $v_n^{(r)}$ at step n, and may add edges to $C_n^{(r)}$ and vertices to $D_n^{(r)}$, etc.

In this section, we introduce the rigorous definition for $\mathbf{G}^{(r)}$ and $\mathbf{G}^{(c)}$. Notice that $Q^{(2)}_{m,q} \geqslant_{\text{st}} Q_{m,p}$ for each $m \in \{1,2,3\}$. For every vertex $v \in \mathbb{Z}^2$, by Strassen's Theorem, there exist three couplings indexed by v: $\{(X_{m,v}, Y_{m,v})\}_{m=1}^3$, satisfying the following properties:

1. $X_{m,v}, Y_{m,v} \in \{0,1\}^m$, with $Y_{m,v} \geqslant X_{m,v}$, for any $v \in \mathbb{Z}^2$, $m = 1,2,3$.

2. $X_{m,v}$ has marginal distribution $Q_{m,p}$, and $Y_{m,v}$ has marginal distribution $Q^{(2)}_{m,q}$ for each $v \in \mathbb{Z}^2$, and each $m \in \{1,2,3\}$.

3. $\{(X_{m,v}, Y_{m,v})\}_{m\in\{1,2,3\}, v\in\mathbb{Z}^2}$ are stochastically independent.

Meanwhile, let $X_{4,\mathbf{0}^{(2)}}$ be a random vector on $\{0,1\}^4$ that is $Q_{4,p}$ distributed such that $X_{4,\mathbf{0}^{(2)}}$ and $\{(X_{m,v}, Y_{m,v})\}_{m\in\{1,2,3\}, v\in\mathbb{Z}^2}$ are mutually independent. Define $\Omega := \{0,1\}^4 \times \prod_{m\in\{1,2,3\}, v\in\mathbb{Z}^2}(\{0,1\}^m \times \{0,1\}^m)$ to be the sample space, $\mathcal{F}$ to be the σ-algebra generated by the associated cylinder sets, and $P_{p,q}$ to be the joint distribution of $X_{4,\mathbf{0}^{(2)}}, \{(X_{m,v}, Y_{m,v})\}_{m\in\{1,2,3\}, v\in\mathbb{Z}^2}$. The Y-variables indicate which edges are possibly included during the growth of $\mathbf{G}^{(r)}$, and the X-variables which edges are possibly included during the growth of $\mathbf{G}^{(c)}$.

We now construct a pair of coupled stochastic processes $(\mathbf{G}^{(r)}_n, \mathbf{G}^{(c)}_n)$ on the probability space $(\Omega, \mathcal{F}, P_{p,q})$ for each $X_{4,\mathbf{0}^{(2)}}, \{X_{m,v}, Y_{m,v}\}_{m\in\{1,2,3\}, v\in\mathbb{Z}^2} \in \Omega$. The process $\mathbf{G}^{(r)}$ shares the state space $\mathcal{S}$ with $\mathbf{G}^{(2)}$. We would like $\mathbf{G}^{(r)}$ to be a copy of $\mathbf{G}^{(2)}$ in

the sense that they both are Markovian and share the same transition probabilities. Meanwhile, we construct a sequence of random variables $\{C_n^{(c)}\}$ from $\{X\}_{m\in\{1,2,3\},v\in\mathbb{Z}^2}$ and $X_{4,\mathbf{0}^{(2)}}$ satisfying the coupling that $\{C_n^{(c)}\}$ is always a subset of $\{C_n^{(r)}\}$. (There is no $Y_{4,\mathbf{0}^{(2)}}$ since at the first step of $\mathbf{G}^{(r)}$, the four explored edges are all included in the cluster with probability 1). We will use $\{C_n^{(c)}\}$ to prove the survival of $\mathbf{G}^{(r)}$ in Chapter 7.

Definition 6.2.1 (Replicated process and coupled process)**.** For the probability space $(\Omega,\mathcal{F},P_{p,q})$, and a labeling function l, we initialize $(A_0^{(r)},B_0^{(r)},C_0^{(r)})$ as follows:

$$A_0^{(r)}:=\emptyset,$$

$$B_0^{(r)}:=\emptyset,$$

$$C_0^{(r)}:=\emptyset.$$

For $n\geqslant 1$, we define a stochastic process $(v_n^{(r)},A_n^{(r)},B_n^{(r)},C_n^{(r)},C_n^{(c)}):\Omega\to\mathbb{Z}^2\times 2^{\mathbb{Z}^2}\times 2^{\mathbb{E}^2}\times 2^{\mathbb{E}^2}\times 2^{\mathbb{E}^2}$ on $(\Omega,\mathcal{F},P_{p,q})$ recursively as follows.

For $n=1$, we have

$$v_1^{(r)}:=\mathbf{0}^{(2)},$$

$$A_1^{(r)}:=\{\mathbf{0}^{(2)}\},$$

$$B_1^{(r)}:=I[\mathbf{0}^{(2)}],$$

$$C_1^{(r)}:=B_1^{(r)}.$$

Label the four edges in $B_1^{(r)}$ with $1, 2, 3, 4$ so that for any two edges $\{u, v_1^{(r)}\}$ and $\{v, v_1^{(r)}\} \in B_1^{(r)}$, the labeling of $\{u, v_1^{(r)}\}$ is smaller if and only if $l(u) < l(v)$. Meanwhile, for each edge $e \in B_1^{(r)}$ labeled i, let $\omega^{(c)}(e)$ be the i-th entry of the random vector $X_{4,v_1^{(r)}}$. Define

$$C_1^{(c)} := \{e \in B_1^{(r)} \mid \omega^{(c)}(e) = 1\}.$$

Assume that this stochastic process has been defined through step n. At step $n+1$, if $\bigcup_{C_n^{(r)}} \setminus A_n^{(r)} \neq \emptyset$, define

$$v_{n+1}^{(r)} := \arg\min\{l(v) : v \in \bigcup_{C_n^{(r)}} \setminus A_n^{(r)}\},$$

$$A_{n+1}^{(r)} = A_n^{(r)} \cup \{v_{n+1}^{(r)}\},$$

$$B_{n+1}^{(r)} := I[\{v_{n+1}^{(r)}\}] \setminus I[\bigcup_{C_n^{(r)}} \setminus \{v_{n+1}^{(r)}\}]$$

Label the edges in $B_{n+1}^{(r)}$ with $1, 2, ..., |B_{n+1}^{(r)}|$ so that for any two edges $\{u, v_{n+1}^{(r)}\}$ and $\{v, v_{n+1}^{(r)}\} \in B_{n+1}^{(r)}$, the labeling of $\{u, v_{n+1}^{(r)}\}$ is smaller if and only if $l(u) < l(v)$. Meanwhile, for each edge $e \in B_{n+1}^{(r)}$, let $\omega^{(c)}(e)$ be the i-th entry of random vector $X_{|B_{n+1}^{(r)}|, v_{n+1}^{(r)}}$ and $\omega^{(r)}(e)$ be the i-th entry of random vector $Y_{|B_{n+1}^{(r)}|, v_{n+1}^{(r)}}$, where i is the label of edge e. Define

$$C_{n+1}^{(r)} := C_n^{(r)} \cup \{e \in B_{n+1}^{(r)} \mid \omega^{(r)}(e) = 1\},$$

$$C_{n+1}^{(c)} := C_n^{(c)} \cup \{e \in B_{n+1}^{(c)} \mid \omega^{(c)}(e) = 1\}.$$

Otherwise, if $\bigcup_{C_n^{(r)}} \setminus A_n^{(r)} = \emptyset$ define

$$v_{n+1}^{(r)} := v_n^{(r)},$$

$$B_{n+1}^{(r)} := \emptyset,$$

$$C_{n+1}^{(r)} := C_n^{(r)},$$

$$C_{n+1}^{(c)} := C_n^{(c)}.$$

The *replicated growth process* is the stochastic process $\mathbf{G}_n^{(r)} := (A_n^{(r)}, C_n^{(r)})$ defined on the probability space $(\Omega, \mathcal{F}, P_{p,q})$, and the *coupled growth process* is the stochastic process $\mathbf{G}_n^{(c)} := C_n^{(c)}$ defined on the same probability space.

Notice that for $n = 1$, $C_1^{(c)} \subseteq B_1^{(r)} = C_1^{(r)}$ by construction. Additionally, for any $n \geqslant 2$ such that $B_n^{(r)} \neq \emptyset$, we have $\omega^{(c)}(e) \leqslant \omega^{(r)}(e)$ for each $e \in B_n^{(r)}$ by the coupling that $X_{|B_n^{(r)}|, v_n^{(r)}} \leqslant Y_{|B_n^{(r)}|, v_n^{(r)}}$. This gives us the "step-wise" coupling that $C_n^{(c)} \setminus C_{n-1}^{(c)} \subseteq C_n^{(r)} \setminus C_{n-1}^{(r)}$. Consequently, by induction, we obtain a "global coupling" that $\bigcup_{n=1}^{\infty} C_n^{(c)} \subseteq \bigcup_{n=1}^{\infty} C_n^{(r)}$. For notational convenience, since both $\{C_n^{(c)}\}$ and $\{C_n^{(r)}\}$ are non-decreasing sets of edges, we may denote $\bigcup_{n=1}^{\infty} C_n^{(c)}$ and $\bigcup_{n=1}^{\infty} C_n^{(r)}$ by $C_\infty^{(c)}$ and $C_\infty^{(r)}$, respectively.

Lemma 6.2.2 (Global coupling of $\{\mathbf{G}_n^{(r)}\}$ and $\{\mathbf{G}_n^{(c)}\}$)**.** $C_\infty^{(c)} \subseteq C_\infty^{(r)}$.

Remarks 6.2.3.

(a) Since the stochastic ordering inequalities $Q_{m,q}^{(2)} \geqslant_{\text{st}} Q_{m,p}$ hold for $m \in \{1, 2, 3\}$, the step-wise coupling can be established at each step that the number of explored

edges are less than or equal to 3. However, at the first step of the replicated process $\mathbf{G}^{(r)}$, there are four edges in $B_1^{(r)} = I[\mathbf{0}^{(2)}]$ under exploration. Therefore, there is no guarantee that the edge cluster $C_1^{(r)}$ contains all edges in $C_1^{(c)}$ if edges in $B_1^{(r)}$ are added to $C_1^{(r)}$ following the $Q_{4,q}^{(2)}$ distribution. In order to have the coupling relation at the first step, we let $C_1^{(r)}$ contain all the edges in $B_1^{(r)}$. Thus, we may consider $\mathbf{G}^{(r)}$ to be a replication of $\mathbf{G}^{(2)}$ conditioned on the event $C_1^{(2)} = I[\mathbf{0}^{(2)}]$. Recall that our goal is to prove that $\mathbf{G}^{(2)}$ survives with positive probability. It is sufficient for us to prove that $\mathbf{G}^{(2)}$ conditioned on the event $C_1^{(2)} = I[\mathbf{0}^{(2)}]$ survives with positive probability. Consequently, such a definition of $C_1^{(r)}$ is justifiable. Furthermore, without the manipulation that $C_1^{(r)} = B_1^{(r)}$, an extra stochastic ordering inequality $Q_{4,q}^{(2)} \geqslant_{\text{st}} Q_{4,p}$ would have to be introduced to establish the step-wise couplings. Not only is this computationally expensive, but it also potentially increases the upper bound derived by the growth process. In fact, when $p = \frac{1}{2}$, solving the extra stochastic ordering inequality gives $q \geqslant 0.381966$. Thus, the upper bound for $p_c(\mathbb{L}^3)$ would increase from 0.365606 to 0.381966. Consequently, such manipulation is both justifiable and valuable.

(b) When establishing the couplings, for each vertex $v \neq \mathbf{0}^{(2)}$ we only use one of the random vectors $\{X_{m,v}, Y_{m,v}\}_{m=1}^3$. Thus, it is not necessary for $\{X_{m,v}, Y_{m,v}\}_{m=1}^3$ to be independent.

(c) Readers may notice that the coupling procedure may not assign $\omega^{(c)}$-values for all

edges in $\mathbb{E}^2$, but only for edges in $\bigcup_{n=1}^{\infty} B_n^{(r)}$. Thus, in order to relate the process $\mathbf{G}^{(r)}$ to a standard bond percolation model on $\mathbb{L}^2$, we still need to consider edges in $\mathbb{E}^2 \setminus \bigcup_{n=1}^{\infty} B_n^{(r)}$. This is done in Chapter 7.

(d) Some of the open edges in $C_{\infty}^{(c)}$ may not be connected to $\mathbf{0}^{(2)}$. Figure 6.5 provides an example of such a situation. The red solid line in the lower-right figure represents an edge that is contained in $C_4^{(c)}$. However, this edge is not connected to $\mathbf{0}^{(2)}$. Thus, the growth of $C_n^{(c)}$ differs from a traditional growth process, in which we explore from vertices that are already included in the cluster and only add edges that are connected to $\mathbf{0}^{(2)}$.

6.3 An Example of Establishing Step-wise Couplings

We now provide an example to help readers better understand how we establish a global coupling by step-wise couplings. The existence of the latter is guaranteed by stochastic ordering inequalities.

At step 1 of this coupling, the replicated growth process $\mathbf{G}^{(r)}$ explores from vertex $v_1^{(r)} = \mathbf{0}^{(2)}$, and $B_1^{(r)}$ contains the four edges incident with $\mathbf{0}^{(2)}$ in the square lattice. We consider the random variable $X_{\mathbf{0}^{(2)},4} \in \{0,1\}^4$. The random variable $X_{\mathbf{0}^{(2)},4}$ is $Q_{4,p}$

distributed. Label the four edges in $B_1^{(r)}$ by $1, 2, 3, 4$ according to the rule introduced in Definition 6.2.1, using the same labeling function from before (Figure 6.1). Each edge $e \in B_1^{(r)}$ labeled i is added to $C_1^{(c)}$ if and only if the i-th entry of $X_{\mathbf{0}^{(2)},4}$ is 1. Meanwhile, our construction needs to satisfy the coupling relation that $C_1^{(c)} \subset C_1^{(r)}$. However, we do not have the stochastic ordering inequality for $|B_1^{(r)}| = 4$. That is, the distribution $Q_{4,q}^{(2)}$ does not necessarily stochastically dominate $Q_{4,p}$. In order to ensure $C_1^{(c)} \subset C_1^{(r)}$, we let $C_1^{(r)}$ be $B_1^{(r)}$. By doing so, the coupling relation is satisfied. Figure 6.2 illustrates $C_1^{(r)}$ and $C_1^{(c)}$ assuming $X_{\mathbf{0}^{(2)},4} = (1, 1, 0, 0)$. Lastly, we set $A_1^{(r)} = \{\mathbf{0}^{(2)}\}$.

At step 2, similar to the definition of $\mathbf{G}^{(2)}$, the process $\mathbf{G}^{(r)}$ explores from vertex $v_2^{(r)}$, which is the vertex in $\bigcup_{C_1^{(r)}} \setminus A_1^{(r)}$ that has the smallest label. In our specific example, $v_2^{(r)}$ is the vertex with label 1, and $B_2^{(r)}$ contains three edges incident to $v_2^{(r)}$. As in step 1, the edges in $B_2^{(r)}$ are labeled by $1, 2, 3$. Since $|B_2^{(r)}| = 3$, we consider two coupled random variables $(X_{3,v_2^{(r)}}, Y_{3,v_2^{(r)}})$, satisfying

1. $X_{3,v_2^{(r)}}, Y_{3,v_2^{(r)}} \in \{0, 1\}^3$,

2. $X_{3,v_2^{(r)}} \leqslant Y_{3,v_2^{(r)}}$,

3. $X_{3,v_2^{(r)}}$ and $Y_{3,v_2^{(r)}}$ are distributed as $Q_{3,p}$ and $Q_{3,q}^{(2)}$, respectively.

Recall that in $\mathbf{G}^{(2)}$, the set of edges in $B_2^{(2)}$ that are added to $C_2^{(2)}$ is determined by the underlying configuration on $\mathbb{L}^3$, or more specifically, by the configuration restricted to the exploration region $B_2^{(3)}$. However, in $\mathbf{G}^{(r)}$, which edges in $B_2^{(r)}$ are added to $C_2^{(r)}$

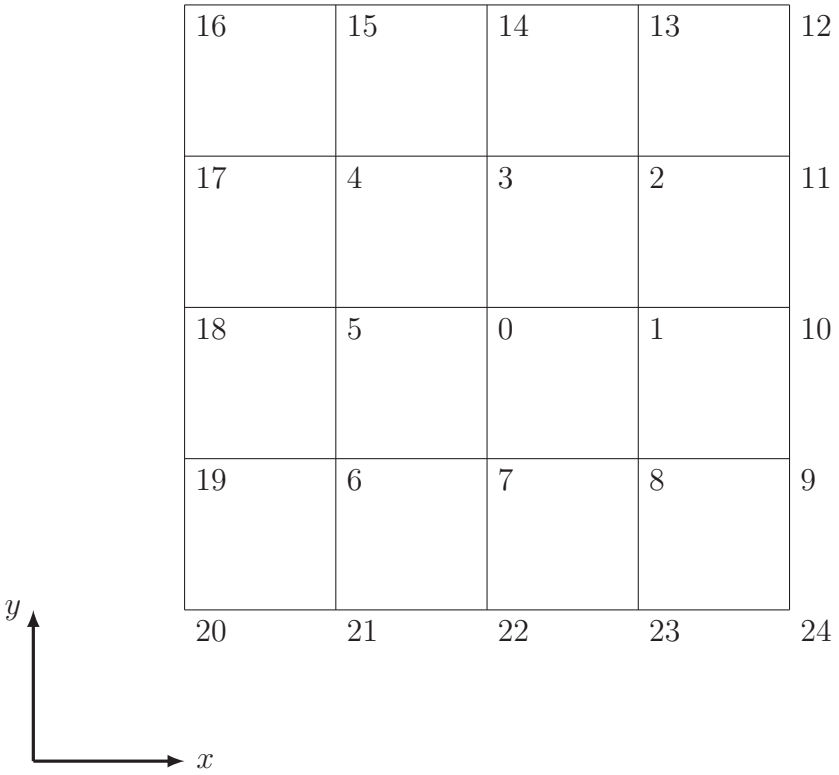

Figure 6.1: An illustration of the labeling function l on a subset of vertices in $\mathbb{L}^2$.

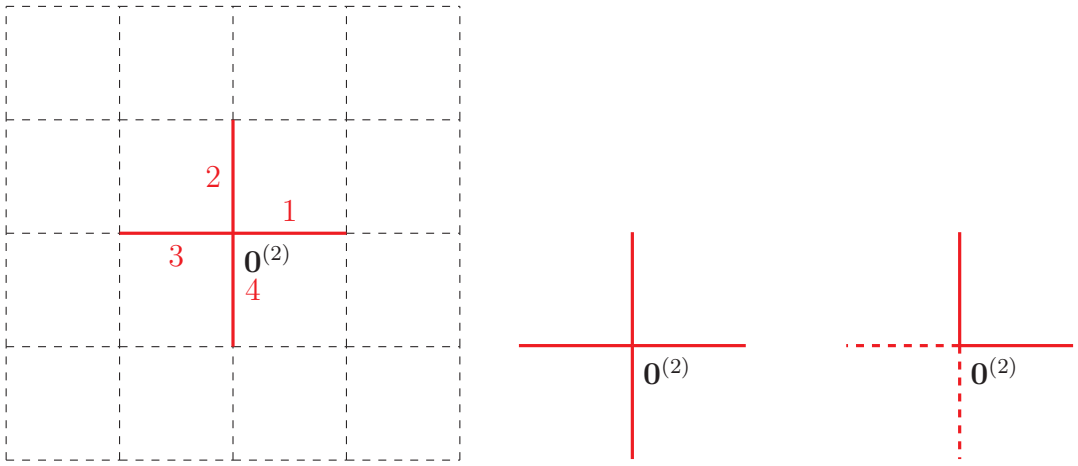

Figure 6.2: An illustration of the construction of $\mathbf{G}^{(r)}$ and $\mathbf{G}^{(c)}$ at step 1. The left figure is an illustration of $B_1^{(r)}$. The red solid line segments are edges in $B_1^{(r)}$, labeled by $1, ..., 4$ in an order characterized by the labeling function l. The middle figure is an illustration of $C_1^{(r)}$. The red solid line segments represent edges in $C_1^{(r)}$. The right figure is an illustration of $C_1^{(c)}$, assuming that $X_{\mathbf{0}^{(2)},4} = (1, 1, 0, 0)$. The red solid line segments are edges in $C_1^{(c)}$. The red dashed lines are edges that are considered, but not added to $C_1^{(c)}$.

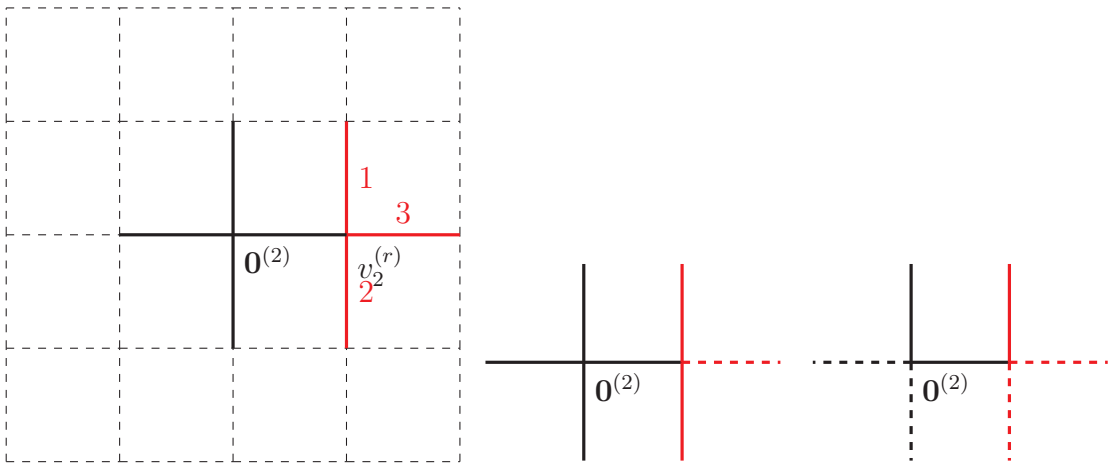

Figure 6.3: An illustration of the construction of $\mathbf{G}^{(r)}$ and $\mathbf{G}^{(c)}$ at step 2. The left figure is an illustration of $B_2^{(r)}$. The red solid line segments are edges in $B_2^{(r)}$, labeled by $1, 2$ and 3 in an order characterized by the labeling function l. The middle figure is an illustration of $C_2^{(r)}$, assuming $Y_{3,v_2^{(r)}} = (1, 1, 0)$. The solid line segments are edges in $C_2^{(r)}$. The right figure is an illustration of $C_2^{(c)}$, assuming $X_{3,v_2^{(r)}} = (1, 0, 0)$. The solid line segments are edges in $C_2^{(c)}$, which is a subset of $C_2^{(r)}$.

is determined by $Y_{3,v_2^{(r)}}$. We add edge $e \in B_2^{(r)}$ labeled i to $C_2^{(r)}$ if and only if the i-th entry of $Y_{3,v_2^{(r)}}$ is 1. Meanwhile, we add edge e into $C_2^{(c)}$ if and only if the i-th entry of $X_{3,v_2^{(r)}}$ is 1. Figure 6.3 illustrates the case that $Y_{3,v_2^{(r)}} = (1, 1, 0)$ and $X_{3,v_2^{(r)}} = (1, 0, 0)$. These two random variables indicate that e_1 and e_2 should be added to $C_2^{(r)}$, and only e_1 should be added to $C_2^{(c)}$. In both figures, the newly added edges are marked in red solid lines, and the edges in $B_1^{(r)}$ that are not added are marked in red dashed lines. Lastly, we update $A^{(r)}$ by $A_2^{(r)} = A_1^{(r)} \cup \{v_2^{(r)}\}$.

At step 3, we explore from vertex $v_3^{(r)}$, which is the vertex in $\bigcup_{C_2^{(r)}} \setminus A_2^{(r)}$ with the smallest label. Following the definition of $\mathbf{G}^{(r)}$, $B_3^{(r)}$ contains two edges incident to $v_3^{(r)}$. We label these two edges by 1 and 2. Since $Q_{2,q}^{(2)} \geqslant_{\text{st}} Q_{2,p}$, there exists two random variables $(X_{2,v_3^{(r)}}, Y_{2,v_3^{(r)}})$ such that

1. $X_{2,v_3^{(r)}}, Y_{2,v_3^{(r)}} \in \{0,1\}^2$,

2. $X_{2,v_3^{(r)}} \leqslant Y_{2,v_3^{(r)}}$,

3. $X_{2,v_3^{(r)}}$ and $Y_{2,v_3^{(r)}}$ are distributed as $Q_{2,p}$ and $Q_{2,q}^{(2)}$, respectively.

As before, the process $\mathbf{G}^{(r)}$ differs from $\mathbf{G}^{(2)}$ in the following aspect: in $\mathbf{G}^{(2)}$, edges in $B_3^{(2)}$ are added to $C_3^{(2)}$ according to underlying configuration on $\mathbb{L}^3$ restricted to the exploration region; in contrast, in $\mathbf{G}^{(r)}$, edges in $B_3^{(r)}$ are added to $C_3^{(r)}$ according to $Y_{2,v_3^{(r)}}$. We add edge e labeled i into $C_3^{(r)}$ if and only if the i-th entry of $Y_{2,v_3^{(r)}}$ is 1. Meanwhile, we add edge e into $C_3^{(c)}$ if and only if the i-th entry of $X_{2,v_3^{(r)}}$ is 1. Figure 6.4 illustrates the case that $Y_{3,v_3^{(r)}} = (1,0)$ and $X_{3,v_3^{(r)}} = (1,0)$. Lastly, we update $A^{(r)}$ by letting $A_3^{(r)} = A_2^{(r)} \cup \{v_3^{(r)}\}$.

In general, at step n of $\mathbf{G}^{(r)}$, a vertex $v_n^{(r)}$ is picked following the analogous rule for expanding $\mathbf{G}^{(2)}$. Meanwhile, $B_n^{(r)}$ is defined in a similar way as $B_n^{(2)}$. Then, the coupled random variable (X, Y) indexed by $|B_n^{(r)}|$ and $v_n^{(r)}$ are considered. The coupled random variables $(Y_{|B_n^{(r)}|,v_n^{(r)}}, X_{|B_n^{(r)}|,v_n^{(r)}})$ indicate which edges in $B_n^{(r)}$ are included in $C_n^{(r)}$ while a subset of these included edges are considered to be open and added to

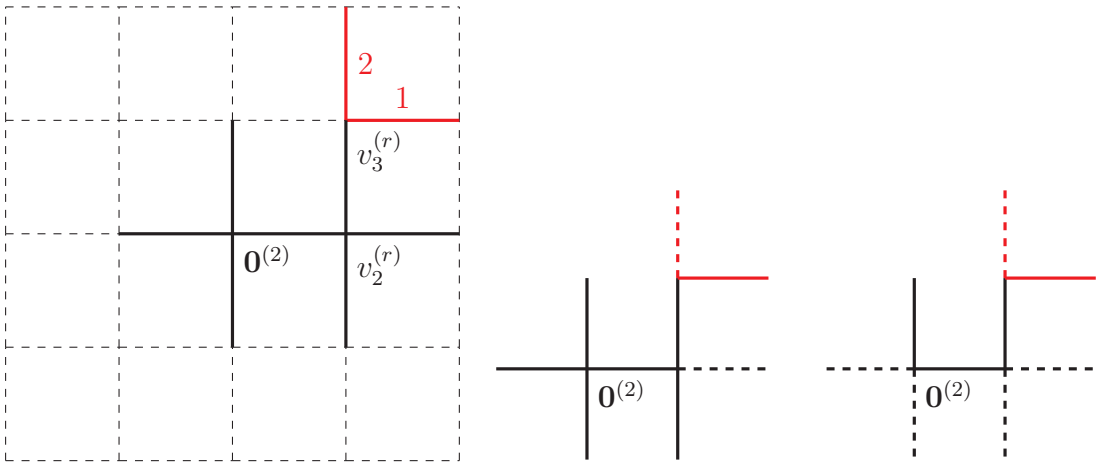

Figure 6.4: An illustration of the construction of $\mathbf{G}^{(r)}$ and $\mathbf{G}^{(c)}$ at step 3. The left figure is an illustration of $B_3^{(r)}$. The red solid line segments are edges in $B_3^{(r)}$, labeled by 1 and 2 in an order characterized by the labeling function l. The middle figure is an illustration of $C_3^{(r)}$, assuming $Y_{3,v_3^{(r)}} = (1,0)$. The red solid line segments are edges in $C_3^{(r)}$. The right figure is an illustration of $C_3^{(c)}$, assuming $X_{3,v_3^{(r)}} = (1,0)$. Edges in $C_3^{(c)}$ are marked by solid line segments

$C_n^{(c)}$. Finally we update $A_n^{(r)}$ by adding $v_n^{(r)}$ to $A_{n-1}^{(r)}$. Figure 6.5 illustrates two more steps of $\mathbf{G}^{(r)}$ and $\mathbf{G}^{(c)}$ following this construction, assuming that $Y_{2,v_4^{(r)}} = (0,0)$ and $X_{2,v_4^{(r)}} = (0,0)$ at step 4, and $Y_{3,v_5^{(r)}} = (0,1,1)$ and $X_{2,v_5^{(r)}} = (0,1,0)$ at step 5.

The process $(\mathbf{G}^{(r)}, \mathbf{G}^{(c)})$ stops growing if for some n, $\bigcup_{C_n^{(r)}} \setminus A_n^{(r)} = \emptyset$. Otherwise, the process continues forever.

6.4 The Similarities between $\mathbf{G}^{(r)}$ and $\mathbf{G}^{(2)}$

In this section we show that $\mathbf{G}^{(r)}$ is a replication $\mathbf{G}^{(2)}$ in the sense that they both are Markovian and have the same transition probabilities, except for the first step. Our proof is based on the reasoning similar to the proof of Theorem 4.2.6.

Theorem 6.4.1. *Let $\mathcal{S}$ denote the state space of $\mathbf{G}^{(2)}$, which is also the state space of $\mathbf{G}^{(r)}$. Then $\mathbf{G}^{(r)}$ is a Markov Chain. Moreover, for each $S_1, S_2 \in \mathcal{S} \setminus \{\emptyset, \emptyset\}$ and for each $m, n \in \mathbb{Z}^+$ such that $P_q^{(3)}(\mathbf{G}_m^{(2)} = S_1) \neq 0$ and $P_{p,q}(\mathbf{G}_n^{(r)} = S_1) \neq 0$,*

$$P_q^{(3)}(\mathbf{G}_{m+1}^{(2)} = S_2 \mid \mathbf{G}_m^{(2)} = S_1) = P_{p,q}(\mathbf{G}_{n+1}^{(r)} = S_2 \mid \mathbf{G}_n^{(r)} = S_1). \tag{6.1}$$

Proof. For any $n \in \mathbb{Z}^+$, let $\mathcal{F}_n^{(r)}$ be the natural filtration of process $\mathbf{G}_n^{(r)}$ up to step n. Using similar reasoning to the proof of Lemma 4.2.5, we conclude that $B_{n+1}^{(r)}$ and

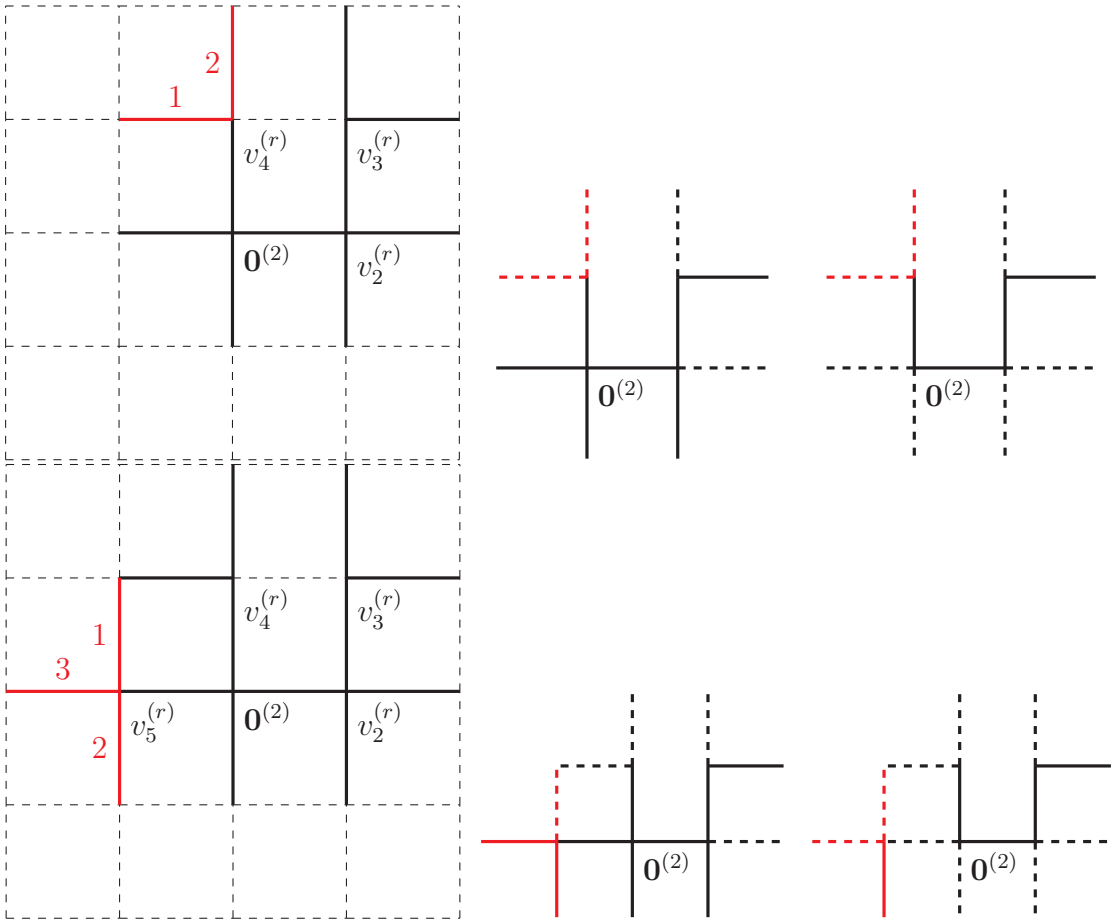

Figure 6.5: An illustration of the construction of $\mathbf{G}^{(r)}$ and $\mathbf{G}^{(c)}$ at steps 4 and 5. The two figures at the left illustrate $B_4^{(r)}$ and $B_5^{(r)}$ respectively. The two figures in the middle illustrate $C_4^{(r)}$ and $C_5^{(r)}$ respectively, assuming that $Y_{2,v_4^{(r)}} = (0,0)$ and $Y_{3,v_5^{(r)}} = (0,1,1)$. The two figures at the right illustrate $C_4^{(c)}$ and $C_5^{(c)}$, assuming that $X_{2,v_4^{(r)}} = (0,0)$ and $X_{2,v_5^{(r)}} = (0,1,0)$.

$v_{n+1}^{(r)}$ are both $\sigma(\mathbf{G}_n^{(r)})$-measurable. By the definition of $\mathbf{G}^{(r)}$, we have

$$P_{p,q}(\mathbf{G}_{n+1}^{(r)} \mid \mathcal{F}_n^{(r)}) = P_{p,q}(\mathbf{G}_{n+1}^{(r)} \mid \mathbf{G}_n^{(r)}) = 0$$

if and only if

$$A_{n+1}^{(r)} \setminus A_n^{(r)} \neq \{v_{n+1}^{(r)}\}, \text{ or } C_{n+1}^{(r)} \setminus C_n^{(r)} \not\subseteq B_{n+1}^{(r)}.$$

Otherwise, we have $A_{n+1}^{(r)} \setminus A_n^{(r)} = \{v_{n+1}^{(r)}\}$, and $C_{n+1}^{(r)} \setminus C_n^{(r)} \subseteq B_{n+1}^{(r)}$. Given $B_{n+1}^{(r)}$ and $v_{n+1}^{(r)}$, the random vector $Y_{|B_{n+1}^{(r)}|,v_{n+1}^{(r)}}$ is conditionally independent of $\{Y_{m,v}\}$, where $m \in \{1,2,3\}$ and $v \in \mathbb{Z}^2 \setminus \{v_{n+1}^{(r)}\}$. Thus, $Y_{|B_{n+1}^{(r)}|,v_{n+1}^{(r)}}$ is conditionally independent of $\mathcal{F}_n^{(r)}$, which gives us

$$\begin{aligned}
&P_{p,q}(\mathbf{G}_{n+1}^{(r)} \mid \mathcal{F}_n^{(r)}) \\
=&P_{p,q}(Y_{|B_{n+1}^{(r)}|,v_{n+1}^{(r)}} = \mathbf{e}_{|C_{n+1}^{(r)} \setminus C_n^{(r)}|,|B_{n+1}^{(r)}|} \mid B_{n+1}^{(r)}, v_{n+1}^{(r)}) \\
=&P_{p,q}(Y_{|B_{n+1}^{(r)}|,v_{n+1}^{(r)}} = \mathbf{e}_{|C_{n+1}^{(r)} \setminus C_n^{(r)}|,|B_{n+1}^{(r)}|} \mid B_{n+1}^{(r)}, v_{n+1}^{(r)}, \mathbf{G}_n^{(r)}) \\
=&P_{p,q}(\mathbf{G}_{n+1}^{(r)} \mid \mathbf{G}_n^{(r)}).
\end{aligned}$$

This shows that $\mathbf{G}^{(r)}$ is a Markov Process. Additionally, for all $n \geqslant 1$,

$$\begin{aligned}
&P_{p,q}(\mathbf{G}_{n+1}^{(r)} \mid \mathcal{F}_n^{(r)}) \\
=&P_{p,q}(Y_{|B_{n+1}^{(r)}|,v_{n+1}^{(r)}} = \mathbf{e}_{|C_{n+1}^{(r)} \setminus C_n^{(r)}|,|B_{n+1}^{(r)}|} \mid B_{n+1}^{(r)}, v_{n+1}^{(r)}) \\
=&Q^{(2)}_{|B_{n+1}|,q}(\mathbf{e}_{|C_{n+1} \setminus C_n|,|B_{n+1}|}),
\end{aligned}$$

where $\mathbf{e}_{|C_{n+1}^{(r)} \setminus C_n^{(r)}|,|B_{n+1}^{(r)}|}$ is a length $|B_{n+1}^{(r)}|$ vector with the first $|C_{n+1}^{(r)} \setminus C_n^{(r)}|$ entries equaling to 1 and the remaining entries equal to 0.

Summarizing the reasoning above, the explicit formulation of the transition prob-

abilities of $\mathbf{G}^{(r)}$ can be written as

$$P_{p,q}(\mathbf{G}^{(r)}_{n+1} \mid \mathbf{G}^{(r)}_{n}) = \begin{cases} 0 \text{ if } A^{(r)}_{n+1} \setminus A^{(r)}_{n} \neq \{v^{(r)}_{n+1}\} \text{ or } C^{(r)}_{n+1} \setminus C^{(r)}_{n} \not\subseteq B^{(r)}_{n+1}, \\ Q^{(2)}_{|B^{(r)}_{n+1}|,q}(\mathbf{e}_{|C^{(r)}_{n+1} \setminus C^{(r)}_{n}|,|B^{(r)}_{n+1}|}) \text{ otherwise,} \end{cases} \tag{6.2}$$

for $n \in \mathbb{Z}_+$. Note that if $\mathbf{G}^{(r)}_n = \mathbf{G}^{(2)}_m$ (i.e., $A^{(r)}_n = A^{(2)}_m$ and $C^{(r)}_n = C^{(2)}_m$), then $v^{(r)}_{n+1} = v^{(2)}_{m+1}$ and $B^{(r)}_{n+1} = B^{(2)}_{m+1}$. Comparing Equation (6.2) with Equation (5.1) for any $S_1, S_2 \in \mathcal{S} \setminus \{\emptyset, \emptyset\}$, we have $P^{(3)}_q(\mathbf{G}^{(2)}_{m+1} = S_2 \mid \mathbf{G}^{(2)}_m = S_1) = P_{p,q}(\mathbf{G}^{(r)}_{n+1} = S_2 \mid \mathbf{G}^{(r)}_n = S_1)$ for each $n \in \mathbb{Z}^+$. □

6.5 Construction of Configuration $\omega^{(2)}$

In the previous sections, we established step-wise couplings $\{\omega^{(r)}(e), \omega^{(c)}(e)\}_{e \in B^{(r)}_n}$, where $n \in \mathbb{N}$. However, $\omega^{(r)}$ is not necessarily a configuration on $\mathbb{L}^2$, since $\bigcup_{n=1}^{\infty} B^{(r)}_n$, which is the set of edges considered by $\mathbf{G}^{(r)}$, does not necessarily include all edges in $\mathbb{E}^2$. Thus, we need to designate edges in $\mathbb{E}^2 \setminus \bigcup_{n=1}^{\infty} B^{(r)}_n$ to be open or closed. This leads us to define a configuration $\omega^{(2)} = \{\omega^{(2)}(e) \in \{0,1\} \mid e \in \mathbb{E}^2\}$ as follows. For $e \in \bigcup_{n=1}^{\infty} B^{(r)}_n$, we simply let $\omega^{(2)}(e) = \omega^{(r)}(e)$; for $e \notin \bigcup_{n=1}^{\infty} B^{(r)}_n$, we let $\omega^{(2)}(e)$ be independent and identically distributed with Bernoulli distribution of parameter p such that $\omega^{(2)}(e)$ is independent of $\{(X_{m,v}, Y_{m,v})\}_{m=1,2,3,v \in \mathbb{Z}^2}$ and $X_{4,\mathbf{0}^{(2)}}$.

We now construct $\omega^{(2)}$ and its corresponding probability space rigorously to make $\omega^{(2)}$ a configuration in $\Omega^{(2)}$. By previous statements, we may consider $\omega^{(2)}$ to be

obtained from the replicated process $\mathbf{G}^{(r)}$, the coupled process $\mathbf{G}^{(c)}$, and states on all edges in $\mathbb{E}^2 \setminus (\bigcup_{n=1}^{\infty} B_n^{(r)})$, the last of which may be regarded as a configuration on the bond percolation model on $\mathbb{L}^2$. In other words, $\omega^{(2)}$ is an infinite dimensional random vector indexed by $e \in \mathbb{E}^2$ defined on the sample space that is a Cartesian product of the following two sample spaces:

- the sample space Ω on which the replicated process $\mathbf{G}_n^{(r)}$ and the coupled process $\mathbf{G}^{(c)}$ are defined,
- the sample space $\Omega^{(2)}$ which is the configuration space of the square lattice bond percolation model.

Meanwhile, the corresponding σ-field can be defined as the sigma field generated by $\mathcal{F} \times \mathcal{F}^{(2)}$. Additionally, the probability measure of $\omega^{(2)}$ is defined by the product measure of $P_{p,q}$ and $P_p^{(2)}$, since we need the edges not considered by $\mathbf{G}_n^{(r)}$ to be open with probability p, independent of $\{(X_{m,v}, Y_{m,v})\}_{m=1,2,3,v\in\mathbb{Z}^2}$ and $X_{4,\mathbf{0}^{(2)}}$. In summary, the probability space for $\omega^{(2)}$ is defined as $(\Omega \times \Omega^{(2)}, \sigma(\mathcal{F} \times \mathcal{F}^{(2)}), P_{p,q} \times P_p^{(2)})$. This leads us to the following definition.

Definition 6.5.1. Let $(\omega, \bar{\omega}^{(2)}) \in \Omega \times \Omega^{(2)}$ be $P_{p,q} \times P_p^{(2)}$ distributed and $\mathbf{G}^{(r)}, \mathbf{G}^{(c)}$ be the replicated process and coupled process associated with ω. An *induced config-*

uration, denoted by $\omega^{(2)}$ is a random vector in $\{0,1\}^{\mathbb{E}^2}$ such that for each $e \in \mathbb{E}^2$,

$$\omega^{(2)}(e) := \begin{cases} 1 & \text{if } e \in \bigcup_{n=1}^{\infty} C_n^{(c)}, \\ 0 & \text{if } e \in (\bigcup_{n=1}^{\infty} B_n^{(r)}) \setminus (\bigcup_{n=1}^{\infty} C_n^{(c)}), \\ \bar{\omega}^{(2)}(e) & \text{if } e \notin \bigcup_{n=1}^{\infty} B_n^{(r)}. \end{cases} \tag{6.3}$$

The definition above assigns $\omega^{(2)}$-values in $\{0,1\}$ to each edge in $\mathbb{E}^2$, Consequently, $\omega^{(2)}$ is a configuration on $\mathbb{L}^2$. Moreover, it is trivial that the definition of $\omega^{(2)}$ agrees with our intuition introduced at the beginning of this chapter: if $e \in \bigcup_{n=1}^{\infty} B_n^{(r)}$, then $\omega^{(2)}(e)$ equals the $\omega^{(c)}$ described in Definition 6.2.1; if $e \notin \bigcup_{n=1}^{\infty} B_n^{(r)}$, then $\omega^{(2)}(e)$ is Bernoulli distributed with parameter p. Notice that in Definition 6.2.1, $\omega^{(c)}(e)$ is the marginal distribution of Q, where Q is the product measure of Bernoulli distributions with parameter p. Consequently, $\omega^{(2)}(e)$ is Bernoulli distributed with parameter p, regardless of whether e is in $\bigcup_{n=1}^{\infty} B_n^{(r)}$ or not. This provides an informal justification of the following theorem.

Theorem 6.5.2. *The distribution of $\omega^{(2)}$ is $P_p^{(2)}$ under $P_{p,q} \times P_p^{(2)}$-measure.*

For simplicity, we write $P_{p,q} \times P_p^{(2)}$ as $P_{p,q}^{(2)}$ throughout the remainder of this chapter.

Proof. Consider the distribution of $\omega^{(2)}$ under $P_{p,q}^{(2)}$ measure. We notice that $\omega^{(2)} \in \Omega^{(2)}$, and the corresponding σ-field $\mathcal{F}^{(2)}$ is generated by the positive cylinder sets of $\Omega^{(2)}$. In other words, for any $E \subset \mathbb{E}^2, |E| < \infty$, let $C_+(E) = \{\omega \in \Omega^{(2)} \mid \omega(e) = 1 \text{ for each } e \in E\} \subset \Omega^{(2)}$ be its corresponding positive cylinder set. We shall have

$\mathcal{F}^{(2)} = \sigma(\{C_+(E) \mid E \subset \mathbb{E}^2, |E| < \infty\})$. Thus, in order to show that $\omega^{(2)}$ is $P_p^{(2)}$ distributed, we only need to show that

$$P_{p,q}^{(2)}(\omega^{(2)} \in C_+(E)) = P_p^{(2)}(C_+(E)) = p^{|E|}. \tag{6.4}$$

We prove it by induction on $|E|$.

For the base case where $|E| = 1$, let $E = \{e\}$ be the set of edges of interest. Furthermore, let $\mathbb{1}(e)$ be the (random) indicator that there exists $n \in \mathbb{N}$ such that $e \in B_n^{(r)}$. We have

$$\begin{aligned}
&P_{p,q}^{(2)}(\omega^{(2)}(e) = 1 \mid \mathbb{1}(e) = 1) \\
=& \sum_{n=1}^{\infty} P_{p,q}^{(2)}(\omega^{(2)}(e) = 1 \mid e \in B_n^{(r)}, \mathbb{1}(e) = 1) \cdot P_{p,q}^{(2)}(e \in B_n^{(r)} \mid \mathbb{1}(e) = 1) \\
=& \sum_{n=1}^{\infty} \sum_{v \in \mathbb{Z}^2} \sum_{m=1}^{4} P_{p,q}^{(2)}(\omega^{(2)}(e) = 1 \mid e \in B_n^{(r)}, \mathbb{1}(e) = 1, v_n^{(r)} = v, |B_n^{(r)}| = m) \\
&\cdot P_{p,q}^{(2)}(e \in B_n^{(r)}, \mathbb{1}(e) = 1, v_n^{(r)} = v, |B_n^{(r)}| = m \mid \mathbb{1}(e) = 1)
\end{aligned}$$

By construction, given $e \in B_n^{(r)}, v_n^{(r)} = v$ and $|B_n^{(r)}| = m$, we have $\omega^{(2)}(e) = 1$ if and only if the corresponding entry of $X_{m,v}$ is 1. Notice that under $P_{p,q}^{(2)}$ measure, $X_{m,v}$ has distribution $Q_{m,p}$, which is the product measure of m Bernoulli distributions with parameter p. Thus, $P_{p,q}^{(2)}(\omega^{(2)}(e) = 1 \mid e \in B_n^{(r)}, \mathbb{1}(e) = 1, v_n^{(r)} = v, |B_n^{(r)}| = m) = p$.

Thus,

$$\begin{aligned}
&P^{(2)}_{p,q}(\omega^{(2)}(e) = 1 \mid \mathbb{1}(e) = 1) \\
&= \sum_{n=1}^{\infty} \sum_{v \in \mathbb{Z}^2} \sum_{m=1}^{4} p \cdot P^{(2)}_{p,q}(e \in B^{(r)}_n, \mathbb{1}(e) = 1, v^{(r)}_n = v, |B^{(r)}_n| = m \mid \mathbb{1}(e) = 1) \\
&= p \cdot \sum_{n=1}^{\infty} \sum_{v \in \mathbb{Z}^2} \sum_{m=1}^{4} P^{(2)}_{p,q}(e \in B^{(r)}_n, \mathbb{1}(e) = 1, v^{(r)}_n = v, |B^{(r)}_n| = m \mid \mathbb{1}(e) = 1) \\
&= p,
\end{aligned}$$

Using the result above, we have

$$\begin{aligned}
&P^{(2)}_{p,q}(\omega^{(2)} \in C_+(E)) \\
&= P^{(2)}_{p,q}(\omega^{(2)}(e) = 1) \\
&= P^{(2)}_{p,q}(\omega^{(2)}(e) = 1 \mid \mathbb{1}(e) = 1) \cdot P^{(2)}_{p,q}(\mathbb{1}(e) = 1) \\
&\quad + P_{p,q}(\omega^{(2)}(e) = 1 \mid \mathbb{1}(e) = 0) \cdot P^{(2)}_{p,q}(\mathbb{1}(e) = 0) \\
&= p \cdot P^{(2)}_{p,q}(\mathbb{1}(e) = 1) + p \cdot P^{(2)}_{p,q}(\mathbb{1}(e) = 0) \\
&= p.
\end{aligned}$$

Thus, Equation (6.4) holds for the base case where $|E| = 1$. Assume that Equation (6.4) holds for any E with $|E| = k$. Consider the situation that the positive cylinder set corresponds to $k + 1$ edges. For simplicity, we write the positive cylinder set as $C_+(E \cup \{e\})$, where $E \subset \mathbb{E}^2$ contains k edges, and $e \in \mathbb{E}^2 \setminus E$. Using the induction

hypothesis, we have

$$\begin{aligned}
&P^{(2)}_{p,q}(\omega^{(2)} \in C_+(E \cup \{e\})) \\
&= P^{(2)}_{p,q}(\omega^{(2)} \in C_+(E \cup \{e\}) \mid \omega^{(2)} \in C_+(E)) \cdot P^{(2)}_{p,q}(\omega^{(2)} \in C_+(E)) \\
&= P^{(2)}_{p,q}(\omega^{(2)} \in C_+(E \cup \{e\}) \mid \omega^{(2)} \in C_+(E)) \cdot p^{|E|}.
\end{aligned}$$

By similar reasoning,

$$\begin{aligned}
&P^{(2)}_{p,q}(\omega^{(2)}(e) = 1 \mid \omega^{(2)} \in C_+(E), \mathbb{1}(e) = 1) \\
&= \sum_{n=1}^{\infty} P^{(2)}_{p,q}(\omega^{(2)}(e) = 1 \mid \omega^{(2)} \in C_+(E), e \in B^{(r)}_n, \mathbb{1}(e) = 1) \\
&\quad \cdot P^{(2)}_{p,q}(e \in B^{(r)}_n \mid \omega^{(2)} \in C_+(E), \mathbb{1}(e) = 1) \\
&= \sum_{n=1}^{\infty} \sum_{v \in \mathbb{Z}^2} \sum_{m=1}^{4} P^{(2)}_{p,q}(\omega^{(2)}(e) = 1 \mid \omega^{(2)} \in C_+(E), e \in B^{(r)}_n, \mathbb{1}(e) = 1, v^{(r)}_n = v, |B^{(r)}_n| = m) \\
&\quad \cdot P^{(2)}_{p,q}(e \in B^{(r)}_n, \mathbb{1}(e) = 1, v^{(r)}_n = v, |B^{(r)}_n| = m \mid \omega^{(2)} \in C_+(E), \mathbb{1}(e) = 1).
\end{aligned}$$

Also, given $e \in B^{(r)}_n, v^{(r)}_n = v$, and $|B^{(r)}_n| = m$, we have $\omega^{(2)}(e) = 1$ if and only if the corresponding entry of $X_{m,v}$ is 1. Notice that $e \notin E$, which makes the corresponding entry of $X_{m,v}$ independent of $\omega^{(2)}$-values of edges in E. Consequently, $P^{(2)}_{p,q}(\omega^{(2)}(e) = 1 \mid \omega^{(2)} \in C_+(E), e \in B^{(r)}_n, \mathbb{1}(e) = 1, v^{(r)}_n = v, |B^{(r)}_n| = m) = p$.

Thus,

$$
\begin{aligned}
&P^{(2)}_{p,q}(\omega^{(2)}(e)=1 \mid \omega^{(2)} \in C_+(E), \mathbb{1}(e)=1) \\
&= \sum_{n=1}^{\infty} \sum_{v \in \mathbb{Z}^2} \sum_{m=1}^{4} p \cdot P^{(2)}_{p,q}(e \in B^{(r)}_n, \mathbb{1}(e)=1, v^{(r)}_n = v, |B^{(r)}_n| = m \mid \omega^{(2)} \in C_+(E), \mathbb{1}(e)=1) \\
&= p \cdot \sum_{n=1}^{\infty} \sum_{v \in \mathbb{Z}^2} \sum_{m=1}^{4} P^{(2)}_{p,q}(e \in B^{(r)}_n, \mathbb{1}(e)=1, v^{(r)}_n = v, |B^{(r)}_n| = m \mid \omega^{(2)} \in C_+(E), \mathbb{1}(e)=1) \\
&= p.
\end{aligned}
$$

Consequently,

$$
\begin{aligned}
&P^{(2)}_{p,q}(\omega^{(2)} \in C_+(E \cup \{e\}) \mid \omega^{(2)} \in C_+(E)) \\
&= P^{(2)}_{p,q}(\omega^{(2)}(e)=1 \mid \omega^{(2)} \in C_+(E)) \\
&= P^{(2)}_{p,q}(\omega^{(2)}(e)=1 \mid \omega^{(2)} \in C_+(E), \mathbb{1}(e)=1) \cdot P^{(2)}_{p,q}(\mathbb{1}(e)=1 \mid \omega^{(2)} \in C_+(E)) \\
&\quad + P^{(2)}_{p,q}(\omega^{(2)}(e)=1 \mid \omega^{(2)} \in C_+(E), \mathbb{1}(e)=0) \cdot P^{(2)}_{p,q}(\mathbb{1}(e)=0 \mid \omega^{(2)} \in C_+(E)) \\
&= p \cdot P^{(2)}_{p,q}(\mathbb{1}(e)=1 \mid \omega^{(2)} \in C_+(E)) + p \cdot P^{(2)}_{p,q}(\mathbb{1}(e)=0 \mid \omega^{(2)} \in C_+(E)) \\
&= p.
\end{aligned}
$$

Thus, we have

$$
P^{(2)}_{p,q}(\omega^{(2)} \in C_+(E \cup \{e\})) = p^{|E|} \cdot p = p^{|E|+1}. \tag{6.5}
$$

Using induction, Equation (6.4) holds for any $E \subset \mathbb{E}^2, |E| < \infty$ and the proof is complete. □

6.6 Relating $\mathbf{G}^{(r)}$ to the Bond Percolation Model

In this section, we show that edges in $\mathbb{E}^2$ that are added to the cluster of the replicated growth process, which is $C_\infty^{(r)}$, cover every vertex in the open cluster of the configuration $\omega^{(2)}$. We prove the following theorem.

Theorem 6.6.1. $D(\omega^{(2)}) \subseteq \bigcup_{C_\infty^{(r)}}$.

Proof. For any $v \in D(\omega^{(2)})$, by the definition of an open cluster, there exists an open path $\{w_0 = \mathbf{0}^{(2)}, w_1, w_2, ..., w_k = v\}$ of some length k that connects v to $\mathbf{0}^{(2)}$, i.e., $\omega^{(2)}(\{w_i, w_{i+1}\}) = 1$ for each $i \in \{0, 1, ..., k-1\}$. We prove that $w_i \in \bigcup_{C_\infty^{(r)}}$ for each $i \in \{0, 1, ..., k\}$ by applying induction on i.

For $i = 1$, we have $\{w_0, w_1\} \in B_1^{(r)}$. Since $\omega^{(2)}(\{w_0, w_1\}) = 1$, according to Equation (6.3) we obtain $1 = \omega^{(c)}(\{w_0, w_1\})$. This implies $\{w_0, w_1\} \in C_\infty^{(c)} \subseteq C_\infty^{(r)}$. Consequently, $w_1 \in \bigcup_{C_\infty^{(r)}}$.

Assume that $w_0, w_1, ..., w_i \in \bigcup_{C_\infty^{(r)}}$. We need to show that $w_{i+1} \in \bigcup_{C_\infty^{(r)}}$ as well. By the induction hypothesis, $w_i \in \bigcup_{C_\infty^{(r)}}$. Thus, there exists j such that $v_j^{(r)} = w_i$. Consider the following two cases.

- Case 1: If $\{w_i, w_{i+1}\} \in B_j^{(r)}$, then $\mathbb{1}_{\{\{w_i, w_{i+1}\} \in C_\infty^{(c)}\}} = \omega^{(c)}(\{w_i, w_{i+1}\}) = 1$. This

further implies that $\{w_i, w_{i+1}\} \in C_\infty^{(r)}$. Consequently, $w_{i+1} \in \bigcup_{C_\infty^{(r)}}$.

- Case 2: If $\{w_i, w_{i+1}\} \notin B_j^{(r)}$, then w_{i+1} is an endpoint of some edge in the edge cluster $C^{(r)}$ before step j. More rigorously, since $B_j^{(r)} = I[v_j^{(r)}] \setminus I[\bigcup_{C_{j-1}^{(r)}} \setminus \{v_j^{(r)}\}]$, $\{w_i, w_{i+1}\} = \{v_j^{(r)}, w_{i+1}\} \notin B_j^{(r)}$ if and only if $w_{i+1} \in \bigcup_{C_{j-1}^{(r)}}$. Consequently, $w_{i+1} \in \bigcup_{C_\infty^{(r)}}$.

In summary, $w_{i+1} \in \bigcup_{C_\infty^{(r)}}$. Using induction, we conclude that $v \in \bigcup_{C_\infty^{(r)}}$. Notice that v is an arbitrary vertex in $D(\omega^{(2)})$, so we have $D(\omega^{(2)}) \subseteq \bigcup_{C_\infty^{(r)}}$.

□

Remark 6.6.2. The conclusion can be strengthened to $D(\omega^{(2)}) \subseteq \bigcup_{C_\infty^{(c)}}$.

6.7 Appendix

We provide detailed proofs of the following two lemmas in this section.

Lemma 6.7.1. *If $Q_{3,q}^{(2)}(U_i) \geqslant_{st} Q_{3,p}(U_i)$ for every $i \in \{1,2,3\}$, then $Q_{3,q}^{(2)} \geqslant_{st} Q_{3,p}$.*

Lemma 6.7.2. *If $Q_{3,q}^{(2)} \geqslant_{st} Q_{3,p}$, then $Q_{2,q}^{(2)} \geqslant_{st} Q_{2,p}$ and $Q_{1,q}^{(2)} \geqslant_{st} Q_{1,p}$.*

Proof of Lemma 6.7.1. Let $p \in (0,1)$ be any fixed value. We claim without a detailed proof that for any non-trivial upset U of the poset $(\{0,1\}^3, \leqslant)$, the function $Q_{3,q}^{(2)}(U) - Q_{3,p}(U)$ is a strictly increasing function of q. One can verify this statement by listing all possible non-trivial upsets U of $\{0,1\}^3$ and examining the corresponding $Q_{3,q}^{(2)}(U) - Q_{3,p}(U)$. An alternative justification of this statement is to consider it to

be a direct application of the Russo's Formula.

For simplicity, we will not continue to mention that the upset is non-trivial in the remaining part of the proof, but simply refer to a non-trivial upset as an upset. For each upset U, the equation $Q^{(2)}_{3,x}(U) - Q_{3,p}(U) = 0$ has a unique solution $x \in [0,1]$. Let $q^* := \max\{x \in [0,1] : Q^{(2)}_{3,x}(U) = Q_{3,p}(U) \text{ for each upsets } U\}$. Then $Q^{(2)}_{3,q^*}(U) \geqslant_{\text{st}} Q_{3,p}(U)$ for every upset U, which gives us $Q^{(2)}_{3,q^*} \geqslant_{\text{st}} Q_{3,p}$. Consequently, we can restate the lemma in the following way:

$$\begin{aligned} & \max\{x \in [0,1] : Q^{(2)}_{3,x}(U) = Q_{3,p}(U) \text{ for each upsets } U\} \\ = \ & \max\{x \in [0,1] : Q^{(2)}_{3,x}(U) = Q_{3,p}(U) \text{ for each } U \in \{U_1, U_2, U_3\}\}. \end{aligned} \tag{6.6}$$

We prove Equation (6.6) by contradiction. Assume that Equation (6.6) does not hold. Define $\mathcal{U}^* := \arg\max_{U \text{ is an upset}}\{x : Q^{(2)}_{3,x}(U) = Q_{3,p}(U)\}$. By assumption, $U_1, U_2, U_3 \notin \mathcal{U}^*$. Let U^* be an upset in $\mathcal{U}^*$ that contains the largest number of elements in $\{0,1\}^3$. If such an upset is not unique, we pick an arbitrary one. Let u be a minimal element in U^*. We claim that there exists u' and an order isomorphism f_0 from the poset $\{0,1\}^m$ to itself such that $f_0(u) = u' \notin U^*$. Otherwise, for any order isomorphism f, $f(u) \in U^*$. This implies that for any $\bar{u} \in U^*$ and $\bar{u} \geqslant u$, we have $f(\bar{u}) \in U^*$ as well. Notice that this holds for any order isomorphism f. Thus, the upset U^* consists of entirely complete classes, so it must be one of U_1, U_2, U_3. This contradicts the assumption that $U_1, U_2, U_3 \notin \mathcal{U}^*$.

Define $f_0(U^*) := \{f_0(u^*) : u^* \in U^*\}$. Then $f_0(U^*)$ is an upset, and furthermore $f_0(U^*) \cup U^*$ and $f_0(U^*) \cap U^*$ are both upsets. Thus, by the monotonicity of $Q^{(2)}_{3,q}(U) - Q_{3,p}(U)$ with respect to q, and by the definition of q^*, we have

$$Q^{(2)}_{3,q^*}(f_0(U^*) \cup U^*) \geqslant Q_{3,p}(f_0(U^*) \cup U^*),$$

$$Q^{(2)}_{3,q^*}(f_0(U^*) \cap U^*) \geqslant Q_{3,p}(f_0(U^*) \cap U^*).$$

We can rewrite the above equations by letting $M^* = f_0(U^*) \cap U^*$ and $N^* = U^* \setminus M^*$. By construction, we have $f_0(U^*) = M^* \cup f_0(N^*)$ and $N^* \cap f_0(N^*) = \emptyset$ (Figure 6.6). Furthermore, we observe that $U^* \cup f_0(N^*) = U^* \cup f_0(U^*)$ and $U^* \setminus N^* = U^* \cap f_0(U^*)$ are both upsets. By the definition of q^* and monotonicity of the probability of an upset, we obtain the following:

$$Q^{(2)}_{3,q^*}(U^* \cup f_0(N^*)) \geqslant Q_{3,p}(U^* \cup f_0(N^*)),$$

$$Q^{(2)}_{3,q^*}(U^* \setminus N^*) \geqslant Q_{3,p}(U^* \setminus N^*).$$

Equivalently,

$$Q^{(2)}_{3,q^*}(U^*) + Q^{(2)}_{3,q^*}(f_0(N^*)) \geqslant Q_{3,p}(U^*) + Q_{3,p}(f_0(N^*)),$$

$$Q^{(2)}_{3,q^*}(U^*) - Q^{(2)}_{3,q^*}(N^*) \geqslant Q_{3,p}(U^*) - Q_{3,p}(N^*).$$

We notice that $Q^{(2)}_{3,q^*}(U^*) = Q_{3,p}(U^*)$. Consequently,

$$Q^{(2)}_{3,q^*}(f_0(N^*)) \geqslant Q_{3,p}(f_0(N^*)),$$

$$-Q^{(2)}_{3,q^*}(N^*) \geqslant -Q_{3,p}(N^*).$$

Using symmetry, since f_0 is an order isomorphism, we have $Q^{(2)}_{3,q^*}(f_0(N^*)) = Q^{(2)}_{3,q^*}(N^*)$ and $Q_{3,p}(f_0(N^*)) = Q_{3,p}(N^*)$. Thus, the two inequalities above prove that

$$Q^{(2)}_{3,q^*}(f_0(N^*)) = Q_{3,p}(f_0(N^*)).$$

Combining with $Q^{(2)}_{3,q^*}(U^*) = Q_{3,p}(U^*)$, we have

$$Q^{(2)}_{3,q^*}(U^* \cup f_0(N^*)) = Q_{3,p}(U^* \cup f_0(N^*)).$$

Since $U^* \cup f_0(N^*) = U^* \cup f_0(U^*)$ is an upset, and $f_0(N^*)$ is non-empty ($f_0(u) \in f_0(N^*)$), we have found a larger upset $U^* \cup f_0(N^*)$ in $\mathcal{U}^*$. This contradicts our assumption that U^* contains the largest number of elements. □

Proof of Lemma 6.7.2. We begin by showing that $Q^{(2)}_{2,q} \geqslant_{\text{st}} Q_{2,p}$. For any fixed upset U in the poset $(\{0,1\}^2, \leqslant)$, let $U' = \bigcup_{(u_1,u_2)\in U} \{(u_1,u_2,0),(u_1,u_2,1)\}$. We claim that U' is an upset in the poset $(\{0,1\}^3, \leqslant)$.

We prove that U' satisfies the definition of an upset, i.e., for any $(u'_1,u'_2,u'_3) \in U'$, and any $(u_1,u_2,u_3) \in \{0,1\}^3$ such that $(u_1,u_2,u_3) \geqslant (u'_1,u'_2,u'_3)$, we have $(u_1,u_2,u_3) \in U'$. In fact, by $(u_1,u_2,u_3) \geqslant (u'_1,u'_2,u'_3)$, we have $(u_1,u_2) \geqslant (u'_1,u'_2)$. Notice that $(u'_1,u'_2) \in U$, and U is an upset. Thus, $(u_1,u_2) \in U$. Consequently, by the construction of U', we have $(u_1,u_2,u_3) \in U'$.

Since $Q^{(2)}_{3,q} \geqslant_{\text{st}} Q_{3,p}$ and U' is an upset of $\{0,1\}^3$, we have $Q^{(2)}_{3,q}(U') \geqslant Q_{3,p}(U')$. By the definition of $Q^{(2)}$ and Q, we have $Q^{(2)}_{2,q}$ and $Q_{2,p}$ are marginal distributions of $Q^{(2)}_{3,q}$

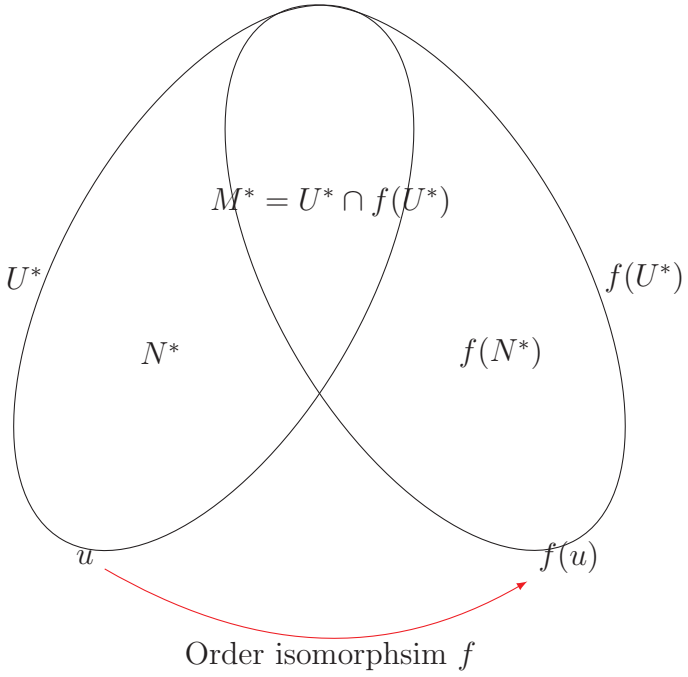

Figure 6.6: An illustration of upset U^* and order isomorphism f operating on U^*, where f satisfies $f(u) \notin U^*$ for some minimal element $u \in U^*$.

and $Q_{3,p}$, respectively. Thus, $Q^{(2)}_{2,q}(U) = Q^{(2)}_{3,q}(U')$ and $Q_{2,p}(U) = Q_{3,p}(U')$, which gives $Q^{(2)}_{2,q}(U) \geqslant Q_{2,p}(U)$. Since U is arbitrary, we obtain $Q^{(2)}_{2,q} \geqslant_{\text{st}} Q_{2,p}$.

Similar reasoning proves that $Q^{(2)}_{1,q} \geqslant_{\text{st}} Q_{1,p}$. □

Chapter 7

Global Coupling and a Summary of the Proof

7.1 An Upper Bound for $p_c(\mathbb{L}^3)$

In this chapter, we summarize the results obtained previously and reach the final conclusion that

Theorem 7.1.1. $p_c(\mathbb{L}^3) \leqslant 0.365606302$.

Recall that for non-decreasing sequences of edge sets $\{C_n^{(2)}\}$ and $\{C_n^{(r)}\}$, we denote $\bigcup_{n=1}^{\infty} C_n^{(2)}$ and $\bigcup_{n=1}^{\infty} C_n^{(r)}$ by $C_\infty^{(2)}$ and $C_\infty^{(r)}$, respectively.

Proof. Consider the percolation probability of the cubic lattice bond percolation model, i.e., $P_q^{(3)}(|D(\omega^{(3)})| = \infty)$. From Lemma 4.1.2, the survival of $\mathbf{G}^{(2)}(\omega^{(3)})$ is

a sufficient condition that $|D(\omega^{(3)})| = \infty$. Thus, we have

$$\begin{aligned} P_q^{(3)}(|D(\omega^{(3)}) \mid \ = \infty) &\geqslant P_q^{(3)}(\mathbf{G}^{(2)}(\omega^{(3)}) \text{ survives}) \\ &= P_q^{(3)}(|C_\infty^{(2)}| = \infty) \\ &\geqslant P_q^{(3)}(|C_\infty^{(2)}| = \infty \mid C_1^{(2)} = B_1^{(2)}) \cdot P_q^{(3)}(C_1^{(2)} = B_1^{(2)}) \\ &\geqslant P_q^{(3)}(|C_\infty^{(2)}| = \infty \mid C_1^{(2)} = B_1^{(2)}) \cdot q^4 \end{aligned} \tag{7.1}$$

From Chapter 6, with $q = 0.365606302$, there exists $p > 0.5$ such that $Q_{m,q}^{(2)} \geqslant_{\text{st}} Q_{m,p}$ for all $m \in \{1, 2, 3\}$. Thus, there exists a probability space $(\Omega, \mathcal{F}, P_{p,q})$ on which a replicated process $\mathbf{G}^{(r)}$ and coupled process $\mathbf{G}^{(c)}$ are defined. By Theorem 6.4.1, $\mathbf{G}^{(r)}$ has the same transition probabilities as $\mathbf{G}^{(2)}$ except for the first step. Notice that for the replicated growth process $\mathbf{G}^{(r)}$, we have $C_1^{(r)} = B_1^{(r)} = B_1^{(2)}$. Consequently,

$$\begin{aligned} P_q^{(3)}(|C_\infty^{(2)}| = \infty \mid C_1^{(2)} = B_1^{(2)}) &= P_{p,q}(|C_\infty^{(r)}| \ = \infty \mid C_1^{(r)} = B_1) \\ &= P_{p,q}(|C_\infty^{(r)}| = \infty \mid C_1^{(r)} = B_1^{(r)}) \cdot P_{p,q}(C_1^{(r)} = B_1^{(r)}) \\ &= P_{p,q}(|C_\infty^{(r)}| = \infty) \\ &= P_{p,q}(|\textstyle\bigcup_{C_\infty^{(r)}}| = \infty). \end{aligned}$$

Furthermore, we extend the probability space $(\Omega, \mathcal{F}, P_{p,q})$ to $(\Omega \times \Omega^{(2)}, \sigma(\mathcal{F} \times \mathcal{F}^{(2)}), P_{p,q} \times P_p^{(2)})$ on which the induced configuration $\omega^{(2)}$ is defined. Recall that we denote $P_{p,q} \times P_p^{(2)}$ by $P_{p,q}^{(2)}$ in Chapter 6. By Theorem 6.6.1, we have that $\bigcup_{C_\infty^{(r)}}$ contains

all vertices in $D(\omega^{(2)})$. Thus,

$$\begin{aligned} P_q^{(3)}(|C_\infty^{(2)}| = \infty \mid C_1^{(2)} = B_1^{(2)}) &= P_{p,q}(|\bigcup_{C_\infty^{(r)}}| = \infty) \\ &= P_{p,q}^{(2)}(|\bigcup_{C_\infty^{(r)}}| = \infty) \\ &\geqslant P_{p,q}^{(2)}(|D(\omega^{(2)})| = \infty). \end{aligned}$$

Finally, $\omega^{(2)}$ is distributed as $P_p^{(2)}$ under $P_{p,q}^{(2)}$ measure, and $p > p_c(\mathbb{L}^2) = 0.5$. We then have

$$\begin{aligned} P_q^{(3)}(|C_\infty^{(2)}| = \infty | C_1^{(2)} = B_1^{(2)}) &\geqslant P_{p,q}^{(2)}(|D(\omega^{(2)})| = \infty) \\ &= P_p^{(2)}(|D(\omega^{(2)})| = \infty) \\ &> 0. \end{aligned}$$

Substituting the result back into Equation (7.1), we obtain

$$\begin{aligned} P_q^{(3)}(|D(\omega^{(3)})| = \infty) \; &\geqslant P_q^{(3)}(|C_\infty^{(2)}| = \infty \mid C_1^{(2)} = B_1^{(2)}) \cdot q^4 \\ &\geqslant P_p^{(2)}(|D(\omega^{(2)})| = \infty) \cdot q^4. \\ &> 0 \end{aligned}$$

This shows that the percolation probability is strictly positive for $q = 0.365606302$, which proves that $p_c(\mathbb{L}^3) \leqslant 0.365606302$. □

7.2 Summary

We end this chapter by providing a summary of the proof of Theorem 7.1.1.

1. Let $\omega^{(3)} \in \Omega^{(3)}$ be a configuration on $\mathbb{L}^3$. Define a growth process $\mathbf{G}_n^{(3)}(\omega^{(3)})$ recursively. The process $\mathbf{G}_n^{(3)}(\omega^{(3)})$ describes the expansion of the open cluster $D(\omega^{(3)})$.

2. Perform the natural projection of $\mathbf{G}_n^{(3)}$ onto $\mathbb{L}^2$. This gives us a projected growth process $\mathbf{G}_n^{(2)}$ which is a growth process on $\mathbb{L}^2$ that describes the expansion of the projection of $D(\omega^{(3)})$.

3. Show that the projected growth process $\mathbf{G}_n^{(2)}$ is a Markov Chain on the probability space $(\Omega^{(3)}, \mathcal{F}^{(3)}, P_q^{(3)})$.

4. Show that the survival of $\mathbf{G}_n^{(2)}(\omega^{(3)})$ implies $|D(\omega^{(3)})| = \infty$.

5. Represent the transition probabilities of $\mathbf{G}_n^{(2)}$ in terms of $Q_{m,q}^{(2)}$, where $Q_{m,q}^{(2)}$ is the joint distribution of adding edges to the edge cluster $C^{(2)}$ at each step of $\mathbf{G}^{(2)}$.

6. Let $Q_{m,p}$ be the joint distribution of m Bernoulli distributions with parameter p. For $m \in \{1, 2, 3\}$, calculate $Q_{m,q}^{(2)}$, and show that for $q = 0.365606302$, there exists $p > 0.5$, satisfying $Q_{m,q}^{(2)} \geqslant_{\text{st}} Q_{m,p}$. Set $q = 0.365606302$ and $p > 0.5$ such that $Q_{m,q}^{(2)} \geqslant_{\text{st}} Q_{m,p}$.

7. With these stochastic ordering inequalities, define a replicated growth process $\mathbf{G}^{(r)}$ and a coupled process $\mathbf{G}^{(c)}$, where $\mathbf{G}^{(r)}$ is a copy of $\mathbf{G}^{(2)}$, and the set of edges in $\mathbf{G}^{(c)}$ is a subset of the edge cluster of $\mathbf{G}$.

8. Construct the induced configuration $\omega^{(2)}$ using $\mathbf{G}^{(r)}$ and $\mathbf{G}^{(c)}$, and prove that $\omega^{(2)}$ is a configuration on $\mathbb{L}^2$ with probability distribution $P_p^{(2)}$.

9. Relate the replicated growth process $\mathbf{G}^{(r)}$ to the standard percolation process on $\mathbb{L}^2$ by showing that $D(\omega^{(2)}) \subset \bigcup_{C_\infty^{(r)}}$.

10. By $p_c(\mathbb{L}^2) = \frac{1}{2}$ and $p > \frac{1}{2}$, the probability that $|D(\omega^{(2)})| = \infty$ is strictly positive. This shows that the probability that $C_\infty^{(r)}$ is infinite is also strictly positive. Consequently, both $\mathbf{G}^{(r)}$ and $\mathbf{G}^{(2)}$ survive with strictly positive probability.

11. The survival of $\mathbf{G}^{(2)}$ implies that $|D(\omega^{(3)})| = \infty$. Consequently, $q = 0.365606302$ is a sufficient condition for $|D(\omega^{(3)})| = \infty$ with positive probability, i.e., $p_c(\mathbb{L}^3) \leqslant 0.365606302$.

Chapter 8

Applications to Stacked Lattices

In this chapter, we introduce several straightforward applications of this growth process approach by applying it to "stacked" lattices. A brief description of stacked lattices is included in Section 8.1. In section 8.2, we introduce modifications made to the growth process approach so that it can be applied to stacked lattices. A summary of the results is provided in Section 8.3.

8.1 Introduction to Stacked Lattices

Stacked lattices are a family of lattices that is used frequently for models in solid-state physics. For instance, the stacked triangular lattice can be found in studies of antiferromagnets and hard-core bosons [3, 13–15, 21, 23]. Consequently, it is impor-

tant to analyze the percolation properties of stacked lattices. Currently, simulation results provide relatively accurate estimates for the percolation thresholds of these lattices. For example, here we list several simulation results for the stacked triangular lattice bond percolation threshold. In 1997, van der Marck [32] showed that this threshold value is approximately 0.1859 ± 0.0002. The latest result was obtained by Schrenk *et al.* [27] in 2013, providing a more accurate estimate for this threshold value: 0.18602 ± 0.00002. While there are many simulation results that provide accurate approximations of the percolation thresholds of the stacked lattices, no published results providing rigorous bounds were found.

We now provide a formal description of stacked lattices. Assume that we have a planar lattice graph G^2 embedded in the two-dimensional Euclidean space $\mathbb{R}^2$. We pile them up to form a graph $G^3 = (V^3, E^3)$ in $\mathbb{R}^3$ that contains a countably infinite collection of parallel layers. For simplicity, we assume that for each $k \in \mathbb{Z}$, there is a layer of G^3 on the $z = k$ plane. We further assume that the third coordinates of the vertices in V^3 are all integers. For each layer, there is a graph isomorphic to G^2 embedded in it in such a way that the projections of the graphs in the layers coincide. The isomorphic copies of G^2 in two adjacent layers are connected by vertical edges: vertices in any two adjacent layers are connected by an edge if and only if their projections are the same. More specifically, for each vertex $v \in V^2$ and each layer $z = k$, there exists a vertex $(v, k) \in V^3$. In G^3, vertex (v_1, k) and (v_2, k) are adjacent if and

only if v_1 and v_2 are adjacent in G^2. Additionally, (v, k) and $(v, k+1)$ are adjacent in G^3, for any $v \in V^2, k \in \mathbb{Z}$. One specific example of stacked lattices is that the cubic lattice can be regarded as the stacked square lattice by choosing G^2 to be the square lattice.

Apart from the cubic lattice, we are interested in other stacked lattices as well, including the stacked kagome lattice and the stacked honeycomb lattice. The kagome lattice (Figure 8.1) consists of equilateral triangles and regular hexagons, arranged in such a way that each hexagon is surrounded by triangles and vice versa, forming a tri-hexagonal tiling. Using the procedure above, we pile up countably infinitely many kagome lattices to form a stacked kagome lattice (Figure 8.2). Similarly, the honeycomb lattice (Figure 8.3), in which each vertex is surrounded by three regular hexagons, can be piled up to form a stacked honeycomb lattice (Figure 8.4). We illustrate how the growth process approach can be applied to these two lattices in the following subsections. In fact, one may see from these two examples that the growth process approach can be applied to a more generalized family of stacked lattices.

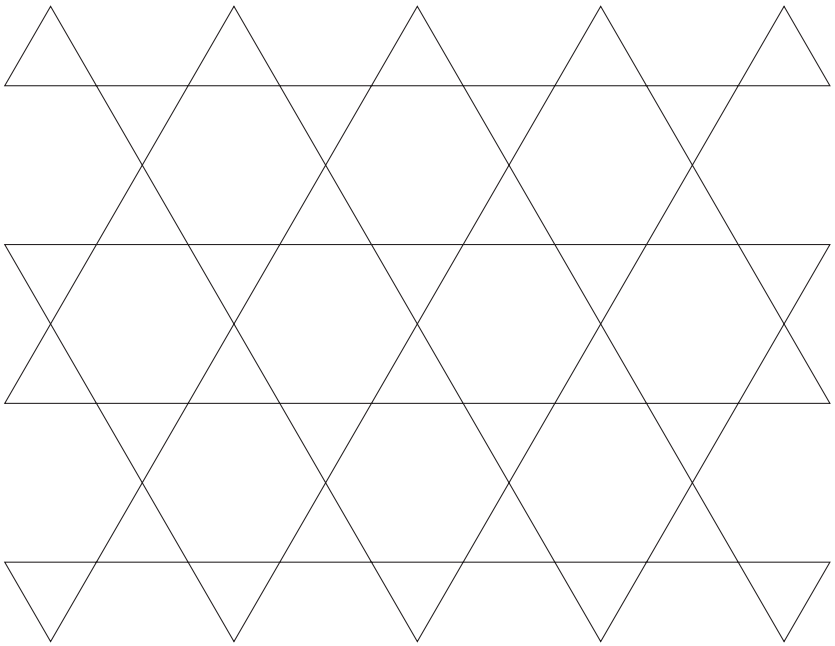

Figure 8.1: The kagome lattice

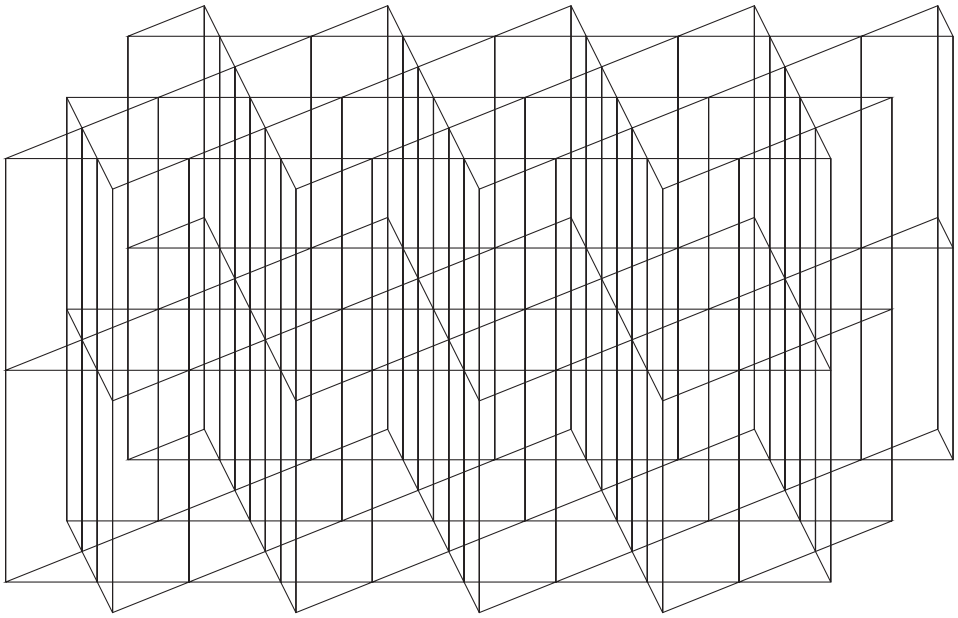

Figure 8.2: The stacked kagome Lattice

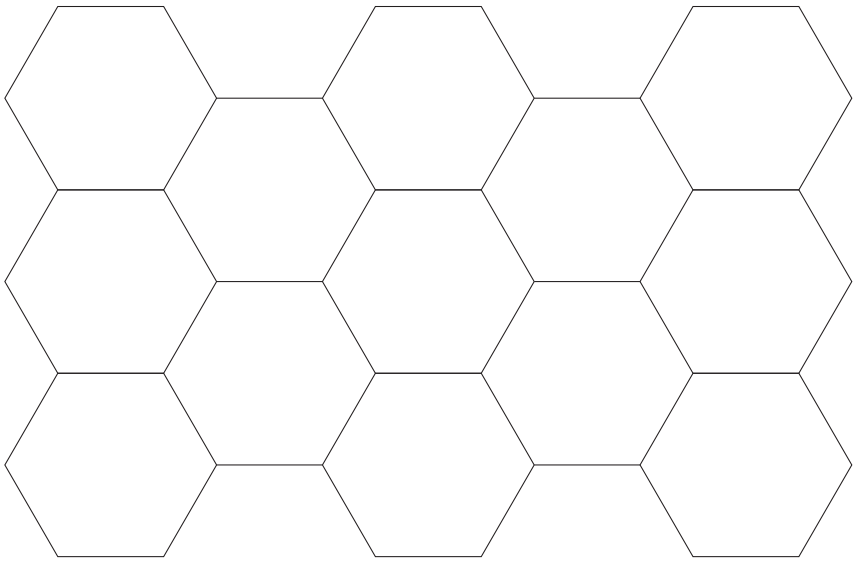

Figure 8.3: The honeycomb lattice

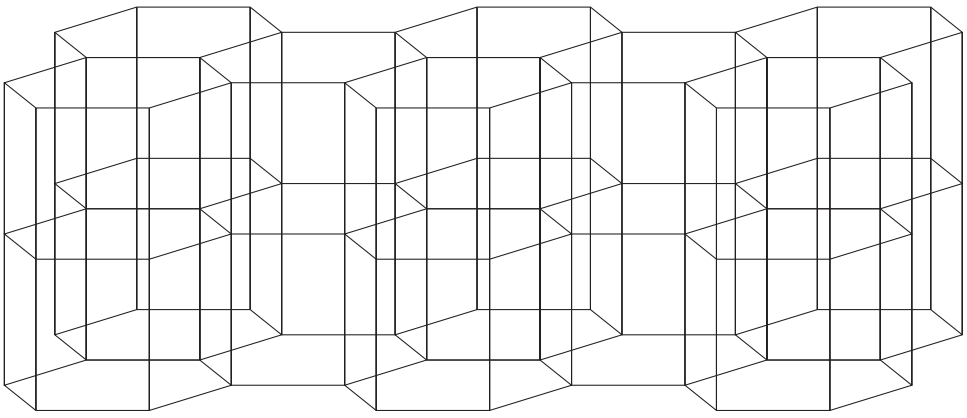

Figure 8.4: The stacked honeycomb lattice

8.2 Applying the Growth Process Approach to Stacked Lattices

In this section, we demonstrate how the growth process approach can be applied to homogeneous bond percolation models on the stacked lattices. We begin by pointing out the differences between applying the growth process approach to the cubic lattice bond model and to other stacked lattice bond models in Section 8.2.1. We then provide two examples of solving for the upper bounds for the bond percolation thresholds of the two stacked lattices: the stacked kagome lattice in Section 8.2.2 and the stacked honeycomb lattice in Section 8.2.3. Detailed calculations to obtain rigorous upper bounds for the bond percolation thresholds of these two models are provided.

8.2.1 New Stochastic Ordering Equations

For simplicity, we continue to use the same notation as in the previous chapters. We denote the planar regular lattice graph by $G^2 = (V^2, E^2)$. Let k be the degree of vertices in the regular graph G^2 minus 1. Specifically, G^2 represents the kagome lattice in Section 8.2.2 and the honeycomb lattice in Section 8.2.3. Denote the corresponding three-dimensional stacked lattice of G^2 by $G^3 = (V^3, E^3)$. Let p be the parameter of the homogeneous bond percolation model on G^2 and q be the param-

eter of the homogeneous bond percolation model on G^3. Moreover, with G^3 being embedded in $\mathbb{R}^3$ as described in the previous section, the projection of vertices and edges of G^3 are defined analogously as described in Chapter 3.

As for the cubic lattice, for any configuration $\omega^{(3)}$ on G^3 and a fixed vertex of G^3, we denote this vertex by $\mathbf{0}^{(3)}$ and the open cluster containing $\mathbf{0}^{(3)}$ by $D(\omega^{(3)})$. For a fixed labeling function l on G^2, define a growth process $\mathbf{G}^{(3)}$ associated with $\omega^{(3)}$ in the same way as we did for the cubic lattice. Furthermore, projecting $\mathbf{G}^{(3)}$ onto $\mathbb{R}^2$ provides us with a growth process on G^2. We name this growth process $\mathbf{G}^{(2)}$, and all the other related notations are carried over analogously. At step n of $\mathbf{G}^{(2)}$, a vertex $v_n^{(2)}$ is chosen from $\bigcup_{C_{n-1}^{(2)}} \setminus A_{n-1}^{(2)}$ according to l. Afterwards, each edge in $B_n^{(2)}$ adjacent to $v_n^{(2)}$ is considered and may be added to the edge cluster: edge $e \in B_n^{(2)}$ is included in $C_n^{(2)}$ if there is a "L-shaped" open path in the corresponding $B_n^{(3)}$ whose projection is e (Remark 8.2.1). This gives us a Markov process $\mathbf{G}^{(2)}$ with its transition probabilities represented in terms of $Q_{m,q}^{(2)}$, where $m = \{1, 2, ..., k\}$. Using the same reasoning as in Chapter 6, if p and q are chosen such that $p > p_c(G^2)$ and $Q_{m,q}^{(2)} \geqslant_{\text{st}} Q_{m,p}$ for all $m \in \{1, 2, .., k\}$, a replicated growth process $\{\mathbf{G}_n^{(r)} = (A_n^{(r)}, C_n^{(r)})\}$ and a process $\{\mathbf{G}_n^{(c)} = C_n^{(r)}\}$ coupled with $\{\mathbf{G}_n^{(r)}\}$ can be established, where $A_n^{(r)} \subseteq V^2, C_n^{(r)} \subseteq E^2$ and $C_n^{(c)} \subset E^2$. The replicated process $\mathbf{G}^{(r)}$ and the projected process $\mathbf{G}^{(2)}$ share the same transition probabilities. The coupled process $\mathbf{G}^{(c)}$ satisfies that at each step, $C_n^{(c)}$ is a subset of $C_n^{(r)}$, meaning that edges that are considered to be open in graph

G^2 are a subset of edges included in $C_n^{(r)}$. Since we pick $p > p_c(G^2)$, which is above criticality, by the definition of bond percolation threshold and the global coupling, we conclude that the process $(A_n^{(r)}, C_n^{(r)})$ survives with strictly positive probability, making q an upper bound of $p_c(G^3)$.

The process of obtaining a rigorous upper bound for $p_c(G^3)$ is exactly the same as introduced previously. All reasoning carries over once p is above $p_c(G^2)$ and stochastic dominance between measures $Q^{(2)}$ and Q is established. Thus, in order to apply the growth process approach to G^3, we only need to solve a new set of stochastic ordering inequalities.

Remark 8.2.1. Notice that the exploration regions corresponding to the stacked lattice G^3 have similar geometry as the exploration regions corresponding to the cubic lattice $\mathbb{L}^3$: both contain edges in an infinite vertical path that passes through the corresponding vertex $v_n^{(2)}$, and edges that are incident to the endpoints of edges along this vertical path. In other words, to calculate the transition probabilities of $\mathbf{G}^{(2)}$ corresponding to G^3, we use the same approach as the one that calculates $Q^{(2)}$. Consequently, it is justifiable that the transition probabilities of the growth process $\mathbf{G}^{(2)}$ that correspond to G^3 are still represented in terms of $Q_{m,q}^{(2)}$.

8.2.2 The Stacked Kagome Lattice

In this subsection, we provide some details about solving stochastic ordering inequalities corresponding to the stacked kagome lattice. Before listing the stochastic ordering inequalities, we pick p above the bond percolation threshold of the kagome lattice (denoted by $p_c(kagome)$). The kagome lattice bond model is not among the solved models. Fortunately, in 2017, Wierman [39] provided a rigorous upper bound for $p_c(kagome)$ that $p_c(kagome) < 0.526490$. The upper bound is very close to its simulation value, which is approximately 0.5244. Notice that the kagome lattice is a 4-regular graph, which gives us $k = 3$. Thus, we choose $p = 0.52649$, and then we pick q such that $Q^{(2)}_{m,q} \geqslant_{\text{st}} Q_{m,p}$, for any $m \in \{1, 2, 3\}$. Consequently, by Lemmas 6.7.1 and 6.7.2, it is sufficient that we check the following three inequalities:

$$Q^{(2)}_{3,q}(U_1) = Q_{3,q}(1,1,1) \geqslant Q_{3,p}(U_1) = p^3,$$

$$Q^{(2)}_{3,q}(U_2) = Q^{(2)}_{3,q}(1,1,1) + 3Q^{(2)}_{3,q}(1,1,0) \geqslant Q_{3,p}(U_2) = p^3 + 3p^2(1-p),$$

$$Q^{(2)}_{3,q}(U_3) = Q^{(2)}_{3,q}(1,1,1) + 3Q^{(2)}_{3,q}(1,1,0) + 3Q^{(2)}_{3,q}(1,0,0) \geqslant Q_{3,p}(U_3) = 1 - (1-p)^3,$$

where U_1, U_2, U_3 are three upsets in $\{0,1\}^3$ that contain the whole equivalence classes:

$$U_1 = \{(1,1,1)\},$$

$$U_2 = U_1 \cup \{(1,1,0), (1,0,1), (0,1,1)\},$$

$$U_3 = U_2 \cup \{(1,0,0), (0,1,0), (0,0,1)\}.$$

Plugging in the calculation results for the $Q^{(2)}$ measure obtained in Chapter 5 and $p = 0.52649$, we obtain:

$$\begin{aligned}
&(1-\bar{q})^3(1-\bar{q}^3+2\bar{q}^4-\bar{q}^5)\times \\
&\quad\frac{(1+\bar{q}+\bar{q}^2+\bar{q}^3-2\bar{q}^4-3\bar{q}^5+2\bar{q}^6+\bar{q}^7+2\bar{q}^8-4\bar{q}^9+\bar{q}^{10})}{[(1-\bar{q}+\bar{q}^2)(1-\bar{q}^2+\bar{q}^3)(1-\bar{q}^3+\bar{q}^4)]^2} \geqslant \frac{5257994672366739}{36028797018963968}, \\
&(1-\bar{q})^2\times \\
&\frac{(1+2\bar{q}+\bar{q}^2-\bar{q}^4+2\bar{q}^5-\bar{q}^6-2\bar{q}^7+4\bar{q}^9-2\bar{q}^{10}-2\bar{q}^{11}+\bar{q}^{12})}{[(1-\bar{q}^2+\bar{q}^3)(1-\bar{q}^3+\bar{q}^4)]^2} \geqslant \frac{19444663311727647}{36028797018963968}, \\
&\frac{(1-\bar{q})(1+\bar{q}+\bar{q}^2)(1-\bar{q}^3+2\bar{q}^4-\bar{q}^5)}{(1-\bar{q}^3+\bar{q}^4)^2} \geqslant \frac{32203746043448635}{36028797018963968},
\end{aligned}$$

where $\bar{q} := 1 - q$. Solving them, we have $q \geqslant 0.3849677751$, $q \geqslant 0.3470432870$, and $q \geqslant 0.3091871401$, respectively. Thus, 0.38497 is an upper bound for the bond percolation threshold of the stacked kagome lattice. Compared with the simulation result of 0.2563 ± 0.0002 obtained by van der Marck [32] in 1997, the upper bound still has much room to improve.

Remark 8.2.2. Readers may have noticed that the left hand side of the three stochastic ordering inequalities are exactly the same as the ones we obtained in Chapter 6. This is because the $B_n^{(3)}$ associated with the kagome lattice is isomorphic to the $B_n^{(3)}$ associated with the square lattice, given that the corresponding two $B_n^{(2)}$'s have the same cardinality.

8.2.3 The Stacked Honeycomb Lattice

Unlike the kagome lattice, the honeycomb lattice, also known as the hexagonal lattice, has an exactly known bond percolation threshold [30], which is $1-2\sin(\pi/18)$. Thus, in this situation, we pick $p = 1-2\sin(\pi/18)$. Furthermore, notice that the honeycomb lattice is 3-regular. Thus, for any $n \in \mathbb{Z}^+ \setminus \{1\}$, at step n of the corresponding projected growth process $\mathbf{G}^{(2)}$, at most two edges are included. Subsequently, $Q^{(2)}_{2,q} \geqslant_{\text{st}} Q_{2,p}$ is the stochastic dominance we need when applying the growth process approach. In other words, it is sufficient that we solve the following two inequalities:

$$Q^{(2)}_{2,q}((1,1)) \geqslant Q_{2,p}((1,1)) = p^2,$$

$$Q^{(2)}_{2,q}(\{(1,0),(0,1),(1,1)\}) \geqslant Q_{2,p}(\{(1,0),(0,1),(1,1)\}) = p^2 + 2p(1-p).$$

Recall that in the previous section, we worked out the distribution $Q^{(2)}_{3,q}$ by programming in MATLAB following algorithm 1 in Chapter 5. This program can be slightly modified to support calculating $Q^{(2)}_{2,q}$ by reducing the triple loop to two "for loops". Alternatively, we can simply use the fact that $Q^{(2)}_{2,q}$ is a marginal distribution of $Q^{(3)}_{3,q}$ to calculate the former measure using the latter. With the methods described above, we write the above two inequalities in terms of p and q:

$$\frac{q^2(q^8 - 4q^7 + 4q^6 + 4q^5 - 13q^4 + 14q^3 - 8q^2 + 2q + 1)}{(q^5 - 3q^4 + 4q^3 - 4q^2 + 2q - 1)^2} \geqslant p^2,$$

$$\frac{q(q^5 - 4q^4 + 5q^3 - 2q^2 - q + 2)}{(q^3 - 2q^2 + q - 1)^2} \geqslant 2p - p^2.$$

Setting $p = 1 - 2\sin(\pi/18)$, and solving the two inequalities above, we obtain $q \geqslant 0.398617136$ and $q \geqslant 0.452127831$, respectively. Thus, the upper bound for the

bond percolation threshold of the stacked honeycomb lattice is 0.452127831. For comparison, our literature research found one simulation estimate [32], which is 0.3093.

8.2.4 Other Stacked Lattices

From the previous examples, readers may have noticed that when applying the growth process approach to compare a $(k+1)$-regular lattice and its corresponding stacked lattice, there are two parameters that are taken into account: one is the degree of the regular lattice, denoted by $k+1$; the other is the upper bound for the percolation threshold of the regular lattice, denoted by p. We have shown that q is an upper bound of the bond percolation threshold if and only if $Q_{k,q}^{(2)} \geqslant_{\text{st}} Q_{k,p}$. The proof is illustrated by a specific example that compares the square lattice $\mathbb{L}^2$ with the stacked square lattice, which is the cubic lattice $\mathbb{L}^3$. However, the same reasoning follows for a more general family of lattices.

Consider a periodic planar lattice graph $G^2 = (V^2, E^2)$ with $c < \infty$ classes of vertices: $\Gamma_1, ..., \Gamma_c$, where vertices of the same class have the same degrees. Denote the degree of vertex in class Γ_i by $k_i + 1$, where $i \in \{1, ..., c\}$. For vertex v of graph G^2, we let $\gamma(v) \in \{1, ..., c\}$ be its corresponding class. The planar lattice G^2 can be piled up and form a three-dimensional stacked lattice $G^3 = (V^3, E^3)$. Our goal is to bound the bond percolation threshold of G^3 from above using the growth process approach.

Following the growth process approach, we generate a growth process $\mathbf{G}^{(3)}$ associated with the open cluster of G^3. Performing the natural projection of $\mathbf{G}^{(3)}$ results in the projected growth process $\mathbf{G}^{(2)}$. At step n of $\mathbf{G}^{(2)}$, the vertex $v_n^{(2)}$ from which $\mathbf{G}^{(2)}$ explores, is $\mathbf{G}_{n-1}^{(2)}$-measurable. Meanwhile, its class $\gamma(v_n^{(2)})$ is $G_{n-1}^{(2)}$-measurable because γ is a measurable function. This makes $B_n^{(2)}$ measurable as well. Thus, the proof of Theorem 4.2.8 carries over in this generalized case. This shows that $\mathbf{G}^{(2)}$ is a Markov process. Meanwhile, the transition probabilities of $\mathbf{G}^{(2)}$ can be represented in terms of $Q_{m,q}^{(2)}$, where $m \in \{1, ..., \max\{k_1, ..., k_o\}\}$. Subsequently, we can replicate $\mathbf{G}^{(2)}$ and establish step-wise couplings by introducing a sequence of coupled random vectors $\{X_{m,v}, Y_{m,v}\}_{v\in V^2, m\in\{1,...,k_{\gamma(v)}\}}$, where $X_{m,v}$ is $Q_{m,p}$ distributed, $Y_{m,v}$ is $Q_{m,q}^{(2)}$ distributed and $X_{m,v} \leqslant Y_{m,v}$. Such coupling exists if we have $Q_{m,p} \leqslant_{\text{st}} Q_{m,q}^{(2)}$ for every $m \in \{k_1, ...k_c\}$. Using Lemma 6.7.1 and 6.7.2, this is equivalent to $Q_{\max\{k_1,..,k_c\},p} \leqslant_{\text{st}} Q^{(2)}_{\max\{k_1,...,k_c\},q}$. Once the step-wise coupling is established, the same reasoning can be applied to the multi-class situations and prove that q is our desired rigorous upper bound.

To summarize, the upper bound for the percolation threshold of the stacked lattice percolation bond model is obtained by picking a proper q to establish stochastic dominance. More specifically, it is obtained by solving k stochastic ordering inequalities as we did in Section 8.2.2 and 8.2.3, where $k+1$ is the maximum degree of the

two-dimensional lattice that forms the problem lattice when stacked together. For large k, these calculations are very complicated and almost impossible to be done by hand. Fortunately, we are able to generalize Algorithm 1 to handle arbitrary k. We implement Algorithm 2 in MATLAB and let the computer perform these calculations symbolically. Consequently, there are no numerical errors, which makes it possible for us to obtain the rigorous upper bound. The MATLAB code is included in the Appendix with comments explaining how each command corresponds to the calculations that are done by hand. The results obtained are presented in Table 8.1.

8.3 Applying the Growth Process Approach to the BCC Lattice

Consider a canonical embedding of the BCC lattice $\mathbb{B} = (V^{\mathbb{B}}, E^{\mathbb{B}})$, where $V^{\mathbb{B}} := \mathbb{Z}^3 \cup (\mathbb{Z}^3 + (\frac{1}{2}, \frac{1}{2}, \frac{1}{2}))$ and $E^{\mathbb{B}}$ is the set of pairs of vertices in $V^{\mathbb{B}}$ whose Euclidean distances are $\frac{\sqrt{3}}{2}$ (Figure 8.7). Rotate $\mathbb{B}$ by some rotation matrix R so that the rotated BCC lattice has a similar geometry to the stacked triangular lattice.

Algorithm 2 Rigorous Upper Bound of $P_c(G)$

for all $\boldsymbol{x} \in \{0,1\}^k$ **do**

  $n \leftarrow$ number of 1's in $\boldsymbol{x}$

  $P_{\boldsymbol{\omega}}(\boldsymbol{x}) \leftarrow q^n(1-q)^{k-n}$

  $P_{\boldsymbol{\omega}^+}(\boldsymbol{x}) \leftarrow \sum_{i=0}^{\infty} q^i(1-q)\left[1-(1-q)^i\right]^n\left[(1-q)^i\right]^{k-n}$

for all $\boldsymbol{x}_1 \in \{0,1\}^k$ **do**

  for all $\boldsymbol{x}_2 \in \{0,1\}^k$ **do**

    for all $\boldsymbol{x}_3 \in \{0,1\}^k$ **do**

      $\boldsymbol{x} \leftarrow (\boldsymbol{x}_1 \vee \boldsymbol{x}_2) \vee \boldsymbol{x}_3$

      $P_{\boldsymbol{\omega}_\perp}(\boldsymbol{x}) \leftarrow P_{\boldsymbol{\omega}_\perp}(\boldsymbol{x}) + P_{\boldsymbol{\omega}_\perp^+}(\boldsymbol{x}_1) \cdot P_{\boldsymbol{\omega}_\perp^+}(\boldsymbol{x}_2) \cdot P_{\boldsymbol{\omega}}(\boldsymbol{x}_3)$

for $i \in \{1,2,...,k\}$ **do**

  for $j \in \{i,...,k\}$ **do**

    $Q_{k,q}^{(2)}(U_{k+1-i}) \leftarrow Q_{k,q}^{(2)}(U_{k+1-i}) + \binom{k}{j} P_{\boldsymbol{\omega}_\perp}(\boldsymbol{e}_{j,k})$

    $Q_{k,p}(U_{k+1-i}) \leftarrow Q_{k,q}(U_{k+1-i}) + \binom{k}{j} p^j(1-p)^{k-j}$;

for $i \in \{1,2,...,k\}$ **do**

  $x_i \leftarrow$ root of $Q_{k,q}^{(2)}(U_i) = Q_{k,p}(U_i)$ in $[0,1]$

return $\max_{i\in\{1,2,...,k\}} x_i$

Lattice Name	Figure	p	k	q	Simulation Results
Stacked Square	Figure 2.1	0.5 [17]	3	0.36561	0.2488 [6, 18, 34]
Stacked Kagome	Figure 8.2	0.52649 [38]	3	0.38497	0.2563 [32]
Stacked Honeycomb	Figure 8.4	$1 - 2sin(\pi/18)$ [30]	2	0.45213	0.3093 [32]
Stacked Triangular	Figure 8.8	$2sin(\pi/18)$ [30]	5	0.27455	0.1859 [32], 0.1860 [27]
Stacked Dice	Figure 8.9	0.47761 [39]	5	0.37754	0.2378 [32]
Stacked Bow-tie	Figure 8.10	0.40452 [35]	5	0.31884	0.2092 [32]
Stacked Octagonal	Figure 8.11	0.37181 [36]	7	0.30712	0.1752 [32]

Table 8.1: A summary of the results obtained by the growth process approach. "Lattice Name" is the name of the stacked lattice G^3, formed from the planar lattice G^2. Additionally, p is a rigorous upper bound for $p_c(G^2)$; k is the maximum degree of G^2 minus 1; q is the upper bound for $p_c(G^3)$ provided by the growth process approach. The simulation results are simulation estimates for $p_c(G^3)$, for readers' reference.

More specifically, let

$$R = \begin{bmatrix} \frac{1}{\sqrt{6}} & \frac{1}{\sqrt{2}} & \frac{1}{\sqrt{3}} \\ \frac{1}{\sqrt{6}} & -\frac{1}{\sqrt{2}} & \frac{1}{\sqrt{3}} \\ -\frac{2}{\sqrt{6}} & 0 & \frac{1}{\sqrt{3}} \end{bmatrix}.$$

Denote the rotated BCC lattice by matrix $\mathbb{B} \cdot R = (V^{\mathbb{B}} \cdot R, E^{\mathbb{B}} \cdot R)$, where $V^{\mathbb{B}} \cdot R = \{\boldsymbol{x} \cdot R \mid \boldsymbol{x} \in V^{\mathbb{B}}\}$ and $E^{\mathbb{B}} \cdot R = \{\{\boldsymbol{x}, \boldsymbol{y}\} \cdot R \mid \{\boldsymbol{x}, \boldsymbol{y}\} \in E^{\mathbb{B}}\}$. The natural projection of $\mathbb{B} \cdot R$ onto $\mathbb{R}^2$ is a triangular lattice, denoted by $\mathbb{T} = (V^{\mathbb{T}}, E^{\mathbb{T}})$ (See Figure 8.5). As in previous examples, we consider vertices in $V^{\mathbb{B}} \cdot R$ that share the same projection to be in the same column so that the nearest connected column-neighbors can be defined analogously. Subsequently, for each configuration of $\mathbb{B} \cdot R$, we can consider the open cluster containing the origin expanding from one vertex to its nearest-connected column neighbors, and thus construct a 3D growth process in a similar manner to $\mathbf{G}^{(3)}$. The 3D process is then projected onto $\mathbb{R}^2$ to obtain a projected process on $\mathbb{T}$. Notice that this 3D process on $\mathbb{B} \cdot R$ has exploration regions isomorphic to the corresponding exploration regions of the growth process defined on the stacked triangular lattice (See Figure 8.6). Thus, the projected process defined for the rotated BCC lattice has the same distribution as the one defined for the stacked triangular lattice. Since both projected processes are compared to the bond percolation process on $\mathbb{T}$, same set of stochastic ordering inequalities are solved for both applications. Consequently, the upper bound for $p_c(\mathbb{B} \cdot R)$ is the same as the growth process upper bound for the percolation threshold of the stacked triangular lattice, which is 0.27455.

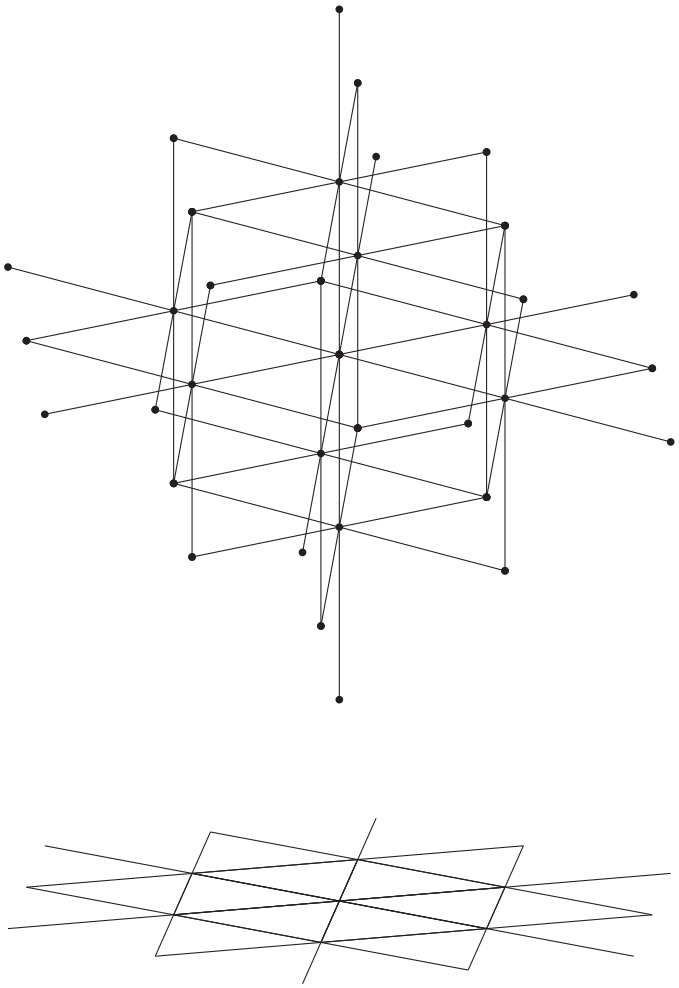

Figure 8.5: An illustration of the rotated BCC lattice and its projection, the latter of which is a triangular lattice.

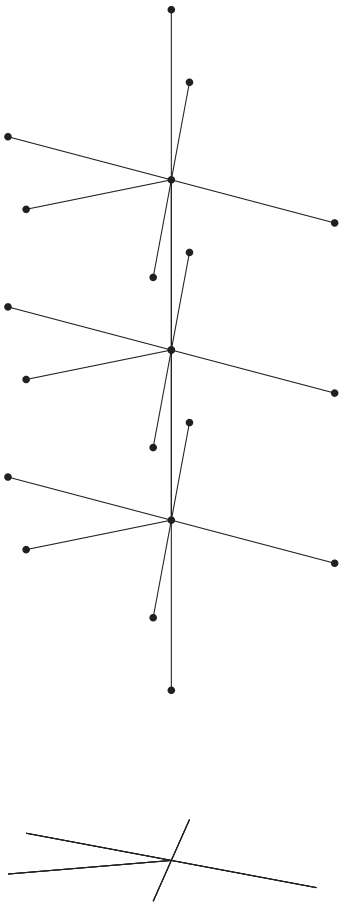

Figure 8.6: An illustration of the exploration region of the 3D process defined on $\mathbb{B} \cdot R$, whose projection contains 5 edges. The figure shows 3 layers of the exploration region, whereas the actual exploration region contains infinitely many layers, and is isomorphic to the exploration region defined on the stacked triangular lattice.

Theorem 8.3.1.

$$p_c(\mathbb{B}) = p_c(\mathbb{B} \cdot R) \leqslant 0.27455. \tag{8.1}$$

8.4 Appendix

We provide figures of the stacked lattices for which simulation estimates have been published in the physics literature, and the MATLAB code that calculates the corresponding upper bounds.

8.4.1 MATLAB Code

```
% roots = growth_model_general(k, p)
% roots are a vector
function roots = growth_model_general(k, p)
% k = Vertex degree of reference graph - 1
% p = p_c(reference graph)
% p = sym(2*sin(pi/18));

% q is the parameter of the problem lattice, n is the height
    of the
% L-shaped open path
syms q;
```

```
11 syms n;
12 % specify the scope of the parameters
13 assume(0<q<1);
14
15 p_plus = sym(zeros(2^k, 1));
16 p_pm = sym(zeros(2^k, 1));
17 p_cond = sym(zeros(2^k, 1));
18 p0 = (1-q)^n;
19 p1 = 1-(1-q)^n;
20
21 % For p_*(x), the index x corresponds to the decimal of a
     length k 0-1
22 % vector PLUS 1, where * can be plus, minus, or cond
23 % p_plus is the probability distribution of \omega_{\perp}^+,
     and by
24 % symmetry, it is also the probability distribution of \
     omega_{\perp}^-
25 % p_cond is the probability distribution of \omega
26 for i = 0:(2^k-1)
27     p_cond(i+1) = q^sum(de2bi(i, k))*(1-q)^(k - sum(de2bi(i,k
         )));
```

```
28 end
29 for i = 0:(2^k-1)
30     index = de2bi(i,k);
31     % Using infinite summation to calculate the corresponding
           probability
32     % distribution of $\omega_{\perp}^+
33     p_plus(i+1) = symsum(expand(p1^sum(index)*p0^(k-sum(index
           ))*q^n*(1-q)), n, 0, Inf);
34 end
35
36 p_plus = simplify(p_plus);
37 p_cond = simplify(p_cond);
38 % Convert binary
39 for i = 0:(2^k-1)
40     index = de2bi(i,k);
41     for i_plus = 0:(2^k-1)
42         for i_minus = 0:(2^k-1)
43             for i_cond = 0:(2^k-1)
44                 % index_i_plus is the possible outcome of
45                 % \omega_{\perp}^{+}
46                 % index_i_minus is the possible outcome of
```

```
47                  % \omega_{\perp}^{+}
48                  % index_i_cond is the possible outcome of
49                  % \omega
50                  % index_combine is given \omega_{\perp}^{+},
51                  % \omega_{\perp}^{-} and \omega, the
                        resulting
52                  % \omega_{\perp}
53                  index_i_plus = de2bi(i_plus, k);
54                  index_i_minus = de2bi(i_minus, k);
55                  index_i_cond = de2bi(i_cond, k);
56                  index_combine = bsxfun(@or, index_i_plus,
                        index_i_minus);
57                  index_combine = bsxfun(@or, index_combine,
                        index_i_cond);
58                  if isequal(index, index_combine)
59                      p_pm(i+1) = simplify(p_pm(i+1) + p_plus(
                            i_plus+1)*p_cond(i_cond+1)*p_plus(
                            i_minus+1));
60                  end
61              end
62          end
```

```
63      end
64  end
65
66  % upset_prob(i) is the upset equation that contains k-i+1
        layers of elements in
67  % the Poset lattice
68
69  upset_prob = sym(zeros(k, 1));
70
71  roots = zeros(k, 1);
72  for i = 1:k
73      for j = i:k
74          % there are j 1's in each vector
75          upset_prob(i) = upset_prob(i) + p_pm(2^j)*nchoosek(k,
                j) - nchoosek(k,j)*p^j*(1-p)^(k-j);
76      end
77  end
78
79  for i = 1:k
80      roots(i) = fzero(matlabFunction(upset_prob(i)), [0,1]);
81  end
```

8.4.2 Figures of the BCC Lattice and Stacked Lattices

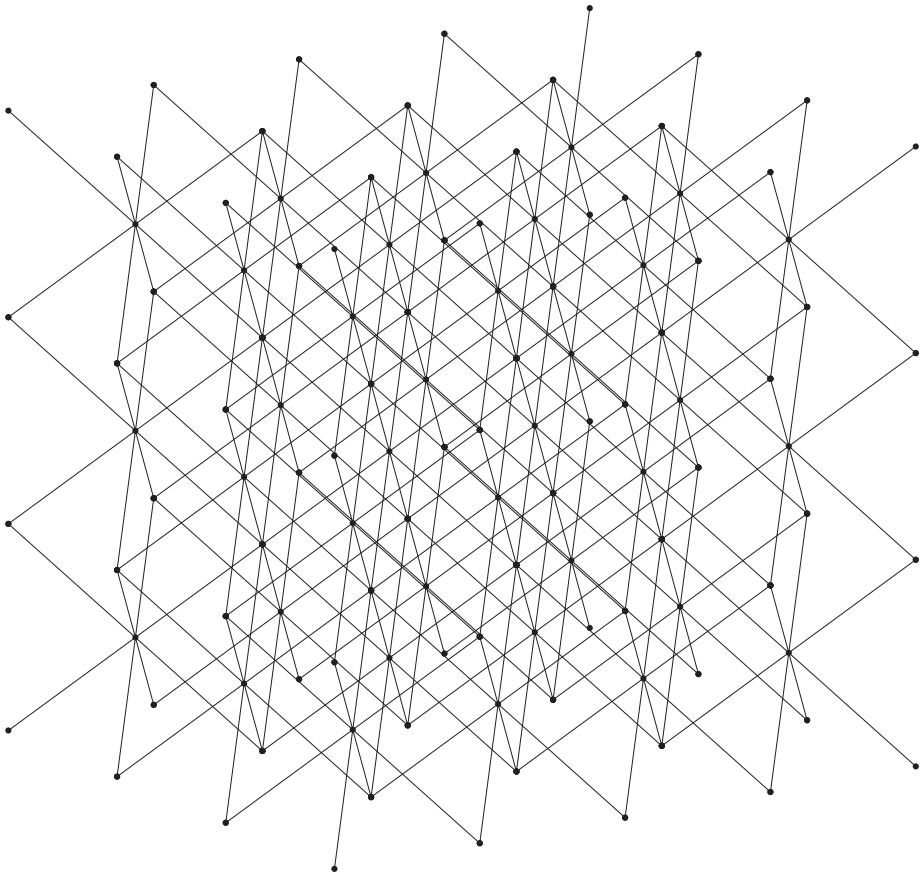

Figure 8.7: The BCC lattice.

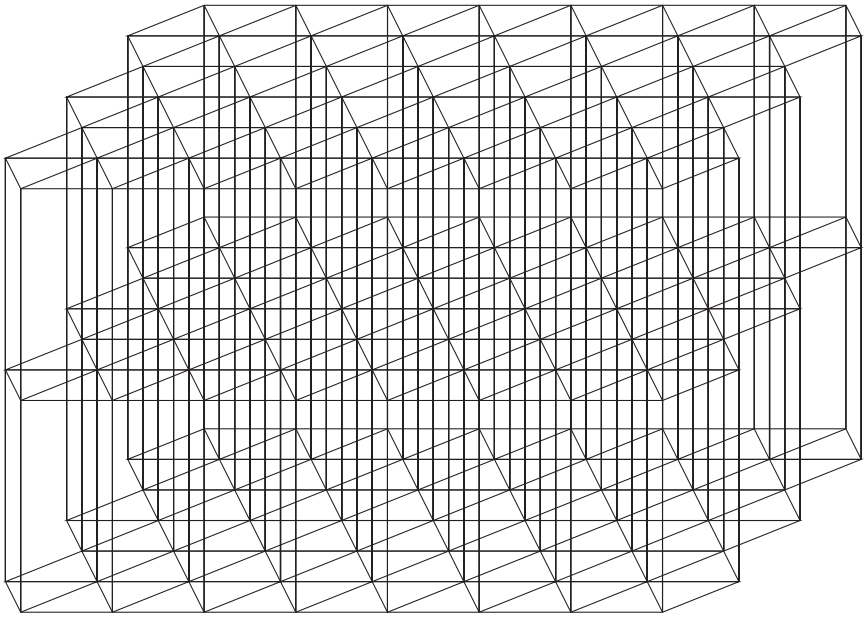

Figure 8.8: The stacked triangular lattice

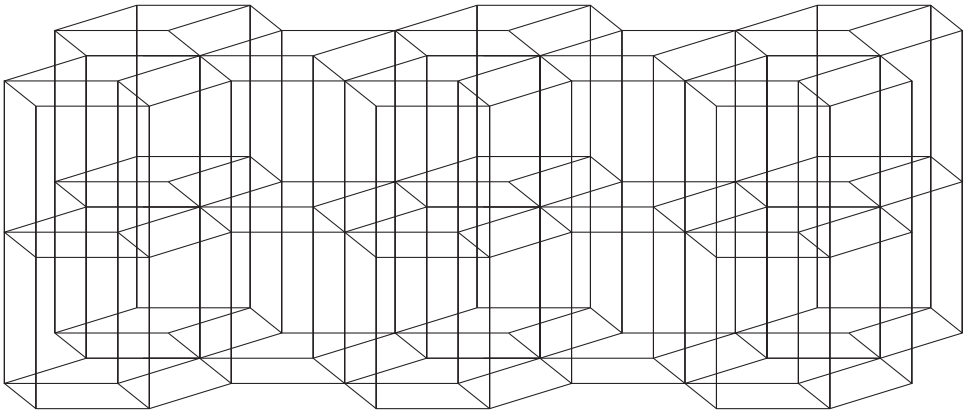

Figure 8.9: The stacked dice lattice

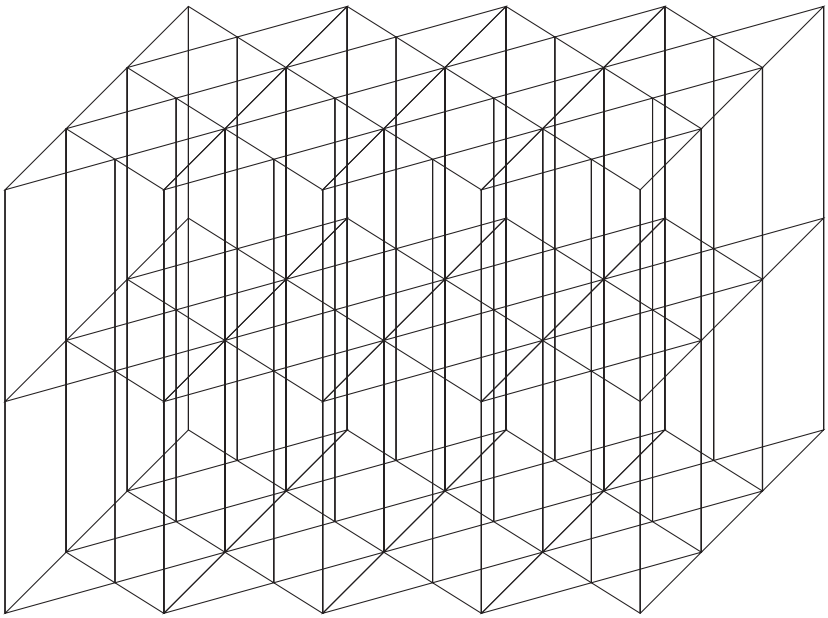

Figure 8.10: The stacked bow-tie lattice

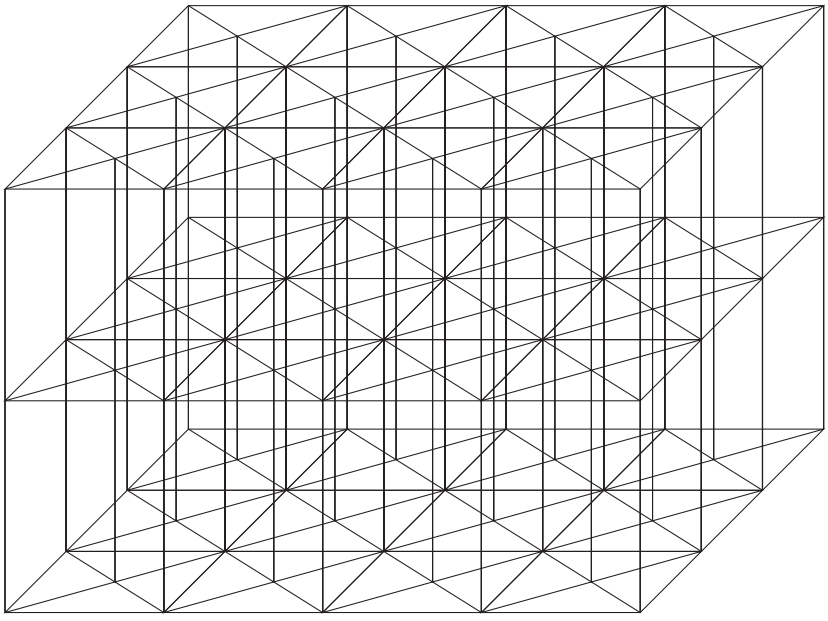

Figure 8.11: The stacked octagonal lattice, or stacked $(4, 8^2)$ dual lattice

Chapter 9

Other Implementations of the Growth Process Approach

9.1 Applying the Growth Process Approach to the Cubic lattice

9.1.1 The Rotated Cubic Lattice

In Chapter 8, we compared the rotated BCC lattice to the triangular lattice. For each embedding of the three-dimensional problem lattice, we may relate it to its natural projection. Thus, by considering different embeddings of the problem lattice, we may compare the problem lattice bond model to bond models on different

two-dimensional lattices. For the simple cubic lattice $\mathbb{L}^3$, a very straightforward comparison is to compare it with the square lattice. However, we can consider another embedding of $\mathbb{L}^3$ by rotating the canonical embedding so that after the rotation, its natural projection is a triangular lattice. More specifically, we give the following two definitions.

Definition 9.1.1 (The rotated cubic lattice $\mathbb{L}^3 \cdot R$)**.** Let

$$R =: \begin{bmatrix} \frac{1}{\sqrt{6}} & \frac{1}{\sqrt{2}} & \frac{1}{\sqrt{3}} \\ \frac{1}{\sqrt{6}} & -\frac{1}{\sqrt{2}} & \frac{1}{\sqrt{3}} \\ -\frac{2}{\sqrt{6}} & 0 & \frac{1}{\sqrt{3}} \end{bmatrix}.$$

be a rotation matrix on $\mathbb{R}^3$. The *rotated cubic lattice*, denoted by $\mathbb{L}^3 \cdot R = (\mathbb{Z}^3 \cdot R, \mathbb{E}^3 \cdot R)$, is an alternative embedding of the cubic lattice, where $\mathbb{Z}^3 \cdot R = \{\boldsymbol{x} \cdot R \mid \boldsymbol{x} \in \mathbb{Z}^3\}$ and $\mathbb{E}^3 \cdot R = \{\{\boldsymbol{x} \cdot R, \boldsymbol{y} \cdot R\} \mid (\boldsymbol{x}, \boldsymbol{y}) \in \mathbb{E}^3\}$.

Definition 9.1.2 (The triangular lattice $\mathbb{T}$)**.** Let $\mathbb{T} = (V^{\mathbb{T}}, E^{\mathbb{T}})$ be an embedding of the *triangular lattice* in $\mathbb{R}^2$, where $V^{\mathbb{T}} = \text{proj}(\mathbb{Z}^3 \cdot R) = \{k_1(\frac{1}{\sqrt{6}}, \frac{1}{\sqrt{2}}) + k_2(\frac{2}{\sqrt{6}}, 0) \mid k_1, k_2 \in \mathbb{Z}\}$ and $E^{\mathbb{T}} = \text{proj}(\mathbb{E}^3 \cdot R) = \{\{\boldsymbol{x}, \boldsymbol{y}\} \mid \boldsymbol{x}, \boldsymbol{y} \in V^{\mathbb{T}}, \|\boldsymbol{x} - \boldsymbol{y}\| = \frac{2}{\sqrt{6}}\}$.

For the rotated cubic lattice $\mathbb{L}^3 \cdot R$, one observation is that its natural projection is the triangular lattice $\mathbb{T}$ (Figure 9.1). Thus, in this section, we shall describe how the growth process approach is implemented to relate the bond percolation model on $\mathbb{L}^3 \cdot R$ to the one on $\mathbb{T}$.

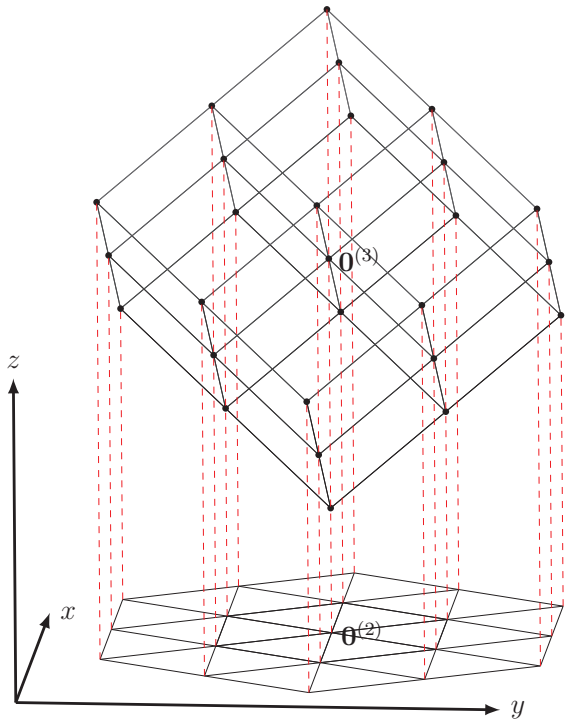

Figure 9.1: An illustration of the rotated cubic lattice $\mathbb{L}^3 \cdot R$ and its projection onto $\mathbb{R}^2$, the latter of which is the triangular lattice $\mathbb{T}$.

9.1.2 The Three-dimensional Growth Process on $\mathbb{L}^3 \cdot R$

Unlike the stacked lattices, vertices of $\mathbb{L}^3 \cdot R$ that share the same projections are no longer connected by vertical edges. Thus, we construct the three-dimensional growth process on $\mathbb{L}^3 \cdot R$ in a different manner by modifying its exploration regions: at each step, the exploration region is a subset of edges incident with the vertex currently under exploration. In other words, the open cluster on the rotated cubic lattice is considered to be exploring from one vertex to its neighbors, instead of its column-neighbors. A formal description and notation are given in the following definition.

Definition 9.1.3 (The growth process $\mathbf{G}^{(3)}$)**.** We initialize $(A_0^{(3)}, C_0^{(3)}, D_0^{(3)})$ as follows:

$$A_0^{(3)} := \emptyset,$$

$$C_0^{(3)} := \emptyset,$$

$$D_0^{(3)} := \{\mathbf{0}^{(3)}\}.$$

Let l be a labeling function on $\mathbb{T}$ and $(\Omega^{(3)}, \mathcal{F}^{(3)}, P_q^{(3)})$ be the probability space for the rotated cubic lattice bond percolation model. Define a stochastic process $(v_n^{(3)}, A_n^{(3)}, B_n^{(3)}, C_n^{(3)}, D_n^{(3)}) : \Omega^{(3)} \to \mathbb{Z}^3 \cdot R \times 2^{\mathbb{Z}^3 \cdot R} \times 2^{\mathbb{E}^3 \cdot R} \times 2^{\mathbb{E}^3 \cdot R} \times 2^{\mathbb{Z}^3 \cdot R}$ on $(\Omega^{(3)}, \mathcal{F}^{(3)}, P_q^{(3)})$ recursively as follows. For each $\omega^{(3)} \in \Omega^{(3)}$, assume that the process has been defined

up to step n. At step $n+1$, if $D_n^{(3)} \setminus A_n^{(3)} \neq \emptyset$, we define

$$\begin{aligned}
v_{n+1}^{(3)} &:= \arg\min\{l(v) : v \in D_n^{(3)} \setminus A_n^{(3)}\},\\
A_{n+1}^{(3)} &:= A_n^{(3)} \cup \{v_{n+1}^{(3)}\},\\
B_{n+1}^{(3)} &:= I[v_{n+1}^{(3)}] \setminus I[\mathrm{col}(D_n^{(3)} \setminus \{v_{n+1}^{(3)}\})],\\
C_{n+1}^{(3)} &:= C_n^{(3)} \cup \{e \in B_{n+1}^{(3)} : \omega^{(3)}(e) = 1\},\\
D_{n+1}^{(3)} &:= D_n^{(3)} \cup (\textstyle\bigcup_{C_{n+1}^{(3)}}).
\end{aligned}$$

Otherwise, we define

$$\begin{aligned}
v_{n+1}^{(3)} &:= v_n^{(3)},\\
A_{n+1}^{(3)} &:= A_n^{(3)},\\
B_{n+1}^{(3)} &:= \emptyset,\\
C_{n+1}^{(3)} &:= C_n^{(3)},\\
D_{n+1}^{(3)} &:= D_n^{(3)},
\end{aligned}$$

The *growth process associated with* $\omega^{(3)}$ is the stochastic process $\mathbf{G}_n^{(3)} := (A_n^{(3)}, C_n^{(3)})$ defined on the probability space $(\Omega^{(3)}, \mathcal{F}^{(3)}, P_q^{(3)})$.

We observe the following properties regarding the growth process $\mathbf{G}^{(3)}$.

Lemma 9.1.4. *For each $\omega^{(3)} \in \Omega^{(3)}$ and $n \in \mathbb{N}$, we have*

$$D_n^{(3)}(\omega^{(3)}) \subseteq D(\omega^{(3)}).$$

Lemma 9.1.5. *The conditional joint distribution of* $C_n^{(3)} \setminus C_{n-1}^{(3)}$ *given* $B_n^{(3)}$ *is*

$$P_q^{(3)}(C_n^{(3)} \setminus C_{n-1}^{(3)} \mid B_n^{(3)}) = \begin{cases} 0 & \text{if } C_n^{(3)} \setminus C_{n-1}^{(3)} \not\subseteq B_n^{(3)}, \\ Q_{|B_n^{(3)}|,q}(\mathbf{e}_{|C_n^{(3)} \setminus C_{n-1}^{(3)}|,|B_n^{(3)}|}) & \text{otherwise.} \end{cases}$$

The properties above follow directly from Definition 9.1.3. Particularly, we let each $e \in B_n^{(3)}$ be added to $C_n^{(3)} \setminus C_{n-1}^{(3)}$ if and only if $\omega^{(3)}(e) = 1$, which results in the transition probabilities of $\mathbf{G}^{(3)}$ characterized by Q-measures.

9.1.3 The Projected Process on $\mathbb{T}$

Definition 9.1.6 (The projected growth process $\mathbf{G}^{(2)}$)**.** Let $(v_n^{(2)}, A_n^{(2)}, B_n^{(2)}, C_n^{(2)}, D_n^{(2)}) \in V^{\mathbb{T}} \times 2^{V^{\mathbb{T}}} \times 2^{E^{\mathbb{T}}} \times 2^{E^{\mathbb{T}}} \times 2^{V^{\mathbb{T}}}$ be a stochastic process on $(\Omega^{(3)}, \mathcal{F}^{(3)}, P_q^{(3)})$, where $v_n^{(2)} := \text{proj}(v_n^{(3)})$, $A_n^{(2)} := \text{proj}(A_n^{(3)})$,..., and $D_n^{(2)} := \text{proj}(D_n^{(3)})$. Define the *projected growth process associated with* $\omega^{(3)}$ as $\mathbf{G}_n^{(2)} := (A_n^{(2)}, C_n^{(2)})$.

Naturally, the process $\mathbf{G}^{(2)}$, which is the projection of $\mathbf{G}^{(3)}$, also has these similar properties that are described in Chapter 4.

Lemma 9.1.7. *For each* $\omega^{(3)} \in \Omega^{(3)}$ *and* $n \in \mathbb{N}$*, we have*

$$D_n^{(2)}(\omega^{(3)}) \subseteq \text{proj}(D(\omega^{(3)})). \tag{9.1}$$

Lemma 9.1.8. *The conditional joint distribution of* $C_n^{(2)} \setminus C_{n-1}^{(2)}$ *given* $B_n^{(2)}$ *is*

$$P_q^{(3)}(C_n^{(2)} \setminus C_{n-1}^{(2)} \mid B_n^{(2)}) = \begin{cases} 0 & \text{if } C_n^{(2)} \setminus C_{n-1}^{(2)} \not\subseteq B_n^{(2)}, \\ Q_{|B_n^{(2)}|,q}(\mathbf{e}_{|C_n^{(2)} \setminus C_{n-1}^{(2)}|,|B_n^{(2)}|}) & \text{otherwise.} \end{cases} \tag{9.2}$$

Both Lemma 9.1.7 and Lemma 9.1.8 are direct consequences of Lemma 9.1.4 and Lemma 9.1.5, respectively.

9.1.4 The Induced Configuration

Notice that the transition probabilities of the projected process $\mathbf{G}^{(2)}$ are already characterized by Q-measures instead of $Q^{(2)}$-measures. Thus, we no longer need to introduce the replicated process and coupled process to relate the $\mathbf{G}^{(2)}$ to a standard bond percolation model on $\mathbb{T}$. Instead, we can construct a configuration on $\mathbb{T}$ directly from $\mathbf{G}^{(2)}$ as follows.

Definition 9.1.9 (The induced configuration $\omega^{(2)}$)**.** Let $(\Omega^{(2)}, \mathcal{F}^{(2)}, P_q^{(2)})$ be the probability space of the triangular lattice bond percolation model. For each $(\omega^{(3)}, \tilde{\omega}^{(2)}) \in \Omega^{(3)} \times \Omega^{(2)}$, let $\mathbf{G}^{(2)}$ be the projected growth process associated with $\omega^{(3)}$. The *induced configuration* is a configuration in $\Omega^{(2)}$ such that

$$\omega^{(2)}(e) := \begin{cases} 1 & \text{if } e \in \bigcup_{n=1}^{\infty} C_n^{(2)}, \\ 0 & \text{if } e \in (\bigcup_{n=1}^{\infty} B_n^{(2)}) \setminus (\bigcup_{n=1}^{\infty} C_n^{(2)}), \\ \tilde{\omega}^{(2)}(e) & \text{otherwise,} \end{cases} \tag{9.3}$$

for each $e \in V^{\mathbb{T}}$.

Lemma 9.1.10. *If $(\omega^{(3)}, \tilde{\omega}^{(2)}) \in \Omega^{(3)} \times \Omega^{(2)}$ is P_q distributed, where $P_q := P_q^{(3)} \times P_q^{(2)}$, then the induced configuration $\omega^{(2)}$ is $P_q^{(2)}$ distributed.*

Lemma 9.1.11. *For each* $(\omega^{(3)}, \tilde{\omega}^{(2)}) \in \Omega^{(3)} \times \Omega^{(2)}$*, let* $\omega^{(2)}$ *be the induced configuration and* $\mathbf{G}^{(2)}$ *be the projected growth process associated with* $\omega^{(3)}$*. Then*

$$D(\omega^{(2)}) \subseteq \bigcup_{C_\infty^{(2)}} . \tag{9.4}$$

9.1.5 An Upper Bound for $p_c(\mathbb{L}^3)$

Now we provide an improved upper bound for $p_c(\mathbb{L}^3)$.

Theorem 9.1.12.

$$p_c(\mathbb{L}^3) \leqslant p_c(\mathbb{T}) = 2\sin\left(\frac{\pi}{18}\right). \tag{9.5}$$

Proof. Since under P_q measure the marginal distribution of $\omega^{(3)}$ is $P_q^{(3)}$, we have

$$P_q^{(3)}(|D(\omega^{(3)})| = \infty) = P_q(|D(\omega^{(3)})| = \infty). \tag{9.6}$$

By Fact 9.1.4,

$$P_q(|D(\omega^{(3)})| = \infty) \geqslant P_q(|\bigcup_{n=1}^{\infty} D_n^{(3)}(\omega^{(3)})| = \infty). \tag{9.7}$$

From Definition 9.1.3 and 9.1.6,

$$\begin{aligned} P_q(|\bigcup_{n=1}^{\infty} D_n^{(3)}(\omega^{(3)})| = \infty) &= P_q(|\bigcup_{C_\infty^{(3)}(\omega^{(3)})}| = \infty) \\ &\geqslant P_q(|\bigcup_{C_\infty^{(2)}(\omega^{(3)})}| = \infty). \end{aligned} \tag{9.8}$$

Using Lemma 9.1.11, we have

$$P_q(|\bigcup_{C_\infty^{(2)}(\omega^{(3)})}| = \infty) \geqslant P_q(|D(\omega^{(2)})| = \infty). \tag{9.9}$$

Also, in Lemma 9.1.10 we proved that $\omega^{(2)}$ is $P_q^{(2)}$ distributed. Thus,

$$P_q(|D(\omega^{(2)})| = \infty) = P_q^{(2)}(|D(\omega^{(2)})| = \infty) > 0 \tag{9.10}$$

for all $q > p_c(\mathbb{T})$. This implies that $P_q^{(3)}(|D(\omega^{(3)})| = \infty) > 0$ for all $q > p_c(\mathbb{T})$ by Equation (9.6) – (9.10). Consequently, $p_c(\mathbb{L}^3) = p_c(\mathbb{L}^3 \cdot R) \leqslant p_c(\mathbb{T})$. □

9.2 Applying the Growth Process Approach to the FCC lattice

9.2.1 The FCC Lattice and Its Rotation

The face-centered cubic (FCC) lattice is a periodic non-planar lattice. Its canonical embedding in $\mathbb{R}^3$, denoted by $\mathbb{F} = (V^{\mathbb{F}}, E^{\mathbb{F}})$, is shown in Figure 9.2: vertices in $V^{\mathbb{F}}$ correspond to the points in $\{(z_1, z_2, z_3) \in \mathbb{Z}^3 \mid z_1 + z_2 + z_3 \equiv 0 \ (mod\ 2)\}$, and edges in $E^{\mathbb{F}}$ correspond to pairs of vertices whose Euclidean distance is $\sqrt{2}$. Intuitively, one may consider the embedding as replacing each cubic unit of the canonical embedding of the cubic lattice by the graph shown in Figure 9.3. Notice that the four edges on each face of the cubic unit are shared by the adjacent cubic unit, i.e., the cubic unit that has the same face. Unlike the stacked lattices, the growth process approach can not be applied to the FCC lattice in a straightforward manner. Thus, we would like to rotate the FCC lattice and modify the approach so that it can be applied to the

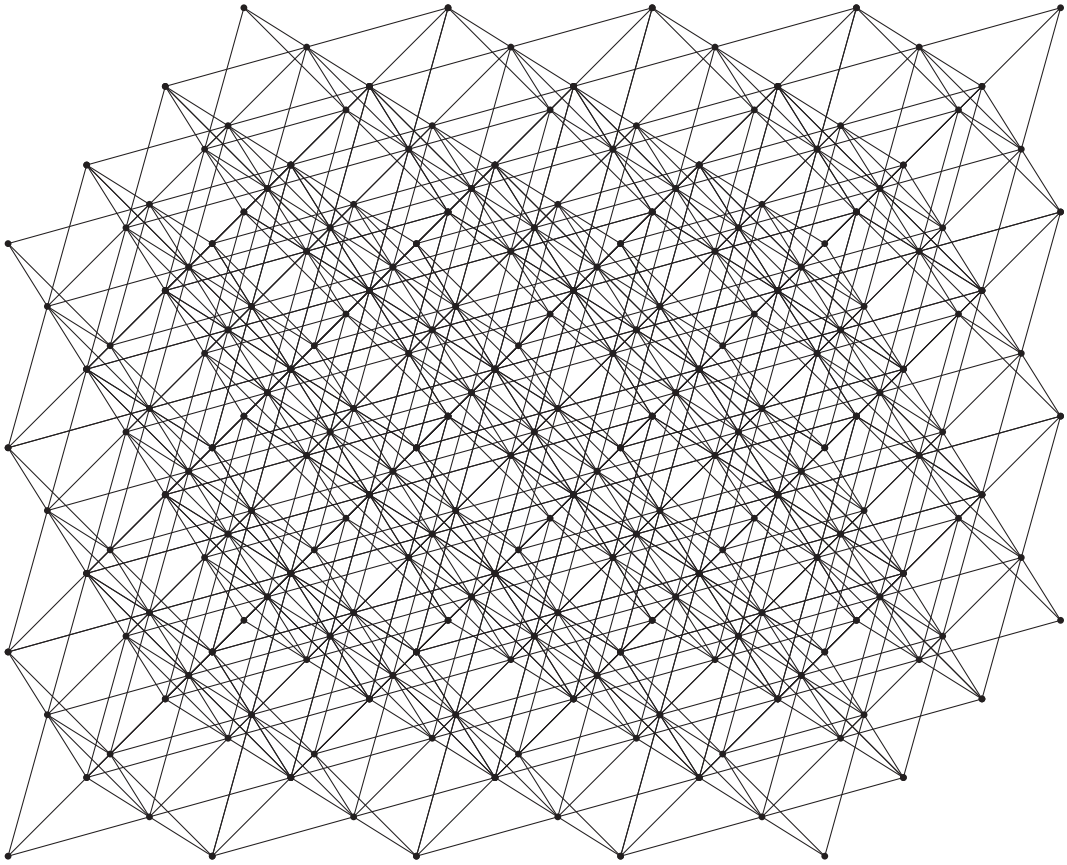

Figure 9.2: The FCC lattice

rotated FCC lattice.

Consider the rotation matrix

$$R = \begin{bmatrix} \frac{\sqrt{2}}{2} & 0 & \frac{\sqrt{2}}{2} \\ -\frac{\sqrt{2}}{2} & 0 & \frac{\sqrt{2}}{2} \\ 0 & 1 & 0 \end{bmatrix}.$$

Rotating the FCC lattice by matrix R and then projecting onto $\mathbb{R}^2$ results in a triangular lattice. (See Figure 9.4). Denote this rotated FCC lattice by $\mathbb{F} \cdot R = (V^{\mathbb{F}} \cdot R, E^{\mathbb{F}} \cdot R)$

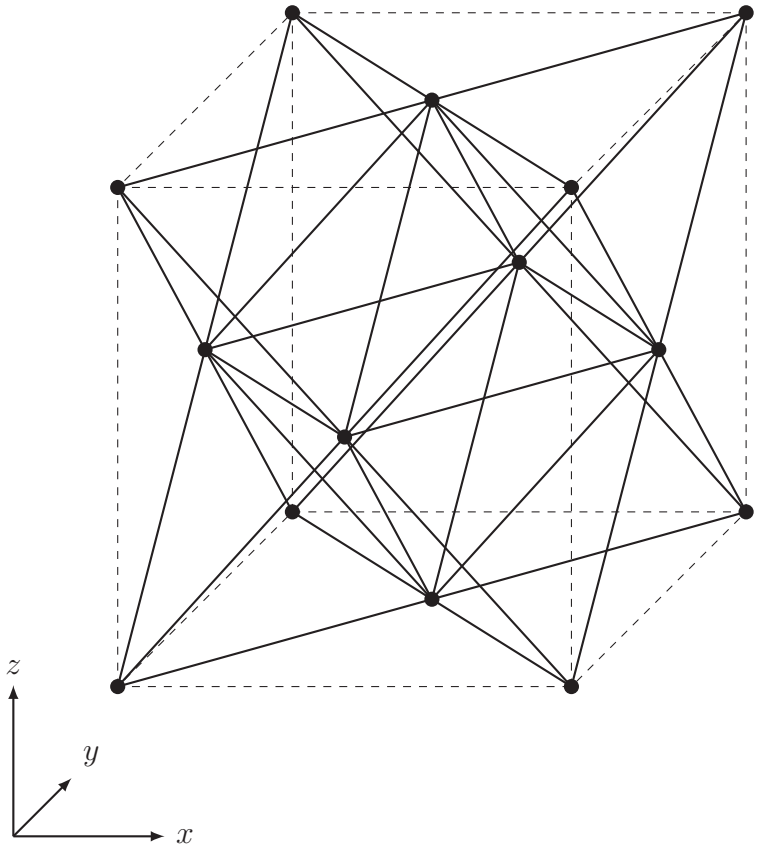

Figure 9.3: One cubic unit of the FCC lattice. The dashed lines illustrate the boundaries of the cubic unit. They are not edges of the FCC lattice. This convention applies to the remaining figures in this chapter.

and its projection by $\mathbb{T} = (V^{\mathbb{T}}, E^{\mathbb{T}})$. As in previous applications, we let q be the parameter of the homogeneous bond percolation model on $\mathbb{F} \cdot R$. Notice that when applying the growth process approach to the rotated FCC lattice, the exploration regions are similar (but not isomorphic) to the corresponding exploration regions of the growth process of the stacked triangular lattice (See Figure 9.5). On this rotated FCC lattice, vertices sharing the same natural projection are considered to be in the same column. Thus, the definition of the nearest connected column-neighbor carries over. Given a labeling function l on $\mathbb{T}$, we define a 3D growth process $\mathbf{G}^{(3)}$ for each configuration on $\mathbb{F} \cdot R$ analogously. Projecting $\mathbf{G}^{(3)}$ onto $\mathbb{R}^2$ results in a growth process on $\mathbb{T}$. Denote the projected process by $\mathbf{G}^{(2)}$. Our goal is to solve for the joint distribution of adding edges in the projected growth process $\mathbf{G}^{(2)}$. Notice that the geometry of the exploration regions (Figure 9.5) differ from the geometry of the exploration regions of the stacked lattices in the sense that the former one contains zig-zag edges forming loops while the latter one is simply a tree. Our approach for calculating the joint distribution of including new edges in the projected process $\mathbf{G}^{(2)}$ is modified accordingly.

We now partition $E^{\mathbb{T}}$ into two types: s-type and t-type, as illustrated in Figure 9.5. Each s-type edge (marked in red) is the projection of a sequence of parallel edges in $E^{\mathbb{F}} \cdot R$, and each t-type edge (marked in black) is the projection of a sequence of zig-zag edges in $E^{\mathbb{F}} \cdot R$. More rigorously, the s-type edges are the projections of edges in $\{(\boldsymbol{x}, \boldsymbol{y}) \cdot R \mid (\boldsymbol{x}, \boldsymbol{y}) \in E^{\mathbb{F}}, x_1 = y_1 + 1, x_2 = y_2 - 1, x_3 = y_3\}$, and t-type edges are

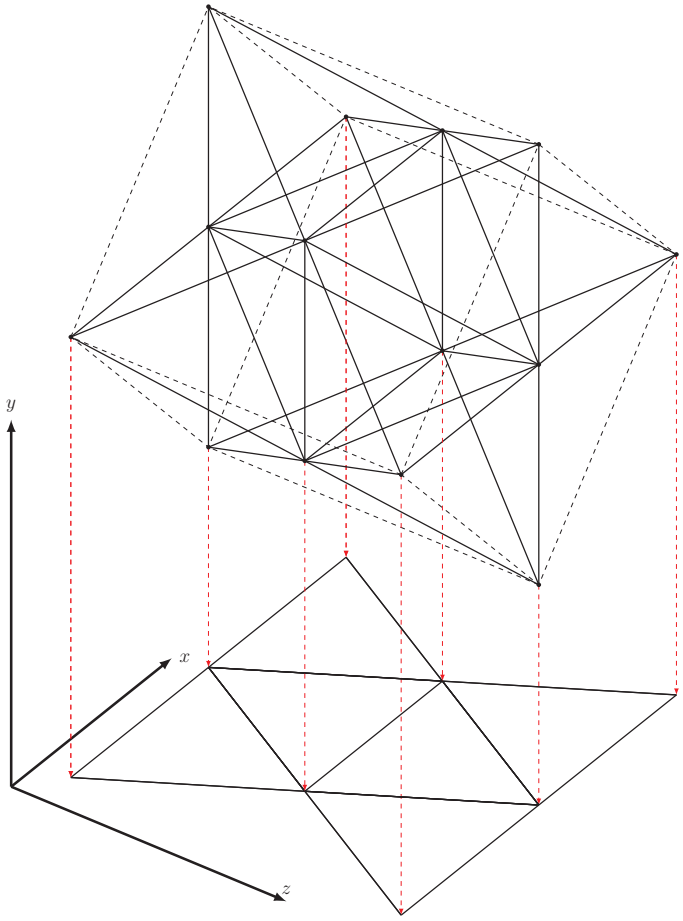

Figure 9.4: An illustration of one cubic unit of the rotated FCC lattice and its projection.

the projections of the remaining edges in $E^{\mathbb{F}} \cdot R$.

9.2.2 The 3D Growth Process on the FCC Lattice

We provide a detailed description of the 3D growth process process $\mathbf{G}^{(3)}$. Let $(\Omega^{(3)}, \mathcal{F}^{(3)}, P_q^{(3)})$ be the probability space of the homogeneous bond percolation model of $\mathbb{F} \cdot R$ with parameter q, and let l be a labeling function on $\mathbb{T}$. Furthermore, the

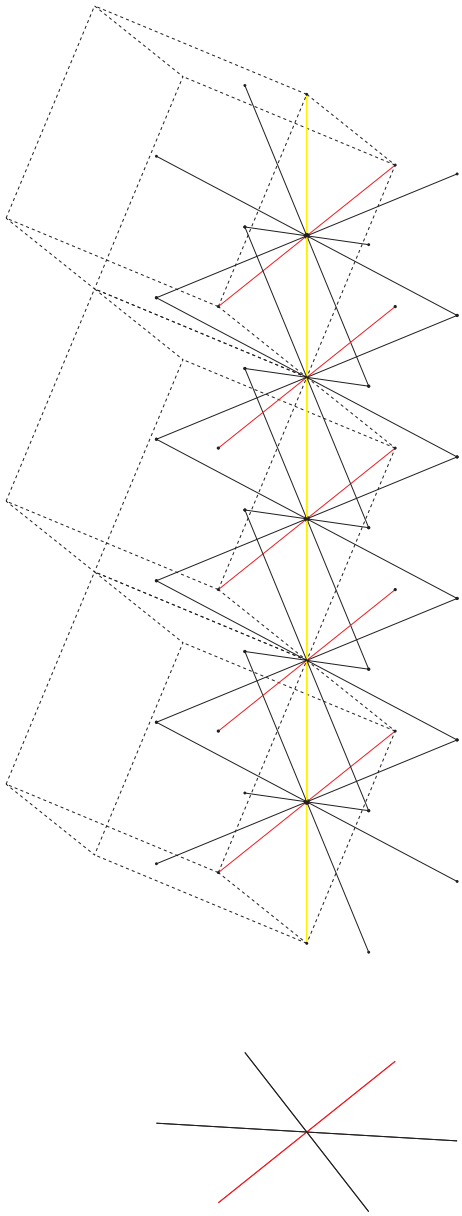

Figure 9.5: An illustration of the exploration region of the 3D process defined on the FCC lattice, where s-type edges are illustrated by red line segments, t-type edges are illustrated by black line segments, and the vertical edges are illustrated by yellow line segments.

notation defined in Definitions 3.1.1 to 3.1.4 used in this chapter is all with respect to $G = \mathbb{F} \cdot R$.

For the rotated FCC lattice, we define the projection of its vertices and edges and the labeling function in the most straightforward manner. Correspondingly, we may define the nearest connected-column neighbor and its related terms for the FCC lattice as follows. The definitions are not very different from the one defined for the cubic lattice.

Definition 9.2.1. For any $\boldsymbol{x} \in V^{\mathbb{F}} \cdot R$, define its *associated column* as $\mathrm{col}(\boldsymbol{x}) := \{\boldsymbol{x} + k(1,1,0) \cdot R \mid k \in \mathbb{Z}\}$. More generally, for any $A \subset \mathbb{Z}^3$, their *associated columns* are $\mathrm{col}(A) := \bigcup_{\boldsymbol{x} \in A} \mathrm{col}(\boldsymbol{x})$.

Definition 9.2.2. The *column-neighbors* of a vertex $\boldsymbol{x} \in V^{\mathbb{F}} \cdot R$ is the set of vertices in $V^{\mathbb{F}} \cdot R$ incident to $\mathrm{col}(\boldsymbol{x})$.

Definition 9.2.3. For an arbitrary vertex $\boldsymbol{x} \in V^{\mathbb{F}} \cdot R$, a collection of edges $B \subseteq I[\mathrm{col}(\boldsymbol{x})]$ and a configuration $\omega^{(3)} \in \Omega^{(3)}$, the *nearest connected column-neighbors* of $\boldsymbol{x}$, denoted by $N[\boldsymbol{x}, \omega^{(3)}, B]$, is a set of vertices, each vertex $\boldsymbol{y}$ of which satisfies the following:

1. $\boldsymbol{y}$ is a column-neighbor of $\boldsymbol{x}$,
2. $\boldsymbol{y} \xleftrightarrow{B,\omega^{(3)}} \boldsymbol{x}$,
3. for all $\boldsymbol{z} \in V^{\mathbb{F}} \cdot R$ such that

(a) $\mathrm{proj}(\boldsymbol{z}) = \mathrm{proj}(\boldsymbol{y})$, and

(b) $\boldsymbol{z} \xleftarrow{B,\omega^{(3)}} \boldsymbol{x}$,

either $|y_3 - x_3| < |z_3 - x_3|$ or both $|y_3 - x_3| = |z_3 - x_3|$ and $(y_3 - x_3) > 0$. Additionally, if the configuration $\omega^{(3)}$ has been pre-specified and is clear from context, we simply omit $\omega^{(3)}$ and refer the nearest connected column-neighbors of $\boldsymbol{x}$ as $N[\boldsymbol{x}, B]$.

Meanwhile, notice that the exploration regions we are about to define for the FCC lattice may contain loops, but there exists a unique shortest-path from the vertex currently under exploration to each of its nearest connected column-neighbors. We may slightly modify the notation "*path*" as follows.

Definition 9.2.4. Let $B \subset E^{\mathbb{F}} \cdot R$ be a collection of edges, and $u, v \in V^{\mathbb{F}} \cdot R$ be two vertices of $\mathbb{F} \cdot R$ such that there exists a unique shortest-path from u to v using only edges in B. Denote the set of edges in such path by $\mathrm{path}(u, v, B)$.

After modifying the related terms, we may define a 3D growth process on $\mathbb{F} \cdot R$ for each $\omega^{(3)} \in \Omega^{(3)}$.

Definition 9.2.5. Initialize $(A_0^{(3)}, D_0^{(3)}, C_0^{(3)})$ as follows:

$$A_0^{(3)} := \emptyset,$$

$$D_0^{(3)} := \{\mathbf{0}^{(3)}\},$$

$$C_0^{(3)} := \emptyset.$$

We then define a stochastic process $(v_n^{(3)}, A_n^{(3)}, B_n^{(3)}, C_n^{(3)}, D_n^{(3)}) : \Omega^{(3)} \to V^{\mathbb{F}} \cdot R \times 2^{V^{\mathbb{F}} \cdot R} \times 2^{E^{\mathbb{F}} \cdot R} \times 2^{E^{\mathbb{F}} \cdot R} \times 2^{V^{\mathbb{F}} \cdot R}$ on $(\Omega^{(3)}, \mathcal{F}^{(3)}, P_q^{(3)})$ for $n \geqslant 1$ recursively as follows. Assume that this stochastic process has been defined up to step n. At step $n+1$, if $D_n^{(3)} \setminus A_n^{(3)} \neq \emptyset$, we define

$$v_{n+1}^{(3)} := \arg\min\{l(v) : v \in D_n^{(3)} \setminus A_n^{(3)}\},$$

$$A_{n+1}^{(3)} := A_n^{(3)} \cup \{v_{n+1}^{(3)}\},$$

$$B_{n+1}^{(3)} := I[\mathrm{col}(v_{n+1}^{(3)})] \setminus I[\mathrm{col}(D_n^{(3)} \setminus \{v_{n+1}^{(3)}\})],$$

$$D_{n+1}^{(3)} := D_n^{(3)} \cup N[v_{n+1}^{(3)}, B_{n+1}^{(3)}],$$

$$C_{n+1}^{(3)} := C_n^{(3)} \cup \left(\bigcup_{v \in N[v_{n+1}^{(3)}, B_{n+1}^{(3)}]} \mathrm{path}(v_{n+1}^{(3)}, v, B_{n+1}^{(3)}) \right).$$

Otherwise, we define

$$v_{n+1}^{(3)} := v_n^{(3)},$$

$$A_{n+1}^{(3)} := A_n^{(3)},$$

$$B_{n+1}^{(3)} := \emptyset,$$

$$D_{n+1}^{(3)} := D_n^{(3)},$$

$$C_{n+1}^{(3)} := C_n^{(3)}.$$

The *growth process associated with* $\omega^{(3)}$ is the stochastic process $\mathbf{G}_n^{(3)} := (A_n^{(3)}, C_n^{(3)})$ defined on the probability space $(\Omega^{(3)}, \mathcal{F}^{(3)}, P_q^{(3)})$.

9.2.3 The Projected Growth Process on the Triangular Lattice

Performing the natural projection of $\mathbf{G}^{(3)}$ results in a projected process on $\mathbb{T}$. Denote the projected process by $\mathbf{G}^{(2)}$, and all the associated notation carries over. Notice that the probability measure of the rotated FCC lattice bond percolation model, still denoted by $P_q^{(3)}$, satisfies the translation invariance property (Lemma 4.2.2), which further implies that $\mathbf{G}^{(2)}$ satisfies the vertex transitive property (Theorem 4.2.3 and 4.2.4). It can also be verified that $v_{n+1}^{(2)}$ and $B_{n+1}^{(2)}$ is $\sigma(\mathbf{G}_n^{(2)})$-measurable, as in Lemma 4.2.5. Additionally, the construction of the exploration regions $\{B_n^{(3)}\}$ implies pair-wise disjointness, which provides conditional independence of $\mathbf{G}_{n+1}^{(2)}$ and $\mathcal{F}_n^{(2)} = \sigma(\{\mathbf{G}_i^{(2)}\}_{i=1}^n)$ given $v_{n+1}^{(2)}$, $z_{v_{n+1}^{(2)}}$ and $B_{n+1}^{(2)}$. Consequently, we may conclude that $\mathbf{G}^{(2)}$ is a Markov process based on similar reasoning in the proof of Theorem 4.2.6.

Suppose that at step n of $\mathbf{G}^{(2)}$, the number of s-type edges and t-type edges in $B_n^{(2)}$ are s_n and t_n, respectively. Label the s-type edges by $\{1, 2, ..., s_n\}$ and the t-type edges by $\{s_n + 1, ..., s_n + t_n\}$ deterministically. Consider two sequences of indicators, $\boldsymbol{\omega}_{\perp,s}^{(2)} \in \{0,1\}^{s_n}$ and $\boldsymbol{\omega}_{\perp,t}^{(2)} \in \{0,1\}^{t_n}$. The i-th indicator in $\boldsymbol{\omega}_{\perp,s}^{(2)}$ indicates whether the s-

type edge with label i is in $C_n^{(2)}$ or not, and the i-th indicator in $\boldsymbol{\omega}_{\perp,t}^{(2)}$ indicates whether the t-type edge with label s_n+i is in $C_n^{(2)}$ or not. Let $Q_{s_n,t_n,q}^{(2)}$ be the joint distribution of $(\boldsymbol{\omega}_{\perp,s}^{(2)}, \boldsymbol{\omega}_{\perp,t}^{(2)})$ under $P_q^{(3)}$-measure. Then the transition probability of $\mathbf{G}^{(2)}$ can be characterized by $Q_{s_n,t_n,q}^{(2)}$-measure, which will be calculated later. Namely,

Theorem 9.2.6 (Transition Probabilities of $\mathbf{G}^{(2)}$ in the FCC lattice)**.** *The transition probability of* $\mathbf{G}^{(2)}$ *can be explicitly expressed as:*

$$P_q^{(3)}(\mathbf{G}_{n+1}^{(2)}|\mathbf{G}_n^{(2)}) = \begin{cases} 0 & \text{if} A_{n+1}^{(2)} \setminus A_n^{(2)} \neq \{v_{n+1}^{(2)}\}, \\ 0 & \text{if} C_{n+1}^{(2)} \setminus C_n^{(2)} \not\subseteq B_{n+1}^{(2)}, \\ Q_{s_{n+1},t_{n+1},q}^{(2)}(\boldsymbol{\omega}_{\perp,s}^{(2)}, \boldsymbol{\omega}_{\perp,t}^{(2)}) & \text{otherwise.} \end{cases} \tag{9.11}$$

Notice that the transition probabilities above are well-defined in the sense that both s_{n+1} and t_{n+1} are obtained from $B_{n+1}^{(2)}$ and thus is $\sigma(\mathbf{G}_n^{(2)})$-measurable.

We further let $Q_{s_n,t_n,s,t}$ denote the product measure of s_n Bernoulli measures with parameter s and t_n Bernoulli measures with parameter t. Here we introduce two parameters s and t since there are two types of edge in the triangular lattice, and the marginal distribution of adding s-edge and t-edge to $C^{(2)}$ are not the same because of the geometry of $B_n^{(3)}$. This inspires us to compare $Q^{(2)}$ measures to product measures of Bernoulli measures with two-parameters, and relate the FCC lattice bond percolation model to a triangular lattice inhomogeneous bond percolation model. We shall provide detailed descriptions of the inhomogeneous percolation in Section 9.2.5.

For the construction of a replicated process and a coupled process to derive the upper bound for $p_c(\mathbb{F})$, we need the stochastic ordering inequalities

$$Q^{(2)}_{s_n,t_n,q} \geqslant_{\text{st}} Q_{s_n,t_n,s,t} \tag{9.12}$$

for all $n \in \mathbb{N}$. Notice that for $n \geqslant 2$, either $s_n \leqslant 2$ and $t_n \leqslant 3$, or $s_n \leqslant 1$ and $t_n \leqslant 4$. Consequently, given s and t, our goal is to find the smallest q such that Equation (9.12) holds for each of the 13 pairs of (s_n, t_n) satisfying the condition above. In Chapter 6, we reduced the amount of calculation in checking stochastic ordering inequalities by introducing equivalence classes and marginal distribution arguments (Lemma 6.7.1 and Lemma 6.7.2). However, these two lemmas can not be applied to the $Q^{(2)}$ distributions for the FCC lattice. More specifically, for any pair $(s_m, t_m) \neq (s_n, t_n)$ such that $s_m \leqslant s_n$ and $t_m \leqslant t_n$, the $Q^{(2)}$ distribution no longer has the property that $Q^{(2)}_{s_m,t_m,q}$ is a marginal distribution of $Q^{(2)}_{s_n,t_n,q}$. Meanwhile, for any two vectors $\boldsymbol{x} \sim \boldsymbol{y} \in \{0,1\}^{s_n+t_n}$ (recall that $\boldsymbol{x}$ and $\boldsymbol{y}$ are in the same equivalence class if both vector have the same number of ones), $Q^{(2)}_{s_n,t_n,q}(\boldsymbol{x}) = Q^{(2)}_{s_n,t_n,q}(\boldsymbol{y})$ is not necessarily correct. Thus, we need to check these 13 inequalities in an exhaustive method. We will discuss this further in the next two subsections.

9.2.3.1 The Transition Probabilities $Q^{(2)}$

Approximating $Q^{(2)}$ by Exploration Regions of Finite Height

Since the exploration regions of $\mathbf{G}^{(3)}$ for $\mathbb{F} \cdot R$ may contain loops, we no longer follow the idea of calculating the transition probabilities of the projected process defined for stacked lattices. We introduce a new probability measure $\bar{Q}^{(2)}_{s_n,t_n,q}$ for each pair (s_n, t_n) that satisfies the following conditions:

1. $\bar{Q}^{(2)}_{s_n,t_n,q}$ is defined on the same sample space as $Q^{(2)}_{s_n,t_n,q}$;

2. $\bar{Q}^{(2)}_{s_n,t_n,q}$ is a good approximation of $Q^{(2)}_{s_n,t_n,q}$;

3. $\bar{Q}^{(2)}_{s_n,t_n,q} \leqslant_{\mathrm{st}} Q^{(2)}_{s_n,t_n,q}$.

We illustrate this approximation by considering a specific example that $(s_n, t_n) = (2, 3)$. Apparently, the exploration region is a subgraph of the exploration region shown in Figure 9.5 and is isomorphic to the graph illustrated in Figure 9.6. Notice that in Figure 9.6, the red edges correspond to the red edges in Figure 9.5 whose projections are s-edges. For any $\boldsymbol{\omega}^{(2)}_{\perp,s} \in \{0,1\}^2$ and $\boldsymbol{\omega}^{(2)}_{\perp,t} \in \{0,1\}^3$, by Definitions 9.2.3 and 9.2.5, we may interpret $Q^{(2)}_{2,3,q}(\boldsymbol{\omega}^{(2)}_{\perp,s}, \boldsymbol{\omega}^{(2)}_{\perp,t})$ as follows. It is the probability that in Figure 9.6, there exists a vertex in the i-th column connected to vertex $v^{(3)}_n$ by open paths if and only if the i-th entry in the vector $(\boldsymbol{\omega}^{(2)}_{\perp,s}, \boldsymbol{\omega}^{(2)}_{\perp,t})$ is 1. Since there are infinitely many layers in the exploration region, this probability is difficult to calculate. A very straightforward approximation of $Q^{(2)}$ is by only considering the vertices that are not too "far away" from $v^{(3)}_n$. We shall define and calculate $\bar{Q}^{(2)}_{s_n,t_n,q}$-measure based on this idea.

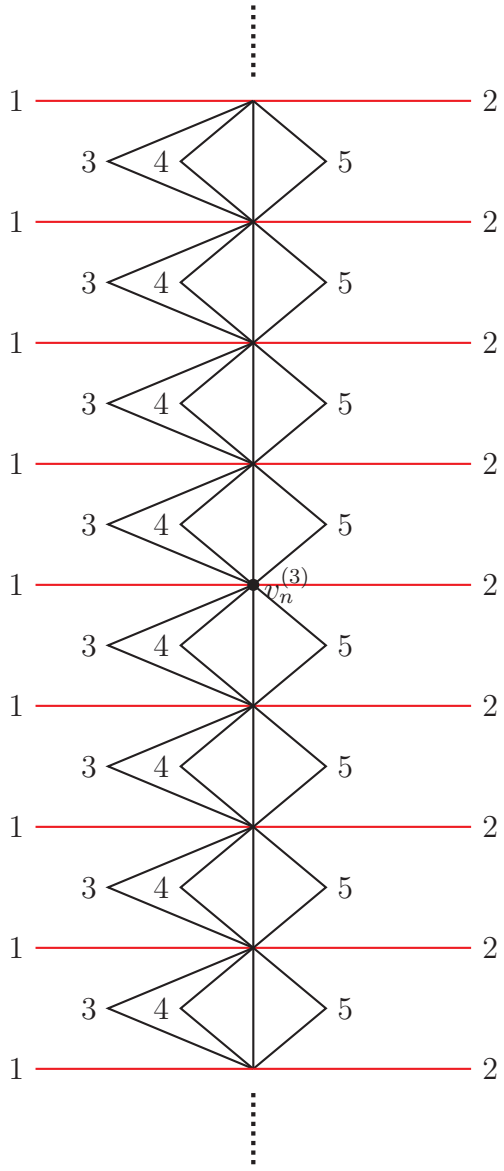

Figure 9.6: An illustration of a graph isomorphic to the exploration region $B_n^{(3)}$, the latter of whose projection contains 2 s-edges and 3 t-edges. For simplicity, we label the vertices by $\{1, 2, ..., 5\}$, which might differ from the labeling function l used in establishing $\mathbf{G}^{(3)}$.

More specifically, for each specified $h \in \mathbb{Z}^+$, we consider two vector indicators, $\boldsymbol{\omega}_{\perp,s}^{\pm h} \in \{0,1\}^{s_n}$ and $\boldsymbol{\omega}_{\perp,t}^{\pm h} \in \{0,1\}^{t_n}$. The i-th indicator of $\boldsymbol{\omega}_{\perp,s}^{\pm h}$ is 1 if and only if

1. the s-type edge with label i is in $C_n^{(2)}$; and
2. in $\mathbb{F} \cdot R$ (Figure 9.5), the Euclidean distance between $v_n^{(3)}$ and the nearest connected column-neighbor whose projection is an endpoint of the s-edge is smaller than or equal to $\sqrt{2h^2+2}$.

Analogously, the i-th indicator of $\boldsymbol{\omega}_{\perp,t}^{\pm h}$ is 1 if and only if

1. the t-type edge with label $s_n + i$ is in $C_n^{(2)}$; and
2. in $\mathbb{F} \cdot R$ (Figure 9.5), the Euclidean distance between $v_n^{(3)}$ and the nearest connected column-neighbor whose projection is an endpoint of the s-edge is smaller than or equal to $\sqrt{2h^2-2h+2}$.

Equivalently, Figure 9.6 shows that the exploration region is formed by piling up infinitely many isomorphic layers (Figure 9.7). We consider a truncated exploration region that only contains $2h$ layers, while there are h layers above $v_n^{(3)}$ and h layers below $v_n^{(3)}$. Then $(\boldsymbol{\omega}_{\perp,s}^{\pm h}, \boldsymbol{\omega}_{\perp,t}^{\pm h})$ is an indicator vector of the nearest connected column-neighbors of $v_n^{(3)}$ that are connected to $v_n^{(3)}$ by open paths in the $2h$-layer truncated exploration region. Simple observation yields

$$(\boldsymbol{\omega}_{\perp,s}^{\pm 1}, \boldsymbol{\omega}_{\perp,t}^{\pm 1}) \leqslant (\boldsymbol{\omega}_{\perp,s}^{\pm 2}, \boldsymbol{\omega}_{\perp,t}^{\pm 2}) \leqslant (\boldsymbol{\omega}_{\perp,s}^{\pm 3}, \boldsymbol{\omega}_{\perp,t}^{\pm 3}) \leqslant \cdots \leqslant (\boldsymbol{\omega}_{\perp,s}^{(2)}, \boldsymbol{\omega}_{\perp,t}^{(2)})$$

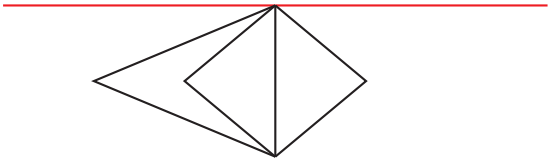

Figure 9.7: An illustration of one "layer" of the exploration region in the rotated FCC lattice. The exploration region can be decomposed into isomorphic layers.

and

$$\lim_{h\to\infty}(\boldsymbol{\omega}_{\perp,s}^{\pm h},\boldsymbol{\omega}_{\perp,t}^{\pm h})=(\boldsymbol{\omega}_{\perp,s}^{(2)},\boldsymbol{\omega}_{\perp,t}^{(2)})$$

We define $\bar{Q}^{(2)}$ be the joint probability distribution of $(\boldsymbol{\omega}_{\perp,s}^{\pm 8},\boldsymbol{\omega}_{\perp,t}^{\pm 8})$, which satisfies the three conditions listed at the beginning of the subsection.

Calculation of $\bar{Q}^{(2)}$

For consistency, we illustrate the calculation procedure by considering the situation that $(s_n,t_n)=(2,3)$ as in the previous subsection. Notice that there are 146 edges in the 16-layer truncated exploration region. Thus, it is impossible to check all the 2^{146} configurations of the truncated exploration region. To simplify our calculation, we introduce a simple graph welding technique that calculates the distribution of $(\boldsymbol{\omega}_{\perp,s}^{\pm h},\boldsymbol{\omega}_{\perp,t}^{\pm h})$ recursively. We name the vertices in the exploration region as illustrated in Figure 9.8. For the convenience of illustrating the calculation procedure, for each $h\in\mathbb{Z}^+$, define $\boldsymbol{\omega}_{\perp}^{+h}\in\{0,1\}^5$ to be the indicator vector whose i-th entry indicates

whether there exists $1 \leqslant j \leqslant h$ such that $u_{i,j} \overset{B_n^{(3)}}{\longleftrightarrow} v_n^{(3)}$. Similarly, the i-th entry of $\boldsymbol{\omega}_\perp^{-h} \in \{0,1\}^5$ indicates whether there exists $-h \leqslant j \leqslant -1$ such that $u_{i,j} \overset{B_n^{(3)}}{\longleftrightarrow} v_n^{(3)}$. Applying the law of total probability, the following recursive formulas hold for each $\boldsymbol{e} \in \{0,1\}^5$:

$$\begin{aligned}
&P_q^{(3)}(\boldsymbol{\omega}_\perp^{+2h} = \boldsymbol{e}, u_{6,2h} \overset{B_n^{(3)}}{\longleftrightarrow} v_n^{(3)} \mid \mathbf{G}_{n-1}^{(2)}) \\
&= \sum_{\boldsymbol{e}_1,\boldsymbol{e}_2} P_q^{(3)}(\boldsymbol{\omega}_\perp^{+h} = \boldsymbol{e}_1, u_{6,h} \overset{B_n^{(3)}}{\longleftrightarrow} v_n^{(3)} \mid \mathbf{G}_{n-1}^{(2)}) \cdot P_q^{(3)}(\boldsymbol{\omega}_\perp^{+h} = \boldsymbol{e}_2, u_{6,h} \overset{B_n^{(3)}}{\longleftrightarrow} v_n^{(3)} \mid \mathbf{G}_{n-1}^{(2)}),
\end{aligned}$$

and

$$\begin{aligned}
&P_q^{(3)}(\boldsymbol{\omega}_\perp^{+2h} = \boldsymbol{e}, u_{6,2h} \overset{B_n^{(3)}}{\not\longleftrightarrow} v_n^{(3)} \mid \mathbf{G}_{n-1}^{(2)}) \\
&= P_q^{(3)}(\boldsymbol{\omega}_\perp^{+h} = \boldsymbol{e}, u_{6,h} \overset{B_n^{(3)}}{\not\longleftrightarrow} v_n^{(3)} \mid \mathbf{G}_{n-1}^{(2)}) + \\
&\quad \sum_{\boldsymbol{e}_1,\boldsymbol{e}_2} P_q^{(3)}(\boldsymbol{\omega}_\perp^{+h} = \boldsymbol{e}_1, u_{6,h} \overset{B_n^{(3)}}{\longleftrightarrow} v_n^{(3)} \mid \mathbf{G}_{n-1}^{(2)}) \cdot P_q^{(3)}(\boldsymbol{\omega}_\perp^{+h} = \boldsymbol{e}_2, u_{6,h} \overset{B_n^{(3)}}{\not\longleftrightarrow} v_n^{(3)} \mid \mathbf{G}_{n-1}^{(2)}),
\end{aligned}$$

where in both summations, we sum over all pairs of $\boldsymbol{e}_1, \boldsymbol{e}_2 \in \{0,1\}^5$ such that $\max(\boldsymbol{e}_1, \boldsymbol{e}_2) = \boldsymbol{e}$. For the base case that $h = 1$, we may calculate $P_q^{(3)}(\boldsymbol{\omega}_\perp^{+1} = \boldsymbol{e}, u_{6,1} \overset{B_n^{(3)}}{\longleftrightarrow} v_n^{(3)} \mid \mathbf{G}_{n-1}^{(2)})$ and $P_q^{(3)}(\boldsymbol{\omega}_\perp^{+1} = \boldsymbol{e}, u_{6,1} \overset{B_n^{(3)}}{\not\longleftrightarrow} v_n^{(3)} \mid \mathbf{G}_{n-1}^{(2)})$ by iterating through all configurations of one layer of the exploration region, which only contains 9 edges and thus there are 2^9 configurations.

Notice that in each of the two recursive formulas above, there are at most 2^{10} terms summed together. Thus, the time cost of calculating the conditional joint distribution of $\boldsymbol{\omega}_\perp^{+2h} = \boldsymbol{e}$ recursively is acceptable. Applying the recursive formula three times, we obtain $P_q^{(3)}(\boldsymbol{\omega}_\perp^{+h} = \boldsymbol{e}, u_{6,h} \overset{B_n^{(3)}}{\longleftrightarrow} v_n^{(3)} \mid \mathbf{G}_{n-1}^{(2)})$ and $P_q^{(3)}(\boldsymbol{\omega}_\perp^{+h} = \boldsymbol{e}, u_{6,h} \overset{B_n^{(3)}}{\not\longleftrightarrow} v_n^{(3)} \mid \mathbf{G}_{n-1}^{(2)})$

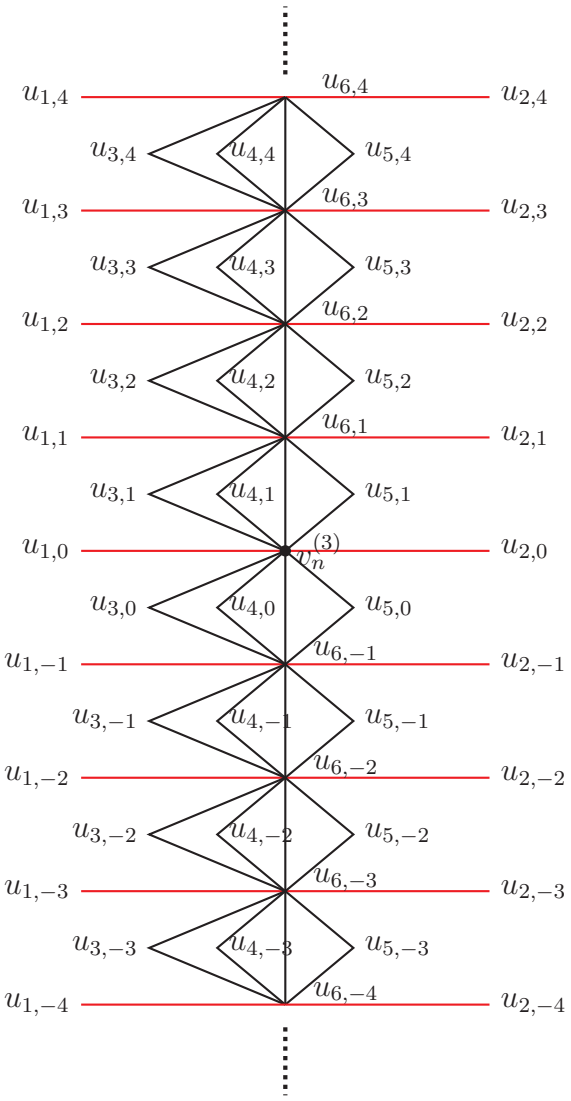

Figure 9.8: An illustration of a graph isomorphic to the exploration region $B_n^{(3)}$, the latter of whose projection contains 2 s-edges and 3 t-edges. For simplicity, we label the vertices by $\{1, 2, ..., 5\}$, which might differ from the labeling function l used in establishing $\mathbf{G}^{(3)}$.

for $h = 2, 4, 8$ and $\boldsymbol{e} \in \{0,1\}^5$. Finally, for $h = 8$, we have

$$\begin{aligned}
&P_q^{(3)}(\boldsymbol{\omega}_\perp^{+8} = \boldsymbol{e} \mid \mathbf{G}_{n-1}^{(2)}) \\
&= P_q^{(3)}(\boldsymbol{\omega}_\perp^{+8} = \boldsymbol{e}, u_{6,8} \overset{B_n^{(3)}}{\longleftrightarrow} v_n^{(3)} \mid \mathbf{G}_{n-1}^{(2)}) + P_q^{(3)}(\boldsymbol{\omega}_\perp^{+8} = \boldsymbol{e}, u_{6,8} \overset{B_n^{(3)}}{\not\longleftrightarrow} v_n^{(3)} \mid \mathbf{G}_{n-1}^{(2)}).
\end{aligned}$$

By symmetry, the conditional distribution of $\boldsymbol{\omega}_\perp^{-8}$ is identical to that of $\boldsymbol{\omega}_\perp^{+8}$. Notice that when considering the distribution of $\boldsymbol{\omega}_\perp^{+8}$ and $\boldsymbol{\omega}_\perp^{-8}$, the states of the two red edges incident to $v_n^{(3)}$ are not taken into account. Thus, we apply the law of total probability again by conditioning on the states of edge $(v_n^{(3)}, u_{1,0})$ and $(v_n^{(3)}, u_{2,0})$ to obtain the conditional distribution of $\boldsymbol{\omega}_\perp^{\pm 8}$.

$$\begin{aligned}
&P_q^{(3)}(\boldsymbol{\omega}_\perp^{\pm 8} = \boldsymbol{e} \mid \mathbf{G}_{n-1}^{(2)}) \\
&= \sum_{\boldsymbol{e}_1, \boldsymbol{e}_2} q^2 \cdot P_q^{(3)}(\boldsymbol{\omega}_\perp^{+8} = \boldsymbol{e}_1 \mid \mathbf{G}_{n-1}^{(2)}) \cdot P_q^{(3)}(\boldsymbol{\omega}_\perp^{-8} = \boldsymbol{e}_2 \mid \mathbf{G}_{n-1}^{(2)}) \\
&\quad + \sum_{\boldsymbol{e}_1, \boldsymbol{e}_2} q(1-q) \cdot P_q^{(3)}(\boldsymbol{\omega}_\perp^{+8} = \boldsymbol{e}_1 \mid \mathbf{G}_{n-1}^{(2)}) \cdot P_q^{(3)}(\boldsymbol{\omega}_\perp^{-8} = \boldsymbol{e}_2 \mid \mathbf{G}_{n-1}^{(2)}) \\
&\quad + \sum_{\boldsymbol{e}_1, \boldsymbol{e}_2} q(1-q) \cdot P_q^{(3)}(\boldsymbol{\omega}_\perp^{+8} = \boldsymbol{e}_1 \mid \mathbf{G}_{n-1}^{(2)}) \cdot P_q^{(3)}(\boldsymbol{\omega}_\perp^{-8} = \boldsymbol{e}_2 \mid \mathbf{G}_{n-1}^{(2)}) \\
&\quad + \sum_{\boldsymbol{e}_1, \boldsymbol{e}_2} (1-q)^2 \cdot P_q^{(3)}(\boldsymbol{\omega}_\perp^{+8} = \boldsymbol{e}_1 \mid \mathbf{G}_{n-1}^{(2)}) \cdot P_q^{(3)}(\boldsymbol{\omega}_\perp^{-8} = \boldsymbol{e}_2 \mid \mathbf{G}_{n-1}^{(2)}),
\end{aligned}$$

where the first summation sums over all $\boldsymbol{e}_1, \boldsymbol{e}_2$ such that $\max(\boldsymbol{e}_1, \boldsymbol{e}_2, (1,1,0,0,0)) = \boldsymbol{e}$; the second summation sums over all $\boldsymbol{e}_1, \boldsymbol{e}_2$ such that $\max(\boldsymbol{e}_1, \boldsymbol{e}_2, (1,0,0,0,0)) = \boldsymbol{e}$; the third summation sums over all $\boldsymbol{e}_1, \boldsymbol{e}_2$ such that $\max(\boldsymbol{e}_1, \boldsymbol{e}_2, (0,1,0,0,0)) = \boldsymbol{e}$; and the fourth summation sums over all $\boldsymbol{e}_1, \boldsymbol{e}_2$ such that $\max(\boldsymbol{e}_1, \boldsymbol{e}_2) = \boldsymbol{e}$. Noting that $\bar{Q}_{2,3,q}^{(2)}(\boldsymbol{e}) := P_q^{(3)}(\boldsymbol{\omega}_\perp^{\pm 8} = \boldsymbol{e} \mid \mathbf{G}_{n-1}^{(2)})$, we obtain the $\bar{Q}_{s_n,t_n,q}^{(2)}$ measure for $(s_n, t_n) = (2,3)$. By a similar approach, we can calculate $\bar{Q}_{s_n,t_n,q}^{(2)}$ for all pairs (s_n, t_n) such that $s_n \leqslant 2$

and $t_n \leqslant 3$ or $s_n \leqslant 1$ and $t_n \leqslant 4$.

Stochastic ordering as a max-flow problem

We now have the $\bar{Q}^{(2)}_{s_n,t_n,q}$ measure, which is dominated by the $Q^{(2)}_{s_n,t_n,q}$ measure. Fix $(s,t) \in (0,1)^2$. In order to find q such that $Q^{(2)}_{s_n,t_n,q} \geqslant_{\text{st}} Q_{s_n,t_n,s,t}$ for each $s_n \leqslant 2$ and $t_n \leqslant 3$ or $s_n \leqslant 1$ and $t_n \leqslant 4$, we find q such that $\bar{Q}^{(2)}_{s_n,t_n,q} \geqslant_{\text{st}} Q_{s_n,t_n,s,t}$. Noting that the sample spaces for $\bar{Q}^{(2)}$ and Q measures may contain up to 2^5 elements, which makes solving stochastic ordering inequalities of $\bar{Q}^{(2)}$ and Q by enumerating all the upsets very time-consuming. The time cost is also raised because the symmetry reduction by introducing equivalence classes no longer holds for these stochastic ordering inequalities. Consequently, we need an efficient algorithm to solve the stochastic ordering inequalities. Such an algorithm can be obtained by turning the stochastic ordering verification problem into a network flow problem.

Recall that the two probability measures we need to compare are $\bar{Q}^{(2)}_{s_n,t_n,q}$ and $Q_{s_n,t_n,s,t}$, both of which are defined on the σ-field generated by all the subsets of $\{0,1\}^{s_n+t_n}$. To determine if $\bar{Q}^{(2)}_{s_n,t_n,q}$ is stochastically larger than $Q_{s_n,t_n,s,t}$, we construct a weighted graph, also called a network, as follows.

- Vertices of the network

    1. Consider each length $s_n + t_n$ zero-one vector as a vertex.

2. For each vector, introduce a new vertex representing a "copy" of the vector. This provides us with another $2^{s_n+t_n}$ vertices.

3. As in all network flow problems, there are two dummy vertices: a source node and a sink node.

- Edges of the network

1. For each length $s_n + t_n$ zero-one vector (considered to be a vertex), there is a directed edge connecting the source node to the vector. The weight of this edge is the probability of the vector under $\bar{Q}^{(2)}_{s_n,t_n,q}$-measure.

2. For each "copy" of the vector there is a directed edge connecting the vector to the sink node. The weight of this edge is the probability of the vector under $Q_{s_n,t_n,s,t}$-measure.

3. For each original vector and each copy vector which may not be the copy of the former vector, there is a weight 1 edge connecting the former vector to the latter if and only if the former vector is larger than or equal to the latter.

For instance, by taking $s_n = 1, t_n = 2$, the corresponding network is shown in Figure 9.9.

A max-flow problem involves finding the maximum amount of flow in a pre-specified network that can reach to the sink from the source satisfying the edge constraint: the amount of flow through each edge can not exceed the weight of the

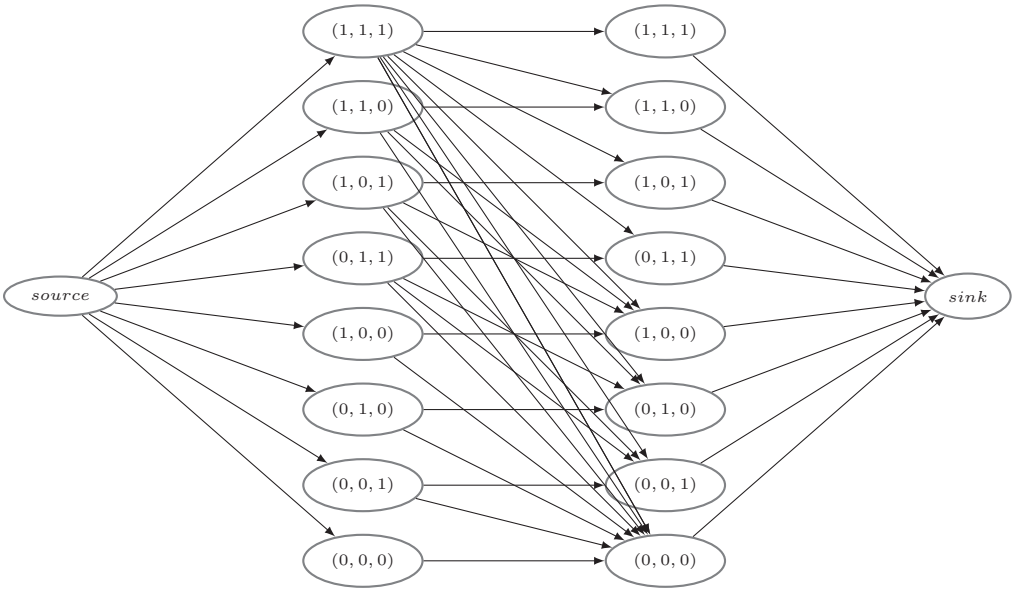

Figure 9.9: The network for verification of $\bar{Q}^{(2)}_{1,2,q} \geqslant_{\text{st}} Q_{1,2,s,t}$. The right-column contains 8 vertices that represents "copies" of the vertices in the left column.

edge.

Now we have a stochastic ordering problem and a corresponding max-flow problem. They are related in the following manner.

Theorem 9.2.7. $\bar{Q}^{(2)}_{s_n,t_n,q} \geqslant Q_{s_n,t_n,s,t}$ *if and only if there is a max-flow of* 1 *in the corresponding network.*

The proof of this theorem is based on the famous max-flow min-cut theorem in combinatorial optimization. Note that most mainstream max-flow algorithms solve the problem in polynomial time (in terms of number of vertices in the network). They provide us with a powerful approach to check stochastic ordering for each fixed

$q \in [0,1]$ efficiently. To find the smallest q such that $\bar{Q}^{(2)}_{s_n,t_n,q} \geqslant_{\text{st}} Q_{s_n,t_n,s,t}$, we perform a binary search algorithm, which provides an accuracy of 10^{-6} within 20 iterations.

We briefly introduced how to prove a stochastic ordering inequality by solving max-flow problems. For detailed description and discussion, including a formal proof of Theorem 9.2.7, we refer the interested reader to Preston [24] and May [19].

9.2.4 The Replicated Process and the Coupled Process

Given stochastic ordering inequalities (9.12), we can construct a replicated process $\{\mathbf{G}^{(r)}_n\}$ and a coupled process $\{\mathbf{G}^{(c)}_n\}$. For each vertex $v \in V^{\mathbb{T}}$, there exist 13 couplings: $\{(X_{s_v,t_v,v}, Y_{s_v,t_v,v})\}_{s_v,t_v}$, satisfying the following properties:

1. $X_{s_v,t_v,v}, Y_{s_v,t_v,v} \in \{0,1\}^{s_v+t_v}$, with $Y_{s_v,t_v,v} \geqslant X_{s_v,t_v,v}$ for each $v \in V^{\mathbb{T}}$, $s_v \leqslant 1, t_v \leqslant 4$ and each $s_v \leqslant 2, t_v \leqslant 3$.

2. $X_{s_v,t_v,v}$ has marginal distribution $Q_{s_v,t_v,s,t}$, and $Y_{s_v,t_v,v}$ has marginal distribution $Q^{(2)}_{s_v,t_v,q}$ for each $v \in V^{\mathbb{T}}$, $s_v \leqslant 1, t_v \leqslant 4$ and each $s_v \leqslant 2, t_v \leqslant 3$.

3. $\{(X_{s_v,t_v,v}, Y_{s_v,t_v,v})\}_{s_v,t_v,v}$ are stochastically independent.

Meanwhile, let $X_{2,4,\mathbf{0}^{(2)}}$ be a random vector in $\{0,1\}^6$ that is $Q_{2,4,s,t}$ distributed (Here $\mathbf{0}^{(2)}$ is the origin of $\mathbb{T}$). For simplicity, we simply refer to $X_{2,4,\mathbf{0}^{(2)}}$, together

with $\{X_{s_v,t_v,v}\}_{s_v,t_v,v}$ as the X-variables, and $\{Y_{s_v,t_v,v}\}_{s_v,t_v,v}$ as the Y-variables. Let Ω be the sample space of the X-variables and Y-variables. Let $\mathcal{F}$ be the corresponding σ-algebra, and $P_{s,t,q}$ to be the joint distribution of the the X-variables and Y-variables.

We now construct two stochastic processes $\{\mathbf{G}_n^{(r)}\}$ and $\{\mathbf{G}_n^{(c)}\}$ on the probability space $(\Omega, \mathcal{F}, P_{s,t,q})$ based on the X-variables and Y-variables such that $\{\mathbf{G}_n^{(r)}\}$ is a copy of $\{\mathbf{G}_n^{(2)}\}$, and $\{\mathbf{G}_n^{(c)}\}$ is coupled with $\{\mathbf{G}_n^{(r)}\}$.

Definition 9.2.8. We initialize $(A_0^{(r)}, B_0^{(r)}, C_0^{(r)}, C_0^{(c)})$ as follows:

$$A_0^{(r)} := \emptyset,$$

$$B_0^{(r)} := \emptyset,$$

$$C_0^{(r)} := \emptyset,$$

$$C_0^{(c)} := \emptyset.$$

Using the same labeling function that appeared in Definition 9.2.5, for $n \geqslant 1$, we define a stochastic process $(v_n^{(r)}, A_n^{(r)}, B_n^{(r)}, C_n^{(r)}, C_n^{(c)}) : \Omega \to V^{\mathbb{T}} \times 2^{V^{\mathbb{T}}} \times 2^{E^{\mathbb{T}}} \times 2^{E^{\mathbb{T}}} \times 2^{E^{\mathbb{T}}}$ on $(\Omega, \mathcal{F}, P_{s,t,q})$ recursively as follows.

For $n = 1$, we have

$$v_1^{(r)} := \mathbf{0}^{(2)},$$

$$A_1^{(r)} := \{\mathbf{0}^{(2)}\},$$

$$B_1^{(r)} := I[\mathbf{0}^{(2)}],$$

$$C_1^{(r)} := B_1^{(r)}.$$

Label the six edges in $B_1^{(r)}$ with $1, 2, ..., 6$ deterministically, so that the s-edges are labeled by 1 and 2 and the t-edges are labeled by $3, 4, 5$ and 6. Meanwhile, for each edge $e \in B_1^{(r)}$ whose label is i, let $\omega^{(c)}(e)$ be the i-th entry of the random vector $X_{2,4,v_1^{(r)}}$. Define

$$C_1^{(c)} := \{e \in B_1^{(r)} \mid \omega^{(c)}(e) = 1\}.$$

Assume that this stochastic process has been defined up to step n. At step $n+1$, if $\bigcup_{C_n^{(r)}} \setminus A_n^{(r)} \neq \emptyset$, define

$$v_{n+1}^{(r)} := \arg\min\{l(v) : v \in \bigcup_{C_n^{(r)}} \setminus A_n^{(r)}\},$$

$$A_{n+1}^{(r)} = A_n^{(r)} \cup \{v_{n+1}^{(r)}\},$$

$$B_{n+1}^{(r)} := I[\{v_{n+1}^{(r)}\}] \setminus I[\bigcup_{C_n^{(r)}} \setminus \{v_{n+1}^{(r)}\}].$$

Let s_{n+1} and t_{n+1} be the number of s-edges and t-edges in $B_{n+1}^{(r)}$, respectively. Label the edges in $B_{n+1}^{(r)}$ with $1, 2, ..., |B_{n+1}^{(r)}|$ so that the s-edges are labeled by $1, ..., s_{n+1}$ and the t-edges are labeled by $s_{n+1}+1, ..., s_{n+1}+t_{n+1}$. Meanwhile, for each edge $e \in B_{n+1}^{(r)}$,

let $\omega^{(c)}(e)$ be the i-th entry of random vector $X_{s_{n+1},t_{n+1},v_{n+1}^{(r)}}$ and $\omega^{(r)}(e)$ be the i-th entry of random vector $Y_{s_{n+1},t_{n+1},v_{n+1}^{(r)}}$, where i is the label of edge e. Define

$$C_{n+1}^{(r)} := C_n^{(r)} \cup \{e \in B_{n+1}^{(r)} \mid \omega^{(r)}(e) = 1\},$$

$$C_{n+1}^{(c)} := C_n^{(c)} \cup \{e \in B_{n+1}^{(r)} \mid \omega^{(c)}(e) = 1\}.$$

Otherwise, if $\bigcup_{C_n^{(r)}} \setminus A_n^{(r)} = \emptyset$ define

$$v_{n+1}^{(r)} := v_n^{(r)},$$

$$B_{n+1}^{(r)} := \emptyset,$$

$$C_{n+1}^{(r)} := C_n^{(r)},$$

$$C_{n+1}^{(c)} := C_n^{(c)}.$$

The *replicated growth process* is the stochastic process $\{\mathbf{G}_n^{(r)}\} := \{(A_n^{(r)}, C_n^{(r)})\}$ defined on the probability space $(\Omega, \mathcal{F}, P_{s,t,q})$, and the *coupled growth process* is the stochastic process $\{\mathbf{G}_n^{(c)}\} := \{C_n^{(c)}\}$ defined on the same probability space.

As in Chapter 6, the X-variables and Y-variables guarantee that $C_n^{(c)} \setminus C_{n-1}^{(c)} \subset C_n^{(r)} \setminus C_{n-1}^{(r)}$ for all $n \in \mathbb{N}$. Meanwhile, the distribution of the X-variables and Y-variables ensure that $\mathbf{G}^{(r)}$ has the same transition probabilities as $\mathbf{G}^{(2)}$. Consequently, $\mathbf{G}^{(r)}$ is indeed a copy of $\mathbf{G}^{(2)}$ and we have the global coupling relation that $\bigcup_{n=1}^{\infty} C_n^{(c)} \subseteq \bigcup_{n=1}^{\infty} C_n^{(r)}$. Alternatively, using abbreviation defined before, $C_\infty^{(c)} \subseteq C_\infty^{(r)}$.

Theorem 9.2.9. *Let $\mathcal{S}$ denote the state space of $\{\mathbf{G}_n^{(2)}\}$, which is also the state space of $\{\mathbf{G}_n^{(r)}\}$. Then $\{\mathbf{G}_n^{(r)}\}$ is a Markov Chain satisfying that each pair of $S_1, S_2 \in \mathcal{S}$ and*

$m, n \in \mathbb{Z}_+$ such that $P_q^{(3)}(\mathbf{G}_m^{(2)} = S_1) \neq 0$ and $P_{s,t,q}(\mathbf{G}_n^{(r)} = S_1) \neq 0$,

$$P_q^{(3)}(\mathbf{G}_{m+1}^{(2)} = S_2 \mid \mathbf{G}_m^{(2)} = S_1) = P_{s,t,q}(\mathbf{G}_{n+1}^{(r)} = S_2 \mid \mathbf{G}_n^{(r)} = S_1). \tag{9.13}$$

Theorem 9.2.10 (Global coupling of $\{\mathbf{G}_n^{(r)}\}$ and $\{\mathbf{G}_n^{(c)}\}$)**.** *The processes $\{\mathbf{G}_n^{(r)}\}$ and $\{\mathbf{G}_n^{(c)}\}$ defined in Definition 9.2.8 satisfy*

$$C_\infty^{(c)} \subseteq C_\infty^{(r)}. \tag{9.14}$$

9.2.5 Inhomogeneous Bond Percolation Models and the Induced Configuration

In a homogeneous bond percolation model, each edge is open with the same probability. This can be generalized to an inhomogeneous bond percolation model, in which different edges may have different probabilities to be open.

Definition 9.2.11 (The inhomogeneous Bernoulli bond percolation model)**.** For a connected graph $G = (V, E)$ with E partitioned into n disjoint edge sets $\{E_i\}_{i=1}^n$, the *inhomogeneous Bernoulli bond percolation model on G* is a random designation of a state (open or closed) to each edge of G, with each edge e independently designated as open with a pre-specified probability p_i, where $i \in \{0, 1, ..., n\}$ satisfies $e \in E_i$.

In this chapter, we consider G to be the triangular lattice $\mathbb{T}$. Since we have partitioned the edges of $\mathbb{T}$ into two types: the s-edges and t-edges, we shall focus on the two-parameter inhomogeneous model. In Definition 9.2.11, we take E_1 and E_2

to be the s-edges and t-edges of $\mathbb{T}$, respectively. We also take $p_1 = s$ and $p_2 = t$. Subsequently, we get a two-parameter inhomogeneous bond percolation model on $\mathbb{T}$, in which each s-edge is open independently with probability s and each t-edge is open independently with probability t. Denote the probability space of the two-parameter model on $\mathbb{T}$ by $(\Omega^{(2)}, \mathcal{F}^{(2)}, P^{(2)}_{s,t})$. More specifically, the sample space $(\Omega^{(2)}, \mathcal{F}^{(2)})$ is the same as the homogeneous percolation model on $\mathbb{T}$, and the probability measure of the two-parameter model is

$$P^{(2)}_{s,t} = \prod_{e \in E^{\mathbb{T}}} \mu_e,$$

where μ_e is Bernoulli distributed with parameter s if $e \in E_1$ and with parameter t if $e \in E_2$.

For the two-parameter percolation model on $\mathbb{T}$, we can define its percolation probability as the probability that there exists an infinite open cluster containing the origin in $\mathbb{T}$.

Definition 9.2.12 (The percolation probability)**.** The percolation probability of the two-parameter percolation model on $\mathbb{T}$ is defined as:

$$\theta^{\mathbb{T}}(s,t) = P^{(2)}_{s,t}(|D(\omega^{(2)})| = \infty),$$

where $D(\omega^{(2)})$ is the open cluster containing $\mathbf{0}^{(2)}$ for each $\omega^{(2)} \in \Omega^{(2)}$.

As in the homogeneous percolation model, the percolation probability is a non-decreasing function with respect to the both of the edge parameters s and t. Thus,

there exists a critical surface such that when the edge parameters are "above" the critical surface, the percolation probability is strictly positive, and when the parameter are "below" the critical surface, the percolation probability is zero.

Definition 9.2.13 (Critical surface)**.** The *critical surface* $\mathbf{p}_c(\mathbb{T})$ is defined as

$$\mathbf{p}_c(\mathbb{T}) = \{(s,t) \in [0,1]^2 \mid \forall\ \mathbf{x} > (s,t), \theta^{\mathbb{T}}(\mathbf{x}) > 0 \text{ and } \forall\ \mathbf{x} < (s,t), \theta^{\mathbb{T}}(\mathbf{x}) = 0\}.$$

We can now construct a configuration on $\mathbb{T}$, called the induced configuration, using $\{\mathbf{G}_n^{(r)}\}$ and $\{\mathbf{G}_n^{(c)}\}$ and a random configuration in $\Omega^{(2)}$ as follows.

Definition 9.2.14 (Induced Configuration)**.** Let $(\omega, \bar{\omega}^{(2)}) \in \Omega \times \Omega^{(2)}$ be $P_{s,t,q} \times P_{s,t}^{(2)}$ distributed. Let $\{(\mathbf{G}_n^{(r)}\}$ and $\{\mathbf{G}_n^{(c)})\}$ be the stochastic processes associated with ω defined in Definition 9.2.8, where the X-variables and Y-variables are obtained from ω. An *induced configuration* on $\mathbb{T}$, denoted by $\omega^{(2)}$, is a random vector in $\{0,1\}^{E^{\mathbb{T}}}$ such that

$$\omega^{(2)}(e) := \begin{cases} 1 & \text{if } e \in C_\infty^{(c)}, \\ 0 & \text{if } e \in (\bigcup_{n=1}^{\infty} B_n^{(r)}) \setminus C_\infty^{(c)}, \\ \bar{\omega}^{(2)}(e) & \text{if } e \notin (\bigcup_{n=1}^{\infty} B_n^{(r)}), \end{cases} \tag{9.15}$$

for each $e \in E^{\mathbb{T}}$.

Not surprisingly, the induced configuration, by construction, satisfies the following two properties.

Theorem 9.2.15. *The distribution of* $\omega^{(2)}$ *is* $P_{s,t}^{(2)}$ *under* $P_{s,t,q} \times P_{s,t}^{(2)}$ *distribution.*

Theorem 9.2.16. $D(\omega^{(2)}) \subseteq \bigcup_{C_\infty^{(r)}}$.

The proofs of the two theorems above are quite similar to the corresponding proofs provided in Chapter 6. For Theorem 9.2.15, we apply the induction method on the number of edges in the edge set E that generate the positive cylinder set $C_+(E)$. At the induction step, we consider two cases, which are distinguished by the type of the new edge in E. Each case can be proved by the same reasoning in the proof of Theorem 6.5.2. As for Theorem 9.2.16, this is a point-wise argument over the configuration space and no probability measure is involved. Thus, the result can be extended to the triangular lattice without worrying about the difference brought by introducing the extra parameters in the inhomogeneous model.

9.2.6 An Upper Bound for $p_c(\mathbb{F})$

From Chapter 7, we conclude that to make q an upper bound for $p_c(\mathbb{F})$, the following two conditions are sufficient.

1. Certain stochastic ordering inequalities are satisfied so that the X-variables and Y-variables exist, and the two processes $\mathbf{G}^{(r)}$ and $\mathbf{G}^{(c)}$ can be constructed.

2. The parameterization for the induced configuration is chosen so that the induced configuration has an infinite open cluster containing the origin with strictly positive probability.

We begin by considering the second condition first. In 1964, Sykes and Essam [30] solved for the critical surface for the three-parameter inhomogeneous bond percolation model on the triangular lattice. As a corollary of their results, the critical surface of our two-parameter model is

$$s = \frac{1-2t}{1-t^2},\ t \in [0, 0.5]. \tag{9.16}$$

Thus, by choosing s and t slightly above the critical surface specified by Equation (9.16), the second condition is satisfied.

We now turn to the first condition. Notice that the first condition implies $Q^{(2)}_{s_n,t_n,q} \geqslant_{\text{st}} Q_{s_n,t_n,s,t}$ for each $s_n \leqslant 1, t_n \leqslant 4$ or $s_n \leqslant 2, t_n \leqslant 3$. Recall that it is difficult to calculate $Q^{(2)}_{s_n,t_n,q}$ explicitly. However, we do have an approximation of the $Q^{(2)}$-measures obtained by considering the "truncated" exploration regions satisfying $Q^{(2)}_{s_n,t_n,q} \geqslant_{\text{st}} \bar{Q}^{(2)}_{s_n,t_n,q}$. Thus, to satisfy the both conditions, it is sufficient that we vary (s,t) on the critical surface $\boldsymbol{p}_c(\mathbb{T})$ and then, for each (s,t), choose q large enough so that

$$\bar{Q}^{(2)}_{s_n,t_n,q} \geqslant_{\text{st}} Q_{s_n,t_n,s,t}$$

for each $s_n \leqslant 1, t_n \leqslant 4$ or $s_n \leqslant 2, t_n \leqslant 3$. We set an accuracy for the binary search at 10^{-7} and performed symbolic calculations in MATLAB (so no numerical error other than the one from binary search may arise). Part of the results are summarized in the following table. Each row of the table contains 13 entries indicating the smallest q such that the corresponding stochastic ordering inequalities holds. Thus, for each

row, the largest value of the 13 entries is an upper bound for $p_c(\mathbb{F})$. Notice that we are free to choose any $t \in [0, 0.5]$. The upper bound for $p_c(\mathbb{F})$ when varying (s, t) along side the whole critical surface is summarized in Figure 9.10 and 9.11, where an optimized upper bound of 0.19170 is achieved by choosing $t = 0.394$.

Theorem 9.2.17. $p_c(\mathbb{F}) \leqslant 0.19170$.

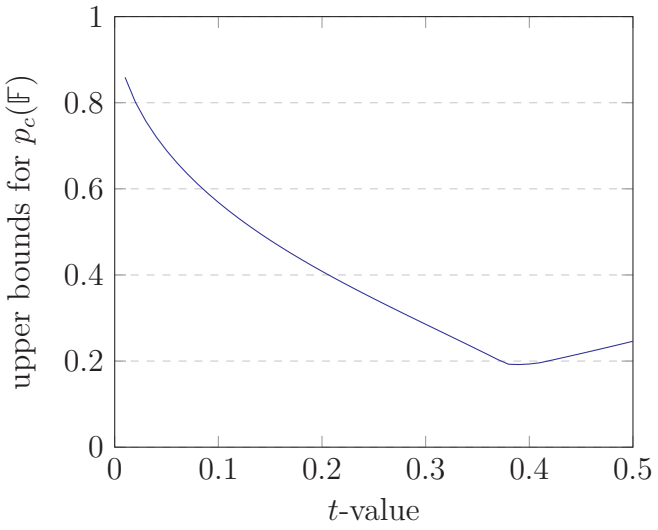

Figure 9.10: An illustration of the upper bound for $p_c(\mathbb{F})$ obtained by the growth process approach by tuning the parameter t from 0.0 to 5.0 with a step-length of 0.1. The curve suggests that an optimized lower bound can be achieved for some $t \in [0.38, 0.40]$.

Table 9.1: The smallest q satisfying the corresponding stochastic ordering inequalities. The t-values are chosen ranging from 0.34 to 0.40 with a step-length of 0.01 and the corresponding s-values are calculated by Equation (9.16). Each length 2 vector specifies the choice of (s_n, t_n) in the stochastic ordering inequality 9.12, and numbers in the same column illustrate the smallest q-values such that the inequality holds. Notice that our algorithm performs the binary search to find the minimum of the q-values. We set an accuracy of 10^{-7}. That is, the binary search stops when the intervals for the q-values has length smaller than 10^{-7}.

t-value	(2,3)	(2,2)	(2,1)	(2,0)
0.34	0.2084418535	0.2165257931	0.2263403535	0.2387548089
0.35	0.1994870305	0.2068859339	0.2158039212	0.2269676328
0.36	0.1944107413	0.1970734596	0.2051178217	0.2150796056
0.37	0.1934564114	0.1929475069	0.1942601800	0.2030576468
0.38	0.1926332116	0.1903607249	0.1886971593	0.1908653975
0.39	0.1919363141	0.1878980994	0.1832246780	0.1784619689
0.40	0.1913614869	0.1855540872	0.1778345108	0.1658006310

t-value	(1,4)	(1,3)	(1,2)	(1,1)	(1,0)
0.34	0.1912959814	0.1975106597	0.2048299909	0.2137016058	0.2249141932
0.35	0.1838200688	0.1895723939	0.1963135004	0.2044292688	0.2145857811
0.36	0.1829784513	0.1815256476	0.1875858903	0.1949576735	0.2040885687
0.37	0.1853865385	0.1830733418	0.1810120344	0.1852536201	0.1933898926
0.38	0.1878936887	0.1847249866	0.1813274026	0.1785216928	0.1824533939
0.39	0.1904982328	0.1864781976	0.1817498803	0.1763866544	0.1712375283
0.40	0.1931986213	0.1883307695	0.1822762489	0.1743509769	0.1596940756

t-value	(0,4)	(0,3)	(0,2)	(0,1)
0.34	0.1599559784	0.1566064954	0.1528141499	0.1485911012
0.35	0.1649544835	0.1613711715	0.1573001742	0.1527565122
0.36	0.1699947715	0.1661694646	0.1618083715	0.1569297314
0.37	0.1750788689	0.1710033417	0.1663405895	0.1611121297
0.38	0.1802086234	0.1758748293	0.1708986163	0.1653053164
0.39	0.1853860021	0.1807858944	0.1754842401	0.1695107222
0.40	0.1906129718	0.1857385039	0.1800994277	0.1737298965

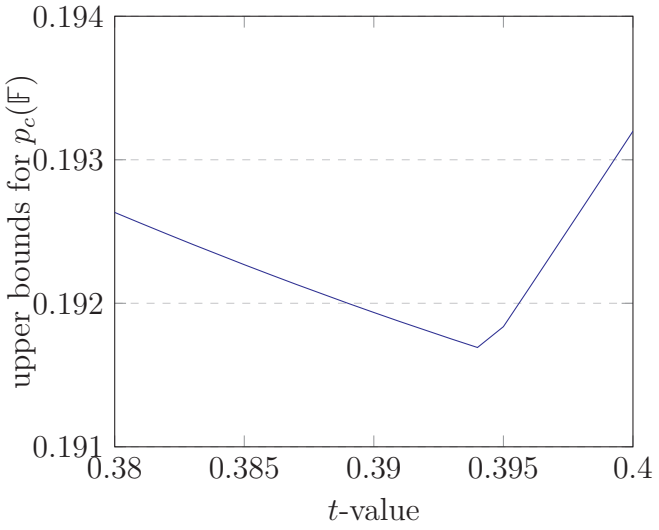

Figure 9.11: An illustration of the upper bound for $p_c(\mathbb{F})$ obtained by the growth process approach by tuning the parameter t from 0.38 to 0.40 with a step-length of 0.01. The curve suggests that an optimized lower bound of 0.19170 by choosing $t = 0.394$.

Bibliography

[1] Adler, J. A second look at a controversial percolation exponent–Is η negative in three dimensions? *Zeitschrift für Physik B Condensed Matter*, 55(3):227–229, 1984.

[2] Adler, J., Meir, Y., Aharony, A., and Harris, A. B. Series study of percolation moments in general dimension. *Physical Review B*, 41(13):9183–9206, 1990.

[3] Boubcheur, E.H., Loison, D., and Diep, H.T. Phase diagram of xy antiferromagnetic stacked triangular lattices. *Physical Review B*, 54(6):4165, 1996.

[4] Broadbent, S.R., and Hammersley, J.M. Percolation processes. *Mathematical Proceedings of the Cambridge Philosophical Society*, 53(3):629–641, 1957.

[5] Campanino, M., and Russo, L. An upper bound on the critical percolation probability for the three-dimensional cubic lattice. *The Annals of Probability*, 13(2):478–491, 1985.

[6] Dammer, S. M., and Hinrichsen H. Spreading with immunization in high dimensions. *Journal of Statistical Mechanics: Theory and Experiment*, 2004(07):P07011, 2004.

[7] de Magalhães, A. C., Tsallis, C., and Schwachheim, G. Probability renormalisation group treatment of bond percolation in square, cubic and hypercubic lattices. *Journal of Physics C: Solid State Physics*, 13(3):321–330, 1980.

[8] Galam, S., and Mauger, A. Universal formulas for percolation thresholds. ii. extension to anisotropic and aperiodic lattices. *Physical Review E*, 56(1):322–325, 1997.

[9] Gaunt, D. S., and Sykes, M. F. Series study of random percolation in three dimensions. *Journal of Physics A: Mathematical and General*, 16(4):783–799, 1983.

[10] Grassberger, P. Surface and edge exponents for the spreading of 3d percolation. *Journal of Physics A: Mathematical and General*, 19(5):L241–L246, 1986.

[11] Grassberger, P. Numerical studies of critical percolation in three dimensions. *Journal of Physics A: Mathematical and General*, 25(22):5867–5888, 1992.

[12] Heermann, D. W., and Stauffer, D. Phase diagram for three-dimensional correlated site-bond percolation. *Zeitschrift für Physik B Condensed Matter*, 44(4):339–344, 1981.

[13] Kataoka, K., Kuno, Y., and Ichinose, I. Bosonic t–j model in a stacked triangular lattice and its phase diagram. *Journal of the Physical Society of Japan*, 81(12):124502, 2012.

[14] Kawamura, H. Commensurate and incommensurate helical orderings in stacked-triangular antiferromagnets: CsMnBr3 and RbMnBr3. *Progress of Theoretical Physics Supplement*, 101:545–556, 1990.

[15] Kawamura, H. Universality of phase transitions of frustrated antiferromagnets. *Journal of Physics: Condensed Matter*, 10(22):4707, 1998.

[16] Kesten, H. The critical probability of bond percolation on the square lattice equals 1/2. *Communications in Mathematical Physics*, 74(1):41–59, 1980.

[17] Kesten, H. *Percolation Theory for Mathematicians*. Springer, Birkhäuser, Boston, 1982.

[18] Lorenz, C. D., and Ziff, R.M. Precise determination of the bond percolation thresholds and finite-size scaling corrections for the sc, fcc, and bcc lattices. *Physical Review E*, 57(1):230–236, 1998.

[19] May, W. D. *Computational Improvements in the Substitution Method for Bounding Percolation Threshold*. PhD thesis, Johns Hopkins University, 2005.

[20] Men'shikov, M.V., and Pelikh K.D. Percolation with several defect types. an estimate of critical probability for a square lattice. *Mathematical Notes*, 46(4):778–785, 1989.

[21] Ngo, V. T., and Diep, H.T. Phase transition in heisenberg stacked triangular antiferromagnets: End of a controversy. *Physical Review E*, 78(3):031119, 2008.

[22] Odagaki, T., and Chang, K. C. Real-space renormalization-group analysis of quantum percolation. *Physical Review B*, 30(3):1612–1614, 1984.

[23] Ozawa, H., and Ichinose, I. Phase structure of repulsive hard-core bosons in a stacked triangular lattice. *Physical Review A*, 86(1):015601, 2012.

[24] Preston, C. J. A generalization of the FKG inequalities. *Communications in Mathematical Physics*, 36(3):233–241, 1974.

[25] Sahimi, M., Hughes, B. D., Scriven, L. E., and Davis, H. T. Real-space renormalization and effective-medium approximation to the percolation conduction problem. *Physical Review B*, 28(1):307–311, 1983.

[26] Schram, R. D., Barkema, G. T., and Bisseling, R. H. Exact enumeration of self-avoiding walks. *Journal of Statistical Mechanics: Theory and Experiment*, 2011(06):P06019, 2011.

[27] Schrenk, K. J., Araújo, N. A. M., and Herrmann, H. J. Stacked triangular lattice: Percolation properties. *Physical Review E*, 87(3):032123, 2013.

[28] Stauffer, D., Adler, J. and Aharony, A. Universality at the three-dimensional percolation threshold. *Journal of Physics A: Mathematical and General*, 27(13):L475–L480, 1994.

[29] Stauffer, D. and Zabolitzky, J. G. Re-examination of 3d percolation threshold estimates. *Journal of Physics A: Mathematical and General*, 19(17):3705–3706, 1986.

[30] Sykes, M. F., and Essam, J. W. Exact critical percolation probabilities for site and bond problems in two dimensions. *Journal of Mathematical Physics*, 5(8):1117–1127, 1964.

[31] Van den Berg, J., and Ermakov, A. A new lower bound for the critical probability of site percolation on the square lattice. *Random Structures and Algorithms*, 8(3):199–212, 1996.

[32] van der Marck, S. C. Percolation thresholds and universal formulas. *Physical Review E*, 55(2):1514–1517, 1997.

[33] Vyssotsky, V. A., Gordon, S. B., Frisch, H. L., and Hammersley, J. M. Critical percolation probabilities (bond problem). *Physical Review*, 123(5):1566–1567, 1961.

[34] Wang, J., Zhou, Z., Zhang, W., Garoni, T. M., and Deng, Y. Bond and site percolation in three dimensions. *Physical Review E*, 87(5):052107, 2013.

[35] Wierman, J. C. A bond percolation critical probability determination based on the star-triangle transformation. *Journal of Physics A: Mathematical and General*, 17(7):1525–1530, 1984.

[36] Wierman, J. C. Bond percolation critical probability bounds for three Archimedean lattices. *Random Structures & Algorithms*, 20(4):507–518, 2002.

[37] Wierman, J. C. An improved upper bound for the bond percolation threshold of the cubic lattice. In *the 2015 Joint Statistics Meetings*. American Statistical Association, 2015.

[38] Wierman, J. C. On bond percolation threshold bounds for Archimedean lattices with degree three. *Journal of Physics A: Mathematical and Theoretical*, 50(29):295001, 2017.

[39] Wierman, J. C., Yu, G., and Huang, T. A disproof of Tsallis' bond percolation threshold conjecture for the kagome lattice. *Electronic Journal of Combinatorics*, 22(2):P2–52, 2015.

[40] Wierman, J.C., and Ziff, R.M. Self-dual planar hypergraphs and exact bond percolation thresholds. *Electronic Journal of Combinatorics*, 18(1):61–80, 2011.

[41] Wilke, S. Bond percolation threshold in the simple cubic lattice. *Physics Letters A*, 96(7):344–346, 1983.

[42] Yu, G., and Wierman, J. C. Exact enumeration of self-avoiding walks on FCC and BCC lattices. *Congressus Numerantium*, 226:199–212, 2016.

[43] Ziff, R. M. Generalized cell–dual-cell transformation and exact thresholds for percolation. *Physical Review E*, 73(1):016134, 2006.

[44] Ziff, R. M., and Scullard, C. R. Exact bond percolation thresholds in two dimensions.. *Journal of Physics A: Mathematical and General*, 39(49):15083, 2006.

[45] Ziff, R. M., Scullard, C. R., Wierman, J. C., and Sedlock, M. R. The critical manifolds of inhomogeneous bond percolation on bow-tie and checkerboard lattices. *Journal of Physics A: Mathematical and Theoretical*, 45(49):494005, 2012.

Vita

Gaoran Yu was born in Jiangsu, China in 1988. He received the Sc. B. degree in Probability and Statistics from Peking University in 2010, and the M. A. degree in Statistics from Columbia University in 2012. He then enrolled in the Applied Mathematics Ph.D. program at Johns Hopkins University in 2012, and was awarded a Gregory Fellowship in engineering. His research focuses on percolation theory under the supervision of John C. Wierman. Their joint research includes developing probabilistic methods and combinatorial tools to bound percolation thresholds rigorously. Gaoran's other areas of expertise include statistics, computer science, economics and finance. He is a CFA level two candidate and is earning a Master's degree in computer science.